

Analysis of asphalt concrete fatigue through energy methods

H.R. Stegeman

Technische Universiteit Delft



 **TU Delft**

 **KWS**

Analysis of asphalt concrete fatigue through energy methods

by

H.R. Stegeman

in partial fulfillment of the requirements for the degree of

Master of Science
in Structural Engineering

at the Delft University of Technology,
to be defended publicly on Wednesday July 01, 2020 at 11:00 AM.

Student number:	1528645	
Thesis committee:	Prof. dr. ir. S.M.J.G Erkens,	Delft University of Technology
	Dr. ir. K. Anupam,	Delft University of Technology
	Dr. O. Copuroglu,	Delft University of Technology
	Ir. C. Kasbergen,	Delft University of Technology
	Dr. ir. E. Hagos,	KWS @vice
	Ir. A. van der Wall,	KWS @vice

An electronic version of this thesis is available at <http://repository.tudelft.nl/>.



Acknowledgements

In front of you lies the thesis I have written to complete my Master degree in Structural Engineering with a specialisation in Road Engineering at the Technical University Delft. The study I performed is a collaboration between the company Koninklijke Wegenbouw Stevin (KWS) at the department of KWS @vice and the TU Delft. The majority of the tests are conducted at the central laboratory of KWS @vice in Hoogblokland with the new experimental work done at the University in Delft.

I enjoyed carrying out my own research for this Master Thesis. Developing and testing different methods in finding a theoretical and practical solution for a current and developing topic in the Dutch pavement industry. I would like to thank KWS for giving me a graduation internship position. Spending the first part at the central laboratory in Hoogblokland, I want to specially thank Otto and Hans for their guidance and who learned me a great deal about the practical aspects of the different fatigue tests. The time and precision it takes to perform a good test, as given all the different factors involved. Eyassu Hagos for his daily supervision and taking me with him when we had our Python course or meetings in Vianen. I want to thank Alex van der Wall for helping me seeing the greater perspective of the research. Giving me the option not only to do research but also to broaden my views by allowing me to follow a course at the company. Thank you for the time you gave me to complete this work. At last a great thanks for all the other staff at the Hoogblokland facility who gave me a great and wonderful time working there.

At the TU Delft I would like to thank the members of the faculty in fixing my additional test setups. Michèle for helping me preparing the specimen, Paul for the help with the measuring software MP3 and Marco for the daily support and intense help with the execution of the fatigue tests. I want to thank them all for the many discussions we had during the coffee breaks both topic related and the asphalt business in general. Kumar Anupam, I would like to thank you for providing me with this topic and the advice you gave me through the months. You make a great duo with Cor Kasbergen and I would like to thank Cor for being in my committee, your questions about how the research progressed kept me focused and ongoing. Furthermore Oguzhan, thank you for being willing to take place in my graduation committee. I would like to thank Sandra Erkens for being the chair of my committee and the crucial remarks you made for finishing this report. Your time was sparse but your overall expertise and feedback on the topic gave new insights and made completion possible. I would also like to thank Fedde Tolman for reading my draft and delivering accurate remarks about measuring accuracy.

Finally, I would like to thank my parents for their years of support and encouragements to finish my studies, which with this thesis will come to an end.

*H.R. Stegeman
Vianen, May 2020*

Summary

The fatigue life of asphalt concrete is an important parameter in the functional design of a road construction. In the Netherlands it is determined by the four Point Bending (4PB) test on laboratory prepared specimen. During the past years there is an increase in desire to validate the laid down asphalt pavement to the established functional properties. The most practical test setup applicable is the Cyclic Indirect Tensile Test (CY-ITT). Both fatigue tests differ on many fronts from each other. The resulting traditional fatigue line between them is therefore not coherent. A solution is previously sought in applying the energy based method of the Ratio of Dissipated Energy Change (RDEC). Developed by Shen & Carpenter. This research is a continuation of those works. The objective of this research is therefore formulated as follows: Establishing a fatigue life relation through the energy methods, which couples the fatigue life results of both the CY-ITT and 4PB fatigue tests and preserve the asphalt mixture characteristics.

In total 12 different mixtures were used to establish a wide field of mixture variation. Differences in RAP content, bitumen, PEN-grade and max aggregate size were used. Each mixture was tested on both force controlled CY-ITT and displacement controlled 4PB. Additional 4PB force controlled and Uni-axial displacement controlled fatigue tests were conducted on a single mixture.

The results were analysed by the two main energy methods: The RDEC and the Viscous-Elastic Continuum Damage (VECD) model of Kim. The RDEC method is based on the slope ratio of the dissipated energy. The dissipated energy is calculated by the hysteresis loop. The VECD method is based on the linearization of the strain by the pseudostrain energy function. The rate of the pseudostrain energy function (G^R) is then used for the fatigue relation.

A single failure criteria (N_{fat}) was first determined for both fatigue tests. The 50% stiffness reduction criteria of the 4PB is replaced by the simplified version of the original Energy Ratio failure criteria: the Stiffness Repetition method. Resulting in a consistent determination of the tilting point on the stiffness curve. The use of this method leads in the 4PB traditional fatigue life relation to a small decrease of slope of the fatigue line. For the application of the energy methods the original Energy Ratio failure criteria was applied. The difference is insignificant, but proved more robust. The failure criteria proved to be dependent, resulting that the failure in RDEC is directly related to failure in stiffness.

The applied RDEC method resulted in large amounts of scatter. Making it impossible to determine the assumed Plateau Value (PV) or the N_{fat} . The assumed linear state interval of the dissipated energy curve with a applied fitting method was used to determine a consistent PV. The resulting dissipated energy slope parameter $x(1)$ is the crucial factor for the subsequent PV. The $x(1)$ is found to be mixture unique and different between the CY-ITT and 4PB. The normalisation of the $x(1)$ through the averaged dissipated energy interval delivered a high consistent Plateau Value.

In literature the VECD method proved to be loading mode independent and mixture type dependent. This result was validated with the force controlled 4PB tests. The calculation method for G^R showed empirically to be more consistent over a fitting method. The resulting relation for the fatigue life on $\log(G^R - N_{fatSN})$ is similar to the found $\log(x(1) - N_{fatER})$ of the RDEC.

For the RDEC is concluded that the method is a single line relationship. Independent of frequency, temperature, mixture type, mixture density and stress strain relation for each mode of loading. The test setup independence between the CY-ITT and 4PB was found for 6 out of the 12 mixtures. The 4PB force controlled test did not deliver an evident result. The Uni-axial displacement controlled fatigue test validated the RDEC independence of test setup. It is therefore not recommended to use the RDEC in the current configuration as a practical application for validation between laboratory prepared specimen

and the road constructed asphalt concrete layer.

For the VECD is concluded that the CY-ITT and 4PB did not form a single coherent fatigue line in the $\log(G^R - N_{fatSN})$ relation. The relation is for a single test setup however mixture type dependent. The hypothesis that the fatigue line is dependent on the linear stiffness from the frequency sweep and could be shifted similar as on the mastercurve, proved preliminary to be true for the same test setup. However to be untrue between the CY-ITT and 4PB G^R fatigue relation. The used relation between $\log(G^R - N_{fatSN})$ is therefor not applicable in linking the CY-ITT and 4PB fatigue test setups.

Recommendations for future research include a further increase of knowledge about the measurement accuracy and variability in results of the CY-ITT test setup. Furthermore the direct theoretical application of the dissipated energy on the practical CY-ITT with the assumptions made regarding to permanent and vertical deformations should definitely be checked and or reconsidered if a research continuation is sought in this direction. The last recommendation is a third energy model option, namely the full VECD theory in the C-S relation. Releasing the dependence on the N_{fat} to a different parameter as a possible answer in a mixture type unique solution. Linking the CY-ITT and 4PB fatigue tests through a single relation.

Contents

Acknowledgements	x
Summary	x
List of Figures	xi
List of Tables	xv
Nomenclature	xviii
1 Introduction	1
1.1 Background information	1
1.2 Scope	2
1.3 Research objective and research questions.	2
1.4 Methodology	3
1.4.1 Phase 1: Literature study	3
1.4.2 Phase 2: Data collection	3
1.4.3 Phase 3: RDEC method	4
1.4.4 Phase 4: Additional testing	4
1.4.5 Phase 5: VECD method	4
1.4.6 Phase 6: Comparison and conclusion	4
1.5 Outline of the Report.	4
2 Theoretical background fatigue	5
2.1 Introduction fatigue life	5
2.2 Fatigue tests	6
2.2.1 4 Point Bending test	7
2.2.2 Cyclic Indirect Tensile Test	9
2.2.3 Overview differences	13
2.3 Energy methods	14
2.3.1 Introduction to dissipated energy	14
2.3.2 Dissipated energy for 4PB & CY-ITT	15
2.3.3 RDEC method	16
2.3.4 VECD method	20
2.4 Failure Criteria	27
2.4.1 Conventional $N_{fat50\%}$	28
2.4.2 Dissipated Energy Ratio	28
2.4.3 Phase angle	31
2.4.4 Summary	31
2.5 Summary	32
3 Classical fatigue results	33
3.1 Mixtures.	33
3.1.1 Overview	33
3.1.2 Sample preparation.	34
3.1.3 Test procedure	35
3.2 Frequency sweep	35
3.2.1 Stiffness	35
3.2.2 Phase angle	36
3.2.3 Results	37

3.3	Fatigue	43
3.3.1	Failure criteria	43
3.3.2	Fatigue life strain vs stress	46
3.3.3	Results	47
3.3.4	All mixtures.	50
3.4	Conclusion	52
4	Results RDEC	53
4.1	General behaviour	53
4.1.1	Force & displacement signals.	54
4.1.2	Phase angle	57
4.1.3	Hysteresis loop	59
4.1.4	Force & displacement	61
4.1.5	Stress-strain distribution CY-ITT	61
4.2	General RDEC results	62
4.2.1	Dissipated energy	62
4.2.2	RDEC	62
4.3	Failure criteria & Plateau Values	64
4.3.1	Energy Ratio	64
4.3.2	Stiffness Repetition.	64
4.3.3	Fitting method	67
4.3.4	Statistical method	70
4.4	Theoretical approach and result	70
4.5	Influence of the non normalised RDEC	72
4.6	Mixture results	74
4.6.1	Individual $PV - N_{fat}$ Results	74
4.6.2	All mixtures.	78
4.7	4PB force controlled	80
4.7.1	Stiffness Repetition on 4PB force controlled	80
4.7.2	RDEC result	81
4.8	Uni-axial displacement controlled	86
4.8.1	Stiffness Repetition failure criteria.	86
4.8.2	RDEC result	87
4.9	Influence of mass density on RDEC	88
4.10	Conclusion	89
5	Results VECD	91
5.1	General behaviour	91
5.2	General VECD results	92
5.2.1	Total released pseudostrain energy W_c^R	92
5.2.2	Failure Criteria	93
5.2.3	Rate of pseudostrain energy G^R	93
5.3	4PB force controlled	97
5.3.1	Li results	97
5.3.2	18619TU results	99
5.3.3	Conclusion	100
5.4	VECD shift hypothesis	101
5.5	Mixture Results.	101
5.5.1	Individual $G^R - N_{fatSN}$ Results.	102
5.5.2	All mixtures.	104
5.6	Conclusion	106
6	Conclusions and recommendations	107
6.1	Conclusions to the research question	107
6.1.1	Main research question	107
6.1.2	Sub-questions	107
6.1.3	Research related conclusions	109

6.2 Recommendations	109
Bibliography	111
A Mixture details	115
A.1 Overview	115
A.2 Test remarks	116
B Results mixtures KWS	117
B.1 18501 results	118
B.1.1 4PB	118
B.1.2 CY-ITT	120
B.2 18502 results	122
B.2.1 4PB	122
B.2.2 CY-ITT	124
B.3 18523 results	126
B.3.1 4PB	126
B.3.2 CY-ITT	128
B.4 18590 results	130
B.4.1 4PB	130
B.4.2 CY-ITT	132
B.5 18607 results	134
B.5.1 4PB	134
B.5.2 CY-ITT	136
B.6 18619 results	138
B.6.1 4PB	138
B.6.2 CY-ITT	140
B.7 19018 results	142
B.7.1 4PB	142
B.7.2 CY-ITT	144
B.8 19020 results	146
B.8.1 4PB	146
B.8.2 CY-ITT	148
B.9 19051 results	150
B.9.1 4PB	150
B.9.2 CY-ITT	152
C Results based on works of Li	155
C.1 4PB strain controlled	155
C.2 4PB stress controlled	158
D Results 18619TU	161
D.1 Stiffness and Stiffness Repetition	161
D.2 Phase angle, dissipated energy and RDEC	164
D.3 Table	168
E Uni-axial Tensile Compression test	169
E.1 Specimen preparation	169
E.2 Test setup	170
E.3 Test Procedure	170
E.4 Measuring software and calculations	171
E.5 Results	172
E.5.1 Stiffness and Stiffness ratio	172
E.5.2 Phase angle, dissipated energy and RDEC	175
E.5.3 Log strain & Log PV	179
E.5.4 Table	179

F	Statistical method	181
G	Matlab code	185
	G.1 4PB185
	G.2 CY-ITT186

List of Figures

1.1	Research framework	3
2.1	Typical fatigue curve distinguishing between the three phases	5
2.2	Schematic diagram of the 4PB test	7
2.3	4PB specimen with glued clamps	7
2.4	Sinusoidal displacement waveform	8
2.5	TU Delft 4PB test setup	9
2.6	Zwick-Roell 4PB test setup	9
2.7	Schematic diagram of the CY-ITT test	10
2.8	CY-ITT LVDT frame	10
2.9	MTS CY-ITT test setup with specimen	10
2.10	Captured CY-ITT displacement and force signals	11
2.11	Stress distribution of a 100 mm ITT sample [Li, 2013]	12
2.12	Strain distribution of a 100 mm ITT sample [Li, 2013]	12
2.13	Linear elastic and visco-elastic loading behaviour[Li, 2013]	14
2.14	Hysteresis loop obtained from plotting load versus deflection[Francken and Clauwaert, 1987]	14
2.15	Dissipated energy change between loading cycles [Tolman et al., 2018]	17
2.16	Theoretical PV curve [Carpenter, 2003]	18
2.17	PV line for different mixtures [Shen and Carpenter, 2007]	18
2.18	RDEC scatter of a DSR fatigue test [Airey et al., 2017]	19
2.19	PV calculated over phase two [Airey et al., 2017]	20
2.20	The concept of C vs S curve. [Kutay and Lanotte, 2017]	21
2.21	schematic view of stress, pseudo strain, pseudo based stiffness [Zhang and Kim, 2012]	23
2.22	Schematic representation of total released pseudo strain energy in the stress pseudostrain space[Zhang and Kim, 2012]	24
2.23	G^R [Sabouri and Kim, 2014]	25
2.24	Rate of pseudo energy G^R for two different mixtures [Zhang and Kim, 2012]	26
2.25	Description of equal stress [Kim and Koh, 2012]	27
2.26	CY-ITT sample 55021 & 22020 after testing	28
2.27	Displacement amplitude sample 55022	28
2.28	Energy Ratio [Hopman et al., 1989]	29
2.29	Controlled strain vs controlled stress [Rowe, 1993]	30
3.1	Phase angle [Abedali, 2015]	36
3.2	Phase angle [Abedali, 2015]	37
3.3	Frequency sweep 18501	39
3.4	Frequency sweep result 18502	39
3.5	Frequency sweep result 18523	39
3.6	Frequency sweep result 18531	39
3.7	Frequency sweep result 18590	39
3.8	Frequency sweep result 18593	39
3.9	Frequency sweep result 18596	40
3.10	Frequency sweep result 18607	40
3.11	Frequency sweep result 18619	40
3.12	Frequency sweep result 19018	40
3.13	Frequency sweep result 19020	40
3.14	Frequency sweep result 19051	40
3.15	Mixtures at single frequency 8Hz, CY-ITT and 4PB	41

3.16	Fatigue line for different mixtures on 4PB	42
3.17	Phase angle for different mixtures 4PB	42
3.18	Stiffness and stiffness repetition 18501 test 50012F	43
3.19	Stiffness and stiffness repetition 18501 test 50022F	43
3.20	Stiffness and stiffness repetition 18590 test 52832F	44
3.21	Stiffness and stiffness repetition 18590 test 52828F	44
3.22	Fatigue line 18501 with different N_{fat}	44
3.23	Fatigue line 18590 with different N_{fat}	44
3.24	Stiffness and stiffness ratio 19020 test 55204F	45
3.25	Stiffness and stiffness ratio 19020 test 55209F	45
3.26	Fatigue line 18501, strain at initial	46
3.27	Fatigue line 18501, strain at failure	46
3.28	Fatigue line 18501, stress at initial	47
3.29	Fatigue line 18501, stress at failure	47
3.30	Fatigue line 18501	47
3.31	Fatigue line 18502	47
3.32	Fatigue line 18523	48
3.33	Fatigue line 18531	48
3.34	Fatigue line 18590	48
3.35	Fatigue line 18593	48
3.36	Fatigue line 18596	48
3.37	Fatigue line 18607	48
3.38	Fatigue line 18619	49
3.39	Fatigue line 19018	49
3.40	Fatigue line 19020	49
3.41	Fatigue line 19051	49
3.42	Fatigue line for different mixtures on 4PB	51
3.43	Fatigue line for different mixtures on CY-ITT	51
4.1	19020 CY-ITT measurement, force applied high	55
4.2	19020 CY-ITT measurement, force applied medium	55
4.3	19020 CY-ITT measurement, force applied low	55
4.4	CY-ITT measured noise	56
4.5	CY-ITT measured noise vs low amplitude displacement signal	56
4.6	Frequency sweep, sample 55205 on 10 Hz	56
4.7	Frequency sweep, sample 55205 on 0.1 Hz	56
4.8	19018 4PB measurement at cycle 100	57
4.9	19018 4PB measurement at cycle 1.250.000	57
4.10	Phase angle and dissipated energy B-15-1	58
4.11	19018 stiffness & phase angle	58
4.12	19018 4PB measurement at cycle 1.350.000	58
4.13	19018 4PB measurement at cycle 1.400.000	59
4.14	19018 4PB measurement at cycle 1.450.000	59
4.15	19020 CY-ITT Hysteresis loop, force applied high	60
4.16	19020 CY-ITT Hysteresis loop, force applied low	60
4.17	19018 4B Hysteresis loop, load cycle 100	60
4.18	19018 4PB Hysteresis loop, load cycle $1.4 \cdot 10^6$	60
4.19	19018 4PB Hysteresis loop, load cycle $1.45 \cdot 10^6$	60
4.20	Comparison in dissipated energy for the CY-ITT	61
4.21	Comparison in dissipated energy for a 4PB test	61
4.22	Dissipated energy 19020 test 55209F	63
4.23	Dissipated energy 19020 test 55199F	63
4.24	RDEC 19020 test 55209F	63
4.25	RDEC 19020 test 55199F	63
4.26	Energy Ratio and dissipated energy 19020 test 55209F	64
4.27	Energy Ratio and dissipated energy 19020 test 55199F	64

4.28	Stiffness and stiffness ratio 19020 test 55210F	65
4.29	Energy Ratio and dissipated energy 19020 test 55210F	65
4.30	Stiffness and stiffness ratio 19020 test 55195F	66
4.31	Energy Ratio and dissipated energy 19020 test 55195F	66
4.32	Dissipated energy CY-ITT 19020 sample 55209F	67
4.33	Dissipated energy 19020 4PB sample 55199F	67
4.34	Dissipated energy CY-ITT 18590 sample 52859	68
4.35	Dissipated energy 18590 4PB sample 52839	68
4.36	RDEC 18590 CY-ITT sample 55209	68
4.37	RDEC 4PB sample 55199F	68
4.38	Modelled 4PB dissipated energy curve	71
4.39	Modelled CY-ITT dissipated energy curve	71
4.40	Modelled 4PB RDEC curve	72
4.41	Modelled CY-ITT RDEC curve	72
4.42	Dissipated energy slope $x(1)$ for mixture 18501	72
4.43	Dissipated energy slope $x(1)$ for mixture 19020	72
4.44	4PB Dissipated energy slope $x(1)$ for mixture 18501 and 18607	73
4.45	4PB Dissipated energy slope $x(1)$ for mixture 18501 and 19020	73
4.46	Plateau value line 18501	74
4.47	Plateau value line 18502	74
4.48	Plateau value line 18523	74
4.49	Plateau value line 18531	74
4.50	Plateau value line 18590	75
4.51	Plateau value line 18593	75
4.52	Plateau value line 18596	75
4.53	Plateau value line 18607	75
4.54	Plateau value line 18619	75
4.55	Plateau value line 19018	75
4.56	Plateau value line 19020	76
4.57	Plateau value line 19051	76
4.58	Plateau value line 19020	77
4.59	Plateau values for different mixtures on 4PB	79
4.60	Plateau values for different mixtures on CY-ITT	79
4.61	Stiffness and Stiffness Repetition, test 55706 force controlled	81
4.62	Stiffness and Stiffness repetition, test 55708 displacement controlled	81
4.63	Stiffness and Stiffness Repetition of test B-11-1 force controlled	81
4.64	Stiffness and Stiffness Repetition of test B-18-4 displacement controlled	81
4.65	Phase angle and dissipated energy B-11-1 force controlled	82
4.66	RDEC B-11-1	82
4.67	Phase angle and dissipated energy B-18-4 displacement controlled	82
4.68	RDEC B-18-4	82
4.69	Plateau values from N. Li force and displacement controlled	83
4.70	Phase angle and dissipated energy 55706	84
4.71	RDEC 55706	84
4.72	Phase angle and dissipated energy 55712	84
4.73	RDEC 55712	84
4.74	Plateau values for 18619 force and displacement controlled	85
4.75	Plateau values for 18619 4PB force and displacement controlled and CY-ITT force controlled loading modes	85
4.76	Stiffness and Stiffness ratio P02	86

4.77	Stiffness and Stiffness ratio P02	86
4.78	Phase angle and dissipated energy P02	87
4.79	RDEC P02	87
4.80	Phase angle and dissipated energy P12	88
4.81	RDEC P12	88
4.82	Plateau values for 18590 4PB, UTCF displacement and CY-ITT force controlled loading modes	88
4.83	Fatigue line mixture 18619 different density's	89
4.84	Plateau Value line mixture 18619 different density's	89
5.1	19018 4PB, change of vector F	92
5.2	19020 CY-ITT, change of vector F	92
5.3	W_c^R 19020 test 55202F	92
5.4	W_c^R 19018 test 55003F	92
5.5	Stiffness and stiffness Repetition 19018 test 55003F	93
5.6	W_c^R 19018 test 55003F	93
5.7	Stiffness and Stiffness Repetition 19020 test 55202F	94
5.8	W_c^R 19020 test 55202F	94
5.9	G^R 19020 test 55202F	95
5.10	G^R 19018 test 55003FF	95
5.11	Total released pseudo strain energy B-18-4 displacement controlled	97
5.12	G^R B-18-4	97
5.13	Total released pseudo strain energy B-11-1 force controlled	97
5.14	G^R B-11-1	97
5.15	G^R calc from Li force and displacement controlled	98
5.16	G^R fitted from Li force and displacement controlled	98
5.17	Total released pseudo strain energy 55692 displacement controlled	99
5.18	G^R 55692	99
5.19	Total released pseudo strain energy 55706 force controlled	99
5.20	G^R 55706	99
5.21	G^R calc from 18619 force and displacement controlled	100
5.22	G^R fitted from 18619 force and displacement controlled	100
5.23	G^R line 19018 CY-ITT on 10 and 30 Hz.	101
5.24	G^R line 19018 CY-ITT shifted to 10 Hz.	101
5.25	G^R line 18590	102
5.26	G^R line 19020	102
5.27	G^R line 19020 CY-ITT shifted to 30 Hz.	102
5.28	G^R line 18501	103
5.29	G^R line 18501 CY-ITT shifted to 30 Hz.	103
5.30	G^R line 19051	103
5.31	G^R line 19051 CY-ITT shifted to 30 Hz.	103
5.32	G^R line for different mixtures on 4PB	105
5.33	G^R line for different mixtures on CY-ITT	105

List of Tables

2.1	Overview fatigue test differences.	13
3.1	Mixture overview.	34
3.2	Number of samples tested.	35
3.3	CY-ITT, sample 50040, mixture 18501 frequency sweep result	37
3.4	4PB, sample 50008, mixture 18501 frequency sweep result	38
3.5	18501 Frequency sweep results	38
3.6	Mixtures stiffness and phase angle at 8 Hz	41
3.7	R^2 and slope parameters from the fatigue tests.	50
4.1	Mixture 19020 CY-ITT different N_{fat}	65
4.2	Mixture 19020 4PB fatigue life for different N_{fat}	66
4.3	Mixture 19020 4PB Plateau Values	69
4.4	Mixture 19020 CY-ITT Plateau Values	69
4.5	Mixture 18619 density's.	89
5.1	Mixture 19020 CY-ITT G^R	95
5.2	Mixture 19018 4PB G^R	96
A.1	Mixture overview including test setup.	115
A.2	Mixture and test remarks overview.	116

Nomenclature

Abbreviations

4PB	4 Point Bending	[-]
CY-ITT	Cyclic Indirect Tensile Test	[-]
DE	Dissipated Energy	[J/m^3]
DER	Dissipated Energy Ratio	[-]
ER	Energy Ratio	[-]
ITT	Indirect Tensile Test	[-]
LVDT	Linear Variable Differential Transformer	[-]
OIA	Ontwerpinstrumentarium Asphaltverhardingen	[-]
PV	Plateau Value	[-]
RDEC	Ratio of Dissipated Energy Change	[-]
SN	Stiffness Repetition	[MPa*n]
SR	Stiffness Ratio	[-]
UTCF-T	Uni-axial Tensile Compression Fatigue Test	[-]
VECD	ViscoElastic Continuum Damage	[-]

Greek Symbols

ϕ	phase angle	[°]
σ	stress	[MPa]
σ_a	stress amplitude	[MPa]
ε	strain	[-]
ε^R	pseudo strain	[-]
ε_a	strain amplitude	[-]
ε_{ini}	strain amplitude at initial load repetition	[-]
ε_{pp}	strain peak-peak	[-]

Latin Symbols

G^R	first derivative of pseudo strain energy	[-]
$N_{fat50\%}$	load cycle at 50% reduction of stiffness failure	[-]
N_{fatSN}	load cycle at failure determined by maximum of SN curve	[-]
N_{fat}	Load cycle at failure	[-]
R^2	Coefficient of determination	[-]
S_d	Damage parameter	[-]

w	dissipated energy	$[J/m^3]$
W_e^R	Total released pseudo strain energy	[-]
$x(1)$	first derivative of dissipated energy	$[J/m^3 * n]$
C	Pseudo stiffness	[-]
E	Elastic Modulus	[MPa]
F	Force applied	[N]
f	frequency	[Hz]
n	Load repetition number	[-]
S	Stiffness	[MPa]



Introduction

This chapter gives an introduction to the performed study. In Section 1.1 the background of the topic is given, which leads to the scope in Section 1.2. In Section 1.3 the research objective and the main and sub research questions are presented, followed by the methodology and outline of the rapport in Section 1.4 and 1.5.

1.1. Background information

Fatigue life is an important property of an asphalt concrete mixture. It specifies the number of wheel passes or load repetitions at a certain load level before the pavement fails in fatigue cracking. It is therefore an important parameter in the design of a road construction. The current Dutch test method uses the *4 Point Bending test* (4PB) to functional specify the fatigue life properties of an asphalt mixture. An asphalt beam is clamped at four points and is sinusoidal displaced with a set strain level. Results are used in the Dutch calculation software 'OntwerpInstrumentarium Asphaltverhardingen' or OIA. It contains all fatigue life results for all the different mixtures and different empirical established factors for conversion from laboratory to practical pavement situations [CROW, a]. Making it the backbone of the current Dutch pavement design methodology.

The laid down asphalt concrete is however only validated empirically by its layer thickness, density, the content of bitumen of the mixture. The verification that the constructed pavement also meets the functional specifications set by the laboratory tested specimen is not checked. To give more insight in the functional properties of the constructed pavement as well in laboratory tested specimens, a program was started to research different methods to verify the constructed pavement on its functional properties and compare them with the results from the laboratory.

The program is called '*Functional Verification*' and is part of a bigger Dutch asphalt research program under the banner Asphalt-Impuls [CROW, b]. The goal of the program is to evaluate the functional properties of the constructed asphalt product and to validate them with the specifications of the Type-Test. The benefits of this method is that the constructed pavement can be validated through its functional properties instead of any empirically based mixture design. Resulting that both the design upfront and delivered construction are based on the same measurable properties [Sluer and Stigter, 2014] .

To directly integrate the Functional Verification program into the Dutch design standard would require to cut beams from the constructed asphalt layer. Dimensions of the beam and the complexities surrounding the removal of the beam from the pavement complicates this. Another more simple method was suggested [Sluer and Stigter, 2014]. The method utilises cores drilled from the constructed pavement, which are tested in the laboratory with the *Cyclic Indirect Tensile Test* or CY-ITT. This test method however differs greatly from the method of the 4PB test. Not only is the shape of the specimen different but also the internal stress strain distribution and most significant, the mode of loading.

The mentioned program requires research to investigate the differences in the two different fatigue test setups on a greater scale. By utilising the results from multiple mixtures, a constant relation between the different fatigue test methods and their differences could possibly be established. The sample size and test setup combined with the measured strain in the traditional fatigue relation are unable to provide that relation [Poeran et al., 2016]. The concept of energy dissipation introduced by Visser & van Dijk [1975] would capture the more fundamental fatigue properties of a viscous elastic material. Creating a different fatigue life relation that represents a more fundamental material fatigue property.

Shen & Carpenter applied the energy dissipation concept through the *Ratio of Dissipated Energy Change* (RDEC) [Shen and Carpenter, 2007]. Replacing the traditional fatigue life relation of the number of load repetitions until failure (N_{fat}) vs the applied strain with a Plateau Value vs N_{fat} . This theory was applied by Poeran on the two different fatigue tests trying to link them together [Poeran et al., 2016]. The published results however didn't show a perfect correlation. The results were later further optimised by Telman using an exponential statistical method on the dissipated energy which gave promising results [Telman, 2017]. However the published work was not very detailed in the final concept. Furthermore the results of Telman were not directly repeated in the succeeding paper published by [Tolman et al., 2018]. The outcome leads to this research in validating, expanding, contributing and investigating a more in depth study into applying both the mentioned RDEC, as the yet to be introduced VECD, energy methods. Both applied on the 4PB and CY-ITT fatigue tests.

1.2. Scope

Much research has been done on the topic of fatigue analysis and different methods have been developed to analyse the results. This thesis focuses on the energy dissipation behaviour of the 4PB and CY-ITT fatigue tests. Not in creating new models and or theories, but applying the current stated energy models on the standardised fatigue tests. Different fatigue failure criteria are discussed in combination with two selected high potential energy dissipating models. The results are used to find a coincident or coherent correlation between the two fatigue tests. A total of 12 different asphalt mixtures are analysed and used to validate the energy models on the CY-ITT and 4PB. The research scale takes place on the mixture or macro level. Testing and researching energy dissipation on a mastic or bitumen micro scale on the *Dynamic Shear Rheometer* (DSR) is not discussed.

1.3. Research objective and research questions

From Section 1.1 it becomes clear that the research on the application of the RDEC energy method is not fully finished or understood. The establishment of a working energy dissipation based methodology to link both CY-ITT, 4PB and the interpretation to a practical application of those fatigue results is meagre or incomplete. The research objective for this study is therefor formulated as follows:

Establishing a fatigue life relation through the energy methods, which couples the fatigue life results of both the CY-ITT and 4PB fatigue tests and preserve the asphalt mixture characteristics.

In order to achieve this objective a main research question and a couple of sub-questions are described below. The sub-questions are formulated as a part of the main question and describes the stated main question each in it's own domain.

Main research question:

How and can the energy methods be applied in coupling the 4PB and CY-ITT fatigue tests?

Sub-questions

1. How are the 4PB and CY-ITT fatigue tests characterized and what are their differences?
2. What are the main energy methods currently found in pavement engineering literature and how are they described?
3. Which failure criteria method applied to both modes of loading describes the specimen failure point the most accurate?

4. How can the energy methods be applied to the different properties and specimen shapes of both fatigue tests?
5. What are the critical influence parameters of each of the two applied energy methods on the resulting fatigue line?
6. Is the resulting fatigue life parameter unique and useful in comparing and coupling the different fatigue tests?
7. How do the two energy methods differ from one another when applied?

1.4. Methodology

The research was conducted in 6 time phases, treating 4 main subjects: Literature study, traditional fatigue life, RDEC and the VECD. The time phases overlapped at some point or had a feedback loop back to the objective of the initial research plan. Phase 4 and 5 were the results of the intermediate results made during the RDEC research phase. They act as an addition and give a broader insight in the different aspects of the energy methods and fatigue life of the CY-ITT and 4PB. The result was that during phase 4 the VECD energy method was researched in literature as a promising alternative to the RDEC. Adding it to the literature chapter and its result analysed in phase 5. In figure 1.1 the total framework of this thesis is given. With highlights to the different aspects treated during each phase and the sub-questions belonging to each topic.

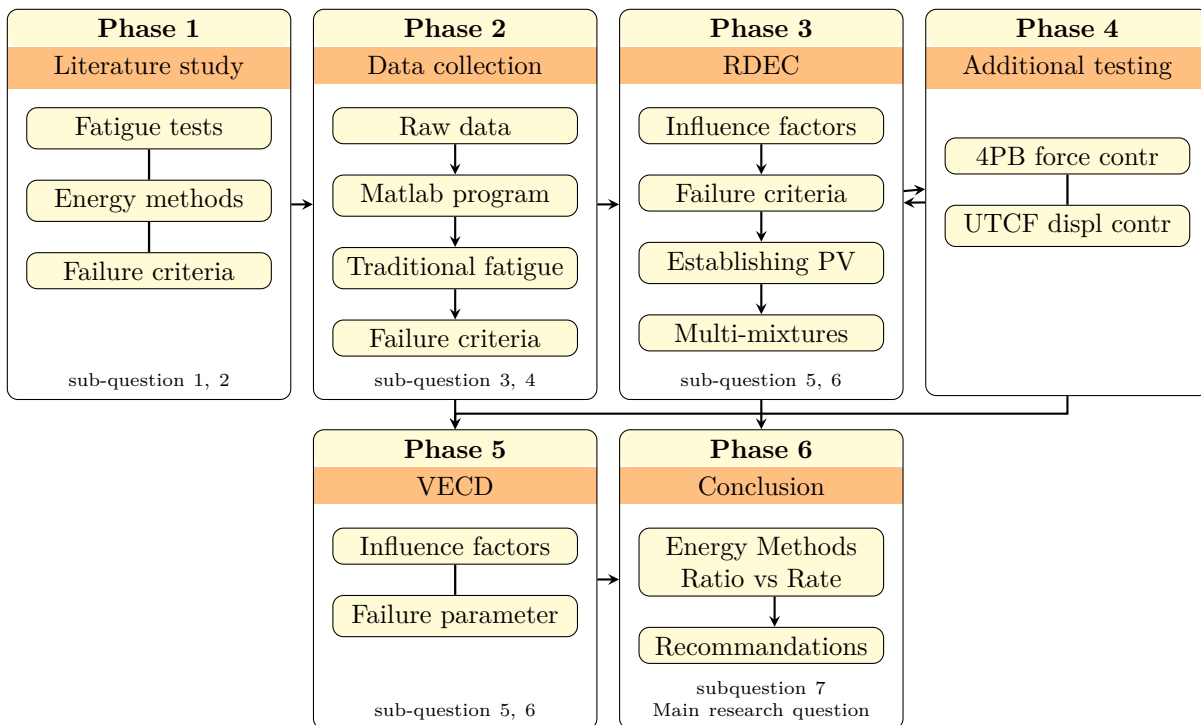


Figure 1.1: Research framework

1.4.1. Phase 1: Literature study

The first phase consisted of a literature study set by the goal of the thesis. The literature study established the knowledge needed about the 3 main subjects: The fatigue tests, the energy methods and failure criteria. The results formed the answer to sub-questions 1 and 2.

1.4.2. Phase 2: Data collection

During the second phase the base layer for the thesis was laid down. The 'raw' data needed and the calculation scripts for fast processing of the results formed the first part of that. To validate the own

developed scripts to the existing 'black box' software, the traditional fatigue results and relation were compared. The result was the established of a single failure parameter and the answering of sub-question 3.

The 'raw' data collection consists out of a wide variety of different mixtures and fatigue test settings to form a broad basis for phase 3 and phase 5. The programming language used is Matlab. It enabled to read and process, processed and unprocessed data files generated by the test setups on a fast and almost automated scale. Making it easy to visually and numerically interpreting the later results.

1.4.3. Phase 3: RDEC method

Phase 3 consisted of the application of the RDEC energy method established from literature through the developed Matlab program. Through program variations the most influenceable factors were established and the failure criteria compared. A fitting equation method was applied to establish the Plateau Value on a trial and error basis with different boundary conditions. Resulting in answering sub-question 4 and 5. The answering of sub-question 5 led to phase 4 and the feedback loop from phase 4 combined with multiple mixtures answers sub-question 6.

1.4.4. Phase 4: Additional testing

The results found and presented in the third phase led to a conclusion to look more in depth to the mode of loading and the stress-strain distribution. The mode of loading influence was researched with one previously and one own conducted 4PB force controlled fatigue test project. The stress-strain distribution influence was studied with the help of the Uni-axial tensile compression test conducted on the displacement controlled loading mode.

1.4.5. Phase 5: VECD method

From literature the VECD seemed to be loading mode independent. This was validated during phase 4 with the 4PB force controlled test. This resulted in the application of the VECD on both the 4PB and CY-ITT. Answering the same sub-questions as for the RDEC method.

1.4.6. Phase 6: Comparison and conclusion

The last phase is defined in comparing and analysing the difference between the two applied energy methods. Their differences are summarized and subquestion 7 is answered. From that the conclusions and later the recommendations for further research are presented.

1.5. Outline of the Report

The layout of the report is divided by the 4 main subjects: Chapter 2 contains the first phase, the performed literature study. Chapter 3 discusses the mixtures used and the traditional fatigue life of both the CY-ITT and 4PB. Holding the research conducted during phase 2. Chapter 4 contains both the research and results of phase 3 and 4 conducted on the application of the RDEC energy model. Chapter 5 discusses the VECD energy model results researched during phase 5 and analysed the additional work of phase 4 through the VECD model. Chapter 6 is formed by the conclusion on both energy models and recommendations for further research made during phase 6.

2

Theoretical background fatigue

This chapter provides the concept and theoretical background of this research. Giving an introduction to the topic of fatigue life and its concepts in the first section. It will be followed by the description of the two main test setups used for fatigue testing, namely the four Point Bending test (4PB) and the Cyclic Indirect Tensile Test (CY-ITT) in section 2.2. The theory of the energy methods on fatigue life is introduced in section 2.3, with subsections for the Ratio of Dissipated Energy Change and the ViscousElastic Continuum Damage model respectfully. With the understanding of fatigue life and the energy methods applied, the different fatigue life failure criteria are discussed in section 2.4.

2.1. Introduction fatigue life

In asphalt pavement fatigue cracking failure occurs from repeated traffic loads. After a certain number of load repetitions the build up of sufficient damage causes the pavement to crack. This cracking behaviour due to the cyclic nature of the loads is called fatigue and the number of load repetitions to a certain threshold of damage is called its fatigue life. The concept of fatigue life is based on the universal idea that most materials undergo a gradual deterioration under repeated loads that are far smaller than the ultimate strength of the material. The deterioration of the asphalt material is defined as the gradual reduction of its stiffness. The classic fatigue crack starts at the bottom of the pavement layer and grows towards the surface. Its development is directly proportional to the strain level at the bottom of the layer [Carpenter, 2003]. This strain level changes with the thickness of the asphalt layer, stiffness of the material, support reaction of the underlying foundation layers and other factors.

To assess the fatigue life of an asphalt specimen a fatigue test is performed. In this the specimen is exposed to a repetitive load at a high frequency. The result is described using a fatigue curve, also known as the S-N curve, where stiffness versus the number of load cycles is graphically shown. A typical traditional fatigue curve is shown in figure 2.1.

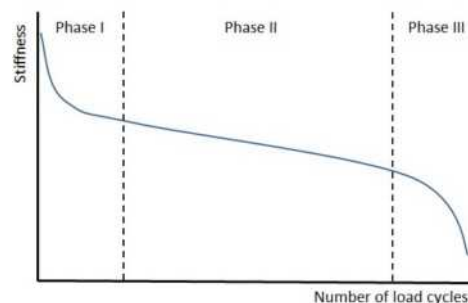


Figure 2.1: Typical fatigue curve distinguishing between the three phases

The typical fatigue curve undergoes three distinct phases, each with its own assigned characteristic features: [Benedetto et al., 2015]

Phase I: Initiation process of micro cracks, in which, apart from fatigue, other factors contribute to the rapid decrease of the stiffness, such as non-linearity, self-heating and thixotropy.

Phase II: Quasi-stationary propagation of micro cracks.

Phase III: The failure process, in which the stiffness rapidly decreases since the micro cracks grow to macro cracks, resulting in failure of the specimen.

From the overall testing time, phase II is the longest and both phase I and phase III are very short with rapid decreases in stiffness. In phase I the sharp decrease in stiffness is often assumed due to the non-linearity, self-heating and thixotropy. These effects are called the biased effects and are not yet fully understood, but they act interdependent, simultaneously and do not describe fatigue damage to the sample. In phase II the previous effects are still present, but are in a constant state. The overall decrease in stiffness here can be attributed to the forming and developing of micro cracks [Pronk, 1996]. Only a general description of the effects are given, as they interconnected and with the current test apparatus hard to not quantifiable.

Material non-linearity plays a significant role in asphalt mixtures at high strain levels. Due to the internal structure of an asphalt mixture, the binder will experience at inter aggregate spaces a higher strain level compared to the overall mix, which results in a higher influence of the non-linearity phenomena overall [Benedetto et al., 2015].

Self-heating is defined as the increase in temperature of the specimen through the cyclic nature of the test. Every moving cycle there is energy that dissipates as heat in the viscous material. The specimen will increase in temperature, but also radiates it's heat out toward the surrounding air. The climate chamber will cool that air and an equilibrium in temperature can occur. This is demonstrated by Pronk where normal bitumen had an increase of around 1 °C [Pronk, 1996].

Thixotropy is a property of a non-newton fluid under which bituminous materials fall. It is defined as the recoverable viscosity reduction after a constant shear or other forms of loading are applied. The phenomenon can be described that due movement, like stirring or bending, the viscosity of the material changes. In other words thinning or thickening of the material. [Benedetto et al., 2015]

With the stated assumption that these biased effects have reached a steady state in the second phase of the test, we will consider their details and influences marginal and don't consider their effects on the results found in this research. We will consider their possible influence however on the measured phase angle in the next section.

2.2. Fatigue tests

Fatigue laboratory testing is an idealised setup of real world practical passing of a wheel on a pavement structure. This passing of a wheel leads to a series of complex stresses and strains in the structure that leads to damage of the pavement. One of those is micro-cracking, which results in loss of stiffness, which we call fatigue. This real world loss in stiffness is measured by a falling weight deflectometer and it's outcome forms a basis for the decision for maintenance or reconstruction in Dutch road construction practices [CROW, a]. In order to understand the complex stress strain distribution and fatigue behaviour from a passing load in a pavement layer a simplification is made in the laboratory by using standardized fatigue tests. These tests represents the passing of a wheel by applying a controlled cyclic or dynamic loading pattern to the visco-elastic material. These loading cycles can be different in shape, loading modes and rest period depending on the fatigue test or tested behaviour. In this section the 4PB and the CY-ITT are discussed in it's overall working, calculations and accuracy.

2.2.1. 4 Point Bending test

2.2.1.1 Description

The 4PB test is a flexural bending beam test in which due to the nature of the test creates a constant bending moment between the two inner clamps. It is developed as an improvement from the 3 point bending test in which the maximum bending moment is located at a single point beneath the clamp. This has the disadvantage with inhomogeneous materials like asphalt in testing just the material under the central clamp. A second advantage is the pure constant bending moment between the two inner clamps, creating almost zero shear forces. The constant bending moment creates a assumed linear strain envelope over the height of this middle part of the beam. It is assumed as the asphaltic beam is none homogeneous and none perfect elastic. The maximum strain occurs at the top and bottom edges of the beam, with the same strain level at both sides of the sample but one end in compression and the other in tension. The dimensions of a standard beam are 450 mm in length, 50 mm in height and 50 mm in width. In figure 2.2 a schematic is given of the test setup. The beam is divided in three equal length parts with a distance of 140 mm in newer test apparatus and 133 mm in the old standard setup. The center frame is considered a rigid stiff frame which is moved by a servo hydraulic cylinder. The displacement of the beam at the center is measured by a single Linear Variable Differential Transformer or LVDT. Depending on the type of machine used, these have a range of -1 to 1 mm or -0.5 to 0.5 mm. Where the accuracy is often stated around $1 \pm 0.5 \mu\text{m}$.

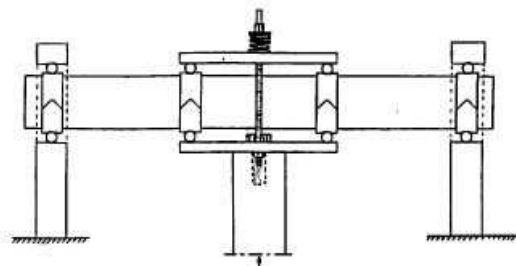


Figure 2.2: Schematic diagram of the 4PB test

In the older days the specimen is prepared by gluing 4 clamps with a hot low pen grade bitumen to the specimen. This is shown in figure 2.3. A special constructed board prevents sacking duo the clamps. On top of these clamps a spindle is placed to act as a hinge. These make sure that the specimen is secured in the vertical direction, but allows free rotation. Because the spindle is smaller in diameter than the groove in the clamp, it allows for a small horizontal translation. The applied force needed to secure the specimen in vertical direction is of influence of the overall measured stiffness [Li, 2013]. The more vertical force applied, the larger the influence of the frame stiffness and the influence on the measured phase lag. So the force applied to the clamps is chosen as low as possible at 100 cNm torque. Applying a lower force results in movement of the beam or spindle in lateral direction.



Figure 2.3: 4PB specimen with glued clamps

The test standard of the 4PB test is a displacement controlled test. This is a type of loading mode in which the displacement and therefore strain, is kept constant over time. Pronk states that the strain

throughout the test still changes and there is need for a second LVDT to keep the relative difference in deflection constant. This leads to a sensitivity drop of a factor 7 in means of measuring the relative deflection [Pronk, 2009]. This sensitivity drop is to great to be measured by a LVDT, so in practice this is not possible. That is why the absolute measured displacement is used and the assumption made that the strain is constant over time. The strain is kept constant by actively controlling the test by the measured displacement of the LVDT and adapting the applied force by the hydraulic cylinder to the specimen. By applying a sinusoidal displacement waveform, see figure 2.4 the specimen is loaded through its neutral line and both sides are put in compression and tension in a single loading cycle.

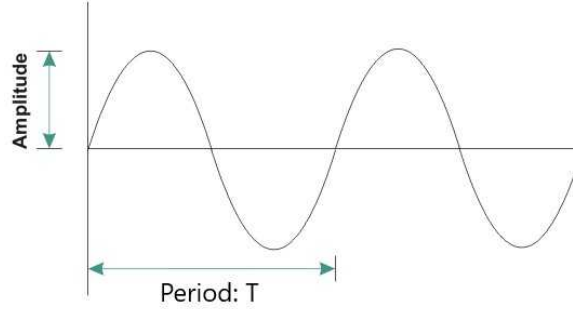


Figure 2.4: Sinusoidal displacement waveform

The test is standard performed at 30 Hz at a temperature of 20 °C [RAW, proef 62]. Three different strain levels are chosen to get the complete Whöhler fatigue curve [Wöhler, 1867], that describes the fatigue line through equation 2.1. The three strain levels are described as long, medium and short in test duration and as a requirement the long test needs to be higher than a million load repetitions to prevent extrapolation [RAW, proef 62]. Tests that take longer than 2 million loading cycles should be disregarded [NEN-EN 12697-24], because of creating a test point that artificial increase the accuracy of the R-squared value.

$$N_f = k_1 \varepsilon_{ini}^{k_2} \quad (2.1)$$

The constants k_1 & k_2 in equation 2.1 describe the linear fatigue line. These values are reported as well as the strain level ε_6 at 1 million load repetitions. These parameters are then used in a design program to calculate pavement thickness for a certain number of equivalent load repetitions. Examples for a complete fatigue curve where the number of load cycles vs the applied strain are given in Chapter 3.

2.2.1.2 Calculations

The basic calculations for the 4PB beam are given below. The test equipment itself take care of the dynamic mass compensation at the different frequencies, as prescribed by NEN-EN-12697-26, resulting that the back calculations can be done with the 'psuedo-static' equations given below. For the painstaking analysis of all the 4PB calculations, including dynamic mass compensation and clamp influences, the reader is referred to [Pronk, 2002]. For further insight in the different factors influencing the outcome of 4PB test results, FEM calculation by Hurman and other corresponding research the author refers to the 4PB platform [civil uminho]. The two most important and 'pseudo-static' used equations for the linear stress strain distribution of the beam are:

$$\sigma_t = \frac{3F_a a}{bh^2} \quad (2.2)$$

where: σ_t = maximum tensile stress [MPa]
 F_a = amplitude of the applied force [N]
 a = distance between clamps [mm]
 b = beam width [mm]
 h = beam height [mm]

$$\varepsilon_t = \frac{12U_a h}{23a^2} \quad (2.3)$$

where: ε_t = maximum tensile strain [-]
 U_a = amplitude of the measured displacement [mm]

Both equation 2.2 and 2.3 are for the outer most fiber of the beam, calculating the highest stress and strain occurring in the beam. The complete and standardised testing procedure is described in NEN-EN 12697-24 Annex D. One remark given to that document is that the clamping force is not mentioned in the current version.

2.2.1.3 Test equipment

In total three different test machines were used for the 4PB fatigue tests. Two commercial and one developed by the TU-Delft. The two commercial ones are delivered by Zwick-Roell and MTS, both used by the central laboratory of KWS. The TU Delft has an in-house developed test setup. In figure 2.5 the 4PB test setup of the TU Delft is shown. It has a lot of experimental possibilities, but with that a lot of complexities. The latest improvement was the addition of a stiffer frame to minimize the deflection of the outer supports in 2013.



Figure 2.5: TU Delft 4PB test setup



Figure 2.6: Zwick-Roell 4PB test setup

The newest test equipment is the Zwick-Roell shown in figure 2.6. This machine is highly automated and a big advantage over the older MTS equipment is the removal of the need of gluing clamps to the specimen as seen in figure 2.3. Resulting in the advantage that the applied torque to hold the beam is applied controlled and automatically, saving the operator valuable time. The measuring frequency is slightly different, the MTS measures with 1600 points per second, the Zwick can do 5000 points per second. This doesn't have a big influence on the calculations directly made by the machine, because both controllers use the Fast Fourier Transform (FFT) method of calculating the peak to peak values and the phase angle. Because of slight differences in setups both machines have a different phase angle correction, these corrections are checked by using an aluminum calibration beam. The biggest difference overall is that the two commercial machines have a high level of automation, including coupled excel macro scripts to speed up the overall test time. Where the TU Delft equipment is more transparent, adaptable and insightful in the way measurements and calculations are made, but a lot slower overall.

2.2.2. Cyclic Indirect Tensile Test

2.2.2.1 Description

The Cyclic Indirect Tensile Test (CY-ITT), also called the dynamic indirect tensile test or Dynamic IDT test. It is development from the monotonic indirect tensile test or (ITT), where the force is applied with a constant rate and the initial linear slope of the force in combination with the measured displacement would give the stiffness or resilient modules of the specimen. The ITT is also called the Brazilian test and was initial developed for concrete strength testing. Performing the test dynamical or cyclic, the test was developed as a fatigue test. Applying a certain force amplitude to the specimen at a loading

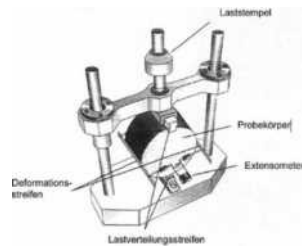


Figure 2.7: Schematic diagram of the CY-ITT test

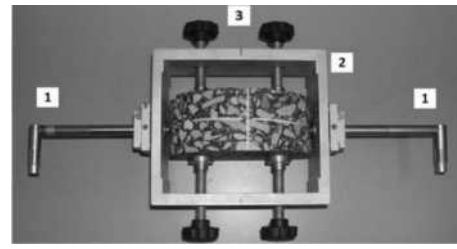


Figure 2.8: CY-ITT LVDT frame

frequency and measuring the amplitude of the displacement in the horizontal direction. This vertical and horizontal relation is then linked through the use of the Poisson number.

In figure 2.7 the schematic overview of the test setup is given. A sample of 100 or 150 mm in diameter and 40 to 50 mm in height is placed in the test setup. The schematic overview suggest the placement of strain gauges, but two LVDT are used in this research for measuring the horizontal displacement. The vertical displacement is not measured. The load is applied by a hydraulic jack through a movable sliding frame to a small steel beam with a width of 12.7 mm. This is the contact area with the specimen and this steel beam is also situated at the bottom of the setup where the specimen is placed upon.

In figure 2.8 next to the schematic overview the LVDT holding frame is shown. This frame is the holding unit for the two LVDT's that measure the horizontal displacement of the sample. This frame is attached on the sample with 4 clamps that are screwed with a 0.25 Nm torque force [NEN-EN12697-24:2018-Annex F]. This is done in a standard mould to ensure horizontal maximum radial placement. The mounting of this measuring frame on the specimen has a possible influence on the measured stiffness of the specimen. A more heavy, stiffer frame applied with an higher torque force to the sample could possible result in a stiffer response, but could also inflict damage to the sample. More quantified research on this topic is recommended. So for fatigue testing the same frame with the same applied torque force is used. Even between the different MTS and Zwick-Roell test setups.

The complete MTS test setup, placed in a climate chamber, is shown in figure 2.9. The sample is placed horizontally with a level and the standard prescribed force of 0.035 MPa [NEN-EN12697-24:2018-Annex F]. This ensures that the sample will not tip over or from the small loading strip where it is placed upon. This 0.035 MPa is the lower bound of the peak-peak force. It is mixture dependent as the strain has to have a certain minimum and maximum value and has to be established with a first test sample. The constant applied force to hold the sample in place is the reason that the frequency sweep, as well as the fatigue test can only be performed with the load controlled mode.



Figure 2.9: MTS CY-ITT test setup with specimen

The load control mode is the force applied through a sinus shaped signal. Due the requirement that the sample has to stay in compression, the load signal is shifted in a continuous compression state called a haversine signal. This results that the horizontal measured displacement is always in a tensile state of extension. In comparison, the 4PB beam is placed in a tensile and compression state during a single load repetition. A second result of this continuous compression state is the permanent vertical and horizontal deformation occurring to the sample. The vertical displacement is not measured in the standard test setup, but is clearly visible at the end of a fatigue test. The 4PB again is kept constant with the set neutral displacement at the start in combination with the displacement controlled feedback loop does not encounter any significant permanent deformations to the sample. An example from this permanent deformation during testing is given in the upper part of figure 2.10

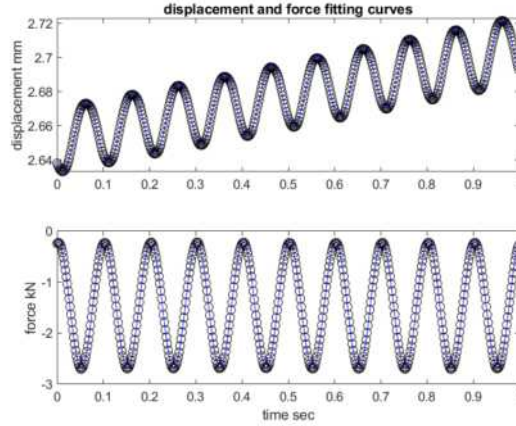


Figure 2.10: Captured CY-ITT displacement and force signals

Figure 2.10 gives the horizontal displacement and force signals of a CY-ITT test performed at 10 Hz. 10 captured load repetitions during a 1 second measurement interval are visible with the blue fitted haversine equation applied through the raw captured data points. This fitting equation is described in equation 2.4 with $u(i)$ being the fitting constants to the raw data.

$$U_t = u(1) \cdot \sin(2\pi ft + u(2)) + u(3)t + u(4) \quad (2.4)$$

where: U_t = displacement function
 f = frequency [Hz]
 t = time [s]
 $u(1)$ = displacement amplitude [mm]
 $u(2)$ = phase angle [rad]
 $u(3)$ = slope of vertical displacement [mm]
 $u(4)$ = shift neutral line [mm]

The CY-ITT is standard performed on 20 °C at 10 Hz with three applied load levels [NEN-EN12697-24:2018-Annex F] to create a fatigue line similar with equation 2.1 used for the 4PB. Instead of the aimed ε at $N \cdot 10^6$ the CY-ITT is set at the 10^5 number of load repetitions [NEN-EN 12697-24-Annex F]. This is the result of the lower test frequency and the otherwise extremely long test time. It also has to be considered that at a lower frequency the sample acts less stiff, so to perform a longer fatigue test the applied force has to be lowered. This will result in a lower measured displacement response from the LVDT's. This displacement response at low applied forces can be checked during testing with an oscillator or by means of an analytical script that uses the raw data to study the measured force and displacement signals as given in figure 2.10.

However equation 2.1 is based on the constant strain relation of a 4PB test, so for the CY-ITT the strain measured at the 100th load cycle is used for equation 2.1. Furthermore not the strain amplitude is taken for this equation, but the peak to peak strain value. This peak to peak strain value is the maximum found strain in the sample through calculations by [Hondros, 1959].

2.2.2.2 Calculations

Assuming that the specimen is homogeneous, isotropic and behaves linear elastic, the solutions of the horizontal stress, vertical stress and horizontal strain along the vertical diameter are derived by Hondros. [Hondros, 1959]

$$\sigma_x(y) = \frac{2F}{\pi ad} \left[\left(\frac{1 - \frac{y^2}{R^2} \sin 2\theta}{1 - 2\frac{y^2}{R^2} \cos 2\theta + \frac{y^4}{R^4}} \right) - \arctan \left(\frac{1 + \frac{y^2}{R^2} \tan \theta}{1 - \frac{y^2}{R^2} \tan \theta} \right) \right] \quad (2.5)$$

$$\sigma_y(y) = -\frac{2F}{\pi ad} \left[\left(\frac{1 - \frac{y^2}{R^2} \sin 2\theta}{1 - 2\frac{y^2}{R^2} \cos 2\theta + \frac{y^4}{R^4}} \right) + \arctan \left(\frac{1 + \frac{y^2}{R^2} \tan \theta}{1 - \frac{y^2}{R^2} \tan \theta} \right) \right] \quad (2.6)$$

$$\varepsilon_x(y) = \frac{1}{E} [\sigma_x(y) - \nu \sigma_y(y)] \quad (2.7)$$

where: F = applied load [N]
 a = loading strip width [mm]
 d = thickness of specimen [mm]
 R = specimen radius [mm]
 θ = half the top angle between loading strip and specimen centre [°]
 y = distance to the centre of the specimen [mm]
 E = Young's modulus [MPa]
 ν = Poisson's ratio

Equation 2.6 and equation 2.7 give the analytical stress distribution along the vertical axis of the sample. Li researched the difference between these equations and a Finite Element Model (FEM) ABAQUS, based on the same assumptions made by Hondros [Li, 2013]. In figures 2.11 and 2.12 the result of both Hondros and the FEM calculations by Li are shown. The vertical and horizontal stresses in figure 2.11 are very close. The maximum horizontal strain occurs at the locations of ± 36 mm from the centre of the specimen in both methods. The values calculated by the FEM model are a little smaller than the results from equation 2.7. Furthermore Li states that the height of a sample has almost no influence on the specimens fatigue life. The reason is because of the almost uniform stress and strain field between the ± 36 mm of the centre [Li, 2013].

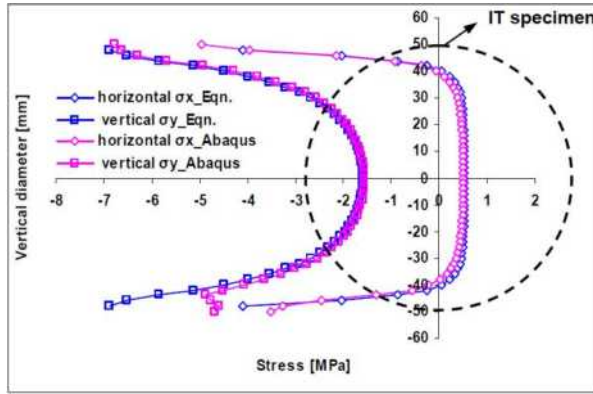


Figure 2.11: Stress distribution of a 100 mm ITT sample [Li, 2013]

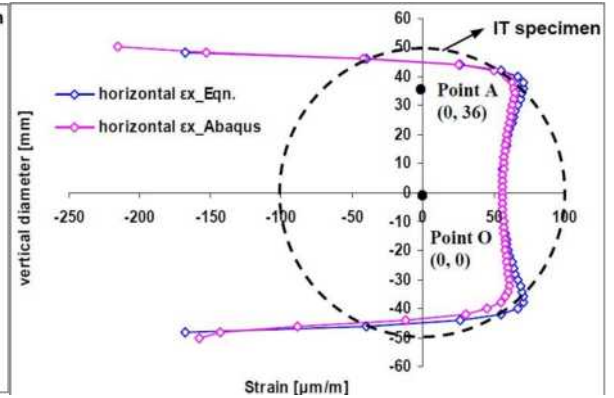


Figure 2.12: Strain distribution of a 100 mm ITT sample [Li, 2013]

With the work of Hondros formulas, it is stated in the NEN-EN 12697-24 that the highest horizontal strain is found in the centre of the specimen. So in $x,y=0,0$ in figure 2.12. We take this position and derive the equations 2.8 and 2.9. These are the same equations as found in NEN-EN 12697-24 Annex F.

$$\sigma_x = \frac{2F_a}{\pi h \Omega} \quad (2.8)$$

where: σ_a = horizontal tensile stress amplitude [MPa]
 F_a = amplitude of the measured vertical force [N]
 Ω = sample diameter [mm]
 h = sample height [mm]

$$\varepsilon_a = \frac{2U_a}{\Omega} * \frac{1 + 3\nu}{4 + \pi\nu - \pi} * 10^6 \quad (2.9)$$

where: ε_a = horizontal tensile strain amplitude [$\frac{\mu m}{m}$]
 U_a = amplitude of the measured horizontal displacement [mm]

From equation 2.9 we could find the maximum strain at the center of the sample, which is $\Delta\varepsilon = 2 \cdot \varepsilon_a$. It has to be realised that the permanent deformation does not play a role in the calculation of the maximum strain at the cycle of loading on which it is calculated. This permanent deformation is no longer considered as a recoverable displacement during the continuous loading signal. So the linear increase of the deformation, as shown in the upper part of figure 2.10 is not in the equation of the strain amplitude. The strain amplitude is calculated namely on this linear increased slope, so any permanent deformation of the sample is not in this strain amplitude, but in the $u(2)$ parameter of equation 2.4. The influence of this is later discussed in Section 2.3.2, where the dissipated energy theory equation is used in combination with the CY-ITT equations.

2.2.2.3 Test equipment

The CY-ITT tests were performed on two different machines, the MTS-07 and the Zwick-Roell. Fatigue testing was performed with time restriction and limited availability, with preferences to perform the 4PB on the Zwick-Roell, the MTS-07 was therefore mostly used for the CY-ITT. To study measurement variations between setups and utilise the higher capture rate, the Zwick-Roell test setup was used thrice for both the CY-ITT and 4PB.

2.2.3. Overview differences

From the previous two subsections it becomes clear that there are number of distinct differences between both fatigue tests. In table 2.1 all differences are summed up. The two main differences are the mode of loading and the shape of the specimen. Resulting from those are the found stress-strain distribution differences. For the CY-ITT the maximum strain is twice the amplitude and is called peak to peak strain, for the 4PB the maximum strain is once the amplitude. The way the fatigue relation of log strain versus the log cycles till failure (N_{fat}) are reported is also different, the CY-ITT strain increases over testing so $N=100$ is taken, the 4PB is strain controlled, so constant. Due the frequency and testing time, the fatigue line result for CY-ITT is reported at 10^5 and the 4PB at 10^6 . The last mentioned difference is the compensation for the moving mass, as 4PB is a beam positive and negative from the neutral, it compensated for the dynamic forces introduced by mass inertia. The CY-ITT does not have such behaviour in principle by the mode of loading. It has however subjected to permanent deformation, which is none to trivial in 4PB.

Table 2.1: Overview fatigue test differences.

Description	CY-ITT	4PB
frequency [Hz]	10	30
mode of loading	force	displacement
controlling signal	haversine (continuous compression)	sinusoidal (tension-compression)
specimen shape	cylinder dxh 100x40 [mm]	beam lxhwx 450x50x50 [mm]
stress-strain distribution	bi-axial	linear
reported strain value	peak to peak	amplitude
reported strain at N_{fat}	$N=100$	constant
strain reported at N	10^5	10^6

If we look to the difference between the number of load cycles needed for the reported strain value we see a difference in time spent performing the test. The CY-ITT is, despite 10 Hz, a faster overall test to perform. Taking less than 3 hours to reach the minimum of one hundred thousand load repetitions. The 4PB performed at 30 Hz needs more than 9 hours to reach the minimum of 1 million load repetitions for the required reported strain level.

2.3. Energy methods

In this section the theory of dissipated energy is defined and explained. Starting with the definition and previous research conducted on this concept of energy dissipation in fatigue testing. Followed by the parts where the developed selected models are explained. These are the RDEC model from Shen & Carpenter [2007] and the principles of the VECD model of Kim [1996].

2.3.1. Introduction to dissipated energy

Dissipated Energy (DE) is defined as the damping energy or energy loss per load cycle in any repeated, cyclic or dynamic test [Carpenter and Ghuzlan, 2001]. Usually when an elastic material is loaded the energy is stored in the system, when the load is removed the material recovers all energy. The loading and unloading follows the same, often linear, path. This can be viewed in figure 2.13. Asphalt concrete under loading and unloading follows a different path in the unloading part, as shown in figure 2.13, creating a loop or an area inside. This is the amount of dissipated energy and is a characteristic of a viscous elastic material like asphalt concrete. The dissipated energy can be in the form of mechanical work, heat generation or damage [Rowe, 1993],[Rowe and Boulding, 2000].

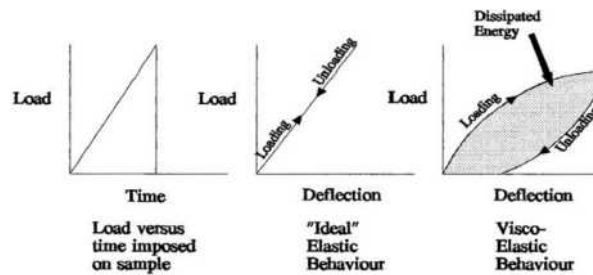


Figure 2.13: Linear elastic and visco-elastic loading behaviour[Li, 2013]

The area from this behaviour is called the hysteresis loop or 'Hysteresis'. The surface of this hysteresis loop is the dissipated energy of the system during that loading cycle. If a visco-elastic material is tested with a sinusoidal load around its neutral line, like in a 4PB test and the force and displacement are plotted against each other, a Hysteresis loop is obtained, as shown in figure 2.14 [Francken and Clauwaert, 1987]. The measured delay or lag between the applied load and measured displacement is the phase angle. This phase angle is variable that describes the viscoelastic behaviour of the material tested. A larger phase angle measured is a more viscoelastic material, resulting in a larger hysteresis loop.

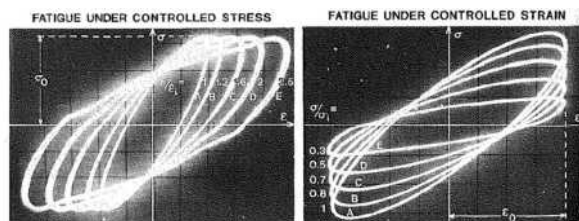


Figure 2.14: Hysteresis loop obtained from plotting load versus deflection[Francken and Clauwaert, 1987]

The resulting loop can be calculated through equation 2.10. Here the dissipated energy is calculated per cycle or load repetition i . Where the force is the calculated stress and the displacement is given by

the strain.

$$w_i = \pi \sigma_i \varepsilon_i \sin \phi_i \quad (2.10)$$

where: w_i = dissipated energy [J/m³]
 σ_i = stress amplitude [MPa]
 ε_i = strain amplitude [-]
 ϕ_i = phase angle [°]

One of the earliest publication that mentions dissipated energy in asphalt concrete fatigue is by van Dijk. Van Dijk researched many different aspects concerning dissipated energy of which the relationship for the cumulative dissipated energy versus the number of load repetitions till failure is one of them [Dijk van and Moreaud, 1975]. The relation is given in equation 2.11.

$$W = \pi \sum_{i=0}^{i=N} \sigma_i \varepsilon_i \sin \phi_i = AN^z \quad (2.11)$$

Van Dijk findings delivered a method that described different mixtures that weren't significantly affected by the mode of loading, temperature, frequency or resting periods [Dijk van and Visser, 1977]. Although relating a ratio between the initial cumulative dissipated energy and the fatigue cumulative energy plotted versus the stiffness showed a difference in the mode of loading.

Hopman and Pronk found a relation by using the Dissipated Energy Ratio (DER) to define at which load cycle the specimen fails in fatigue, called the N_{fat} , for the normal stiffness curves [Hopman et al., 1989]. Stating in a successive paper that the dissipated energy is also responsible for the fatigue damage to the specimen [Hopman and Pronk, 1991]. This method provided the basis, but also the disadvantage that not all dissipated energy is related to damage. Resulting in that the dissipated energy is either material dependent as shown by van Dijk or loading mode dependent by Hopman.

A theory formed by Carpenter and Jansen states that not all dissipated energy is responsible for material damage. For each load cycle the loss of energy due material mechanical work and other environmental influences, like heat dissipation, is almost unchanged. Only if there is a change in the dissipated energy, there is damage to the sample, indicating that large changes of dissipated energy indicates failure [Carpenter and Jansen, 1997].

The developed theory was later examined and refined by Carpenter in a series of publications with different co-authors; [Carpenter and Ghuzlan, 2001], [Carpenter, 2003] and [Shen and Carpenter, 2007]. Eventually Carpenter with Shen state that their modified method of the dissipated energy ratio is fundamental in that it is independent of loading level, loading mode and mixture type [Carpenter, 2003]. In this last specific paper they changed the name from the dissipation energy ratio to the *Ratio of Dissipation Energy Change* (RDEC). Carpenter specifies the theory by not only the change of the dissipated energy per load cycle compared to the previous load cycle, but also by also dividing it by the initial dissipated energy, making it a ratio based value, called the RDEC.

Through the statements that the RDEC could be a load and material independent parameter, Poeran used this theory to combine the 4PB and CY-ITT [Poeran et al., 2016]. Poeran adapted the method by replacing the standard 50% stiffness reduction failure criteria ($N_{fat50\%}$) used by Carpenter, by the method of finding the turning point of the RDEC curve. This research will start at the RDEC methodology explained by Carpenter. Before the RDEC method is discussed in detail in Section 2.3.3 we first look at the application of the dissipated energy concept applied on both the 4PB and CY-ITT.

2.3.2. Dissipated energy for 4PB & CY-ITT

Applying the dissipated energy method on a CY-ITT and 4PB samples we have to take into account the applied load configuration and stress strain distribution in the samples. As we look specifically to fatigue damage and fatigue damage caused by cracking in the tensile strain state, we assume that only the loaded tensile strain parts of the dissipated energy loop causes damage. The compression part of the loop is dissipating energy, only this amount of energy is assumed not to be related to the creation

of tensile fatigue cracking. It is furthermore often assumed that fatigue caused by compression takes a significant amount more energy than by tensile, creating often also other compression related damage to the sample like permanent and plastic deformation.

For the 4PB we assumed the sinusoidal variable linear strain configuration during testing. With the highest strains occurring at the top bottom edges of the beam. In a single load repetition each end is then loaded both in tension and compression. Resulting with the applied sinusoidal displacement controlled loading mode that equation 2.11 can be applied on the 4PB [Mello et al., 2009], [Grenfell, 2019]. As the equation utilize the calculated strain and stress amplitudes the resulting hysteresis loop is both positive and negative. Combined with the assumption that all compression dissipated energy is trivial to fatigue damage, we can state that the positive part of the Hysteresis loop is relevant for one side of the beam and the negative part for the other side of the beam during a single repetition. Resulting that the whole dissipated energy loop is relative relevant to the assumed part of fatigue damage.

For the CY-ITT it is not a straightforward case. The loading signal is haversine and the measured strains are all in a constant tensile state. Combined with the bi-axial stress-strain state and the visible permanent deformation after testing, makes the direct application of the dissipated energy on the CY-ITT at least to say controversial and debatable. This could lead to the discussion if the CY-ITT is even applicable to measure fatigue life as [Cocurullo et al., 2008],[Lytton et al., 2015],[Isailovi et al., 2016] discuss in their research. We take these considerations for a later research discussion and assume for the sake of this research that the permanent deformation influence on energy dissipation on the center of the core is small.

The largest strain for fatigue is assumed to take place horizontal at the center of the core, see Section 2.2.2.2, combined with the calculated tensile stress and phase angle. Take note that the phase angle is taken direct orthogonal constant from vertical to horizontal. These form the input parameters for equation 2.11. However as the CY-ITT is in a constant tension state at the specimen center, the equation, which is based on the amplitude of a tensile-compression fatigue test, should be considered to be peak-peak. So the amplitudes should be multiplied by two. The dissipated energy equation is therefore multiplied with a total factor of four. This direct integration over the total area of the Hysteresis loop result however in still a loop area that is both positive and negative, see also figure 2.14. As the CY-ITT is in a constant tensile state, without a simultaneous opposite compressing part that is loaded in tensile stress-strain in the other half of the loading cycle, we can only take half of this area. So the final assumed CY-ITT dissipated energy equation is given as:

$$w_{CYITT-i} = DE_{CYITT_i} = 2 \cdot \pi \sigma_i \varepsilon_i \sin \phi_i \quad (2.12)$$

A final remark is placed with this formula to describe the amount of dissipated energy. As the amount of dissipated energy is only considered at the normative cut, 4PB two outer edges, CY-ITT center cut, we don't consider the direct sample dimensions and or strain distribution over the amount of dissipated energy, as the cut is set as the fatigue failure point. That is why not the 'Raw' or direct work relation of force and displacement amplitudes are used, but the portion of energy calculated by the strain and stress at that certain critical cut. As the raw work energy is the total energy delivered to the sample. At other critical points in the sample these energies could be relative used as example for permanent deformation and or other damage behaviour.

In this section the applicability of the dissipated energy theory was discussed and for the 4PB the equation 2.11 holds with minor assumptions. For the CY-ITT a lot of different assumptions and or conditions are made to hold the established equation for the CY-ITT. For this research we have simplified and or neglected the different aspects considering permanent deformation in combination with fatigue. In future research it is recommended to study these aspects to validate the use of the CY-ITT as a worthy fatigue test. In Section 4.1.4 we will however see that the influence of the established equations are nullified by the RDEC method.

2.3.3. RDEC method

As described the Ratio of Dissipated Energy Change or 'RDEC' is a method developed by Carpenter and other researchers in numerous papers through the last two decades [Carpenter, 2003],[Carpenter

et al., 2003] [Shen and Carpenter, 2007]. The method is used in the different researches regarding the predictions of fatigue life, endurance limits of asphalt concrete and the influence of healing on that fatigue life [Shen and Carpenter, 2007]. The established main equation is given by equation 2.13. The equation is often named by Plateau Value or *PV* instead of RDEC, but the correct general description for this method is RDEC. *PV* is only valid for the value found in phase 2 where the RDEC should give a steady 'Plateau Value'.

$$RDEC = \frac{DE_{n+1} - DE_n}{DE_n} \quad (2.13)$$

where: $RDEC$ = ratio of dissipated energy change [-]
 DE_n = dissipated energy at load repetition n [kPa]
 DE_{n+1} = dissipated energy at load repetition n+1 [kPa]

A remark can be placed with the units used in the equation for dissipated energy. As only the stress have a unit in the dissipated energy equation, the usage of [kPa] is, although correct, preferable to use the energy term per volume as used by van Dijk [1977]. In this thesis we will use this J/m^3 generic energy per volume term. Which is not directly related to specific volumes of a sample, but purely on the normative cut of the highest strain and coherent value in a sample. If we look at the RDEC equation with a none standard interval, so the interval between measurements point changes over time, we find equation 2.14 [Shen and Carpenter, 2007]. This equation adds the interval over the number of load cycles.

$$RDEC_n = \frac{DE_{n+1} - DE_n}{(N_{n+1} - N_n)DE_n} \quad (2.14)$$

where: DE_n = dissipated energy at load repetition n [J/m^3]
 N_n = load cycle at n [-]

The resulting RDEC is an equation that calculates the difference in dissipated energy between two loading cycles 'Change' and is normalised by dividing it by DE_n 'Ratio'. Setting the dissipated energy as a ratio, similar to the strain value and losing it's parametric character. Equation 2.14 can be visually represented between two measurement cycles in figure 2.15. In which the blue area is the change in dissipated energy between loading cycle i and j. So not the complete energy dissipation from a cycle is used, but only the change to the previous cycle. This change is the assumed amount of dissipated energy used for fatigue damage.

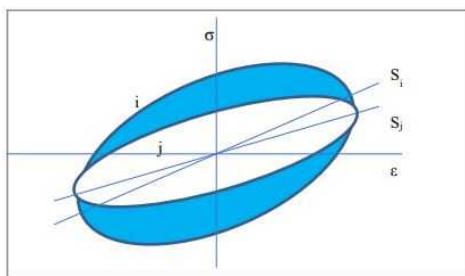


Figure 2.15: Dissipated energy change between loading cycles [Tolman et al., 2018]

In theory the resulting total graph from a fatigue test using equation 2.14 should result in figure 2.16. In which the curve represents a typical 'bathtub' shape with three distinctive phases. These phases and its corresponding phenomenons can be compared to the descriptions given in section 2.1 in figure 2.1 for the fatigue curve. It should be noted that this theoretical curve is dependent on the rate as on the increase or decrease of the dissipated energy itself over the number of load repetitions. Where an increase in DE would result in a smaller RDEC by equation 2.14. In phase 3 during the forming of macro cracks, great amounts of energy are dissipated in forming these cracks, resulting in a rapid increasing slope of the RDEC.

Figure 2.16 is furthermore related to a displacement controlled fatigue test. As later discussed in the Chapter 4 the modelled RDEC curve of a force controlled CY-ITT test is theoretical different in nature. As the initial drop of the RDEC curve is related to the large decrease of the dissipated energy at the start of a displacement controlled fatigue test, a behaviour not witnessed for a theoretical force controlled fatigue test.

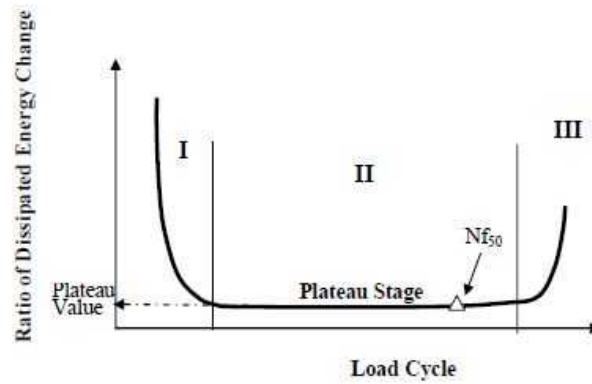


Figure 2.16: Theoretical PV curve [Carpenter, 2003]

Tolman states in contributing to this subject that the correct and full formulation of the RDEC is as given in equation 2.15 [Tolman et al., 2018]. Stating that the complete change of DE at point n is the change compared to the load repetition in front ' $n - 1$ ' as well after ' $n + 1$ ' of the cycle of interest. This method will average the found RDEC value by using in the calculation an extra load repetition, increasing the span over which the slope of the dissipated energy is calculated.

$$RDEC_n = \frac{DE_{n-1} - DE_{n+1}}{(N_{n-1} - N_{n+1})DE_n} \quad (2.15)$$

Figure 2.16 presents $N_{fat50\%}$ as a failure criteria, despite the fact that the method Carpenter presents is based on energy dissipation and not on stiffness. Furthermore take note that the failure criteria is not set at the end of phase two, but at the very first incline of the RDEC curve. Using this failure criteria and using an exponential fitting function on the dissipated energy, Carpenter finds the following relation between different mixtures. Tested both on strain and force controlled loading mode on 4PB beams in figure 2.17 [Carpenter, 2003]. Concluding that found PV line is independent of the mode of loading and that there is no visible difference between different mixtures.

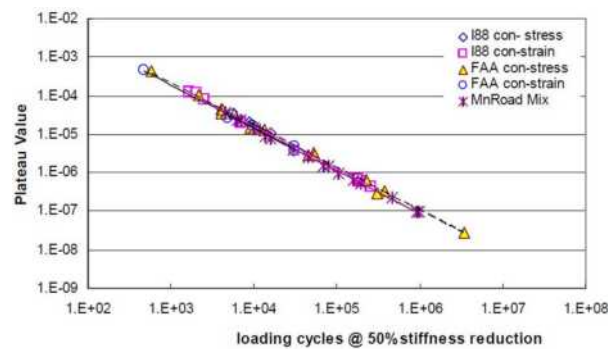


Figure 2.17: PV line for different mixtures [Shen and Carpenter, 2007]

Remarks placed by using this test setup is the fact that Carpenter only uses very high strain levels in the test setups till the reduction of 50% stiffness, as Americans often do. We know that a displacement controlled fatigue test actually never describe a single exponential curve. But consist of 2 curves that have a deflection point in the middle of what looks like a linear decreasing part in phase two, see also figure 2.2 in Section 2.1. This phase two only has the appearance to be linear in long low strain fatigue tests, but still exists of two exponential curves. Annex B gives a multitude of fatigue test results to

show this behaviour. If you would stop the fatigue test performed on high strain levels at a reduction of 50% stiffness, only then you would find a single exponential curve that can be fitted with the Carpenter PV equation. Equation 2.16 gives this fitted exponential PV equation to directly calculate the PV. In which the k is the slope of the exponential fitted function.

$$PV = \frac{1 - \left(1 + \frac{100}{N_{fat50\%}}\right)^k}{100} \quad (2.16)$$

The reason to use a fitting function instead of a measured value is that the found RDEC values are very small. They are in the range of 10^{-6} and subjected to a large scatter in the calculated values, see figure 2.18. Take note that the y-axis is on log scale. This scattering is the result from the very small change that is calculated between the cycles of two successive dissipated energies. With the overall behaviour of the dissipated energy curve is steady on the given scale, the underlying differences are very small, resulting in positive and negative calculated RDEC values. This was in the past one of the reasons not to look further into this method, but measuring accuracy and calculation methods have improved to the point that this can be amended.

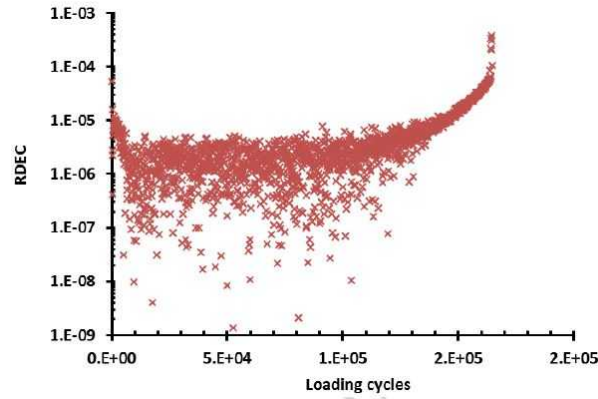


Figure 2.18: RDEC scatter of a DSR fatigue test [Airey et al., 2017]

Airey found the same problem as stated above with fitting a single exponential curve to a double exponential measured dissipated energy curve. In the paper, 'New simplified approach for obtaining a reliable plateau value in fatigue analysis of bituminous materials', Airey states this problem and found the following solution. Stating that the general RDEC equation 2.14 is the description of the slope of the dissipated energy normalised by DE_n [Airey et al., 2017]. Using this and the statement that the PV is constant in phase two Airey found that you could also calculate the PV over the length of phase two. This is shown in figure 2.19. Where w_o is the start of the dissipated energy curve and the range of phase two is set by N_f and a . Tolman mentioned with the previous equation 2.15 also the slope, but only directly around the cycle of interest. Airey takes the mentioned slope over a far greater span of load repetitions. However the term DE_n with the dissipated energy at cycle n is replaced with DE_0 .

Following from these statements we could conclude the RDEC equation and optimise it for this thesis as follows in equation 2.17. With $x(1)$ being the slope or the first derivative of the measured dissipated energy. The range over which $x(1)$ would be set is between the start of phase two, n_i and the failure criteria of n_{fat} . The normalisation factor of DE_n is the mean value of DE over the range of $n_i - n_{fat}$. The challenge now exist in establishing a valid failure criteria, which will be discussed in Section 2.4.

$$PV = x(1)_{n_i..n_{fat}} * \frac{1}{mean(DE_{n_i..n_{fat}})} \quad (2.17)$$

where: $x(1)$ = slope of the dissipated energy over phase two [(J/m³)/n]
 DE_n = mean dissipated energy over phase 2 [(J/m³)]

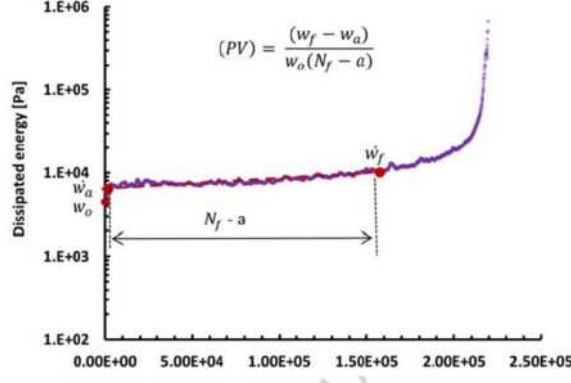


Figure 2.19: PV calculated over phase two [Airey et al., 2017]

2.3.4. VECD method

The Viscous Elastic Continuum Damage (VECD) model is a mechanistic model that calculates the progression of material damage and resulting stiffness reduction under monotonic as well as for cyclic loading. The model is based on three major principles. First, the elastic-viscoelastic correspondence principle that simplifies the viscoelastic problem into an elastic one. Second, the continuum damage mechanics based on the work potential theory for modeling the effects of micro cracking on global constitutive behaviour and the third, the time temperature superposition principle with growing damage to include the effects of frequency, time/rate and temperature [Zhang and Kim, 2012], [Kim and Lee, 1996].

2.3.4.1. Pseudo strain

The elastic-viscoelastic correspondence principle states that the viscoelastic problem can be solved by an elastic formulation where the physical strains are replaced by 'pseudo strains'. This was first proposed by Shapery [1984], in which the pseudo strain is defined as:

$$\varepsilon^R = \frac{1}{E^R} \int_0^t E(t-\tau) \frac{d\varepsilon}{d\tau} d\tau \quad (2.18)$$

where: ε^r = pseudo strain
 ε = physical strain
 τ = variable of integration (time)
 E^R = reference modulus, mostly set as 1
 $E(t)$ = relaxation modulus

This results that the magnitude of the pseudo strain is equal to the Linear ViscoElastic (LVE) stress. This means that for a cyclic test at low frequencies the following statement holds $\varepsilon^R = \varepsilon \cdot |E^*|$. In which the E^* is the measured stiffness at assumed linear strain levels. Equation 2.18 is based on the constitutive relationship for LVE materials and is generally given by the convolution integrals combined as shown in equations 2.19 & 2.21. With D as the creep modulus in the stress convolution integral.

$$\sigma = \int_0^t E(t-\tau) \frac{d\varepsilon}{d\tau} d\tau \quad (2.19)$$

$$\varepsilon = \int_0^t D(t-\tau) \frac{d\sigma}{d\tau} d\tau \quad (2.20)$$

The pseudostrain was initially developed for monotonic testing and did not consider the effects of temperature, age and healing. Park used the work potential theory [Schapery, 1984] and the continuum damage model together with Kim to computed a damage parameter S in the following formulation for the damage evolution law [Park et al., 1996]:

$$\frac{dS}{dt} = \left(-\frac{\partial W^R}{\partial S} \right)^\alpha \quad (2.21)$$

With:

$$W^R = f(\varepsilon^R, S) \quad (2.22)$$

where: S = damage parameter
 W = pseudostrain energy density
 α = damage rate growth

In this equation the pseudostrain energy density is formulated as equation 2.22, where the W^R is set as the area under the curve constructed by the monotonic test. The pseudostrain energy density function W^R is related to the pseudostrain and pseudostiffness from a monotonic load in a constant stress test. All pseudo related variables are taken dimensionless, as their physical meaning is lost. The damage rate growth a is related to the slope of the relaxation modulus from the frequency sweep. Different researchers have found different formulations for number α [Kutay and Lanotte, 2017], but most agree it is $\alpha = 1 + 1/m$, where m is the linear slope of the relaxation modulus for a strain controlled test and $\alpha = 1/m$ for a stress controlled test [Park et al., 1996]. We discuss the Damage parameter S in detail.

2.3.4.2. Damage parameter 'S'

The general VECD method describes the occurring damage to the sample with a damage parameter S . This behaviour is given in the damage characteristic curve, see figure 2.20, which describes the reduction in material integrity, or pseudo stiffness C and the growth of S . The damage parameter normalises the effect of the applied strain level to the effects of temperature and frequency. This should however not normalise the different results from different mixtures [Kutay and Lanotte, 2017].

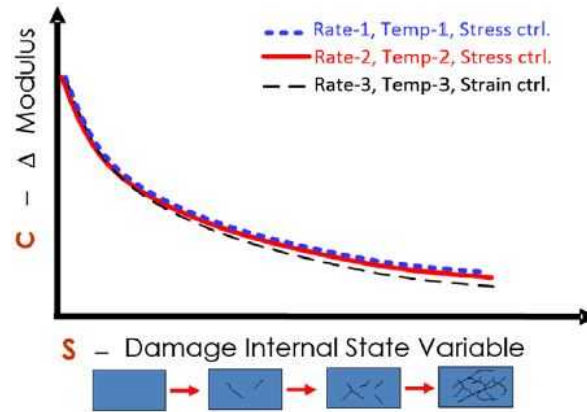


Figure 2.20: The concept of C vs S curve. [Kutay and Lanotte, 2017]

In figure 2.20 the pseudostiffness is no more than a ratio number of the remaining actual measured stiffness of the sample. So it ranges from 1 to zero. The variable S is the cumulative damage over time given in the general equation 2.23. So when the damage increases over time the pseudo stiffness will decrease in a natural logarithm course. The parameter k is the range over time measured and α the relation to the relaxation modulus.

$$S_k = \sum_{j=1}^k \left[\left(\frac{I}{2} (\varepsilon_j^R)^2 \cdot (C_{j-1} - C_j) \right)^{\frac{\alpha}{1+\alpha}} (t_j - t_{j-1})^{\frac{1}{1+\alpha}} \right] \quad (2.23)$$

The previous figure 2.20 is the result from equation 2.23. It should be noted that the C versus S curve is not directly universal applicable for every loading mode, monotonic or cyclic. Kim states that the method is interchangeable within these different test setups [Kim et al., 2002]. Although the summation over the time step interval in equation 2.23 should be modified for cyclic testing.

Further, Kutay states that for cyclic uni-axial testing the C-S curve will be different for a tension only mode compared to a tensile compression loading mode [Kutay and Lanotte, 2017]. Underwood

researched the exemptions and states that only the tensile parts of a cyclic load is considered in the calculated S [Underwood et al., 2010]. However the $C - S$ curve holds for all types of loading [Underwood et al., 2010]. Furthermore Underwood founded that if there are changes to the mixtures the founded $C - S$ curves are unique for different types of mixtures.

The relation of $C - S$ is unfortunately no further explored throughout this thesis due time restrictions for establishing a good and steady parameter S . The reason being that the to establish relation for the relaxation modulus $E(t)$ and the derived slope parameter α will be inaccurate. These parameters are dependent on the complete frequency sweep which will not be performed in full for this study. The relaxation modulus is established through the use of the resulting Prony Serie coefficients from this frequency sweep. These coefficients can be calculated from the same equation 2.24 as used to calculate the dynamic modulus E_{LVE}^* .

However in the case that the frequency sweep is performed at the same temperature and frequency ranges, a fitted Boltzmann equation would hold. Resulting in finding a viscoelastic dynamic modulus that is close to the averaged dynamic modulus found from the individual sample fatigue tests. The full frequency sweep and the resulting established relation with the damage parameter S is set as a recommendation for successive research. The assumed linear elastic dynamic modulus is however needed in establishing the pseudo strain in a cyclic fatigue test as showed in the latter equation 2.28.

$$|E^*|_{LVE} = \sqrt{\left[E_{\infty} + \sum_{m=1}^N \frac{E_m \omega_R^2 \rho_m^2}{\omega_R^2 \rho_m^2 + 1} \right]^2 + \left[\sum_{m=1}^N \frac{E_m \omega_R \rho_m}{\omega_R^2 \rho_m^2 + 1} \right]^2} \quad (2.24)$$

where: ω = angular frequency used in the frequency sweep experiment
 ω_R = reduced angular frequency, $\omega_R = \omega \cdot \alpha_T$
 α_T = time-temperature shift factor for the frequency sweep test temperature
 E_{∞}, E_m, ρ_m = Prony coefficient terms

From literature [Kim et al., 2002] introduced a variability ratio ' I '. It is set as a correction factor between the $|E^*|_{LVE}$ and the measured linear elastic response of each individual sample. This ensures that the viscoelastic properties obtained in the frequency sweep can be used effectively in the VECD analysis. Eliminating the specimen to specimen difference. The ratio is established through equation 2.37. Where the $|E^*|_{fingerprint}$ is the elastic modulus from the individual test at its set temperature and frequency. The $|E^*|_{LVE}$ is the calculated Elastic Modulus from the established master curve. This can be set at the same fatigue type test frequency or shifted. The shifting happens according the master curve, resulting in a change of parameter I over the frequency domain. Establishing a relation of the $C - S$ curve that is frequency independent during fatigue testing [Kim and Koh, 2012].

$$I = \frac{|E^*|_{fingerprint}}{|E^*|_{LVE}} \quad (2.25)$$

where: $|E^*|_{fingerprint}$ = Elastic Modulus at test temperature and frequency
 $|E^*|_{LVE}$ = Elastic Modulus at set temperature and frequency

Equation 2.37 with parameter I can secondly also be set as a limit. In where each sample in the measured linear elastic range is compared to the overall averaged found value of the master curve. If an individual sample deviates outside the set limits the sample should be disregarded. The normal applied limits are between 0.9 and 1.1.

In the previous part the VECD model on monotonic testing was introduced with the pseudo strain energy function and the omitting of the damage parameter. The linear elastic behaviour is introduced as the factor to find the pseudo strain through equation 2.18. With the introduction of the VECD method in cyclic fatigue testing, the model and its parameters are changed. These are discussed in the next section.

2.3.4.3 Simplification approach of VECD for cyclic loading

The VECD model requires the calculation of the pseudo strain and effective pseudo stiffness C at every time step to track the damage evolution of the sample through equation 2.18. For cyclic fatigue testing this is a cumbersome and time consuming process. Underwood developed a simplified VECD model that states that a single cycle does not propagate much damage [Underwood et al., 2010]. Evaluating the effective stiffness at the end of each loading cycle. Resulting in a pseudo strain based secant modulus C^* at the peak of the stress amplitude. Shown in figure 2.21 This can be further simplified if the permanent pseudo strain does not accumulate much over the number of load cycles. This is the case when successive hysteresis loops are set around the same central point zero. The secant modulus is then approximated by the cyclic magnitude based stiffness F .

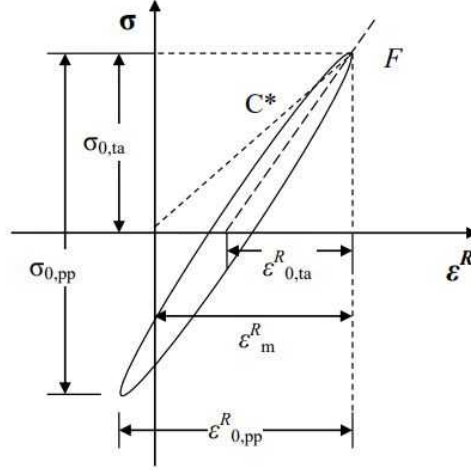


Figure 2.21: schematic view of stress, pseudo strain, pseudo based stiffness [Zhang and Kim, 2012]

Figure 2.21 results in the following simplified calculations for the pseudo secant modulus and cyclic magnitude stiffness:

$$C^* = \frac{\sigma_{0,ta}}{\varepsilon_m^R \cdot I} = \frac{\sigma_{0,ta}}{(\varepsilon_{0,ta}^R + \varepsilon_s^R) \cdot I} \quad (2.26)$$

$$F = \frac{\sigma_{0,ta}}{\varepsilon_{0,ta}^R \cdot I} = \frac{\sigma_{0,pp}}{\varepsilon_{0,pp}^R \cdot I} \quad (2.27)$$

where: ε_m^R = absolute pseudo strain at peak
 $\varepsilon_{0,ta}^R$ = pseudo strain tension amplitude
 $\varepsilon_{0,pp}^R$ = peak-peak pseudo strain amplitude
 ε_s^R = permanent pseudo strain
 I = variability factor
 C^* = instantaneous secant pseudo stiffness
 F = cyclic magnitude-based stiffness

If the cyclic magnitude stiffness F is used, which is possible with the assumption of the steady state solution from the convolution integral, the pseudo strain can be calculated as:

$$\varepsilon_{0,pp}^R = \varepsilon_{0,pp} \cdot |E^*|_{LVE} \quad (2.28)$$

Where $|E^*|_{LVE}$ is the previous established Elastic Modulus from the frequency sweep. This results in establishing a relation between the pseudo secant modulus and the cyclic magnitude stiffness:

$$C^* \approx F = \frac{\sigma_{0,pp}}{\varepsilon_{0,pp}^R \cdot I} = \frac{\sigma_{0,pp}}{|E^*|_{LVE} \cdot \varepsilon_{0,pp} \cdot I} \quad (2.29)$$

Instead of looking at the hysteresis area inside the loop which depends on the variation of the phase angle. The pseudo energy is evaluated in a cumulative sense per load cycle. During a load cycle the

maximum amount of stored pseudo strain energy is at the peak of that occurring pseudo strain value or $\varepsilon_{0,pp}^R$. See also figure 2.21. From that we can calculate the maximum stored pseudo energy as given in equation 2.31. This is the same pseudo energy density function applied in the previous section through equation 2.21 for calculating the damage parameter S during a monotonic test.

$$W^R = W_{total}^R - W_s^R = \frac{1}{2}(1 - C^*)(\varepsilon_p^R)^2 \quad (2.30)$$

where: W = pseudo strain energy density

$$(W_{max}^R)_i = \frac{1}{2}(\sigma_{o,ta})_i \cdot (\varepsilon_{0,ta}^R)_i \quad (2.31)$$

This can be linked through the magnitude-based cyclic pseudo stiffness 'F'

$$(\sigma_{o,ta})_i = F_i \cdot (\varepsilon_{0,ta}^R)_i \quad (2.32)$$

This can be rewritten to the following general equation for the total maximum stored pseudo energy at a load cycle i .

$$(W_{max}^R)_i = \frac{1}{2}F_i \cdot (\varepsilon_{0,ta}^R)_i^2 \quad (2.33)$$

The maximum amount of stored pseudo strain energy W_{max}^R is a measurement of how much energy the material currently can store. When damage accumulates during fatigue testing the material will lose stored energy for the same magnitude as the applied pseudo strain because of the reduction in the pseudostiffness. The now developed approach is the comparison of the current available maximum pseudo strain energy to the corresponding undamaged state at each cycle and assumes that the difference between them represents a cumulative loss of energy in total damage [Zhang and Kim, 2012]. This total dissipated pseudo strain energy function over the number of load repetitions i is called the total released pseudo strain energy W_c^R , is denoted as equation 2.34 and schematically represented in figure 2.22.

$$(W_c^R)_i = \frac{1}{2}(1 - F_i) \cdot (\varepsilon_{0,ta}^R)_i^2 \quad (2.34)$$

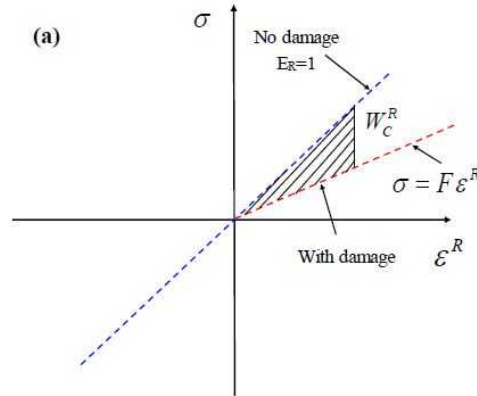


Figure 2.22: Schematic representation of total released pseudo strain energy in the stress pseudostrain space[Zhang and Kim, 2012]

2.3.4.4. Previous results

Work from Shen & Carpenter formed the basis for using the RDEC method on the fatigue relation of the CY-ITT and 4PB in this thesis, so is the published work from Sabouri the basis for using the VECD. In the paper: *Development of a Failure Criterion for Asphalt Mixtures Under Different Modes of Fatigue Loading*, Sabouri states that the generic formula of 2.35 describes a relation for finding a variable that is independent for the mode of loading used for fatigue testing. Sabouri describes the parameter G^R

as the rate of change of the averaged released pseudo strain energy (per cycle) throughout the entire history of the test [Sabouri and Kim, 2014].

$$G^R = \frac{\int_0^{N_f} W_c^R}{N_f^2} \quad (2.35)$$

Sabouri however doesn't show the comparison in how this calculated G^R compares to the overall rate of change of the released pseudo strain energy per single load cycle. So considerations arise on how the equation holds on the expected scatter produced by introducing a rate dependent variable.

Zhang states that as equation 2.34 represents the released pseudostrain energy in a cumulative sense, the derivative of the equation in respect to time or cycles would represent the rate of released pseudo strain energy, which is the released pseudo strain energy per cycle [Zhang and Kim, 2012]. This is a more accurate description of the parameter G^R and can be formulated as equation 2.36. The formulation of this rate dependent parameter G^R is very similar to the general RDEC formulation in section 3.3.3. However take note that G^R is non normalised.

$$G^R = \frac{W_{c,i+1}^R - W_{c,i}^R}{N_{n+1} - N_n} \quad (2.36)$$

In figure 2.23 the concluding results are shown from Sabouri's research. Where the addition 'CX' stands for the controlled displacement by the actuator of the machine fatigue test, CS is a controlled stress test and COS a strain on specimen controlled loading mode. The COS loading mode is comparable to how a 4PB test is conducted.

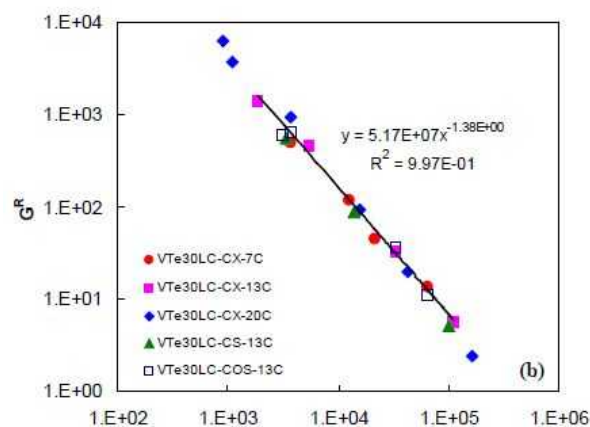


Figure 2.23: G^R [Sabouri and Kim, 2014]

The stated formulation is not tested on a wide variety of asphalt concrete mixtures. Sabouri only tested a single mixture with different levels of PR. In contrast to the works of Shen & Carpenter, the stated method of G^R is not material independent as Zhang showed in his work [Zhang and Kim, 2012]. In figure 2.24 a significant difference between the mixtures is shown. This difference can possibly be explained in the fact that Shen & Carpenter are using a ratio based calculation method and the G^R is a rate dependent variable.

The differences between a rate dependent variable and a ratio dependent variable is that the size of the numbers matters for a rate. The ratio based variable will be normalised, eliminating all size, dimensions and shape effects. For example an error in setting the right dimensions throughout your calculations will be eliminated by a ratio. The rate dependent variable will however show this error. From these perspectives we will look at previous research for applying the pseudo strain energy rate theory to the 4PB and CY-ITT.

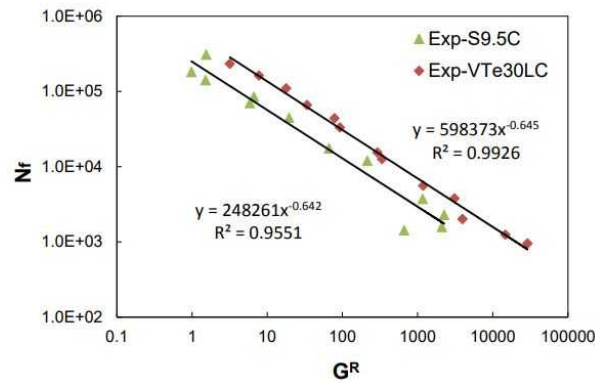


Figure 2.24: Rate of pseudo energy G^R for two different mixtures [Zhang and Kim, 2012]

4.3.2.5. VECD applied on 4PB

Applying the theory and the stated formulas directly from the uni-axial testing test up to the 4PB test is possible. In the considered scope of this thesis the damage parameter S is not used. Resulting that the adjustment of equation 2.23 for the applied tensile load time (t_j) to the specimen is not necessary. However with the previous discussion in Section 2.3.2 we state that tensile strain is causing the significant major amount of damage to the specimen. Therefore we only use the strain amplitude in the 4PB.

This last statement is verified by multiple researchers; [Underwood et al., 2010] for uni-axial testing, [Haddadi and Hosseini, 2015] and [Mello et al., 2010] for the 4PB testing. With a sinusoidal applied displacement controlled test, the specimen stays on a single neutral line. This is theoretical true for both for a uni-axial fatigue test as the 4PB test. Creating the possibility to apply the previous stated equation directly on the 4PB results.

The only concern is placed with a force controlled test that is not held constant over it's neutral line. Due the possibility of permanent deformation or creep during force controlled testing, a certain section, top or bottom, could be shifted over the neutral line. Resulting that the sinusoidal applied force creates a haversine measured strain signal. So that a part of the beam is in a constant strain state. Resulting that the simplification of using the strain amplitude directly for the pseudo strain is incorrect and the correct formulation needs to be derived through figure 2.21.

4.3.2.6. VECD applied on CY-ITT

The CY-ITT setup is with the force control loading mode acting in a constant positive strain state in the horizontal direction. The stress strain distribution derived with the correspondence principle for the uni-axial samples cannot be applied directly to the ITT sample. In multiple papers the VECD method is applied to the CY-ITT. Lee derived all the equations for the VECD method for the IDT in his paper: 'Application of the Viscoelastic Continuum Damage Mechanics to Asphalt Mixtures under Indirect Tensile Load' [Lee, 2015]. In this paper Lee describes the idea and formulations of applying the VECD method to the IDT test with the monotonic strength test.

Previous to that, Kim studied the possible connecting between monotonic and cyclic testing on the IDT in the paper: 'Development of a Predictive System for Estimating Fatigue Life of Asphalt Mixtures Using the Indirect Tensile Test' [Kim and Koh, 2012]. Even in 2002 Kim used the VECD on the IDT test for validation of field extracted cores in his publication: *Fatigue performance evaluation of wet-track asphalt mixtures using viscoelastic continuum damage approach* [Kim et al., 2002]. In that first publication the relation was established for the monotonic strength test which Lee later used with the specific focus on the cyclic variant of the ITT'

In this study the focus is laid on the previous works of Kim. Kim mentioned the formulations of the VECD for the cyclic IDT test [Kim and Koh, 2012] in the formulation of a single $C - S$ curve that can be established for monotonic and cyclic testing. Utilising the modified uni-axial setup for which it was

originally developed. The modification is needed for the correspondence principle getting the damage parameter S in the stress strain distribution of an IDT test. The damage parameter is however due time limitations and limited test results for the relaxation modulus not further explored, but should be considered in a future study.

For cyclic testing only the tensile loading part is considered to cause damage. Underwood presents that considering the cyclic stress strain hysteresis loops, we could find the pseudostiffness vector F [Underwood et al., 2010]. Zhang presents in figure 2.21 the implication of this method. Resulting that the pseudostiffness has to start at zero. With the CY-ITT there is permanent deformation occurring, however this results not in a deviation from the loop leftwards over the strain axis. This is because how the cyclic strain amplitude is measured, stored and used to establish the pseudo strain. The last is discussed in detail in chapter 4.

The relation for the $\varepsilon_{0,ta}^R$ in equation 2.33 is then established through the peak to peak strain values. For the stress relation to the pseudostiffness Kim recognises that the seating stress needs to be added to the damage relation of the test setup [Kim and Koh, 2012]. This stress is constantly added to the sample and is the shift for the found mean value of the force haversine signal. This is shown in figure 2.25. The seating stress is set at 0.034 MPa as prescribed by NEN-EN 12697-24.

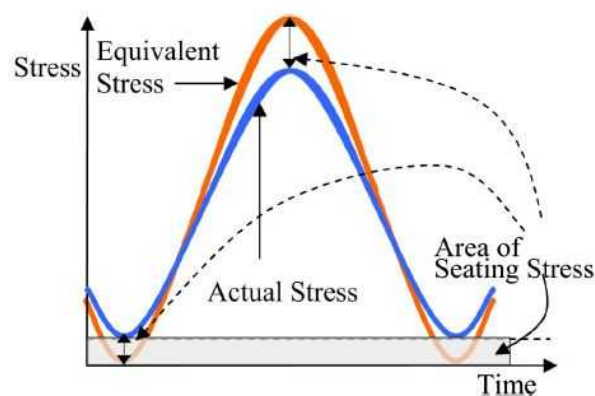


Figure 2.25: Description of equal stress [Kim and Koh, 2012]

The equal stress only influences the pseudostiffness C and with that the pseudostiffness vector F . This is however a very small number compared to the applied stress to the specimen. The influence is then only noticeable at the low applied stress amplitudes for the long fatigue test. Resulting in a shift upwards for the total released pseudo strain energy function of W_c^R , which would result in a higher G^R values for the longer fatigue tests. The exact results and differences between applying a seating stress to the VECD calculations is discussed in chapter 5.

With the general concept of the viscoelastic continuum damage model of Kim, assumptions about permanent deformation, combined with the successive papers by different authors, it is theoretical possible to utilize the VECD principles in the same relation to the number of load cycles as the RDEC method of Shen & Carpenter for both CY-ITT as 4PB. We now discuss in the next section the relation of these energy methods as well the traditional stiffness curve to different failure criteria.

2.4. Failure Criteria

Fatigue life and the definition of failure on that span over the number of load repetitions is a discussing at large in the scientific community. Not only do current fatigue criteria differ per specimen size, test setup and loading mode, but also per country set in their respected standardisation Norms. Still new methods and theoretical concepts about true fatigue failure are published. All with the goal to find the single failure criteria applicable to the whole field of asphalt fatigue testing. To limit the work, we will focus on establishing a single failure criteria that will hold for at least the two fatigue tests studied.

2.4.1. Conventional $N_{fat50\%}$

The standard well known failure expression applied is the $N_{fat50\%}$. This is defined as the load repetition at which the stiffness is decreased to 50% of the initial stiffness. The initial stiffness is set at load repetition at $N=100$ and is a set value by the NEN-EN 12697-24:2018. The reference, exact reason or experimental research for the choice of 50% reduction is unknown to the author. It can be a policy, but can possible be based on old works for finding the transition point. We will discuss that in moment.

The set criteria of $N_{fat50\%}$ gives for the standard displacement controlled loading mode reasonable results in finding the transition point. The transition point is defined as the point where the stage of forming micro-cracks ends and macro-cracking starts to happen, resulting in a fast decreasing stiffness curve. The transition point is then the shift from phase two to phase 3. It can be viewed in the previous figure 2.1 in Section 2.1. However, with developing new mixtures with higher percentages and types of modified bitumen in combinations with high percentages of PR, results became unsatisfactory on defining the transition point through $N_{fat50\%}$. Resulting in a N_{fat} with a significant number of load repetitions left before the set transition point is reached. This was also one of the reasons for the study started by Poeran on the RDEC method [Poeran et al., 2016].

Second the criteria of $N_{fat50\%}$ is a difficult to apply criteria for the CY-ITT. Samples can possible fail in macro cracking before the stiffness has reduced to 50%. The NEN-EN 12697-24:2018 describes the *Energy Ratio* as the method to find the transition point on where macro cracking starts to form. In figure 2.26 sample 55020 and 55021 from mixture 19018 are given. In figure 2.27 the displacement amplitude for sample 55021 is given as an example with both the 50% reduction of stiffness and the Energy Ratio failure criteria, N_{fatER} . In the next part the background of this Energy Ratio is given.

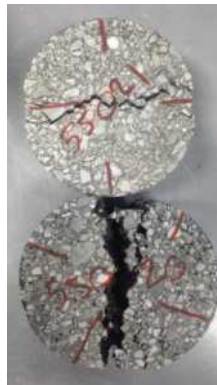


Figure 2.26: CY-ITT sample 55021 & 22020 after testing

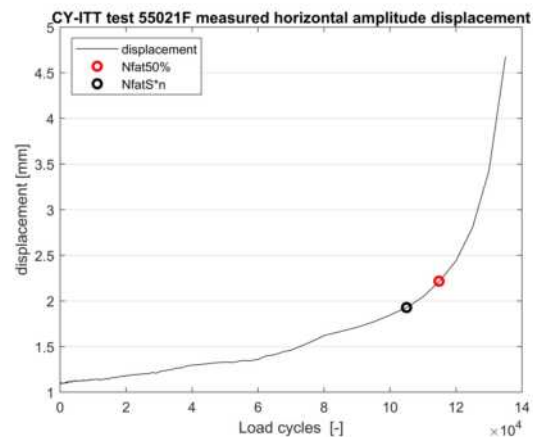


Figure 2.27: Displacement amplitude sample 55022

2.4.2. Dissipated Energy Ratio

From the dissipated energy theory, as described in section 2.3, [Hopman et al.] developed the 'Energy Ratio' for the controlled strain test to define the number of load cycles till failure, called N_1 [Hopman et al., 1989]. This point is set to be the transition point between micro cracking and macro cracking and is given in figure 2.28

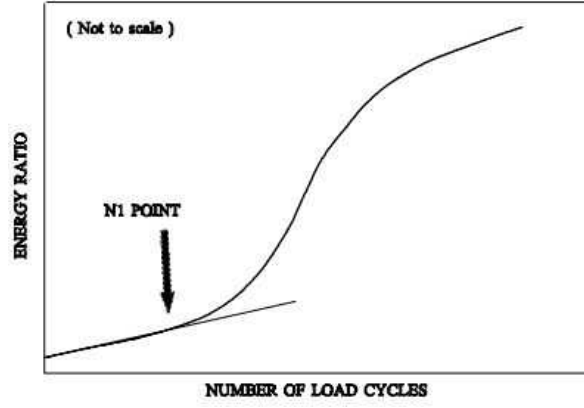


Figure 2.28: Energy Ratio [Hopman et al., 1989]

The Energy Ratio is defined as:

$$ER = \frac{n_i \cdot w_0}{w_i} \quad (2.37)$$

where: ER = Energy Ratio [-]
 n = load repetition [-]
 w_0 = dissipated energy at $n=100$ [J/m^3]
 w_i = dissipated energy at load repetition [J/m^3]

Rowe describes the Energy Ratio and states that it can be written as follows [Rowe, 1993]:

$$ER = \frac{n(\pi\sigma_0\varepsilon_0\sin\phi_0)}{(\pi\sigma_i\varepsilon_i\sin\phi_i)} \quad (2.38)$$

Equation 2.38 shows the used dissipated energy formulas as used in section 2.3. Rowe further simplifies the formula, using the general formula of $E = \sigma\varepsilon$ and states that the resulting E_0 is a constant and can be left out. This results to:

$$ER = \frac{n\sin\phi_0}{E_n\sin\phi_i} \quad (2.39)$$

The next simplification is made by stating that the phase angle is more or less constant during a whole fatigue test, secondly that the change between individual measurement intervals does not change much during the fatigue test [Rowe, 1993]. Resulting that $\phi_i = \phi_0$. This statement is important that now equation 2.39 is made independent of the phase angle, reducing it to only the stiffness and the associated load repetition. This results in equation 2.40 for a controlled strain test and the inverse, as in correspondence with equation 2.39, for the controlled stress test in equation 2.41.

$$ER \approx n/E_n \quad \text{strain controlled} \quad (2.40)$$

$$ER = n \cdot E \quad \text{stress controlled} \quad (2.41)$$

The latter equation is the prescribed method to find N_{fat} in the CY-ITT by NEN-EN 12697-24:2018. It is described as the stiffness multiplied by the load repetition at their respected load cycli. Resulting in a curve where the found maximum is the load repetition at failure, called N_{fat} . The established relation in both equations no longer holds the energy method as a defined relation, but uses the strain and stress through the stiffness. The result is now a Stiffness multiplied with the respected load cycli n . The latter part can be defined as a load repetition or in short repetition. To define the differences between both methods in establishing a repetition dependent failure criteria. We call the original Energy Ratio by equation 2.37 the Energy Ratio ER throughout this thesis and the failure criteria defined by only the stiffness, the Stiffness Repetition SN . The Stiffness Repetition is stated by equation 2.42. It is defined as $S \cdot n$, that is why the more distinctive syntax of SN is used instead of SR , which would stand for Stiffness Repetition.

$$SN = S_n \cdot n \quad (2.42)$$

Equation 2.40 as stated by Rowe is actually no longer a ratio dependent method. As it is no longer divided by it's initial stiffness. Emphasis should be placed on the multiplication by the corresponding load repetition. Resulting in a method that is now defined by it's load repetition instead of the ratio. That is why the resulting end equation 2.42 is defined as the Stiffness Repetition method.

Results from Rowe are presented in figure 2.29. Where in (a) the standard 4PB fatigue test is shown with E as the stiffness modulus. In (b) the ER is given as R with the linear plotted line to find N_1 by equation 2.40. As comparison N_f is given which represents the 50% stiffness reduction. In (d) and (e) the results are shown for a stress controlled fatigue test. From (e) we can see that with stating equation 2.41 that the maximum of function $ER = N_1$ the N_{fat} is easily determined. From figure 2.29 (d) and (e) it is also clear that the $N_{fat50\%}$ makes a poor failure criteria for force controlled 4PB fatigue testing.

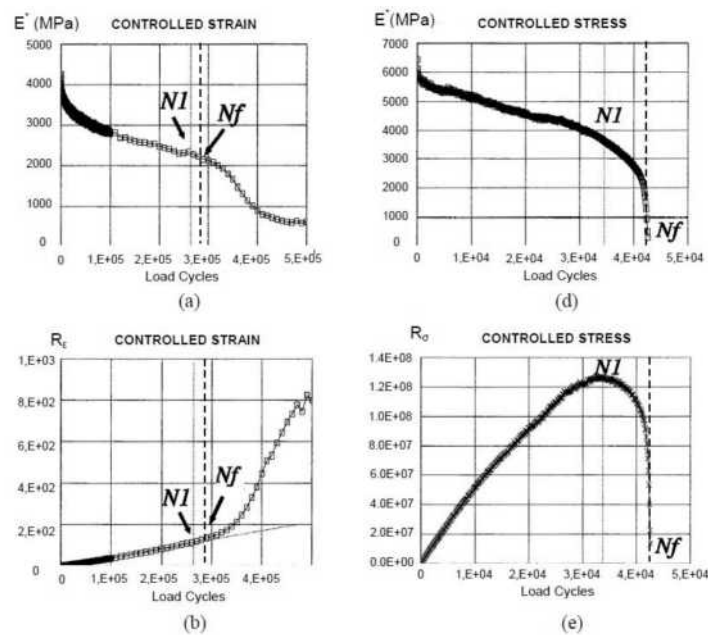


Figure 2.29: Controlled strain vs controlled stress [Rowe, 1993]

Rowe states in a successive paper that the found equation 2.42 can be applied to the strain controlled fatigue test [Rowe and Boulding, 2000]. However theoretical not a correct derivation, it still experimentally holds. Pronk explains in his unpublished paper that this relation can be used for determining the correct N_{fat} [Pronk, 2019] during strain controlled fatigue testing. Pronk adapts the formulation of equation 2.41 with a correction factor k , resulting in $SN = S \cdot n^k$. The correction factor k can correct the influence of the number of load repetitions in a small declining stiffness curve. The correction factor k set at 0.5 will than result in a sharper distinct SN curve, finding the correct N_{fat} [Pronk, 2019]. Pronk finds this behaviour especially in heavy modified PMB mixtures. If the fatigue curve follows the standard sudden drop at failure k can be set at 1.

The established fatigue criteria through the stiffness repetition relation is also mentioned before by recent researchers of the TU Delft. Dijkhuis applied it successfully in her thesis about DSR fatigue testing [Dijkhuis, 2016]. Li used the same derivations for his research the works about the different fatigue type testing on mixture level [Li, 2013]. Li used the work of [Hopman and Pronk, 1991] in which the equation 2.37 is transformed to equation 2.43. Here the cumulative dissipated energy till cycle n is divided by the dissipated energy at cycle n .

$$DER = \frac{\sum_{n=1}^{n=N} w_i}{w_n} \quad (2.43)$$

The drawback of this method is that the found relation has to be compared to a linear line to find N_1 as the failure criteria. This is the same method compared to equation 2.37 and showed in figure 2.28.

Returning to the same problem in finding the N_{fat} in a strain controlled fatigue test. In this thesis we will continue the work of Pronk in validating the developed Stiffness Repetition equation 2.42 and comparing that to the original method of the Energy Ratio through equation 2.37.

Returning from the mentioned point about previous research in establishing $N_{fat50\%}$ as a failure criteria. There is work available from Abojaradeh for finding a comparison between the stress and strain controlled loading modes for the 4PB test [Abojaradeh and Witczak, 2007]. Abojaradeh studied the influence of on which load cycle the initial stiffness should be set. Resulting in different results for the stiffness and Stiffness Ratio. Abojaradeh used the Stiffness Degradation Ratio (SDR) in which the initial stiffness is taken into account. Transforming equation 2.42 to a ratio equation 2.44

$$SDR = \frac{S_n \cdot n}{S_{ini}} \quad (2.44)$$

From this equation and plotted SDR value versus the N_{fat} Abojaradeh found a relation that shows a correlating line if the initial stiffness is set at load repetition 50. This line is a single line for all the different mixtures, making the method load and material independent. From that correlating line Abojaradeh finds a solution in the fitted line that corresponds to $0.48(N_f)^{0.998}$. Stating, compared to equation 2.44, that the slope value of 0.48 is the percentage that form the degradation ratio. In other words: Using 50% stiffness reduction as a failure criteria holds for both strain as load controlled loading modes if initial load repetition is set at $n=50$. In the standard applied test protocol all fatigue type test start at $n=100$. Limiting the possibilities to validate and research the set N_{ini} through this thesis. However the influence of the phase angle in equation 2.39 and as an individual failure criteria can be researched.

2.4.3. Phase angle

The phase angle is in different papers, [Sabouri and Kim, 2014],[Airey et al., 2017] and [Zhang and Kim, 2012] mentioned as a method to find the failure of the sample. During fatigue testing the measured phase angle changes gradually, which can be related to micro damage to the sample. The moment at which the phase angle rapidly increases or decreases is then set as the macro failure of the sample. Resulting in finding the N_{fat} . This sudden phase angle drop often relates to another failure criteria that is based on the measured displacement and or force.

The phase angle is related through the delay between the measured values of the force and displacement signals. A sudden drop or increase would mean that the measured displacement or force suddenly is shifted over its time domain. The behaviour of shifting and changing of the phase angle is of interested, because it is introduced as a third parameter in the dissipated energy approach in fatigue testing. With this introduction as a variable in the calculated dissipated energy, it can also acts as a failure indicator. Especially with the mentioned earlier research by Poeran about the PMB modified bitumen showing a bad correlation between the RDEC and the set failure criteria of 50% reduction of stiffness [Poeran et al., 2016].

With the utilising of the hysteresis loop on the raw data this behaviour of the phase angle can be studied. With the precooked calculated values by the testing equipment these insight are neglected in finding out where the calculated results come from and how they are influenced by their measurement accuracy's. That is why in chapter 4 with the introduction of the dissipated energy results, this behaviour and failure criteria are discussed detail.

2.4.4. Summary

From this section we can summarize that there are three different methods of establishing a failure criteria. The first is by a fixed percentage value which has proven itself in the past. The 50% reduction of initial stiffness is such a fixed criteria. The second is using a 'Repetition' based method. Multiplying the set value by its corresponding load repetition and finding the maximum value on this curve. Well known examples are the original Energy Ratio and the simplified stiffness variant now renamed Stiffness Repetition. Noting that for almost every fatigue related variable this curve can be constructed in a

similar way. The third method is by a sudden phase angle change. Using a material dependent measured parameter that seems to be related to the failure of the specimen.

2.5. Summary

After the general introduction to fatigue life of asphalt concrete three main topics were discussed and two sub-questions were answered. The first main topic was the two fatigue tests and their differences utilised for this thesis. The second was the literature study with the discussion of the RDEC and VECD energy methods. the third topic was the different ways the fatigue criteria could be determined.

- The two fatigue test, CY-ITT and 4PB, differ from each other on almost every front. Not only is the mode of loading and the stress-strain distribution different, the established fatigue life relation are based on different parameters. It should foremost be considered that the 4PB has a constant cyclic bending between clamps and due the displacement controlled loading mode almost no permanent deformation, where the CY-ITT is visible deformed after the constant compression fatigue test. This second damage phenomena can possible influence the fatigue life of the CY-ITT and it is recommended to research this in a future topic.
- The dissipated energy theory, where the hysteresis loop is calculated through the tensile compression dissipated energy equation, is applicable to the 4PB. Under the assumed dissipated energy foremost contributing to the tensile fatigue damage at the center of a CY-ITT fatigue test, we set this equation by a factor two, disregarding the none existing compression counterpart and using the peak-peak values caused by the constant tensile state of the specimen center.
- The RDEC method of Shen & Carpenter is a ratio method describing the normalised slope of the dissipated energy. The method is notorious for the amount of scatter it produces, but with the method employed by G. Airey an accurate value can be calculated for the Plateau Value at failure. The dissipated energy slopes $x(1)$ produced for the CY-ITT are positive and negative for the 4PB.
- The VECD method developed by Kim suggest the method of applying a pseudo strain, creating a linearized strain relation that has removed its viscous component. Through calculations by pseudo stiffness over the number of load repetitions the total released pseudo strain energy W_c^R equation is created. The resulting rate G^R of this released pseudo energy is then a similar formulation as the $x(1)$ parameter of the RDEC method.
- The failure criteria can be set by three different manners; constant, repetition or a measured distinct peak. From the literature study the Energy Ratio is the best substantiated method for both the CY-ITT as for 4PB. Reduced by using only the stiffness, it is called the Stiffness Ratio SR . Further simplified it is called the Stiffness Repetition method which is used greatly throughout this thesis in combination with the original Energy Ratio.

3

Classical fatigue results

In this chapter the classical fatigue results of the different mixture fatigue tests are presented. In total 12 different mixtures were available for analysis. The tests are performed for the standard CE-markings and used in collaboration for this research. Mixture composition is a company's asset, so the overall properties are given but the detailed mixture design is left out. In the first section an overview is given of the used mixtures. In section 3.2 the frequency sweep and phase angles results are given for both the CY-ITT and 4PB. In section 3.3 the fatigue results are given and a single failure criteria is established for both fatigue test. It will also discuss the main differences found in the analyzed results of the two fatigue tests and conclude. These traditional results provide the background why the energy methods are researched in the next chapter.

3.1. Mixtures

To study the behaviour of a new to establish relationship for asphalt concrete mixtures, a wide variety of market conform mixtures should be validated to confirm the theory. This is done in this thesis by using 12 different mixtures that have a practical application in real road construction projects. This also make it possible in the future to validate the to be developed energy relation with the drilled cores from a road construction project. To validate the stated theory in the previous chapter a wide variety of mixtures is chosen that varies in: max size aggregate, bitumen percentage or grade and type of asphalt, base or surface layers and the percentage of recycled asphalt, in Dutch called *PR* 'Partial Recycling', called *RA* or 'Reclaimed Asphalt' in the European Union or *RAP* 'Reclaimed Asphalt Pavement' in the United States). Two extra different types of bitumen are studied: Foam bitumen and PMB's, both now widely used in Dutch road practise.

3.1.1. Overview

The different mixtures in table 3.1 will be designated through its project number in this thesis. Different mixtures do not vary a lot at first sight, but the composition can depend a lot for the different purposes for which they are developed. As an example, there is a mixture that is specially designed to give a great noise reduction on city streets at 50 km/h. This mixture is later adapted and improved for provincial roads to sustain more heavier loaded vehicles. From this a new validation project started for that asphalt mixture. Resulting in a new fatigue test and a new project number.

In table 3.1 the mixture overview is given. In the second column the indication 'AC' stands for asphalt concrete with attached a number as the set largest aggregate size passed. In the same column the specified application layer is given. This is indicated as a surface layer or as a base layer. A top layer is a special surface layer that is only used in special cases. The third column indicates the Penetration grade of bitumen used in the mixture. The last column indicates the percentage of Partial Recycled, 'PR' asphalt.

Table 3.1: Mixture overview.

Projectnumber	Mixture	Pen grade	PR [%]
18501	AC 11 Surf	50/70	30
18502	AC 11 Surf	40/60	0
18523	AC 16 Base	30/45 Foam	50
18531	AC 8 Surf	70/100 Red	0
18590	AC 16 Surf	40/60	0
18593	AC 8 Surf	40/60	0
18596	AC 11 Surf	30/45 Foam	40
18607	AC 11 Surf	PMB	0
18619	AC 16 Base	40/60	85
19018	AC 11 Top	40/60	0
19020	AC 11 Top	-	55
19051	AC 8 Surf	-	50

The principles of the energy methods should be tested on a wide range. A certain number of variations on the test setup are made to achieve this goal. As an addition to the standardised works performed at the laboratory of KWS, there are extra tests done at the Faculty of Civil Engineering at the TU Delft. These extra works are done on mixtures or samples from KWS. To resemble a same mixture, the project number is chosen with the addition of 'TU'. For the few exemptions named below, all tests are performed at 20°C. Including all the frequency sweeps and fatigue tests, both on CY-ITT and 4PB. The standard test frequency for the CY-ITT fatigue test is 10 Hz and all 4PB are performed at 30 Hz.

- Project 18523, From a road construction project with the same mixture a number of samples are cored. These are compared with the samples prepared in the laboratory.
- Project 18590, the complete CY-ITT is executed at 30Hz.
- Project 18590TU, 150x100 mm gyrator compacted and subsequently cored samples are prepared at the TU Delft from this mixture to be tested on uni-axial fatigue. Tests were performed at 10 Hz on a displacement controlled loading mode.
- Project 18619TU, the same samples as 18619 were reused to be tested on force controlled loading mode. The beams have been laid to rest for 3 months and turned 90° to minimize the influence from the previous fatigue test.
- Project 18619D, same mixture with 0% PR is conducted only on 4PB with three different levels of compaction. Namely at 97,100 and 103% mass density.
- Project 18607, the CY-ITT is performed at 10 °C and the 4PB at the standard 20°C. This because the low stiffness of the PMB modified mixture.
- Project 19018, the CY-ITT of this project was partly done on 30 Hz and 10 Hz loading frequency. This project was actually performed on CY-ITT before the CY-ITT of 18590. This to study the difference between the 10 Hz and 30 Hz on the same mixture.

3.1.2. Sample preparation

Samples were prepared in the central laboratory of KWS. Aggregate is collected from the yard and heated to a maximum temperature of 110 °C till a constant mass is reached. After the drying process the aggregate is stored and when needed weighted in per batch. After weighing the aggregate is heated to the desired mixing temperate, which is different for each type of mixture. Bitumen is heated in closed cans separately to the same temperature. Each batch is made to prepare a single asphalt concrete slab. A slab is around 500x500 mm with an height of 100mm. Mixing the batch is done according NEN-EN 12697-35;2016 in a Hobart N50 shear mixer for 180 seconds. After mixing the plate is compacted with a segment-compactator to the desired density of the mixture. The exact procedure for the preparation of the prismatic beams is described in NEN-EN 12697-33;2007. A single compacted slab weighs around 60 kg and a total of 4 to 5 slabs are needed for a full mixture 4PB and CY-ITT fatigue test.

After compaction the asphalt concrete slabs are stored in a climate chamber at a temperature of 5-15°C as prescribed in NEN-EN 13108-20;16. Sawing the slabs to the prismatic beams or coring to cylindrical specimen to the size needed for testing is done within 7 days. After sawing or coring the samples, they are laid to rest for at least two weeks before commencing the fatigue test to a maximum of 8 weeks. The number of samples tested per mixture are given in table 3.2. In total a number of 153 CY-ITT cylindrical and 246 prismatic beams were tested at the central laboratory of KWS during this research.

Table 3.2: Number of samples tested.

Projectnumber	CY-ITT	4PB
18501	13	20
18502	13	19
18523	11	18
18531	9	18
18590	12	18
18593	9	18
18596	9	18
18607	11	18
18619	10	18
19018	16	17
19020	9	18
19051	11	20

3.1.3. Test procedure

Samples are brought from storage and brought to the test temperature for at least 4 till 8 hours before testing. Testing is done on a Zwick-Roell or a MTS dynamic testing setup. Depending which machine is available. Testing is done respectively to the NEN-EN 12697-26 Norm for the stiffness and NEN-EN 12697-26 for fatigue. A elucidation to these procedures was given in Chapter 2. The general procedure was to first perform a frequency sweep test. Followed by a fatigue test. The results of the frequency sweep are discussed in Section 3.2.3 and the fatigue results in Section 3.3.

A few remarks to the testing procedure: The first couple of 4PB projects are all performed with the norm of 4PB till 50% stiffness reduction, called $N_{fat50\%}$. This results in the possibilities that the defined Stiffness Repetition failure criteria, in short N_{fatSN} is not always possible to find. With the adaptations from the author to the standard testing procedure at the KWS laboratory, the later performed projects are done till a lower stiffness reduction percentage. The second is also the case with the testing time of the CY-ITT. Setting the stop criterion a little lower gives a better insight in the stiffness reduction after failure and the later to develop slopes of the energy methods.

The initial short testing projects for the 4PB are 18501, 18502, 18523 and 18531. For the CY-ITT this differs again, because most CY-ITT tests were performed later due time restrictions, so the author had more influence on those tests. The same goes for the different frequencies at which the CY-ITT tests where performed. For a detailed overview of each mixture and the deviations during testing, see appendix A.

3.2. Frequency sweep

In this section the results are presented from the frequency sweep. Both stiffness and phase angle responses are reported and compared for the 4PB and CY-ITT fatigue tests.

3.2.1. Stiffness

An important property of an asphalt concrete mixture is its mechanical stiffness. It is called stiffness or resilient modulus because of its dependency on temperature and load frequency due its viscoelastic nature. The viscoelastic behaviour describes the time difference between when the load is applied and the reaction of the displacement of the material. It also incorporates the permanent and recoverable

deformations the material undergoes in time. Because of this the term elasticity is not used and when strains are very small and the stress-strain relation is kept in the linear visco elastic (LVE) range the stiffness is called the Dynamic or Complex Modulus E^* . This Dynamic Modulus is used to describe the stiffness of the material at different loading frequencies at low strain levels. The complete master curve is the result of multiple frequency sweeps at different temperatures. With the principle of time-temperature superposition (TTS) the individual sweeps can be shifted to a single curved line at the reference temperature, resulting in the master curve. This master curve is a unique curve that describes the viscoelastic behaviour of asphaltic material. With the use of this principle the stiffness can be found at temperatures and frequencies outside the range of the test. Important to note is that the shifting factors are the Prony-series coefficients used in visco-elastic modelling software.

The measured stiffness during the frequency sweep for both CY-ITT and 4PB is different. This difference for all twelve mixtures is given in figures 3.3 till 3.14. In these figures the difference in stiffness are represented through the fitted frequency sweep curve. This fitting is done through the method described in the German method for frequency sweeps dictated by the organisation FGSV in the document of AL-SP Asphalt 09[für Strassen-und Verkehrswesen, 2009]. The method fits a sigmoidal shape through the single frequency sweep result at a single temperature. The test temperature is 20°C, the same temperature at which the fatigue test is performed. This method saves time by reducing the number of sweeps and the long time needed to bring the sample on the right test temperature. The method assumes with using a sigmoidal shape function that all, including PMB's, describe the same stiffness vs frequency curve. Fitting is done through the Boltzmann equation 3.1 in which y_0, w, x, z , are fitting parameters found through the least squared error fitting method.

$$|E| = y_0 + \frac{w}{1 + e^{-\left(\frac{x-x_0}{z}\right)}} \quad (3.1)$$

A note is to be placed with assuming that the sigmoidal fitting is a correct representation of the complete master curve. At frequencies higher than 30 Hz the stiffness can possibly show a drop and does not stay horizontal as the fitted function shows. This behaviour can be observed in frequency sweeps performed on the DSR. The master curve is normally fitted on a log log scale which would show an almost straight line with a bend to the top and bottom of the curve. Because the limited horizontal scale of the frequency sweep with a single temperature this log log curve is not possible to construct. That is the reason why the sigmoidal function is done with only a log function on the x-axis. The use however is still relevant in easily identifying the differences between the CY-ITT and 4PB in stiffness and phase angle.

3.2.2. Phase angle

The phase angle is the measured time difference Δt [s] between when the force is applied and the displacement measured. A graphical distinct representation is given in figure 3.1. The force is given by γ and the following displacement by τ . With the an increase of the time delay between the force and time signal the phase angle increases. A material that is more viscous will react slower to an applied force then a more elastic material.

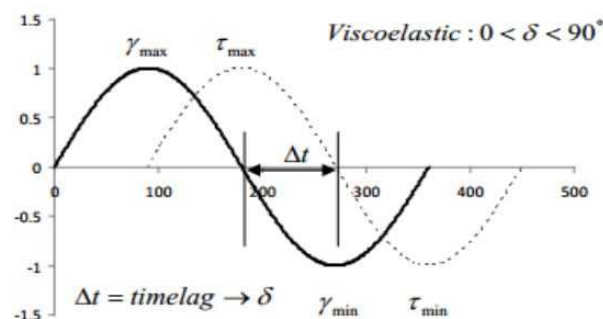


Figure 3.1: Phase angle [Abedali, 2015]

The Δt is more often expressed in δ [°]. Expressing the difference in time to an angle in degrees is called phase angle and limited between 0 and 90 degrees. In which the phase angle is the distribution between

the viscous and elastic part of the stiffness or shear modulus in DSR testing. Figure 3.2 explains this clear with on the y-axis the viscous or loss modulus and on the x-axis the elastic or storage modulus. Combining both moduli with a certain phase angles leads to a total modulus. In figure 3.2 this is called the Shear Modulus G^* . This is because the theory en testing originate from the dynamic shear rheology testing on the DSR. The measured phase angle can also be applied on the CY-ITT and 4PB to split the stiffness into two different parts. However this splitting has no practical use in fatigue testing and is not mentioned further. It is mentioned and taken into account because the energy method of dissipated energy takes the phase angle as an important variable. That is why the phase angle and the stiffness results are both shown in the next section.

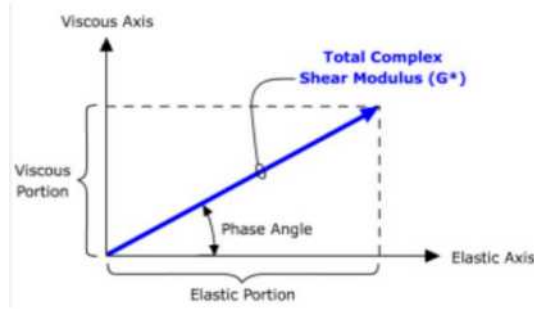


Figure 3.2: Phase angle [Abedali, 2015]

3.2.3. Results

For each sample per a mixture the frequency sweep was performed. For both the CY-ITT and the 4PB the result of a single frequency sweep is given in table 3.3 and 3.4. The overall result on the frequency sweep for both the measured force and displacement amplitude is given. From these values the stress and strain amplitudes are calculated, resulting in the stiffness for each frequency. In the last column the phase angle is given.

The prescribed test conditions for the CY-ITT are with a small applied fixating force of 0.035 [MPa]. In table 3.3 the given applied force is given with the related calculated stress. The force should result in a strain amplitude between 0.05 % and 0.1 % as prescribed by NEN-EN12697-26:2018 Annex E. Table 3.3 shows about half. The reason is that the software reported the strain as ε_{el} , which is the peak to peak value. Not the strain amplitude. The measured displacement is small, even with twice the amount of force. An amplitude of around 1.5 μm is measured by the LVDT's, so each LVDT measures in theory half this amplitude in displacement. It should be noted that these displacements are small. A human hair is for comparison around 60 $\mu\text{m}/\text{m}$. However NEN-EN12697:2018 addresses this problem and states that it of less concern and should be checked with a specimen with a known stiffness. In chapter 4 the accuracy and measurement results are discussed in more detail.

Table 3.3: CY-ITT, sample 50040, mixture 18501 frequency sweep result

frequency	load amplitude [kN]	displ amplitude [μm]	stress amplitude [MPa]	strain amplitude [$\mu\text{m}/\text{m}$]	stiffness [MPa]	phase angle [$^\circ$]
30	0.977	1.543	0.155	32.2	9106	25.7
20	0.894	1.551	0.141	32.3	8285	26.8
10	0.730	1.533	0.116	32.0	6853	28.7
8	0.626	1.391	0.099	29.0	6468	29.3
5	0.546	1.416	0.086	29.5	5547	30.7
2	0.376	1.313	0.060	27.3	4119	33.7
1	0.289	1.297	0.046	27.0	3201	35.7
0.5	0.254	1.489	0.040	31.0	2456	37.7
0.1	0.154	1.711	0.024	35.7	1294	40.5
30.0	0.987	1.559	0.156	32.5	9103	25.0

Table 3.4 shows the results of the frequency sweep of the 4PB. The result is different with the CY-ITT due the displacement mode of loading. Finding an almost constant strain amplitude. The applied force thereby to the specimen is far lower than a force applied to a CY-ITT specimen. The measured displacement of $38 \mu\text{m}$ by the single LVDT is clearly in the measurement range of $1 \pm 0.5 \mu\text{m}$. The frequency sweep for the CY-ITT starts and end at 30 Hz. This is to check if the measurement range was in the linear elastic range of the sample. If the deviation between the two sweeps is larger than 2% the sample is left out of the results. The inverse order between the CY-ITT and 4PB of the frequency sweep has no special reason but is due historical development.

Table 3.4: 4PB, sample 50008, mixture 18501 frequency sweep result

frequency	load amplitude [kN]	displ amplitude [μm]	stress amplitude [MPa]	strain amplitude [$\mu\text{m}/\text{m}$]	stiffness [MPa]	phase angle [$^\circ$]
0.1	0.013	38.383	0.044	50.9	855	47.1
0.2	0.018	38.177	0.061	50.6	1218	46.8
0.5	0.029	38.236	0.097	50.7	1921	44.6
1	0.040	38.797	0.136	51.4	2644	41.7
2	0.055	39.014	0.185	51.7	3570	38.2
5	0.077	38.608	0.260	51.2	5074	33.2
8	0.089	38.569	0.303	51.1	5935	30.6
10	0.095	38.234	0.321	50.7	6356	29.4
20	0.116	38.449	0.393	51.0	7703	26.2
30	0.127	38.355	0.430	50.8	8462	24.5
0.1	0.013	38,333	0.043	50.8	850	47.2

For each sample per mixture the frequency sweep was eventually performed. The resulting stiffness and phase angle measurements presented here below are the average value of all samples per mixture. For comparison both CY-ITT and 4PB are presented in a single table or graph for comparison. In table 3.5 the averaged results for mixture 18501 are presented. From this table it is clear that there is a difference in stiffness between the CY-ITT and 4PB. The stiffness for mixture 18501 is 12% higher for the CY-ITT compared to the 4PB. The phase angle shows comparable behaviour on the higher frequencies, where on the lower frequencies the phase angle slowly deviates between the CY-ITT and 4PB.

Table 3.5: 18501 Frequency sweep results

18501 Frequency sweep results				
Frequency [Hz]	E measured CY-ITT [MPa]	Phi measured CY-ITT [$^\circ$]	E measured 4PB [MPa]	Phi measured 4PB [$^\circ$]
30	9540	26	8383	24
20	8567	27	7654	26
10	7058	29	6324	29
8.0	6588	29	5903	30
5.0	5688	31	5051	33
2.0	4184	34	3565	38
1.0	3230	36	2651	41
0.5	2459	37	1932	44
0.1	1309	39	877	46

The general differences between the CY-ITT and 4PB are better represented in figures 3.3 to 3.14. Each individual frequency sweep per mixture is given. The left y-axis represents the stiffness with on the right y-axis the phase angle. The frequency on the x-axis is on a log scale. Given the 10 Hz sweep results at $x=1$ and the reported stiffness at frequency of 8 Hz close to that. The statement that the CY-ITT returns a higher stiffness applies to all mixtures, except the lowest frequency of mixtures 18619 in figure 3.12. While for most mixtures the stiffness lines show a parallel or close to parallel behaviour over the set frequencies. The phase angle however shows a cross linking behaviour where the 4PB has a higher phase angle for the lower frequencies compared to the CY-ITT. Ending with a lower phase angle than the CY-ITT at the higher frequencies. The phase angle shows a comparable phase angle for frequencies

around 8 to 10 Hz for both CY-ITT and 4PB.

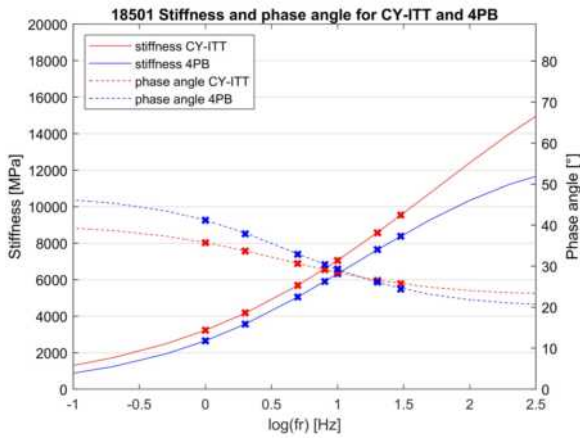


Figure 3.3: Frequency sweep 18501

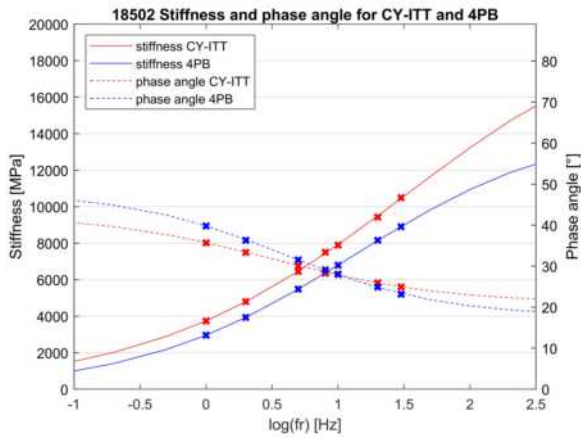


Figure 3.4: Frequency sweep result 18502

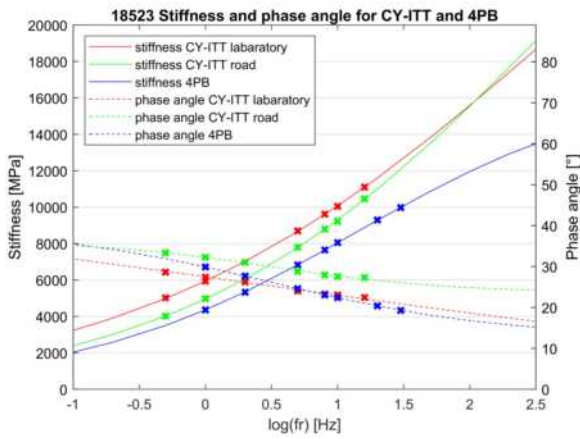


Figure 3.5: Frequency sweep result 18523

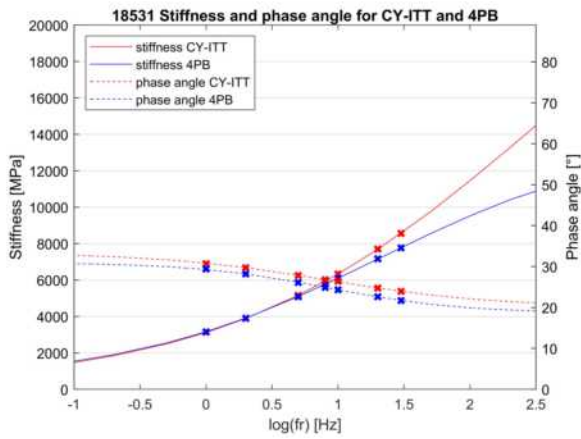


Figure 3.6: Frequency sweep result 18531

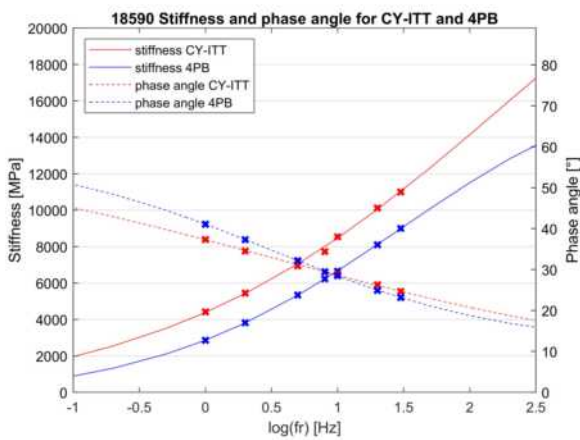


Figure 3.7: Frequency sweep result 18590

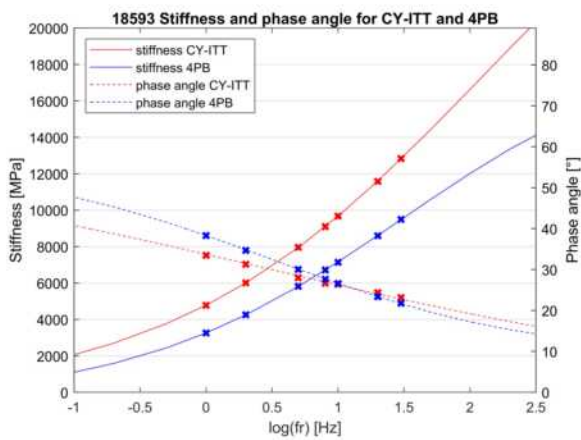


Figure 3.8: Frequency sweep result 18593

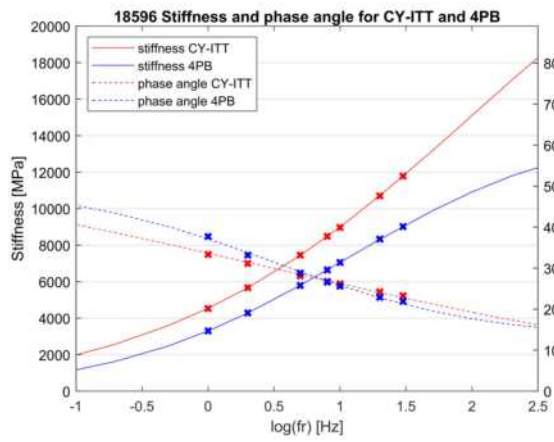


Figure 3.9: Frequency sweep result 18596

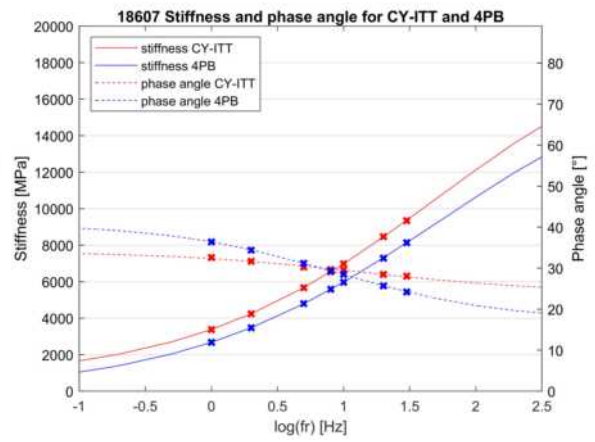


Figure 3.10: Frequency sweep result 18607

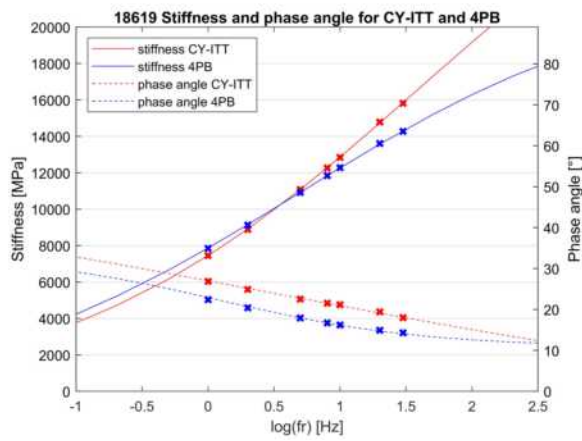


Figure 3.11: Frequency sweep result 18619

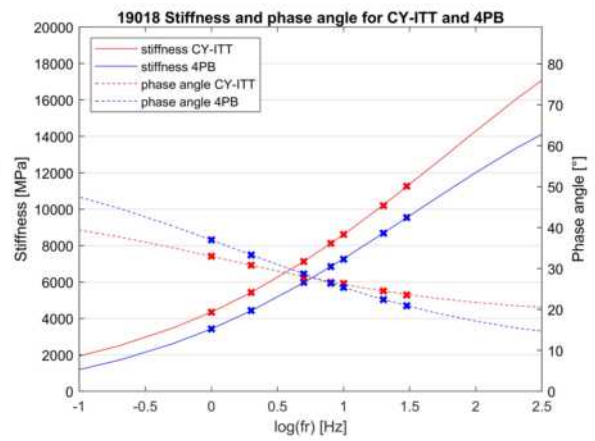


Figure 3.12: Frequency sweep result 19018

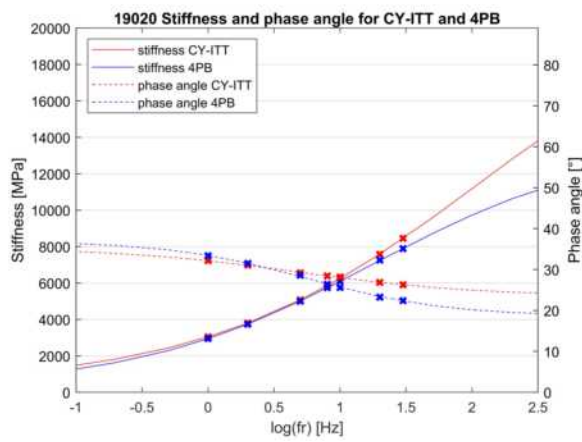


Figure 3.13: Frequency sweep result 19020

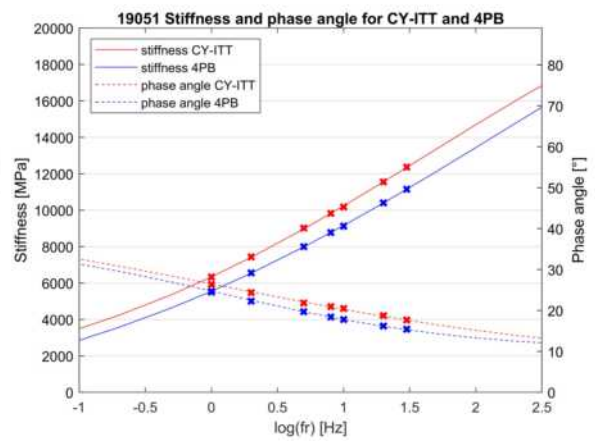


Figure 3.14: Frequency sweep result 19051

In detail we can state from figures 3.3 to 3.14 that there are two mixtures at which there is no constant parallel shift between the measured stiffness. These are mixtures 18531 and 18619. From a general mixture property perspective there is no clear correlation to be found. 18619 has a high PR percentages, but 19051 and 18501 are also high in PR content. The amount of bitumen, aggregate size or other distinct differences in mixture design, which are known to the writer, can not explain this crossing in stiffness for the CY-ITT and 4PB. The intriguing behaviour of these frequency sweeps is that for these two mixtures the phase angles are parallel. Performing the exact opposite phase angle behaviour from the other 10 mixtures. Where the phase angle is the one that is overlapping and crossing between the CY-ITT and 4PB.

For the other two mixtures remaining in figure 3.13 and 3.14 we see other distinct behaviour. Mixture 19020 has an almost overlapping stiffness ratio between the CY-ITT and 4PB. Where 19051 has both a parallel shift between the stiffness and the phase angle. Both mixtures uses a special type of modified bitumen mixed with high percentages of PR. This can explain the more steady response from the samples studied. The behaviour of mixtures 19051 was the expected result for all the different mixtures. Showing a constant shift between the two fatigue tests resulting in a probably convenient shift or calculation correction.

For all 12 different mixture fatigue test result between the 4PB and CY-ITT no correlation is found. There is also no correlating shift factor to be found between the two fatigue test. As a result we will look more closely at the differences found between the results at a single frequency.

Mixtures at single frequency

To study the general behaviour between two mixtures at this linear elastic testing range, the single frequency of 8 Hz is chosen. This is also the standard reported value for the stiffness and used for calculations. In table 3.6 for every mixture the stiffness and phase angles are given at 8Hz. From this we can compare the differences between the CY-ITT and 4PB. The average stiffness difference is 18%, while the phase angle is on average exactly the same.

In figure 3.15 the mixtures are each plotted with the phase angle versus its stiffness for both the CY-ITT and 4PB. In the ideal case this would have been a parallel line between the two fatigue test. Unfortunately there is no such shift directly visible, but if we would leave mixture 18529 with it's high 4PB phase angle out of the figure. We would perceive a more parallel line between the two fatigue tests. Resulting in a more or less parallel structure. In which, with 4PB and CY-ITT having a comparable phase angle, we could see the higher averaged stiffness of the CY-ITT over the phase angle measured.

Table 3.6: Mixtures stiffness and phase angle at 8 Hz

Mixture	S measured CY-ITT [MPa]	Phi measured CY-ITT [°]	S measured 4PB [MPa]	Phi measured 4PB [°]
18501	6588	29.1	5903	30.4
18502	7501	28.5	6361	29.1
18523	9614	23.3	7653	23.1
18529	5098	33.3	3660	39.1
18531	5921	26.8	5763	24.9
18590	7728	29.4	6230	29.5
18592	8386	26.0	6126	28.7
18593	9103	26.7	6721	27.6
18596	8486	26.8	6642	26.6
18607	6539	29.6	5585	29.3
18619	12261	21.5	11842	16.7
19018	8123	26.6	6852	26.4
19020	5859	28.4	5742	26.4
19051	9819	20.9	8779	18.4
Average	7930	26.9	6704	26.9

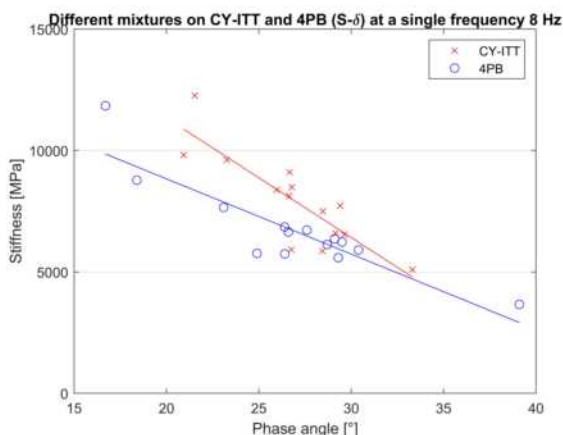


Figure 3.15: Mixtures at single frequency 8Hz, CY-ITT and 4PB

Overview all frequency sweeps

As a final comparison for the frequency sweep all the different mixtures are given in figure 3.16 and 3.17. In these figures the stiffness and phase angles are given for each mixture on the 4PB. We can clearly see that the phase angle and stiffness are proportionately opposites of each other in performances. Stiffer mixtures have a lower phase angle and more flexible mixtures have a higher phase angle. There is a distinct difference visible between the different mixtures. For the CY-ITT we would see the same results, but shifted with the factor that we saw in the previous frequency sweep figures. For trivial reasons these have been left out.

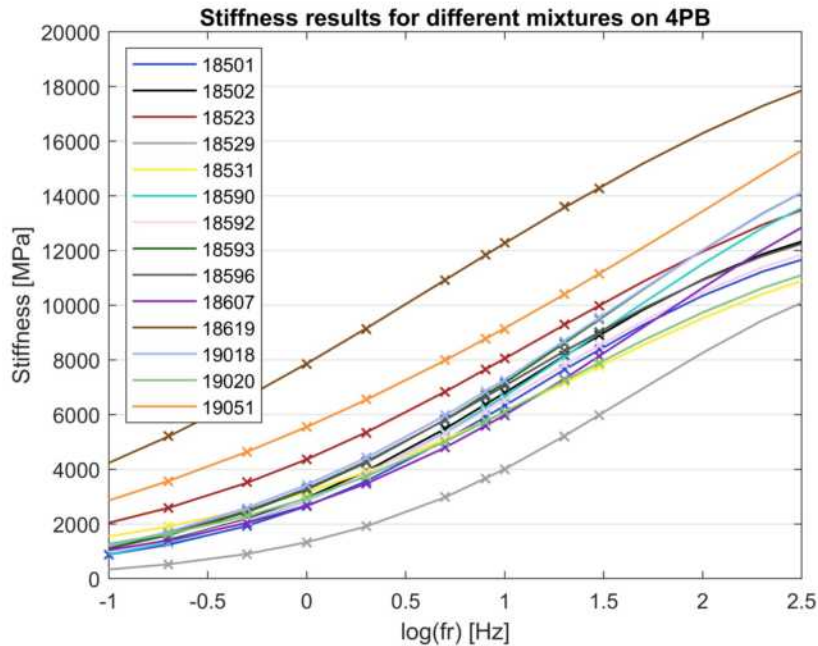


Figure 3.16: Fatigue line for different mixtures on 4PB

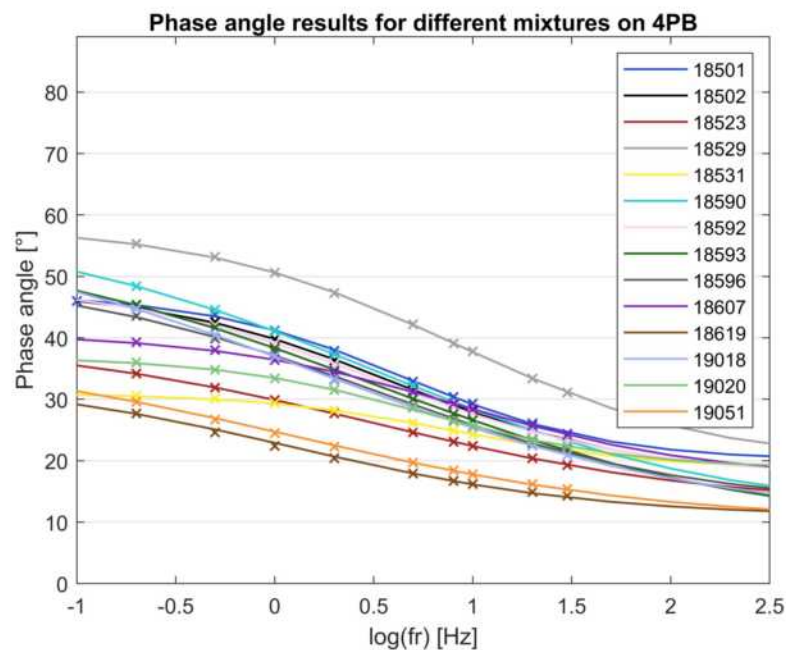


Figure 3.17: Phase angle for different mixtures 4PB

3.3. Fatigue

In this section the fatigue results of both CY-ITT and 4PB are presented and discussed. The traditional fatigue relation is based on the phenomenological equation 2.1 given in the previous chapter. The linear equation fitted on log-log scale on the individual mixtures are given for both the CY-ITT as the 4PB in a single figure. This to comprehensible study the differences for each fatigue test for the current classical fatigue approach. Where the classical approach consists of the $\log(\varepsilon_{ini}-N)$ relation. First the variable of failure criteria N_{fat} for the y-axis is discussed, followed by a general overview for the possible influence of the stress or strain variable on the x-axis. After which for each individual mixture the CY-ITT and 4PB are compared, followed by a final comparison between all the mixtures themselves.

3.3.1. Failure criteria

As described in chapter 2 the fatigue test for the CY-ITT is prescribed by using the stiffness repetition method as a failure criteria. This method is explained in section 2.4. Stating that it can also be used for a displacement control test like the 4PB. Through this we can compare both test in the traditional $\log(\varepsilon_{ini}-N)$ relation with a single failure criteria. Being a failure criteria that is based on the stiffness and not on energy dissipation we only take the behaviour of the failure criteria on the stiffness curve in consideration.

3.3.1.1. Stiffness Repetition on 4PB

The method of using the stiffness repetition in comparison to the traditional $N_{fat50\%}$ is shown in this section. While the stiffness repetition method itself is not used for comparing the CY-ITT and 4PB, the method proves a valuable tool to find the assumed transition point from micro cracking to macro cracking on a stiffness curve. In figure 3.18 the result is shown for mixture 18501 in a long/low strain fatigue test. Resulting is the visible difference between the 50% reduction of stiffness and the failure point set by the maximum of the stiffness repetition curve. In which the stiffness repetition performs noticeable better in setting the transition point than the classical failure method.

For the same mixture a short high strain fatigue test was selected to study the difference. In figure 3.19 again both failure criteria are given. This fatigue test was not conducted long enough to give a correct N_{fatSN} . The stiffness repetition curve has not yet reached a clear maximum value and it is visible that the transition point is not yet reached. Resulting that the 50% reduction of stiffness is on the far safe side of the fatigue life in a high strain fatigue test. Fatigue tests that are performed in the middle of these strain ranges show almost the same N_{fat} between the two criteria. These and the remainder of the 4PB fatigue tests from mixture 18501 are given in Annex B.

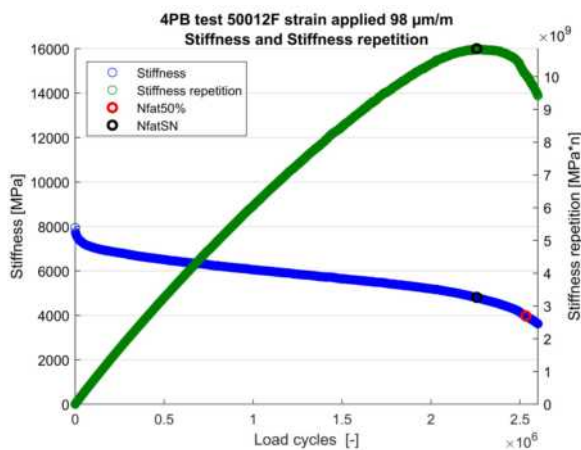


Figure 3.18: Stiffness and stiffness repetition 18501 test 50012F

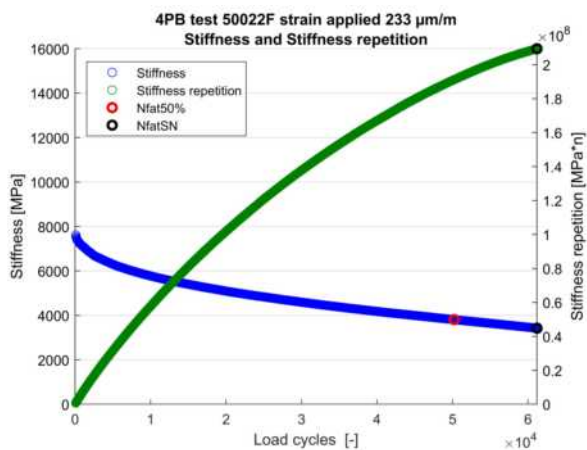


Figure 3.19: Stiffness and stiffness repetition 18501 test 50022F

Given that not all fatigue test were conducted fully to show the potential behaviour of the stiffness repetition SN failure criteria on the stiffness curve for mixture 18501. Mixture 18590 is selected to further validate the SN failure criteria. This test on 4PB was performed long enough to show the

influence of the failure criteria even on short high strain fatigue testing. This is shown in figure 3.21 on the right. In figure 3.20 the result is shown for the low strain fatigue test. Given again a better estimation of the turning point of the stiffness curve. The middle strain range shows comparable behaviour in finding the fatigue life. The remaining stiffness and stiffness repetition curves can be found in Annex B

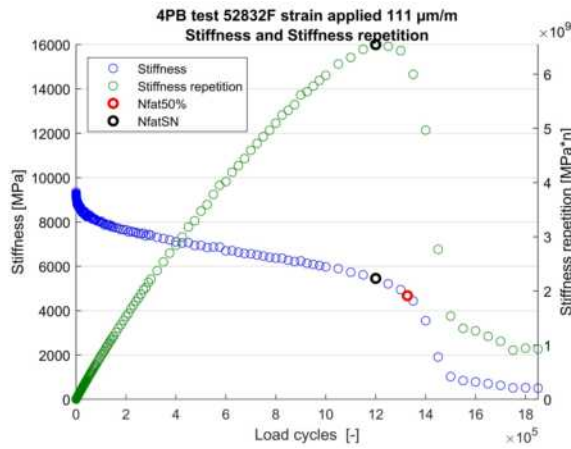


Figure 3.20: Stiffness and stiffness repetition 18590 test 52832F

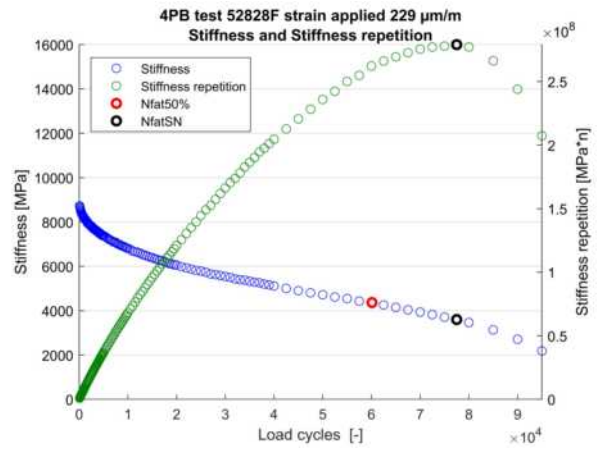


Figure 3.21: Stiffness and stiffness repetition 18590 test 52828F

To prove this influence on the traditional results of a 4PB test, a comparison is made in figure 3.22 and 3.23. Due the log scale for the y-axis N_{fat} the small increments or decrements are not clearly visible. But the change of slope is significant enough to mention. Where the new established fatigue line by the N_{fatSN} failure criteria is given in blue. The $N_{fat50\%}$ criteria is given in green. The difference found between the two different N_{fat} criteria is 8% average for the mixture 18501 presented in figure 3.22. For mixture 18590 in figure 3.23 the average difference is 10%.

As mentioned for mixture 18590 the test time was increased to establish always the maximum stiffness repetition value. This is not the case for 18501, finding sometimes not the correct stiffness repetition which could be higher if the test was performed for a longer duration. So the 8% average difference for the 18501 mixture is on the low side. Both mixtures show the same behaviour in decreasing their slope, validating that, although not all 4PB test did run for the correct time calculating the maximum stiffness repetition. The overall behaviour between the two criteria is close enough on the log-log scale to still be used. Keeping in mind that applying the concept to 4PB tests that were stopped to early can have a slightly bigger slope than perceived.

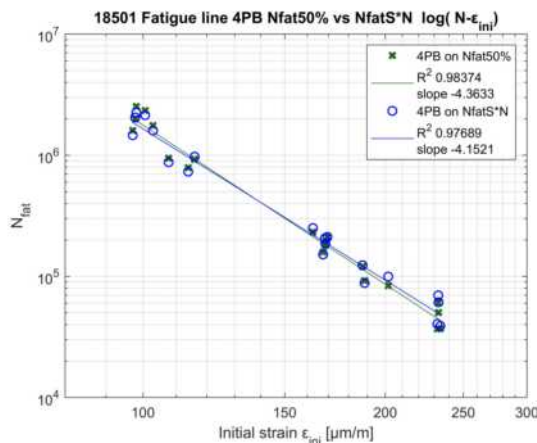


Figure 3.22: Fatigue line 18501 with different N_{fat}

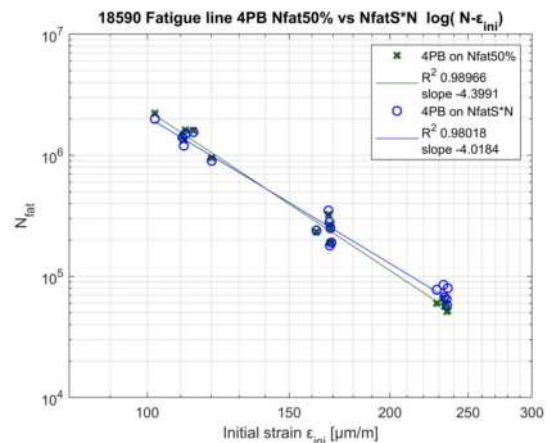


Figure 3.23: Fatigue line 18590 with different N_{fat}

Important to consider is that the shift is especially noteworthy at the higher strain levels. For the 18590

there is a 19% increase in N_{fat} . For the lower strain levels there is an decrease of 7% of the number of load repetitions till failure. For the middle strain levels the stiffness repetition finds the same N_{fat} as the 50% reduction norm. In both figures 3.22 and 3.23 the mentioned slope is directly related to the k_2 value of the fatigue line. The k_1 values, not mentioned, differ around 5% from each other, resulting in lower values for the stiffness ratio failure criteria. Meaning in practical calculations through IOA that the overall fatigue life of mixtures will decrease.

From this part it becomes clear that the influence of using a different failure criteria is present, but as showed in section 2.4 this method is theoretical more correct and should be pursued, although the results are worse for fatigue calculations and that the chapter is titled 'classical fatigue results'.

3.3.1.2. Stiffness repetition on CY-ITT

The stiffness repetition method is from origin a force controlled failure criteria. Set by the stiffness multiplied by the number of load repetitions. The method is called energy ratio in literature and employed in the current NEN-EN-12697-26 as the set failure criteria for the CY-ITT.

In a force controlled fatigue test the overall stiffness reduction can be described as linear. Or to be completely accurate this is the almost linear approach of the natural logarithm. This linear decrease is the result of the constant force amplitude acting on the specimen, resulting in a displacement amplitude that will slowly increase. This is associated with the formation of micro cracks in the specimen [Benedetto et al., 2015]. Continuing till a certain moment where macro cracking appears and the specimen will show visible macro cracks. In a stiffness curve it will appear as an almost linear decreasing slope that slowly accelerate downwards. The turning point from linear to accelerating is the set failure point as discussed previously in chapter 2.

The problem is that this turning point is visually hard to establish and not always noticeable. Second, if applying the reduction of the initial stiffness to 50%, would give a $N_{fat50\%}$ far in the macro cracking region. Using two CY-ITT examples from mixture 19020 this behaviour is shown in figure 3.24 and 3.25. That the 50% stiffness reduction criteria fails is due the increase of stiffness at the start of the test. In the first 500 or so load repetitions the sample still settles under the current testing procedure. Resulting that the set stiffness at $N=100$ is too low. If the highest found stiffness in this range was set as the initial stiffness the 50% reduction norm would be close to failure point established by the Stiffness Ratio.

Also given figure 3.24 and 3.25 is the stiffness repetition. With that the failure point can be established at the linear end of the stiffness curve. With the examples from mixture 19020 this accelerating behaviour was clearly visible. With this result and all other results presented in appendix B the stiffness repetition is set as a good failure criteria for the traditional failure relation.

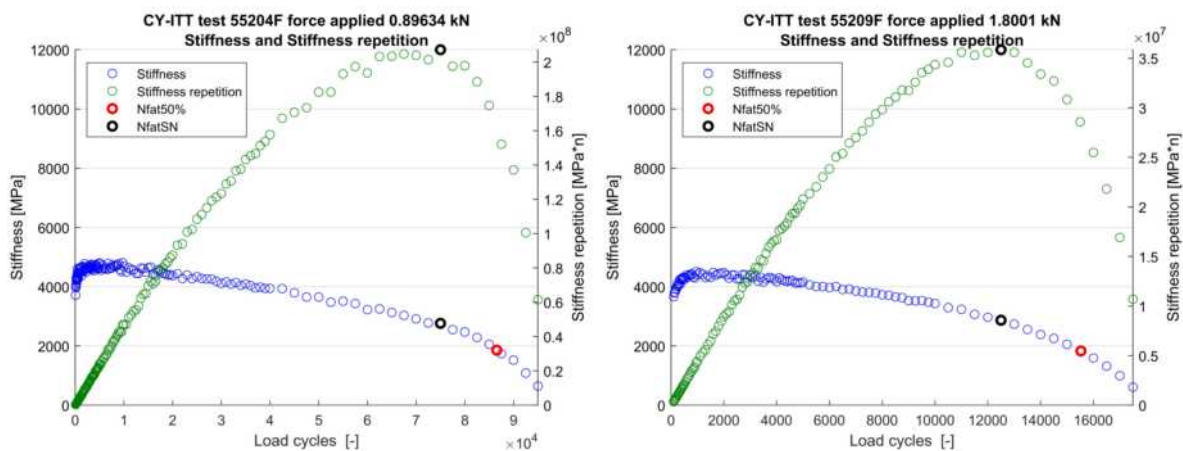


Figure 3.24: Stiffness and stiffness ratio 19020 test 55204F Figure 3.25: Stiffness and stiffness ratio 19020 test 55209F

3.3.2. Fatigue life strain vs stress

In the previous section the N_{fat} influence on the traditional fatigue life was discussed. In this part the portrayed ε on the x-axis is discussed. From the traditional method the strain at the lower parts of an asphalt layer is determinative for it's fatigue life. So all fatigue relations found in 4PB tests are projected on a $\log(\varepsilon_{ini} - N_{fat})$ basis. Given the nature of the CY-ITT, the strain is variable and increasing over the number of load cycles. So the NEN-EN12697-24:2018 prescribes that the strain is reported at $N=100$. Side note, for the 4PB test the strain is constant, but also reported at $N=100$ in all software. For both tests the phenomenological relation is given in figure 3.26 for mixture 18501. As displayed in the title of figure 3.26 the failure criteria applied is the stiffness repetition method.

There is no correlation visible in figure 3.26. Both fatigue test describe a different slope and different ranges in strain and fatigue life. The difference found will be confirmed later in section 3.3.3 for all mixtures. So there is no attempt made to find a constant shift factor. However with the adapted failure criteria we could also change the stated variable of ε_{ini} to ε_{S*N} . Stating that the measured strain at failure as the found strain variable. In figure 3.27 this change of strain is showed. Only the CY-ITT strain values will increase due the increasing deformation measured during testing. The result is still a none correlating relation between the two fatigue tests.

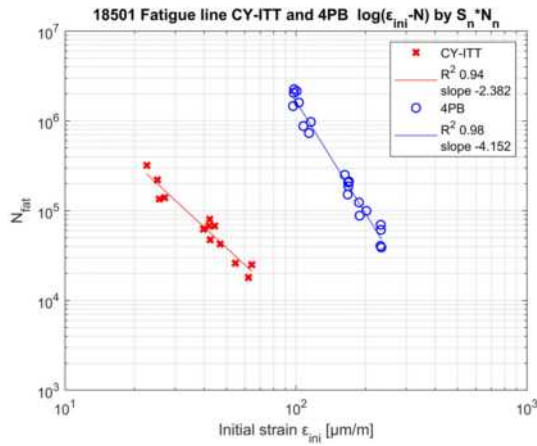


Figure 3.26: Fatigue line 18501, strain at initial

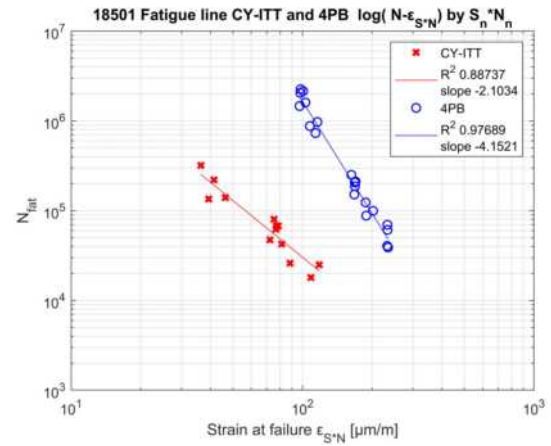


Figure 3.27: Fatigue line 18501, strain at failure

We could replace the variable strain by the variable stress σ . As is the CY-ITT a stress controlled test, we inverse the relation that is traditional strain controlled. Now the CY-ITT is the leading fatigue test, resulting in figures 3.28 and 3.29. In the first figure the $\log(\sigma_{ini} - N_{fat})$ relation is shown. A comparable difference as for the strain based relation in figure 3.26 is found. The CY-ITT is performed on stress levels that are on average a factor 8 lower than the 4PB. But does not result in a correlation shift factor. For a complete insight the stress value at failure SN is given in figure 3.29. Here the 4PB results are shifted towards the CY-ITT. The failure criteria is no longer set at a reduction of 50% of stiffness, this results in a larger or lesser shift in the measured stress at failure. So there is no direct a half shift compared to the σ_{ini} in figure 3.28, but also a change in the slope. However the slope change is opposite of the CY-ITT slope. So all four possible parameters don't show correlation behaviours.

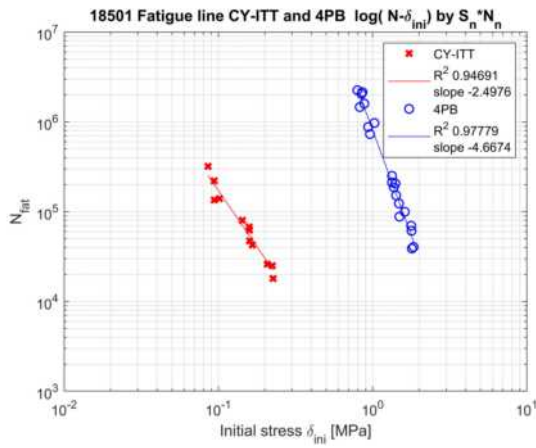


Figure 3.28: Fatigue line 18501, stress at initial

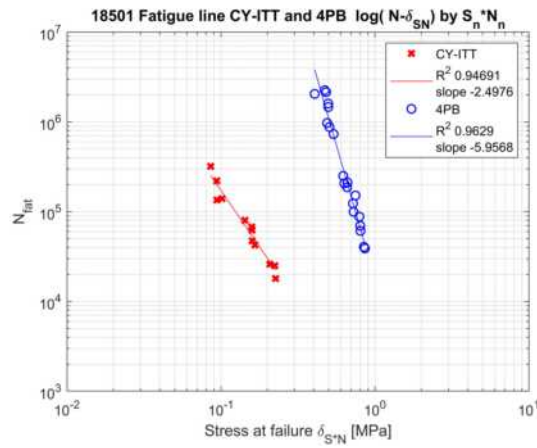


Figure 3.29: Fatigue line 18501, stress at failure

3.3.3. Results

For all the different mixtures the traditional fatigue relations are given in figures 3.30 to 3.41. These form the basis for studying the further relations found between the two fatigue tests. Both tests per mixture has an own calculated R^2 . This is set as the variable in how good the linear relation fits on the found test results. Resulting for a mixture with test results close to that fitted line with a high R^2 . Meaning a low spread and samples that show a low variability between them. The set R^2 found for both fatigue test per mixture forms the lower bound for the new to establish relation. Meaning that it at least should find a R^2 which is the same or higher. This to ensure a better correlation and lower variation then the old fatigue relation.

The overall results and R^2 for both CY-ITT and 4PB per mixture are good. It can be viewed that for mixtures with high PR contents tends to have a larger spread, resulting in a lower R^2 . Mixture 18523, with 50% PR, figure 3.32 and mixture 18619, with 85% PR, in figure 3.38 are examples of that. Figure 3.32 for mixtures 1823 presents the fatigue relation for laboratory prepared specimen on the CY-ITT and the field cored specimen. Both lines do not fall on a single line and both have quite a different slope between them. A field cored specimen does therefor not correlate directly to the lab prepared one. Unknown to the author is the exact procedure applied to the field cored samples, cored after how many weeks, density etc, so more research should be done on the difference in fatigue life for lab en field prepared specimen.

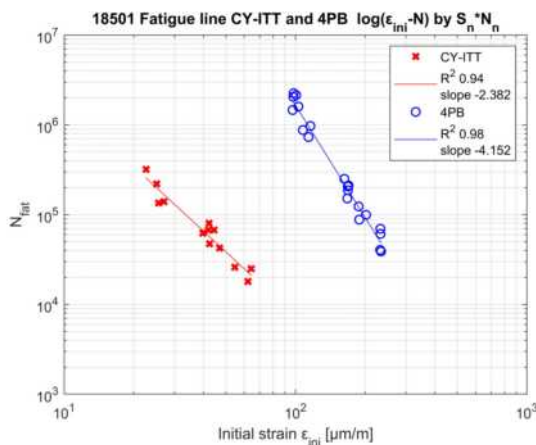


Figure 3.30: Fatigue line 18501

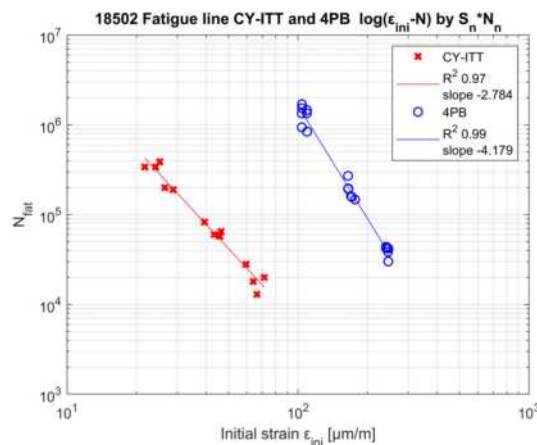


Figure 3.31: Fatigue line 18502

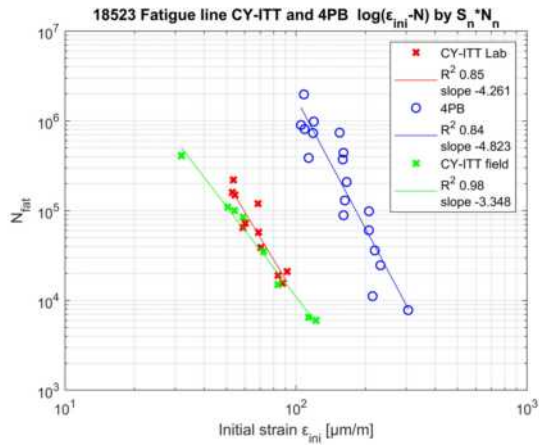


Figure 3.32: Fatigue line 18523

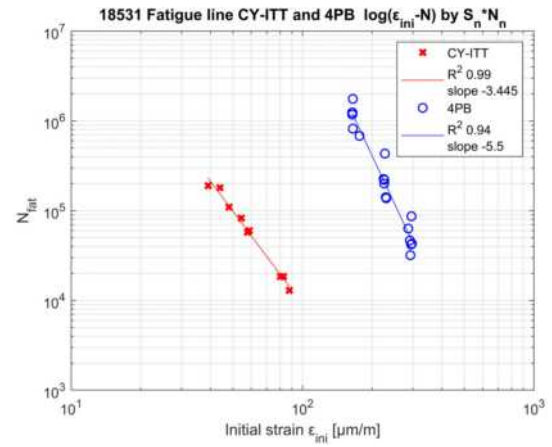


Figure 3.33: Fatigue line 18531

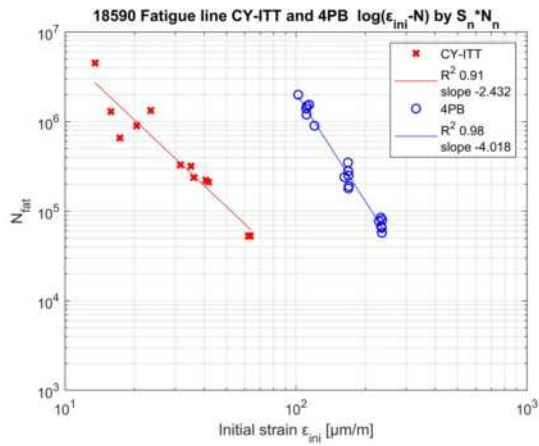


Figure 3.34: Fatigue line 18590

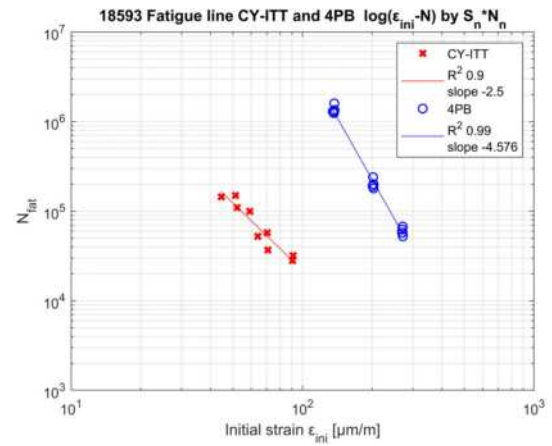


Figure 3.35: Fatigue line 18593

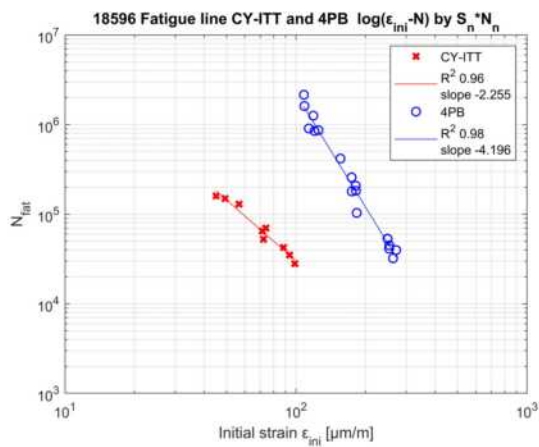


Figure 3.36: Fatigue line 18596

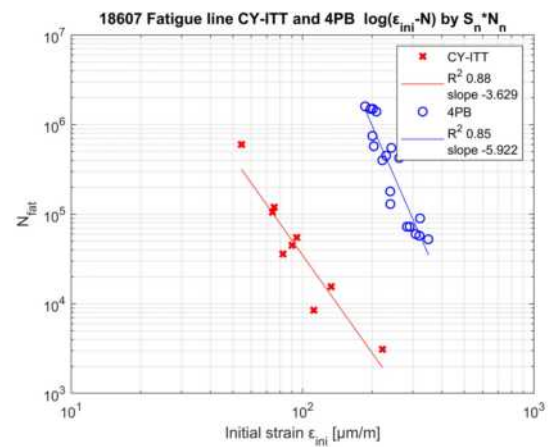


Figure 3.37: Fatigue line 18607

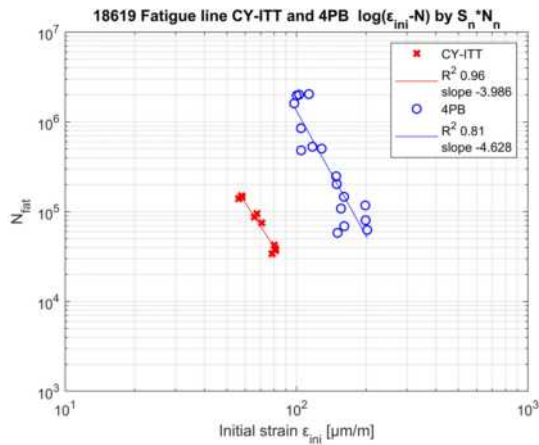


Figure 3.38: Fatigue line 18619

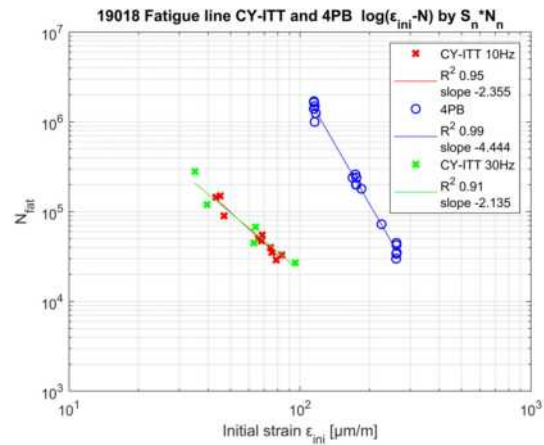


Figure 3.39: Fatigue line 19018

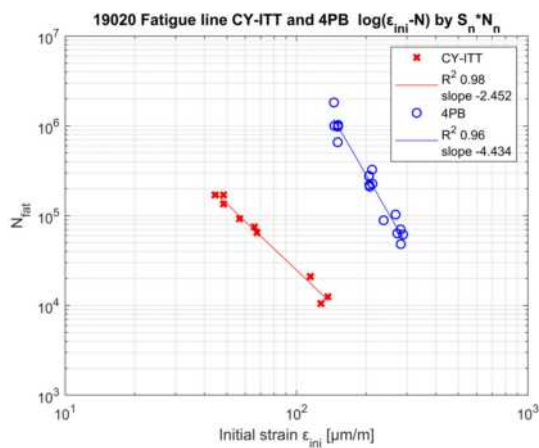


Figure 3.40: Fatigue line 19020

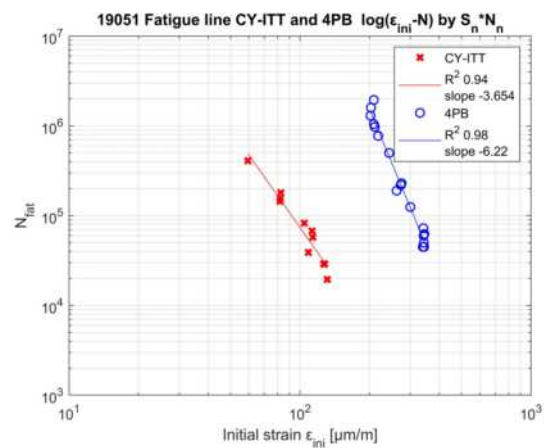


Figure 3.41: Fatigue line 19051

Different details are found in the previous figures. The CY-ITT from 18590 in figure 3.35 is tested in its entirety on 30 Hz and 19018 in figure 3.39 partially on 30 Hz. We see a comparable behaviour between tested on 10 or 30 Hz, but not a distinct correlation. The slopes of both frequencies are quite comparable, but a distinct shift is visible. This is in accordance to the research of Ghuzlan. Ghuzlan founded a distinct shift between different frequencies for the CY-ITT test [Al-Khateeb and Ghuzlan, 2014]. For project 19018 with both 10 and 30 Hz CY-ITT, the applied strain levels aren't that distinct, making it harder to significant describe the frequency dependent behaviour. For both CY-ITT tests we see a different slope and shift compared to their 4PB results. Making a direct correlation with the same frequencies not possible.

To compare the robustness of the two different fatigue tests. The average R^2 for both the CY-ITT and 4PB for all mixtures is calculated. For this it is assumed that with an higher averaged R^2 the fatigue test is a more robust way of testing samples. Resulting in better fitting lines and more reliable fatigue parameters. The presented results from the previous figures is collected in table 3.7 For the 4PB the average $R^2 = 0.943$ and the CY-ITT = 0.924. Therefor there is no significant difference found between the CY-ITT and 4PB. So we state that the sample variance for both fatigue tests is the same.

Table 3.7 also presents the overall slopes. These slope parameters are an important factor for the overall fatigue life of a mixture. A higher slope is equal to more load repetitions the mixture can endure at an imposed lower strain value. For the CY-ITT we notice three deviants mixtures that also contain high percentages of PR. Namely 18523, 18619 and 19051. However mixture 19020 and 18596 also contain high PR percentages, bu are in line with the overall average. For the 4PB in the forth column we

Table 3.7: R^2 and slope parameters from the fatigue tests.

Projectnumber	PR [%]	CY-ITT R^2	4PB R^2	CY-ITT slope	4PB slope
18501	30	0.935	0.977	2.382	4.152
18502	0	0.970	0.986	2.784	4.179
18523	50	0.853	0.841	4.261	4.824
18531	0	0.988	0.944	3.445	5.500
18590	0	0.912	0.980	2.432	4.018
18593	0	0.905	0.994	2.500	4.576
18596	40	0.962	0.978	2.297	4.196
18607	0	0.749	0.850	2.826	5.922
18619	85	0.952	0.851	3.950	4.993
19018	0	0.924	0.990	2.246	4.363
19020	55	0.998	0.960	2.752	4.433
19051	50	0.937	0.963	3.654	5.951
Averaged	-	0.924	0.943	2.960	4.759

see especially for the 18531, 18607 and 19051 higher than averaged measured slopes. These are the mixtures with special types of bitumen. The explanation for the higher slope of mixture 18531 is that the red pigments grains are bounded with an EVA polymer.

A special note is placed with mixture 18523 where the slopes are almost parallel between the CY-ITT and 4PB. This is the only case for all mixture and no comparable situation is found for other mixtures. Otherwise the respective results between the CY-ITT and 4PB mixtures are comparable.

3.3.4. All mixtures

The previous results from each individual mixture are compared in figure 3.42 on page 51 for the 4PB. This comparison leads to finding the best mixture in fatigue life behaviour. The criteria for the best fatigue life is set by the highest fit parameters k_1 and k_2 . The ε_6 value can be computed with equation 2.1. This results that mixture 19051 and 18607 are the best performing mixtures on fatigue. Both mixtures have a modified type of bitumen, where 18607 is a PMB modified and 19051 has a special type of modifier added combined with 50 % PR. Compared to the 18619 which has a 85% PR content and does perform way worse with unmodified bitumen.

The fatigue lines for the CY-ITT are given in figure 3.43. The same overall relations as the 4PB are found. Mixture 19051 is here also the best performing mixture. However the worst performing mixtures on the 4PB are the better performing mixtures on the CY-ITT. These are the 18523 and 18619. The first remark is placed at the 18607 modified mixture. Here the CY-ITT was performed on 10 °C, resulting in the general effect of having a lower fatigue life [Al-Khateeb and Ghuzlan, 2014]. Otherwise there would be an expected shift towards 19051 in accordance with the 4PB result. The second remark is placed with 18590, performed on 30 Hz the range of the fatigue line is different, but the slope is quite the same. As stated by Ghuzlan there is a shift factor between different frequencies so for an exact comparison a single frequency should be set.

From comparing figure 3.42 and 3.43 we can state that the overall fatigue results for the CY-ITT and 4PB are not interchangeable. We cannot conclude that if a mixtures performs well on the 4PB it also has good results for the CY-ITT. This is mainly the case with the high PR mixtures. For all other mixtures the overall comparison in fatigue life are valid. A reason for this can be that PR has a great influence on the relative small beams compared to the bigger cored diameter samples from the CY-ITT. Another reason can be that the found stiffness in Section 3.2 for both 18523 and 18619 is relative quite high. Which results in a stiffer response to vertical deformation. For both are classified as a base layer with a very low permanent deformation. This possible influence of the permanent deformation that is conceived during fatigue testing is previously discussed in Section 2.3.2, explaining the serious influence the permanent deformation could have on the fatigue life. This shift perceived with these high stiffness

and permanent deformation resistance mixtures could be an indicator for this behaviour. It is for these reasons that a study should be performed for explaining and classifying the influence of the permanent deformation in the CY-ITT.

Taking in consideration the log-log scale used on how the different mixtures are graphical represented, there is a distinct difference visible between the mixtures. Making it easy to identify which mixtures perform in the same range or which modification and variable can have a influence on the measured fatigue life. This concept holds for both the CY-ITT and the 4PB as long as the test is performed in the same exact conditions. So the traditional method of N_{fat} plotted against $\log(\epsilon_{ini})$ is a good identification of mixture performance on fatigue.

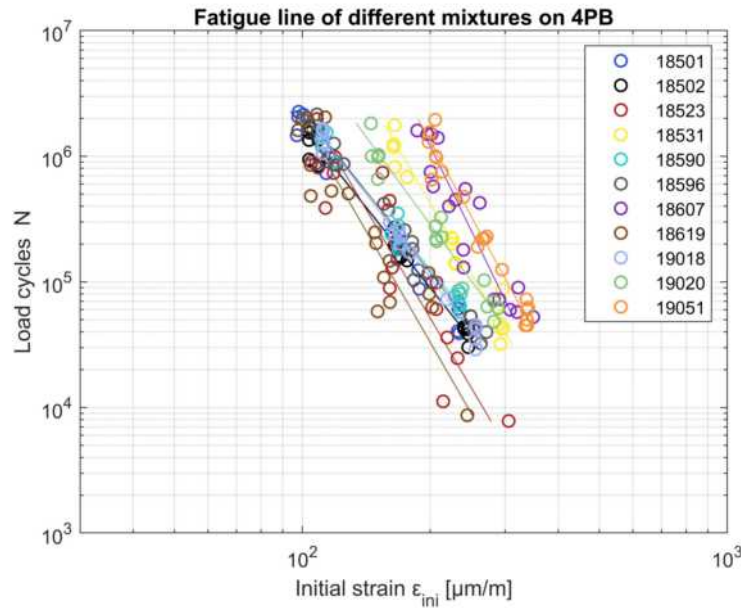


Figure 3.42: Fatigue line for different mixtures on 4PB

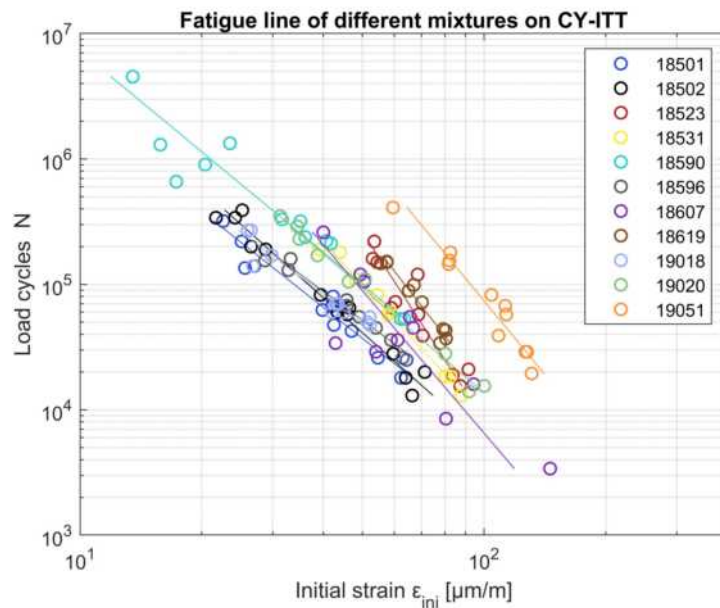


Figure 3.43: Fatigue line for different mixtures on CY-ITT

3.4. Conclusion

In this chapter the traditional fatigue results of the CY-ITT and 4PB were presented. A wide range of 12 different mixtures were analysed and discussed in two main sections. From the frequency sweep the distinct differences between the CY-ITT and 4PB on stiffness and phase angle were established. In the section about the traditional fatigue results, a consistent material dependent, but loading mode independent failure criteria was first established, called the Stiffness Repetition method, SN . With the load cycle at failure defined as N_{fatSN} . With that Sub-question 3 was answered. The resulting fatigue result were established with this failure criteria. Creating the $\log(N_{fatSN} - \varepsilon_{ini})$ relation. The stress and or ε_{SN} were unsuccessfully explored. In short the following conclusions could be drawn.

Frequency sweep

- From the frequency sweep comes forth that the CY-ITT has on average a 18% higher stiffness value at 8 Hz than the 4PB.
- The phase angle is on average the same at 8 Hz for the CY-ITT and 4PB.
- There is no constant coherent parallel behaviour between the CY-ITT and 4PB during the frequency sweep.
- Stiffer mixtures are highly related to the amount of PR or bitumen modifications applied to the mixture.
- The mixtures behaviour on the stiffness and phase angle are opposites of each other. Resulting that stiffer mixtures are less viscous compared to the low stiffness mixtures.

Fatigue

- The Stiffness Repetition method set as failure criteria presents itself as a good method in finding the transition point of the assumed microcracking to macrocracking transition on the stiffness curve in all stiffness curves of the 4PB. Where the $N_{fat50\%}$ is found to be inadequate for the high (too short) and low (to far on N) applied strain tests.
- In The CY-ITT the $N_{fat50\%}$ is due the initial stiffness growth not applicable. Here the used Energy Ratio from NEN-EN12697-24, renamed in this thesis N_{fatSN} proves to be consistent in finding the transition point of the stiffness curve.
- On average both fatigue tests show the same sample to sample variance in the fatigue test.
- It is not possible to compute a constant shift factor between the CY-ITT and 4PB fatigue results. The reason being the different found slopes and strains between every mixtures.
- The classical $\log(\varepsilon_{ini}-N)$ approach is a good method to distinguish the different performances of mixtures in fatigue life.

Recommendations

Although the traditional fatigue life relation is with no discrepancy's researched in this chapter, there can be made a recommendation to look at a certain phenomenon observed during the CY-ITT test, which could indicate that there can be a possible shortcoming, improvement or interference with the fatigue test on the CY-ITT. For mixtures with high stiffness and permanent deformation resistance showed a distinct improved in fatigue on the CY-ITT over the 4PB. This could indicate the interference of these mixture properties on the desired measured 'true' fatigue life.

4

Results RDEC

In this chapter the results of the Ratio of Dissipated Energy Change (RDEC) energy method are presented. In the first section the general behaviour is discussed with the influences of the three parameters on the RDEC. The measured force and displacement amplitudes are discussed. Followed by the calculated phase angle, the resulting hysteresis loops, application of the force method and the stress-strain distribution in the sample. From these the general result of the RDEC method is given in Section 4.2. In Section 4.3 three different methods are discussed to determine the N_{fat} on the RDEC curve. Followed by the fitting method to find PV . First the complete method of the Energy Ratio failure criteria is explained, followed by the derived method of the Stiffness Repetition from Chapter 2. The third method is based on a statistical approach to determine the range of the number of load repetitions and the resulting PV .

In Section 4.4 a theoretical perfect RDEC curve is discussed with the previous methods to find PV . The resulting slope parameter $x(1)$ from Section 4.3 is discussed in Section 4.5. The overall results from these methods for 12 individual mixtures are presented in combination with the average found results of RDEC in Section 4.7. Including an overall comparison of these mixtures. Resulting from this research, additional work is shown in Section 4.7 and 4.8 with the addition of the 4PB executed on force control and the uni-axial displacement controlled test. In Section 4.9 a practical example is given for the influence of the mass density on the RDEC. The chapter is finally concluded in Section 4.10.

4.1. General behaviour

In Chapter 2 the equation for the RDEC was given in equation 2.14. The formula employed resulted in a great scatter of RDEC values [Airey et al., 2017]. This result is one of the largest downside of the method and prevented further research. One of the reason for this scatter is often stated by the measuring accuracy [Tolman et al., 2018]. The measuring accuracy needs to be good and the specimen has to have a stable response to the applied load, otherwise the signals are too much disturbed and the RDEC figures are just a scattering cloud. The measured response result is therefore discussed as first.

The phase angle is the result from both the force and displacement amplitude measurement and used as the third parameter in the dissipated energy equation 2.10. From the fatigue tests different results came forth and are discussed in Section 4.1.2. The resulting Hysteresis loop is validated next, as it forms the basis of the RDEC method. As the dissipated energy principle is validated, the direct principle of *work* in the energy method of RDEC is discussed next. With the influence of that principle explained we can look deeper into the RDEC method by looking at the influence of the calculated dissipated energy of the bi-axial stress-strain distribution of the CY-ITT. The results forms the basis of the RDEC values calculated in section 4.2.

4.1.1. Force & displacement signals

In a CY-ITT test the force is constantly applied, where in the 4PB the force is constantly adjusted. The measured displacement in a CY-ITT is therefore changing and in the 4PB the displacement is held constant through the controller. It is of interest in how accurate the measured signals are compared to the presented RDEC method in chapter 2.

4.1.1.1. CY-ITT

We will first look at the results of a CY-ITT test. For different projects a separate raw data file was collected during testing. This was initially done to establish the hysteresis loop for the dissipated energy, but can also show the amount of scatter of the measured displacement signal. With this we could confirm that the measured displacement holds as a sinusoidal/haversine displacement signal. Or that the occurring displacement is of a too small nature to measure with the current generation of LVDT's. A too small displacement amplitude would mean that the signal is no longer distinct from the 'noise' around the measured signal. This noise consist of small disturbances occurring during testing. Like vibrations, accuracy of the LVDT's or electric noise generated by the equipment itself.

For this part we will focus on the results generated by the current measuring equipment. The detailed study about the calibration of the LVDT's, the resulting signals in voltages, the electronic filters applied to create the measurement in the unit of displacement is out of field of expertise employed in this thesis. At the current moment a validation sample with a known stiffness and zero phase angle is not available to guarantee the exact measurements of a CY-ITT test setup. We will therefore hold true on the statement made in NEN-EN 12697-24 that in practice the correct stiffness of the material is found.

As an example, we have taken three samples from mixture 19020, tested on a high, medium and low force amplitude fatigue to show the differences in the measured displacement response. The CY-ITT type test was performed on the Zwick-Roell equipment. Project 19020 is chosen because it has almost the lowest stiffness of all tested mixtures. Resulting in the lowest range of applied forces. In figure 4.1, 4.2 and 4.3 the displacement and force captured data are given. The negative displacement is the direct result from the initial setup of the LVDT's, set at the maximum range of almost -1 mm at the start to get a maximum testing range of the LVDT's. All three figures show the very small displacement amplitude that is measured. Ranging somewhere between 2 and 0.5 μm . Below the displacement, the applied force signal is given. The blue fitted line is the applied sinusoidal fitting function at the raw data points that results through equation 2.4 to the amplitude and phase angle calculated values.

For the test with the high applied peak to peak force of almost 2 kN in figure 4.1 we observe a very good displacement signal. The raw data scatter plot shows a good haversine displacement function. Resulting in a good fit. If this is compared to a test with the low force applied test in figure 4.3 we see a significant difference. The force applied is almost three times lower. Resulting in a displacement signal with an amplitude of around 0.6 μm . Although the low amplitude and the increase of a disturbed displacement signal, the amount of noise doesn't interfere severely with the created haversine fitting function. Result is that the lowest limit of measurable displacement is not yet reached.

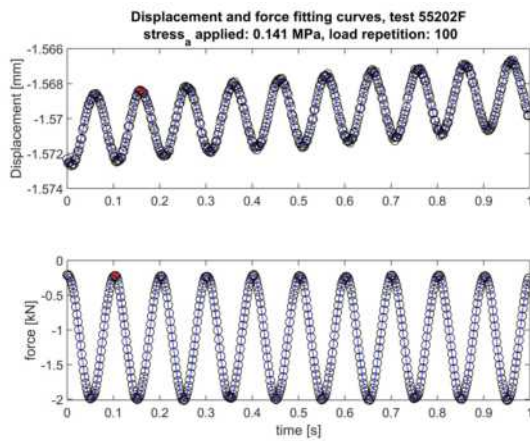


Figure 4.1: 19020 CY-ITT measurement, force applied high

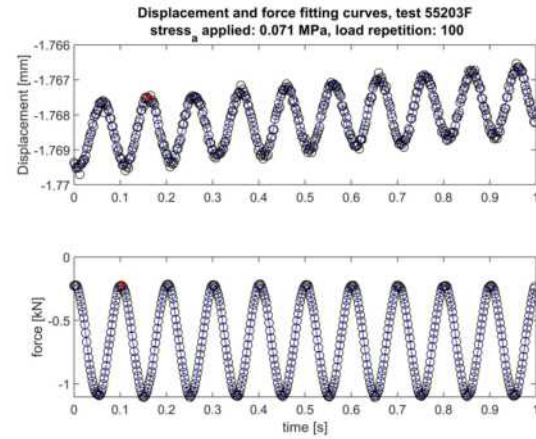


Figure 4.2: 19020 CY-ITT measurement, force applied medium

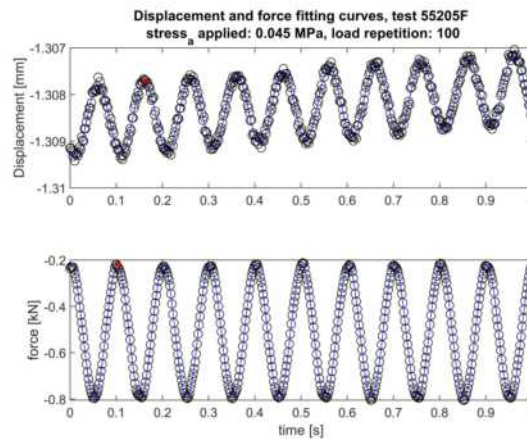


Figure 4.3: 19020 CY-ITT measurement, force applied low

In the previous figures for the CY-ITT the load repetition of $N=100$ is chosen. For the CY-ITT this is the lowest measured amplitude during fatigue testing. After which the displacement amplitude will slightly increase over the number of load repetitions, although this is marginal until failure. The difference between the measured real displacement signal and the amount of measured noise is at first highly dependent on the amount of electronic filters applied to the controller. Second to the computational capabilities of the controller.

To test the influence of the noise on the measured displacement signal, a sample was placed in the setup without applying the load to the sample. The hydraulic jack was positioned 5 cm above the sample and was actively moving while the on sample displacement was measured. The result was the amount of background scatter that was measured on the sample. The scatter was the result of the non filtered noise from the test setup that would be there also during normal testing. In figure 4.4 this registered displacement is plotted in μm . The result is a cloud in the range of around $0.1 \mu m$.

The noise plotted together with the lowest found displacement amplitude from fatigue test 55205F results in figure 4.5. The measured displacement from the fatigue test, here in μm , describes a distinct haversine signal compared to the separate registered noise signal. While the peak to peak displacement is only around $2 \mu m$ it is far larger than the founded scattering of $0.1 \mu m$ in figure 4.4. From this simple test and comparison at 10 Hz, together with the visual inspections on the oscilloscope during testing, we state that the measured signal is distinctive enough to capture the displacements in a CY-ITT fatigue test.

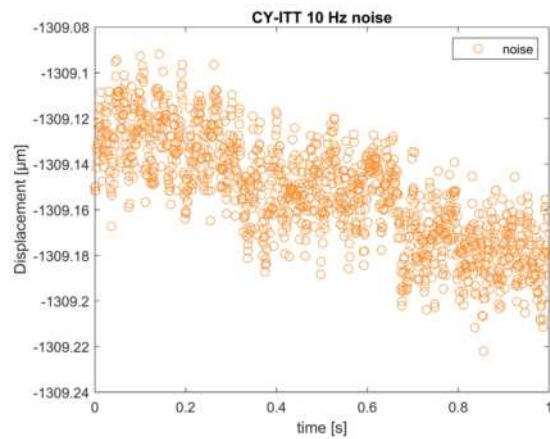


Figure 4.4: CY-ITT measured noise

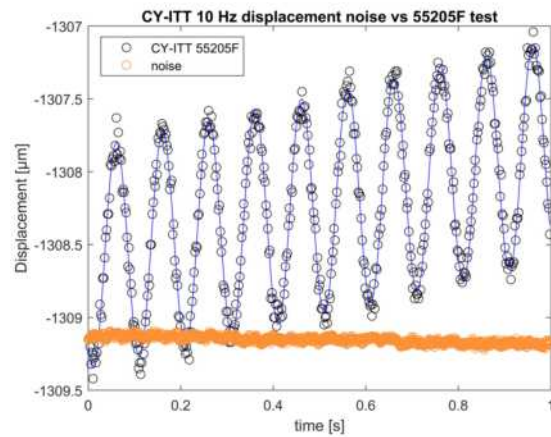


Figure 4.5: CY-ITT measured noise vs low amplitude displacement signal

It should be noted that this is an asphalt concrete mixture with a average stiffness of 6256 MPa at 10 Hz established during the frequency sweep with an 0.125 MPa load amplitude. The measurement result from the frequency sweep is presented in figure 4.6. The frequency sweep is performed with a higher load then the long fatigue test, resulting in a good signal. For the 0.1 Hz frequency sweep in figure 4.6 the applied fore is lower than the low strain performed fatigue test in figure 4.3. Still the measured displacement signal is a distinct haversine shape. So the statement that the measured noise is trivial to the measured displacement holds. The only aspect that still should be considered is a reference sample with a known stiffness to fully validate the test setup in general.

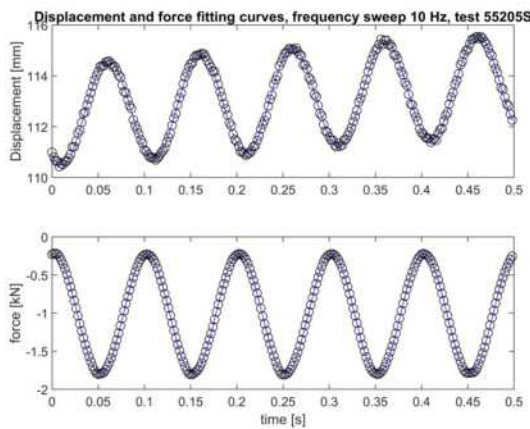


Figure 4.6: Frequency sweep, sample 55205 on 10 Hz

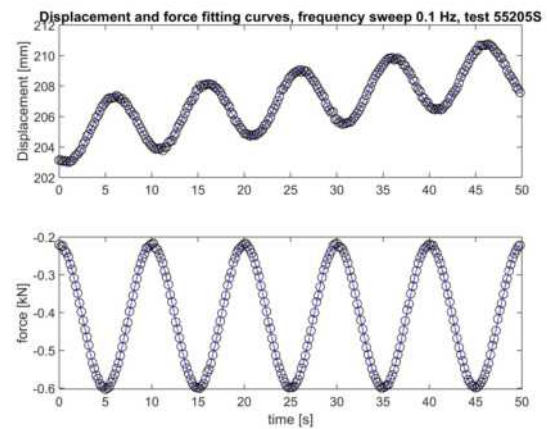


Figure 4.7: Frequency sweep, sample 55205 on 0.1 Hz

4.1.1.2. 4PB

The 4PB test for mixture 19020 was performed on the MTS-86 machine. This setup didn't have a standard raw data output file and the specific raw data output file created for mixture 19020 didn't compile at the right number of load repetitions. So for the 4PB we take mixture 19018 that was performed on the Zwick-Roell testing equipment.

For the 4PB the force applied is constantly adjusted to keep the same strain on the specimen. This force signal decreases over the number of load repetitions parallel to the stiffness. In figure 4.8 and 4.9 the measured displacement and force signals are given with the respective fitted functions through them. In the left figure the signal is given at N=100 and the right figure is at the set failure criteria, in

this case $N=1.250.000$. In total 5 load repetitions at 30 Hz are captured with an frequency of 5000 Hz. The overall results for both the displacement and force functions are sinusoidal in nature and show no scattering. So for the applied testing range in the 4PB with the standard strain ranges the equipment shows no deviant behaviour.

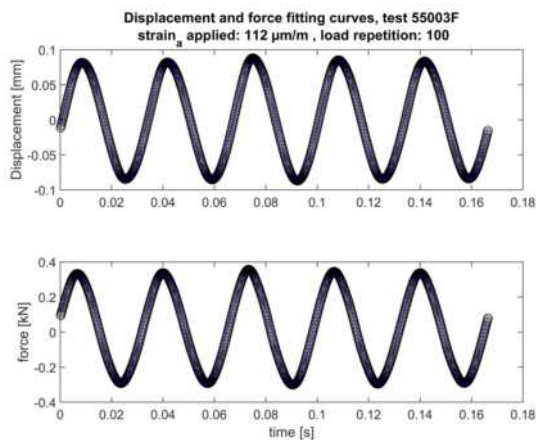


Figure 4.8: 19018 4PB measurement at cycle 100

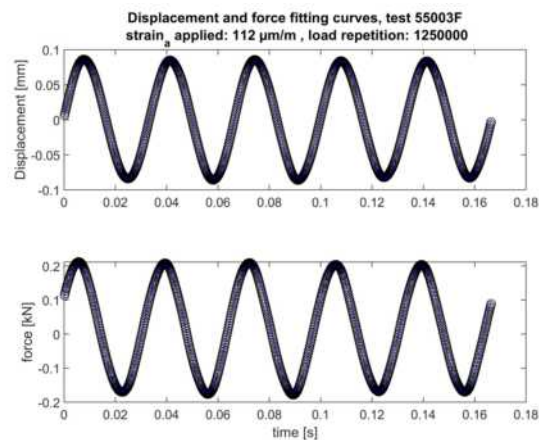


Figure 4.9: 19018 4PB measurement at cycle 1.250.000

However if we look further than the set failure criteria and we look closely at the measured force signal. The resulting phase angle shows strange abnormal responses in both results. Because this has significant effect for the calculated dissipated energy, we will discuss it in the next section about the measured phase angle.

4.1.2. Phase angle

The phase angle is the measurement in time between the applied force and the reaction of the displacement. In modern testing equipment this is done real time during testing through a Fast Fourier Transform (FFT) calculation.[Ebe, 2012] The NEN-EN 12697-24:2018 annex F describes it actually through the process of fitting a sinusoidal curve through the measured data points. The shift in time between the measured sinusoidal force and displacement signals is the phase angle.

The accuracy of measuring the phase angle is of high importance for the calculations of the dissipated energy. Due the nature of the sinus function, a phase angle increase at smaller angles delivers a higher contribution than if the phase angle increases at higher phase angle rates. As an example: A single degree increase at $\sin(15^\circ)$ is a 7% increase for the dissipated energy with the other parameters kept constant. If we have a angle increase at 28° it gives an increase of 3.4%. Higher degree phase angles then 35° we don't come across at the testing temperatures of 20°C , but if we do test at lower temperatures the stiffness increases and the phase angles decreases. If we then measure around 10° phase angle, we have a 11% increase of dissipated energy at a single phase angle degree increase. So at lower temperatures and lower viscous materials the influence of fluctuations in the phase angle have a higher impact than at higher temperatures and high viscous materials.

One of the biggest influences of a lower value of phase angle is shown in the works by Li. Testing a single mixture on both displacement as force controlled loading modes at 5°C . Here the normal shown behaviour of a displacement controlled type test at 20°C is cancelled out and instead of a downward slope, an upward slope behaviour of the dissipated energy is observed in figure 4.10.

That the phase angle measurements are not always accurate is shown in figure 4.11. Here the 4PB stiffness and phase angle curves for sample 55003F on the Zwick-Roell from mixture 19018 are given. The phase angle is completely dispersed after the moment of failure. This resulted in creating the measurement signals at the load repetitions after failure.

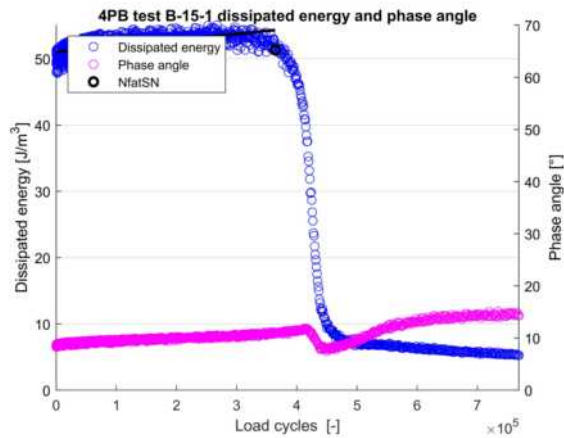


Figure 4.10: Phase angle and dissipated energy B-15-1

In figures 4.12, 4.13 and 4.14 the measured displacement and force signals are given during fatigue testing of sample 55003F. Starting figure 4.12 at $N=1.350.000$ the phase angle is still stable at 26.6° . This is almost the same result as for the force signal at failure in the previous section figure 4.9. In the measured cycle after that in figure 4.13 the first distortions are clearly visible in the force signal. The hydraulic actuator can no longer hold the sinusoidal load signal to keep the displacement constant in the decrease of stiffness happening at this moment. The measured phase angle is at this moment 29.3° at a stiffness of around 3000 MPa.

The next load cycle at 1.450.000 leads to the total scattering of the phase angle to 42.2° in figure 4.14. The force signal is completely distorted with the very small force amplitude it has to apply for the given displacement amplitude. The beam has almost no stiffness left and the force applied is around 50 N. This disrupted force signal is the basis for the scattering of the phase angle and is no longer a valid calculation but a measurement error.

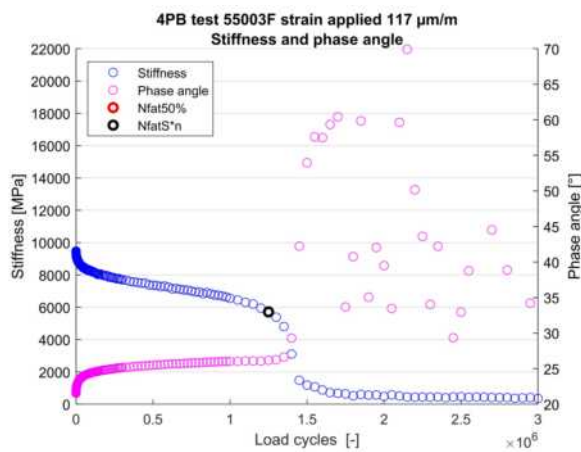


Figure 4.11: 19018 stiffness & phase angle

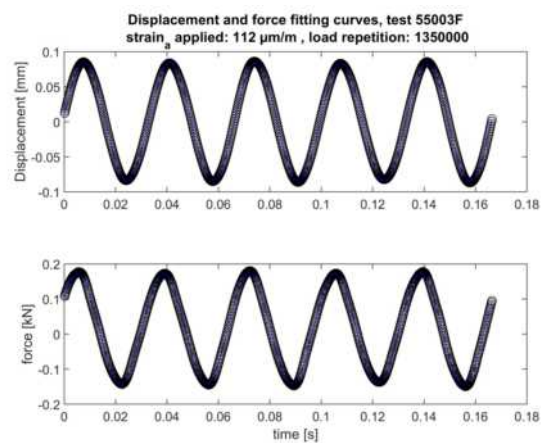


Figure 4.12: 19018 4PB measurement at cycle 1.350.000

The phase angle calculation is dependent of where the software measures the peak. When the to applied load is to small and beyond the capabilities of the load actuator the load cannot be applied anymore in a sinusoidal way. So the measurements beyond the failure point are subjected to the Zwick-Roell equipment incapability to determine the phase angle accurately.

If we compare that with the 4PB result of the TU Delft equipment used in figure F.1 and the 4PB MTS-86 equipment in the later to describe figure 4.33, we don't see this amount of scatter. We observe a

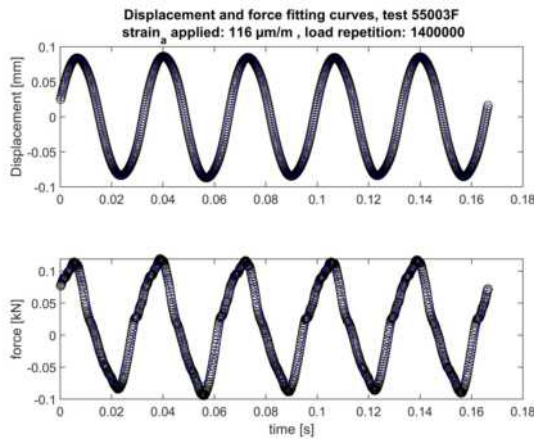


Figure 4.13: 19018 4PB measurement at cycle 1.400.000

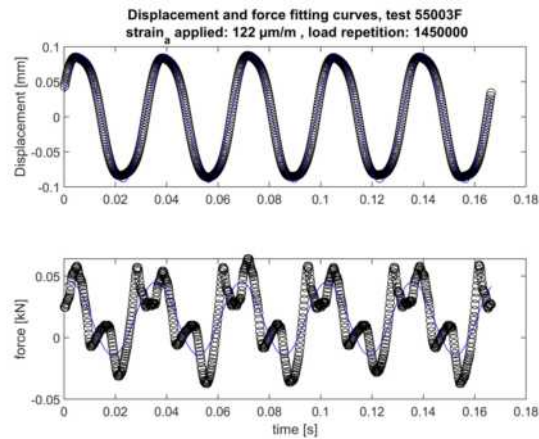


Figure 4.14: 19018 4PB measurement at cycle 1.450.000

drop of the phase angle in the TU Delft equipment at the moment of failure and a steady response after, but no scattering. The same with the MTS-86 equipment where only a steady small overall increase is observed, even at the point where the stiffness rapidly decreases. So this scattering behaviour is only observed with the Zwick-Roell machine during 4PB testing. The reason for this behaviour can be the fact that the the ZWick-Roell machine uses a 10 kN load cell and the MTS a 5 kN load. Making the MTS machine more accurate on the lower applied load levels.

One should consider the effect of the increasing temperature of the beam or cylindrical specimen during testing. This is often, as in chapter 2, described as the cause of the increase of the phase angle at the start of the test. However as described in this section the phase angle increase can also be caused by the inaccuracy from the fast decreasing load amplitude. If this decrease of load amplitude is than assigned to a rapid decrease of material integrity or by the temperature increase is left to additional research.

The CY-ITT is left out of the discussion for the phase angle. The reason is that the force applied is kept constant haversine as proven in the previous section. The same is for the proven haversine displacement function. With the same setup and LVDT's for both the MTS-07 and Zwick-Roell setup the measured phase angle is accurate enough to use.

Concluding from this section we can state that first: The measurements are a distinct sinusoidal shape for both the displacement and force signals. Given a distinct difference for different frequencies for both frequency as fatigue sweep results. Second, the phase angle is dependent on test temperature and with that the non-linear relation to the dissipated energy equation. Resulting in contradiction behaviour at some temperatures. Third, the phase angle is heavily dependent from the measured displacement and force signals. A fast increase of phase angle is therefore not a material failure indicator, but often an equipment error.

4.1.3. Hysteresis loop

The dissipated energy is foremost first described trough the hysteresis loop that the stress and strain describe if plotted together. The total amount of dissipated energy per cycle is calculated by the area inside this loop. For both the CY-ITT and 4PB this loops differs due the nature of the applied mode of loading.

As an example how the loop is constructed we take the same test samples as in the previous sections from mixture 19020 for the CY-ITT and mixture 19018 for the 4PB. First the CY-ITT hysteresis loop is given in figure 4.15. This was done for sample 55202F which was tested with a high force amplitude and didn't show much scatter, comparable to its result in figure 4.1. The fitted function which now represent the area of dissipated energy shows an excellent fit. Due the loading mode all values are in the positive notation with the horizontal strains and stresses all positive in tension.

In figure 4.16 the hysteresis loop is given for the low force amplitude sample 55205F, this more scattered result is comparable to its results from figure 4.3. Although the scatter is more severe, the fitted function still holds true to the concept of the loop. Another result from the scatter is that some datapoints are found in the negative tensile mode. This is the result by the calculation from the displacement to strain with the set point of origin in the strain-stress system.

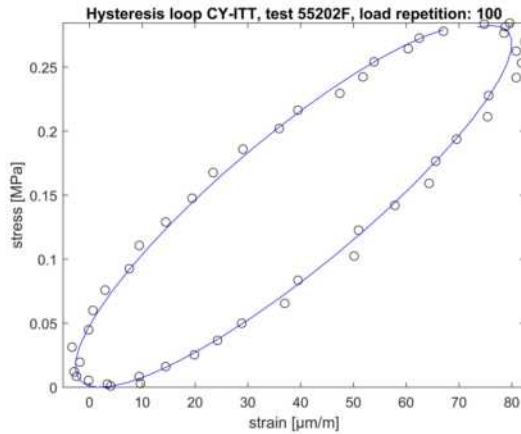


Figure 4.15: 19020 CY-ITT Hysteresis loop, force applied high

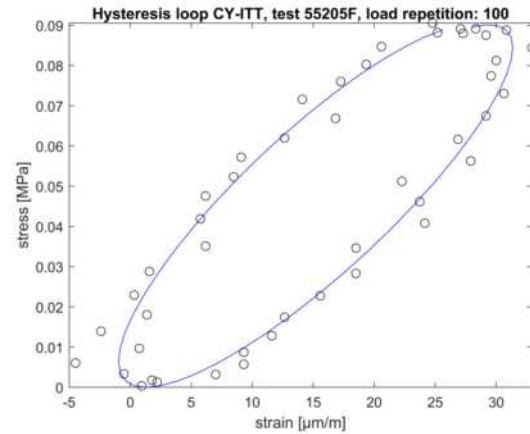


Figure 4.16: 19020 CY-ITT Hysteresis loop, force applied low

For the 4PB we compile the hysteresis loop for sample 55003F for both $N=100$ and $N=1.4 \cdot 10^6$ in figure 4.17 and 4.18. The result is based on the displacement and force relation shown in figure 4.8. The horizontal displacement of the CY-ITT is in a all tensile strain state during testing, for the 4PB the sample is bent through it's neutral line. This result, controlled by it's displacement, is set through the zero axis resulting in even size in positive and negative strain. The stress however is for compensating for own weight not directly proportional in positive and negative measured stress. The applied fitting functions shows an excellent relation to the datapoints and the hysteresis loop.

From the previous results for the fitting function in the range between $N=100$ and N_{fat} and the result in figure 4.17 we see that the hysteresis loop holds. However if we look at the measured force signals in figure 4.9 and combine that with the calculations for the stress and strain for the hysteresis loop, we see the result in figure 4.18. The disrupted force signal results in that the hysteresis loop is no longer a loop. With that the equation, equation 2.10 for the dissipated energy no longer holds. Especially if we look at load cycles after $N=1.4 \cdot 10^6$ where the phase angle distortions became scatter. In figure 4.19 the first major deviation is given at $N=1.45 \cdot 10^6$. The calculated hysteresis loop no longer holds any relation to the measured force signal.

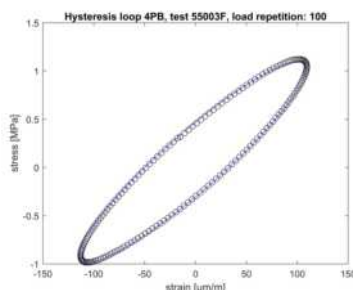


Figure 4.17: 19018 4B Hysteresis loop, load cycle 100

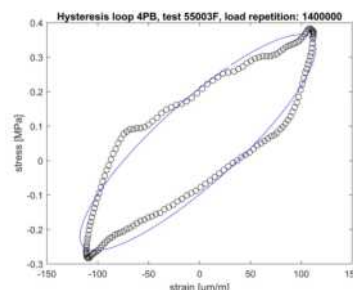


Figure 4.18: 19018 4PB Hysteresis loop, load cycle $1.4 \cdot 10^6$

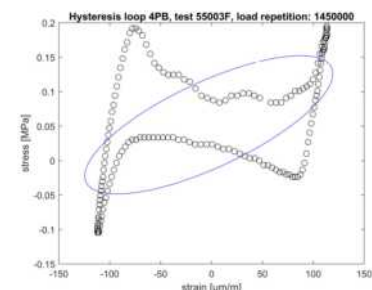


Figure 4.19: 19018 4PB Hysteresis loop, load cycle $1.45 \cdot 10^6$

So for the the dissipated energy calculations we need to consider and validate the equations with the real measured results before applying the concept. In the next section we consider the principle of

'work' compared to the dissipated energy with the concept of the hysteresis loop in mind.

4.1.4. Force & displacement

With the method of the Ratio of Dissipated Energy Change given by equation 2.13, we could state that is a generalised method by normalizing the first derivative of the energy dissipation. See also equation 2.17. This generalisation of the ratio can be proven by using not the calculated stress and strain parameters, but by stating that the equation is independent of these calculations. This makes the overall equation independent of the constant Poisson number, specimen size or clamping distance used. This statement is only true for a ratio dependent method as is RDEC method. The overall measured results, now governing, are of course dependent on the distinct fatigue behaviour.

Only the three raw measured parameters, force amplitude F_a [N], displacement amplitude U_a [mm] and time-derived phase angle $[\circ]$, have a direct influence on the measured normalised slope parameter RDEC. Equation 4.1 gives the formulation of the raw dissipated energy.

$$DE_{raw} = \pi F_a U_a \sin(\varphi) \quad (4.1)$$

To prove this statement we use mixture 18501 as an example for the monitored behaviour for both the CY-ITT and 4PB. Using the equation 4.1 we could calculate the raw dissipated energy. In figure 4.20 both the stress-strain as the force-displacement calculated dissipated energies are given for the CY-ITT test. The stress strain relation are scaled through the specimen size so the dissipated energies are a lot lower then the raw values. To prove the statement a different scale is used for the raw values on the right y-axis and chosen in a way the general behaviour over the number of load cycles is easy to be interpreted. Both dissipated energies plots show the exact same behaviour. For the 4PB the same comparison is made in figure 4.21. The 4PB has the same parallel shift between the two dissipated energies.

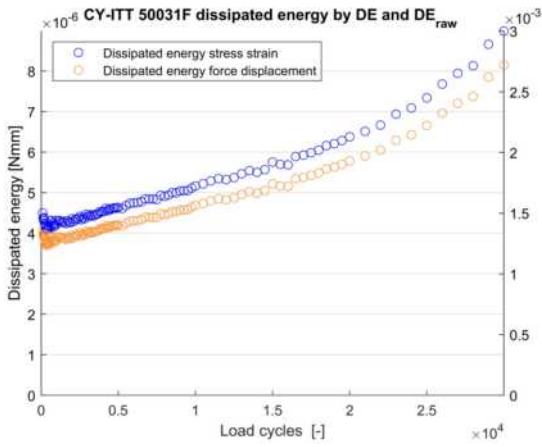


Figure 4.20: Comparison in dissipated energy for the CY-ITT

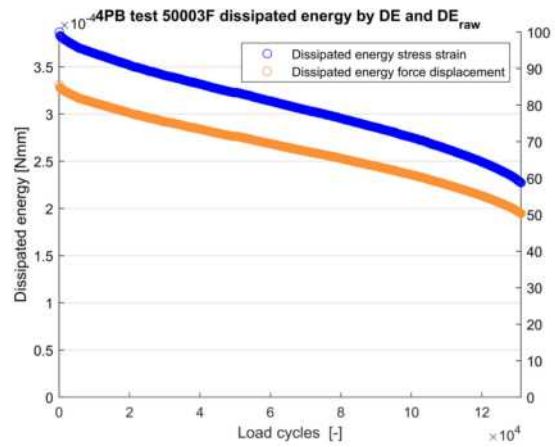


Figure 4.21: Comparison in dissipated energy for a 4PB test

Because of the nature of equation 2.13 and if we use DE_{raw} instead of DE we will find the same RDEC results. So from these results we could state that the normalised or Ratio slope of the dissipated energy is directly related to the measured response, but that this response is of course dependent on the shape and loading mode of the fatigue test. The implication of using the direct measured amplitude values will be further discussed in the next subsection.

4.1.5. Stress-strain distribution CY-ITT

From Chapter 2 we know the description and how the stress-strain distribution varies inside a cylindrical specimen. Using the standard formula 2.2 for the calculation of the dissipated energy with the formulas formulated for the CY-ITT, we calculate the dissipated energy per unit of volume. For the

CY-ITT only the horizontal strain and stress distributions at a certain assumed highest peak value, namely at the center of the specimen. Resulting in disregarding all vertical dissipated energy, as well as the stress-strain distribution in the sample.

With the findings from the previous section and the use of the slope of the dissipated energy, the resulting slope is the crucial variable. Resulting in the fact that all these variables can be calculated, but only the parameters that eventually effect the slope of the dissipated energy are of importance. So only the measured displacement of the sample. So the neglecting of the stress-strain distribution of a CY-ITT sample is a correct assumption. With that statement and assuming a constant Poisson number we can also neglect the vertical dissipated energy. Because of the assumed constant Poisson number over the fatigue life this also result in a constant that falls away by the RDEC normalisation as shown by figures 4.20 and 4.21.

The only extra variable that can have a influence on the slope of the dissipated energy is therefore the measured vertical displacement. This would result in changing the test setup significantly, because the use of LVDT is then no longer possible due how the measuring frame is build up. This will result in using strain gauges in horizontal and vertical direction. These have to be glued to the sample and are under risk of snapping due the force controlled mode of the CY-ITT or the larger applied deformation in a fatigue test. Due these radical changes in test setup and the assumption that only tensile strains leads to fatigue failure, we will not discuss the vertical deformation part any further.

4.2. General RDEC results

The method of Shen & Carpenter establishes a ratio of energy dissipation. As mentioned in Chapter 2 it is the normalised first derivative of the dissipated energy. The method states that when the RDEC is constant, the energy dissipated is constant, this is called the Plateau Value (PV). When the specimen fails in fatigue there is a sudden increase in RDEC. The specific number of load repetitions when this happens is called the N_{fat} . From the previous section we concluded that there are no further external influences on this energy method. So it crucial to establish a highly accurate PV and N_{fat} value.

4.2.1. Dissipated energy

The dissipated energy per load cycle is depicted in the previous section in figure 4.15, where the hysteresis loop is given. The area of the loop can be calculated through equation 2.10. The results is the dissipated energy course during the fatigue test. Where the dissipated energy is a multiplication of three parameters. With the addition of the phase angle to the relation of stress and strain. Simplified the addition of the phase angle to the two stiffness parameters. This results in figure 4.22 and 4.23 where the dissipated energy is given for mixture 19020. Mixture 19020 is chosen above 18501 because of longer test duration and the quality of the latter RDEC values. It is furthermore not influenced by the phase angle distortions as shown in the previous section. Figure 4.22 is for a CY-ITT and 4.23 for a 4PB. The result is a similar trend as with the stiffness results from 3.

The reason for the similarities is that the phase angle, if correctly measured, is almost constant. Finding an almost identical dissipated energy curve to the stiffness curve. The phase angle is projected alongside the dissipated energy curves in both figure 4.22 and 4.23. As these are the general curves described for the dissipated energy, the remainder of the results are given in appendix B. From the calculated dissipated energies the RDEC can be calculated.

4.2.2. RDEC

The Ratio of Dissipated Energy Change is given through equation 2.13. The result from from this equation is given in figure 4.24 for the CY-ITT and in figure 4.25 for the 4PB. From both figures three distinct observations can be made:

- Scatter. The amount of scatter is significant. The result from the CY-ITT is clear, but this is due the short testing time. Longer fatigue tests show the same behaviour as the result from the longer conducted 4PB test. The calculated result is however in line with the work from [Airey et al., 2017].

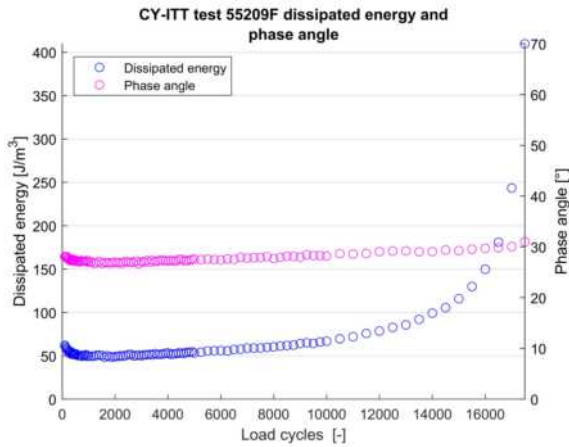


Figure 4.22: Dissipated energy 19020 test 55209F

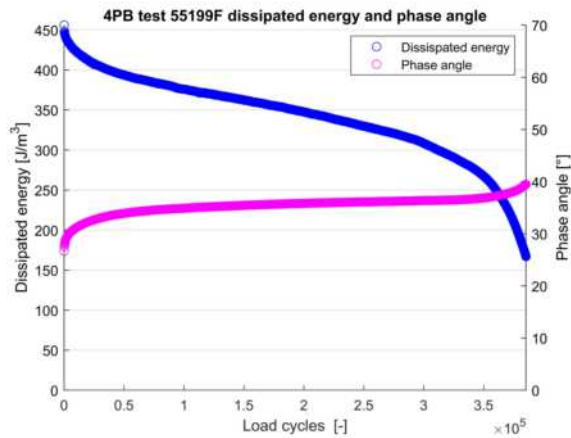


Figure 4.23: Dissipated energy 19020 test 55199F

- Shape. The shape of the curve is in general the theoretical shape of [Shen and Carpenter, 2007] as depicted in figure 2.16. However this is not always the case. For test that are conducted before a clear N_{fatSN} is reached or test that don't show a sudden drop in stiffness can show a very small increment in RDEC values. This can be a define case with the CY-ITT, where the increase of displacement at failure is not so sudden as compared to force reduction of the 4PB.
- Scaling. The scale used on the y-axis can give a wrong impression about the amount of scatter present in a sample. As the decline and incline at start and finish are relative huge, scaling the figure accordingly to those values can hide the amount of scatter. Second, due the amount of scatter RDEC values can become negative. This should be noted as a negative side of the method employed. However as shown in both figures the amount of negative points is relative low and not a mirrored substitute of the positive RDEC values.

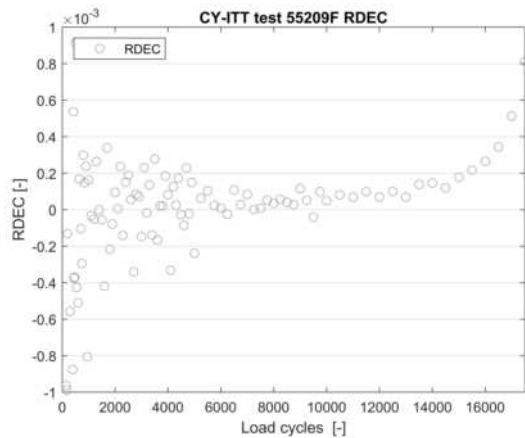


Figure 4.24: RDEC 19020 test 55209F

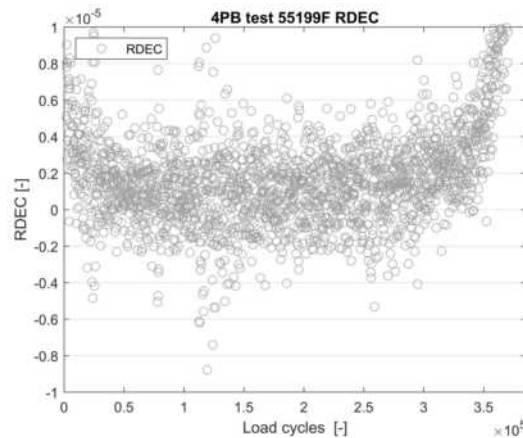


Figure 4.25: RDEC 19020 test 55199F

The three observations leads to three different conclusions. It is not possible to define a definite failure point in the scatter cloud. Second, with the amount of scatter and shape the constant Plateau Value in the RDEC figure is not definable. Third, neglecting of the negative values, or plotting only the positive values of RDEC, is hiding a negative aspect of the method. However if the PV value is established through a method that does not use the direct RDEC values, they can be left out for graphical representation.

From the previous figures is comes forth that establishing a accurate Plateau Value in the scatter is not straightforward. The same goes forth with establishing the N_{fat} . In the next section we discuss

three methods in establishing an accurate method of determining the N_{fat} through different methods and reflect them on the general RDEC curve. For these 3 methods we employ three different ways of calculating the PV.

4.3. Failure criteria & Plateau Values

In chapter 3 we used the simplified version of the full Energy Ratio ER to find the turning point in the stiffness curve. The method employed is the stiffness repetition method SN . To validate if this method can also be applied to the RDEC, we start with the full Energy Ratio as described by Hopman et al. [1989]. We compare the result with the simplified version that neglects the influence of the phase angle. The method most suitable will be applied. It is followed by a statistical approach of determining the N_{fat} . Establishing N_{fat} by either ER or SN will lead to establishing the PV by a fitting function over the linear assumed part of the dissipated energy curve as described in Chapter 2. The second method of calculating PV will be based on the statistical method. This method combines both establishing N_{fat} and PV in a single statistical approach.

4.3.1. Energy Ratio

The basis for the Energy Ratio is given by equation 2.37. Where the ratio based on the initial dissipated energy is multiplied by the load cycle and divided by the DE_n . The formulation is required as the DE-curve of the CY-ITT is only increasing. The 4PB is set by the inverse of $ER = DE_n * n / DE_1$. This method establishes a curve where the maximum reflects the turning point of the dissipated energy curve itself.

The method is applied on the same samples in figure 4.26 for the CY-ITT and in figure 4.27 for the 4PB. It should be noted that with the remarks placed in Chapter 2 the inverse of equation 2.37 is used for the 4PB. The general curve established does not deviate significantly from the SN method. Both the N_{fatSN} and N_{fatER} are given on the dissipated energy curve. The magnitude and the reason for the small difference found between the Energy ratio and Stiffness Repetition method is discussed in the next section.

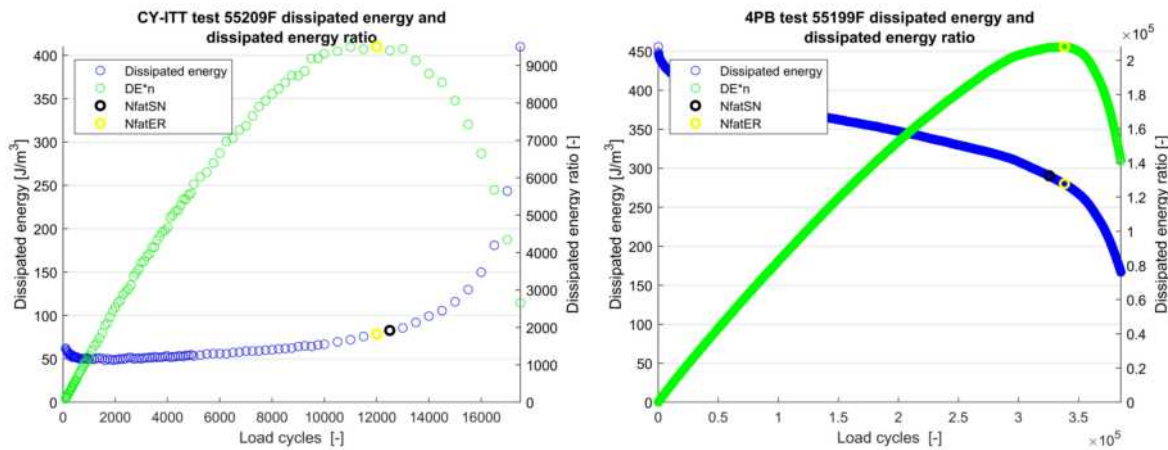


Figure 4.26: Energy Ratio and dissipated energy 19020 test 55209F

Figure 4.27: Energy Ratio and dissipated energy 19020 test 55199F

4.3.2. Stiffness Repetition

The failure criteria set by the simplified stiffness repetition method as explained in Section 2.4 resulted in a more accurate method to establish the transition point on the stiffness curve than the traditional 50% rule. In the previous figures of 4.26 and 4.27 the found N_{fatSN} is also given on the dissipated energy curve. The found difference was insignificant. However this is not always the case.

For the CY-ITT there can be a significant difference between both the N_{fatER} and the N_{fatSN} . For mixture 19020 the three different N_{fat} are given in table 4.1. The sample number and the initial strain

are given as an indication. Furthermore if a 50% reduction of stiffness could be found, it is given and the percentage of increase or decrease to N_{fatSN} . The last column gives the found N_{fatER} and the percentages decrease to the N_{fatSN} . From 4.1 it becomes clear that the Energy Ratio method gives an overall lower fatigue life than the Stiffness Repetition method.

Table 4.1: Mixture 19020 CY-ITT different N_{fat} .

Sample	strain ini	$N_{fat50\%}$	Δ	N_{fatSN}	Δ	N_{fatER}
55202F	115	26846	28%	21000	-10%	19000
55203F	57	125177	35%	92500	8%	100000
55204F	66	86559	15%	75000	-13%	65000
55205F	44			170000	0%	170000
55206F	67			65000	0%	65000
55207F	128	13227	26%	10500	-7%	9750
55208F	48	217892	28%	170000	-6%	160000
55209F	137	15527	24%	12500	-4%	12000
55210F	48			135000	-15%	115000

From table 4.1 we take sample 55210F as an example with the 15% difference found. The difference can be directly explained by figure 4.28. The Stiffness Repetition method based on the inconsistent stiffness curve leads to finding a higher N_{fat} than the curve should result to. It is clear that if the stiffness curve and the sample responded more consistent the SN method would suffice. In figure 4.29 the result by the Energy Ratio is given. The same wobble effect of the stiffness curve combined with the wobbling measured phase angle gives a slightly different curve. Resulting in a different N_{fat} . The phase angle seems to mediate the measured inconsistency and combined in the dissipated energy leads to a lower, more conservative, N_{fat} for the CY-ITT.

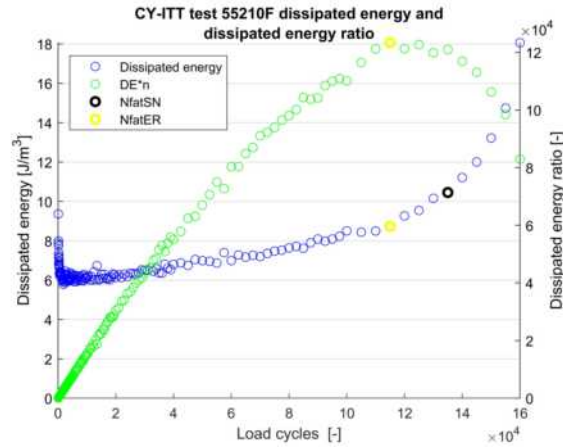
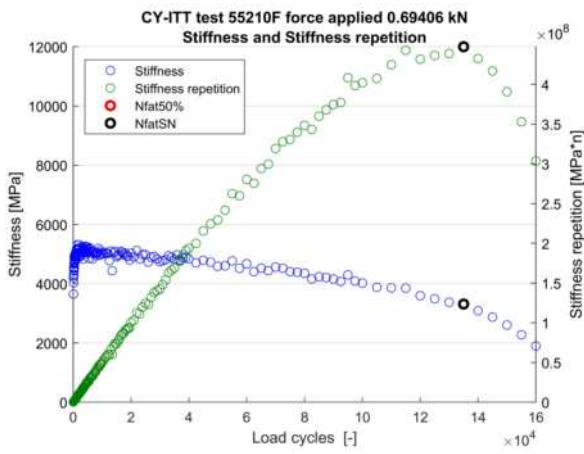


Figure 4.28: Stiffness and stiffness ratio 19020 test 55210F

Figure 4.29: Energy Ratio and dissipated energy 19020 test 55210F

The results for mixture 19020 for the 4PB compared to the CY-ITT show the opposite behaviour. In table 4.2 the results is shown for all 18 beams. Here the same results as given in Chapter 3 is observed for the difference between N_{fatSN} and the $N_{fat50\%}$. Higher fatigue life at the high strain ranges and lower fatigue life at the lower strain ranges applied. The difference between the N_{fatSN} and N_{fatER} is overall insignificant, but show a constant trend of being longer than that of the SN method.

We take sample 55915F with a difference of 9% between both methods. The result is given in figure 4.30 and 4.31, where both the SN and ER result is shown. The reason found for the difference is traced back to the non sudden drop of stiffness in figure 4.30. As mentioned by [Pronk, 2019] if the curve develops after the initial drop to a secondary linear trajectory, the repetition based method will find either one of the transition points based on the steepness of the secondary linear part. This is the case during the fatigue test of sample 55195 as well as of sample 55185F. In these case the full ER method

Table 4.2: Mixture 19020 4PB fatigue life for different N_{fat} .

Sample	strain applied	$N_{fat50\%}$	Δ	N_{fatSN}	Δ	N_{fatER}
55176F	238	87361	-2%	88935	3%	91490
55177F	206	221972	1%	220372	1%	223255
55179F	207	221294	5%	210372	1%	212895
55180F	146	1116344	12%	1000877	0%	1000877
55181F	268	55281	-46%	103106	3%	105910
55182F	151	1083075	8%	1006277	0%	1004477
55185F	145	1983238	9%	1825257	2%	1863056
55186F	273	52204	-18%	63392	5%	66647
55187F	206	277978	0%	278124	9%	303529
55188F	151	1082265	5%	1026076	1%	1036875
55189F	206	273474	-1%	276138	2%	282084
55190F	282	52931	-25%	70258	3%	72311
55194F	213	220768	-3%	226588	3%	234516
55195F	282	45150	-6%	48271	9%	52576
55196F	151	1079738	10%	981077	4%	1024276
55197F	289	53064	-14%	61644	2%	62695
55198F	151	730593	11%	658885	3%	678684
55199F	212	311811	-4%	325687	4%	338300

provides a better fit to the real transition point of both the stiffness as the dissipated energy curves. The method of using a correction factor k as Pronk suggested [Pronk, 2019], is due the rarity of the secondary linear trajectory phenomenon and the details about the exact slope influence parameter, left for a further more exact detailed study.

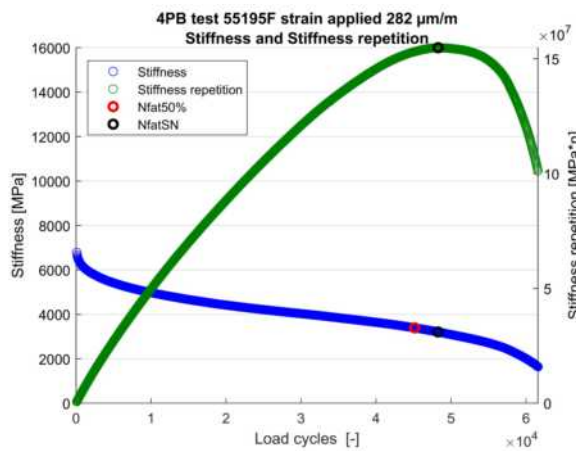


Figure 4.30: Stiffness and stiffness ratio 19020 test 55195F

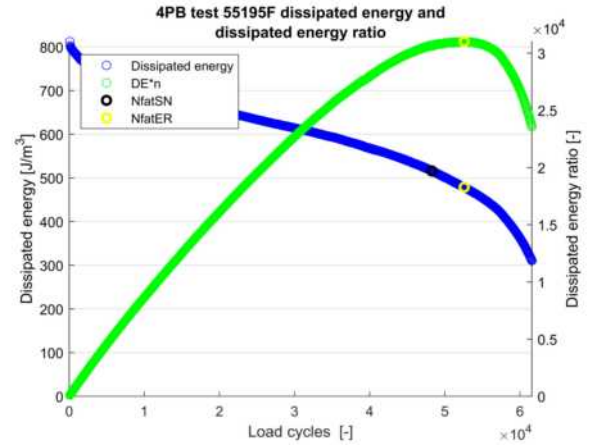


Figure 4.31: Energy Ratio and dissipated energy 19020 test 55195F

It should be considered that for the 4PB the delay caused in the finding of the maximum value of the Energy Ratio curve can be the cause of the increase of the phase angle. As shown in figure 4.23 the phase angle tends to increase at failure and the reason is discussed in Section 4.1.2. As the method determine the N_{fat} relative before this increase, it is considered a small influence on the N_{fatER} . The phase angle results should however be checked to be sure a non scattering or large increase occurs because of equipment failure as shown in the same previous section.

In the comparison between the Energy Ratio and the Stiffness Repetition method the ER method is the overall best method to determine the N_{fat} for the dissipated energy curve. It will therefore be employed in the next section to establish a consistent PV relation.

4.3.3. Fitting method

In Chapter 2 it was discussed that the RDEC is the first derivative of the dissipated energy and normalised with DE_n . Where the RDEC is almost constant is called the Plateau Value. This phase of the RDEC curve is almost same as the second stable phase of the stiffness curve. This can be stated because the phase angle is almost constant linear and the other parameters are directly related. We now can use a linear fitting process to eliminate the 'small' disturbances we see in the measurements which were leading to the high unpredictability of the PV at the moment of failure. This is the same method G. Airey proposed in his paper *New simplified approach for obtaining a reliable plateau value in fatigue analysis of bituminous materials*. In which he applies the RDEC method and finding a better constant PV values for DSR stress controlled testing [Airey et al., 2017].

We apply the fitting method through equation 2.17 on mixture 19020 on both the 4PB in figure 4.33 and on the CY-ITT in figure 4.32. The fitted linear line is applied after the first phase till the set failure point. For the CY-ITT the fitting starts after the initial increase of stiffness, which returns an initial decrease in the dissipated energy. This is set at $N=1000$. The 4PB fitting is applied after the initial exponential reduction and is set at $N=500$. We observe for the 4PB that the dissipated energy curve is not a straight line. Combined with the N_{fatER} we see that the fitted line is more gentle than the actual calculated RDEC value should be at the failure point. The second observation is that the displacement controlled 4PB, as stated before for the stiffness curve, does also not describe a linear slope in a dissipated energy curve. However the overall founded values for the fitted line do approximate a good Plateau Value. Keeping in consideration the limitations from the actual curve course.

For the CY-ITT in figure 4.32 the fitted line, after the initial thousand load repetitions, describes the linear slope in the dissipated energy. Only that the set failure point is above this linear fitted line. Resulting in a calculated RDEC value that correctly describes the second phase Plateau Value, but has a failure point that is outside the range of the linear slope. The remaining results for each individual type test that shows the same behaviour can be found in appendix B. Here for different mixtures with this fitting method are represented graphically to prove this method for the different mixtures, both on CY-ITT and 4PB.

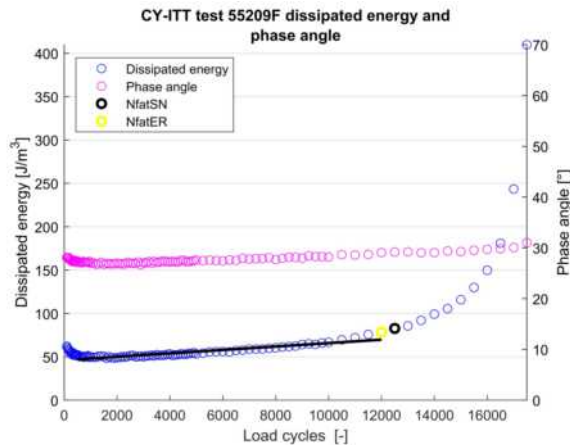


Figure 4.32: Dissipated energy CY-ITT 19020 sample 55209F

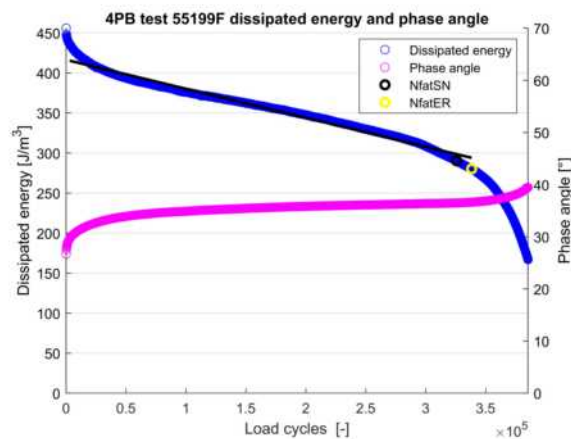


Figure 4.33: Dissipated energy 19020 4PB sample 55199F

For completeness the fitting method a 4PB and CY-ITT example are given for mixture 18590. The 4PB is given in figure 4.35, resulting in a good fit on the dissipated energy curve. So the linear fitted line can be applied as long as the difference in the two natural logarithm curves that describe the dissipated energy curve are not too great. This will result in a general linear line below the dissipated energy at the left side of the dissipated energy and above the dissipated energy curve at the right side. Averaging the overall slope of these natural logarithm curves. As both the N_{fatSN} as N_{fatER} are almost similar they are plotted on top of each other in both figures. For the CY-ITT in figure 4.34 we observe the same steady linear increase of the dissipated energy after the first initial settling of the sample. The applied

failure criteria is a good fit in finding the end of the linear envelope of the dissipated energy.

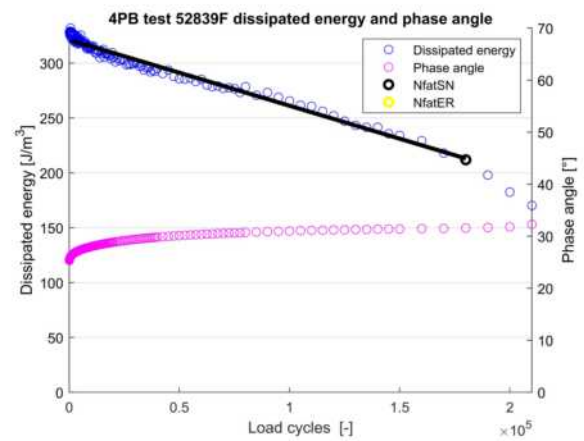
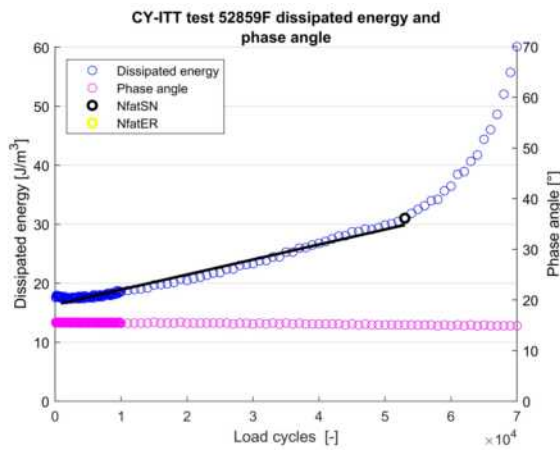


Figure 4.34: Dissipated energy CY-ITT 18590 sample 52859 Figure 4.35: Dissipated energy 18590 4PB sample 52839

The result from the fitted function is the non-normalised constant RDEC value. The result is normalised by the mean function of the same interval as the fitted function was applied. This results in the calculated PV coupled at the N_{fatER} failure criteria. It's result is given in figure 4.36 for the CY-ITT and in figure 4.37 for the 4PB. The scale is set only positive and for comparison the PV mean is also calculated. the PV mean is set as the average of the 10 RDEC values before N_{fatER} . It is given as a reference value towards the calculated PV fitted value. Second it gives a better comparison towards the calculated PV values through fitting and the set N_{fat} . If N_{fatER} is set in the third phase of the RDEC curve, the PV fitted function will still be calculated for the second phase. The reason is the set fitted function on the dissipated energy. However the PV mean will be way larger as these values are set by the RDEC. So it acts as a control. The reason it is not employed as a direct measure to set PV, is by the origin of the large and negative scatter of the RDEC. Note that the scale on y-axis varies with the calculated PV fitted value. It is found that this has to be at least a factor 100 smaller to graphically represent a good RDEC curve.

The result of the CY-ITT in figure 4.36 is given for the PV fitted and PV mean value. The found N_{fatER} seems to define the end of the Plateau Value quite good. The calculated PV does not vary a lot from the PV mean. Overall the applied method of N_{fatEN} and the fitted calculated PV works for the CY-ITT. For the 4PB in figure 4.37 the combination provides a clear and distinct end of the PV phase and provides a good N_{fat} on the RDEC curve. The calculated fitted PV is in the same range as the PV mean. The scattering overall is still significant to clearly define the absolute PV value by only observation. Other remaining results can be found in appendix B.

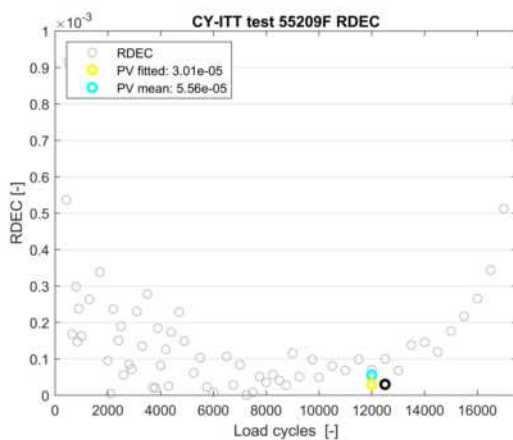


Figure 4.36: RDEC 18590 CY-ITT sample 55209

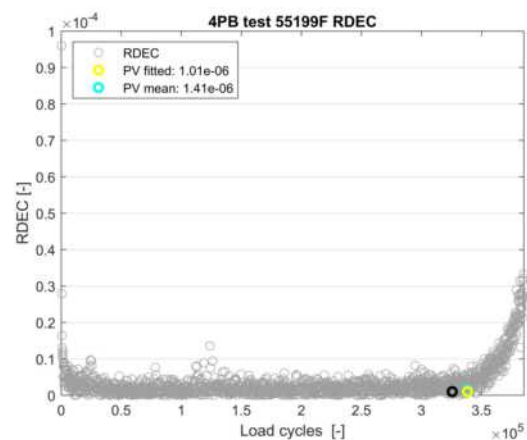


Figure 4.37: RDEC 4PB sample 55199F

Table 4.3: Mixture 19020 4PB Plateau Values

Sample	PV fitted (*10 ⁻⁶)	PV mean (*10 ⁻⁶)	ΔPV
55176F	3,78	0,53	7,1
55177F	1,37	1,47	-1,1
55179F	1,15	5,43	-4,7
55180F	0,22	0,29	-1,3
55181F	5,21	1,19	4,4
55182F	0,22	0,49	-2,2
55185F	0,13	0,35	-2,6
55186F	6,75	15,32	-2,3
55187F	1,20	3,54	-3,0
55188F	0,21	0,31	-1,5
55189F	1,18	21,29	-18,0
55190F	6,44	16,29	-2,5
55194F	1,51	0,49	3,1
55195F	7,89	27,49	-3,5
55196F	0,28	0,79	-2,9
55197F	6,47	5,65	1,1
55198F	0,35	1,27	-3,7
55199F	1,01	1,41	-1,4

Table 4.4: Mixture 19020 CY-ITT Plateau Values

Sample	PV fitted (*10 ⁻⁶)	PV mean (*10 ⁻⁶)	ΔPV
55202F	18,72	19,78	-1,1
55203F	3,66	3,99	-1,1
55204F	5,53	5,32	1,0
55205F	1,74	1,90	-1,1
55206F	5,89	6,02	-1,0
55207F	38,13	37,94	1,0
55208F	1,36	1,63	-1,2
55209F	31,70	30,08	1,1
55210F	2,19	2,72	-1,2

To find the overall comparison between the fitted and mean PV values the results for mixture 19020 is given in table 4.3. Here the results are given for the CY-ITT and 4PB and the magnitude in difference ΔPV between PV fitted and PV mean. At $\Delta PV = 1$ the methods are equal. The factor is set negative if the PV fitted is smaller than the PV mean, meaning that the PV mean results in a higher PV. However it shows that the ΔPV differs greatly for the 4PB. The reason again being the influence of the scattering on the RDEC values. For the CY-ITT the ΔPV is far more consistent. The reason explained by far lesser measurements in the number of load cycles. Resulting in a significant difference between them. Second the increase is almost consistent linear, resulting for both the PV mean as PV fitted in better results.

In this section the previous established N_{fatER} is combined with the fitted function on the dissipated energy. The overall results seems to find a constant and good value of the PV. Both for the CY-ITT and 4PB. The comparison made between the PV mean and PV fitted was clearly in favor for the fitted function approach. In the next section a short result is presented about the application of a statistical approach to establish both the N_{fat} and the PV.

4.3.4. Statistical method

In this section the application of the statistical method result is discussed. The method is employed to establish a relation between the N_{fat} and the resulting PV. In this method both parameters are found through a single statistical equation and boundary condition instead of two different concepts in the previous section. The full description, theory, discussion and results can be found in Appendix F.

The method itself is based on the works of [Telman, 2017]. The goal was to validate and compare the results found with the results obtained in this paper. As stated in Chapter 1 the results presented by Telman are the only working examples in linking the CY-ITT and 4PB through the RDEC method, which makes it important to discuss.

The statistical method is based on a fitted function through the dissipated energy curve. The function itself is based directly on the derived PV equation on the RDEC curve. Resulting in a almost linear line at the lowest established PV. The starting point is chosen arbitrarily but should be at the center of the second phase of the DE curve. The latter is kind hard to establish as each test is in practice determined at a different moment, but can be manually done. The fitted equation is described as:

$$Y = DE_o \cdot R^{n-n_o} \quad (4.2)$$

where: DE_o = Starting point of the fit on DE curve
 R = exponential parameter term for PV = R-1

The boundary condition is set by the absolute difference of the measured DE value minus the fitted predicted value and the 95% confidence interval. Where the confidence interval is build upon the standard error of both the predicted and the measured dissipated energy curve. For a full description see [Telman, 2017] and appendix F.

The overall result was that the 95% confidence interval boundary condition combined with non linear behaviour of the dissipated energy curve terminated to quickly to be representable as a good solution. The two main reasons for this were: The DE curve of the 4PB test has a tilting point halfway the stable assumed phase. Choosing a starting point before or after affected the script in a way the fitting function saw it as the failure point and terminated. the reason for this is that the actual DE slope decreases and increases over the tilting point in phase two. Creating a shift if the fitting functions starts on either side of the tilting point. Second the amount of scatter in the DE curve, especially of the CY-ITT, leads to manually establishing each function by neglecting these local disturbances. Resulting in also having to manually determine the actual failure point, as these could also be subjected to scatter or a local disruption.

In the current setup the method is not further explored or presented, as the manual practical multi mixture application was not feasible in the time frame of the thesis. As the results in the latter sections agree on the results found by Telman, the mechanical-empirical established results could be directly supported with the statistical results. Reinforcing the final results and the findings in this report.

A recommendation from this meager result is therefor to look with the original author to further develop the statistical method and to compare those results with the later presented results established through the Energy Ratio failure criteria and the fitted method. In the next section a theorised optimal RDEC result is presented as a further explanation and comparison of the established methods.

4.4. Theoretical approach and result

For both the 4PB and the CY-ITT a theoretical dissipated energy curve is constructed by the means of a natural logarithm curve that describes a standard dissipated energy curve. The goal is to verify the applied methods on a theoretical perfect Dissipated Energy curve. As the previous section with the statistical method failed to provide a more in depth look. From these curves the RDEC is calculated and the applied methods are given and discussed.

The resulting theoretical curves are given in figures 4.38 and 4.39. The curves describes a $\ln(x)$ function. The 4PB results in figure 4.38 is fitted through a number of curves from mixture 19020. The curve is then mirrored and flipped at $x = 5000$. The CY-ITT result in figure 4.38 is without the initial drop of the DE. This drop is an unwanted practical result of the force controlled test, which in theory should not happen in a force controlled test. The curve is also a $\ln(x)$ function, however the increase over the number of load repetitions is set very low as a force controlled test shows in practise.

The Energy Ratio method is applied to find the N_{fat} on both dissipated energy curves. Both figures show an overall good fit in establishing the end of the fatigue life. It should be mentioned that if the curve of the $\ln(x)$ function is set at a higher increase, the CY-ITT N_{fat} is established far sooner as the linear stage of increase is ended far sooner.

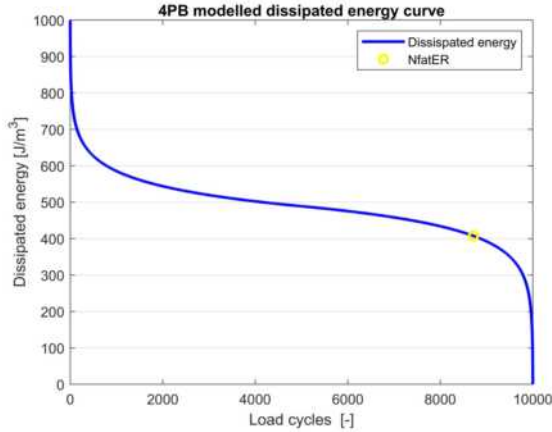


Figure 4.38: Modelled 4PB dissipated energy curve

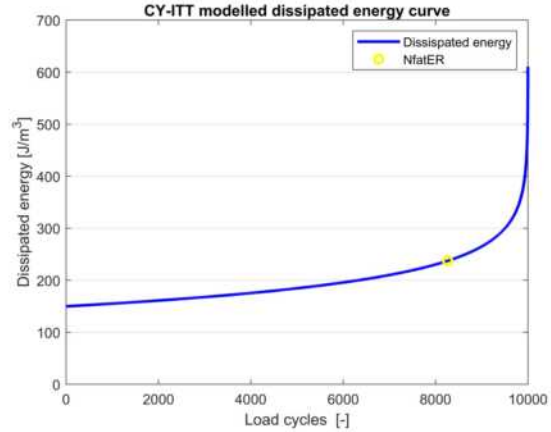


Figure 4.39: Modelled CY-ITT dissipated energy curve

The RDEC results from the DE curves are given in figures 4.40 and 4.41. The Plateau Values are established through the fitted method in combination with the Energy Ratio and the PV mean is given as a reference.

The 4PB result is an almost identical result as 2.16 from Chapter 2. The Plateau Phase is however not an almost straight line. The reason is that the DE is modeled as an $\ln(x)$ function, which is the closest to standard displacement controlled short and medium fatigue type test. Only the longer fatigue type test show an linear development in phase 2. If the second phase is modeled through a linear line in DE, the RDEC result would show a constant increase over n . The reason for that is that with a linear decrease of DE_n over n , the RDEC equation will increase.

For the 4PB the fitted PV value is a factor 10 smaller than the PV mean at N_{fatER} . The explanation and limitations of the fitted approach comes to bear with this perfect RDEC curve. The applied fitted line between $n = 2000$ and N_{fatER} is a linear or almost linear equation. Applying equation 2.17 or equation F.4 does not differ a lot, as the latter method is set as an almost linear equation. The result however does give the PV in the second phase overall. It is not the lowest RDEC value or the average value. The reason again is that DE_n changes non-linear over n . The perfect fitted line equation is therefore not possible. The set equation is however as we have seen in table 4.3 a good overall fit with the overall scattering of the type test values.

In figure 4.41 the RDEC result is given for a modelled CY-ITT. As DE is not influenced by the initial test disturbances, the RDEC curves starts without the initial drop in phase 1. The typical presented bath-up shape is therefore not applicable to a perfect force controlled test. The PV fitted result is again a factor 10 lower as the RDEC value at N_{fatER} . The PV mean is set already in the failure envelope. The PV fitted value is with the assumption that the $\ln(x)$ function is near linear between zero and N_{fatER} , the near average RDEC value in the set range. It is near because again the DE_n changes over n , which gives a slight increase over the RDEC values.

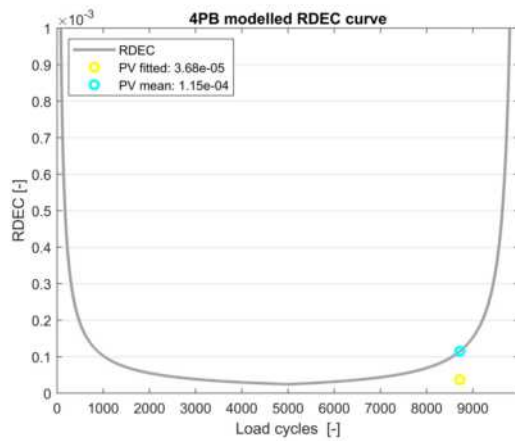


Figure 4.40: Modelled 4PB RDEC curve

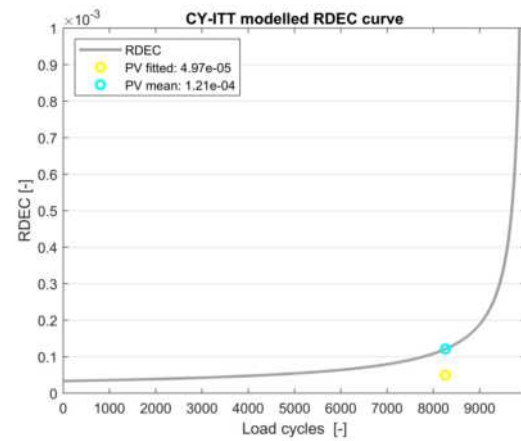
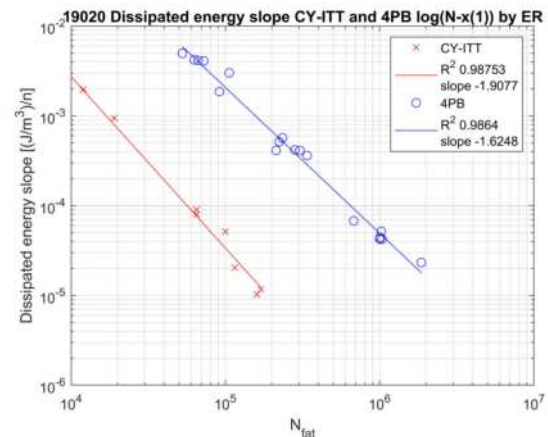
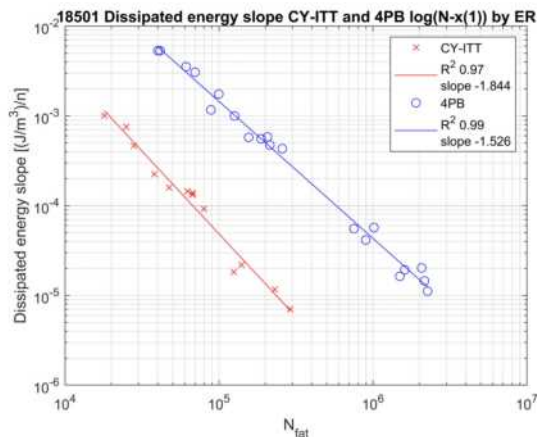


Figure 4.41: Modelled CY-ITT RDEC curve

The modeled dissipated energy curves in this section gives an almost perfect practical representation of the real found RDEC curves. The applied failure criteria holds in these modelled curves. The applied linear fitting method finds Plateau Values far lower as the RDEC values at failure. However the PV represents the assumed constant RDEC values in phase 2. Therefore the relation between PV and RDEC at failure should be decoupled. Meaning that the $PV - N_{fat}$ relation is not directly related to the $RDEC_{N_{fat}} - N_{fat}$.

4.5. Influence of the non normalised RDEC

In the previous subsections the fitting method and the N_{fat} were discussed. As the method is highly dependent on the slope of the dissipated energy curve through equation 2.17. We shortly discuss using only the change of dissipated energy from mixture 18501 and 19020 in combination with the Energy Ratio failure criteria on a log log scale. This results in a comparison on the measured dissipated slope parameter $x(1)$ from equation 2.17. Or the amount of dissipated energy per load cycle plotted against the number of load cycles till fatigue for both the CY-ITT and 4PB. These results are shown in figure 4.42 for mixture 18501 and in figure 4.43 for mixture 19020.

Figure 4.42: Dissipated energy slope $x(1)$ for mixture 18501 Figure 4.43: Dissipated energy slope $x(1)$ for mixture 19020

With the non normalised dissipated energy ratio we observe from figure 4.42 and 4.43 that the 4PB describes a higher dissipated energy rate per loading cycle in the second or stable phase of the fatigue test. It should be compared vertically at a certain number of N_{fat} . This can be due the fact that the 4PB is performed on 30Hz and the CY-ITT on 10 Hz. Another explanation could be that the applied

strains to 4PB are much higher than those applied to a CY-ITT test specimen as we saw in Chapter 3. Resulting with the set formulation of the dissipated energy a higher value will be found. That in combination with the higher N_{fat} the shift factor between the CY-ITT and 4PB is significantly great.

The rate of energy dissipation between the CY-ITT and 4PB is significant. Normalising the dissipated energy slope in figure 4.42 with the average of DE, is an accurate way of bringing the two type tests in line. The question could rise in how the $x(1)$ values are related to each between mixtures. So in how would a different mixtures with an significant higher fatigue life as shown in Chapter 3 would compare in the dissipated energy rate per load cycle?

Concluding from Chapter 3 we use mixture 18607 instead of 19020. 18607 is PMB modified and showed a significant difference in the $\log(\varepsilon - N_{fat})$ values in figure 3.42. Indicating a significant difference in the strains applied to the samples. In figure 4.44 the result is given for the 4PB for mixture 18501 and 18607. The found dissipated energy slope or rate of dissipated energy $x(1)$ for both mixtures show a significant difference if plotted against the N_{fat} . The lines are shifted over the diagonal off the found $x(1) - N_{fat}$ relation. Meaning that a mixture that performs better in fatigue does deviate diagonally with the other mixture. The higher value of $x(1)$ is logical from the fact that the same amount of load repetitions is achieved through a higher strain rate. Which result in relative more fatigue damage per load cycle. From this we can conclude that a relation through $\log(N - x(1))$ is distinctive for a 4PB displacement controlled fatigue test.

Although the resistance to higher strain level is proven for mixture 19020, the slope of dissipated energy is almost the same compared to mixture 18501 in figure 4.45. The $x(1)$ is therefore mixture unique but a hard to distinguish difference between mixtures. If the $x(1)$ is plotted against the ε_{ini} the relation between the applied strain level and the slope would be more significant.

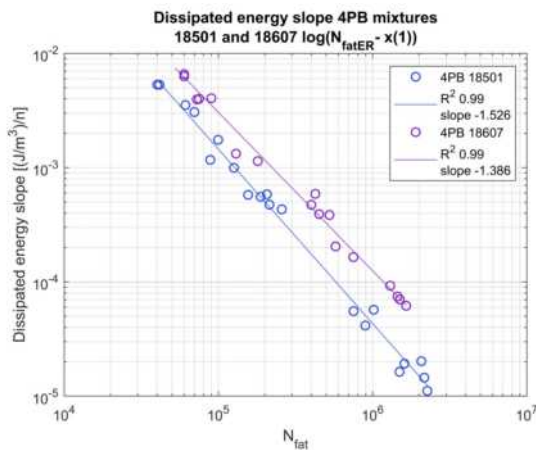


Figure 4.44: 4PB Dissipated energy slope $x(1)$ for mixture 18501 and 18607

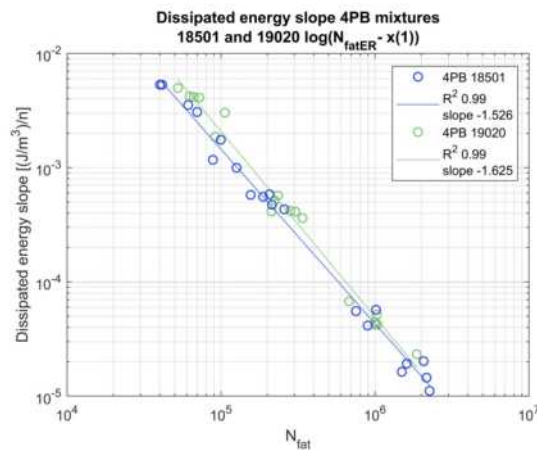


Figure 4.45: 4PB Dissipated energy slope $x(1)$ for mixture 18501 and 19020

4.6. Mixture results

To establish the significance and impact of the RDEC method on the fatigue behaviour of the CY-ITT and 4PB, the result of different mixtures are presented in this section. This to show if the applied methods in the previous sections consistently holds or that a significant difference is found for different type type of mixtures.

4.6.1. Individual $PV - N_{fat}$ Results

Combining the theory, statements and results from the previous sections we can calculate the $\log(N_{fat} - PV)$ relation for all the different mixtures. The Energy Ratio method is used for finding N_{fat} combined with equation 2.17 to find PV. The results for the different mixtures are presented in figure 4.46 till 4.57. The resulting figures are consistent with in red the CY-ITT and the 4PB in blue. Differences as the CY-ITT on road extracted cores in figure 4.48 and CY-ITT partially performed on 30 Hz in figure 4.55, are given in green. The general coherence between the two type tests is given with the black line, representing the overall fit off all measurements combined.

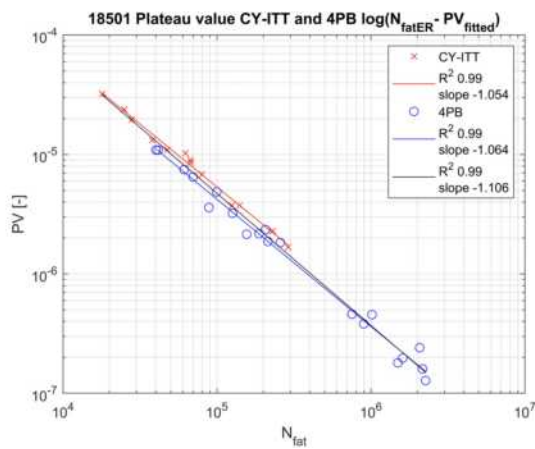


Figure 4.46: Plateau value line 18501

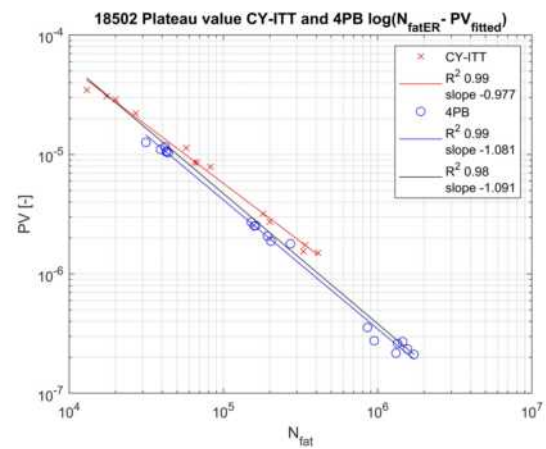


Figure 4.47: Plateau value line 18502

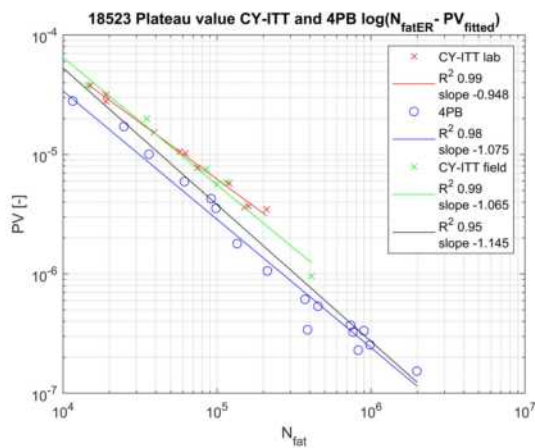


Figure 4.48: Plateau value line 18523

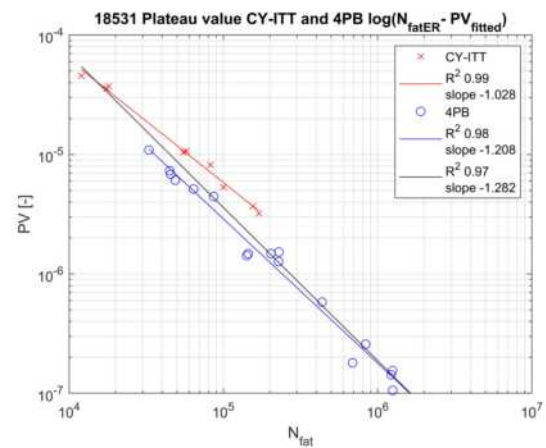


Figure 4.49: Plateau value line 18531

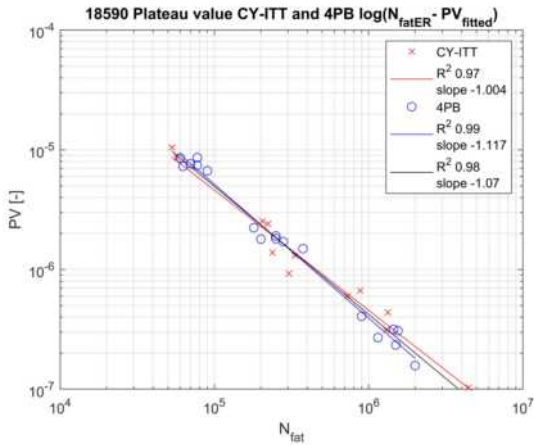


Figure 4.50: Plateau value line 18590

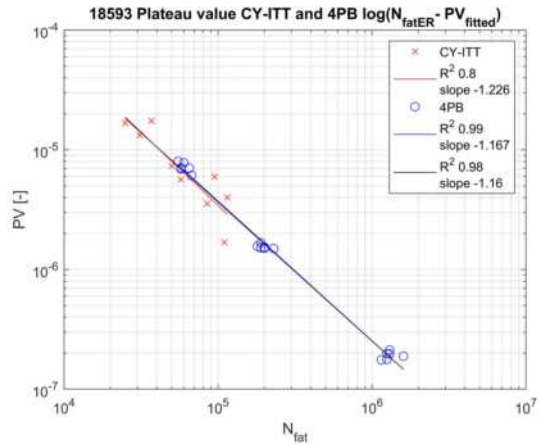


Figure 4.51: Plateau value line 18593

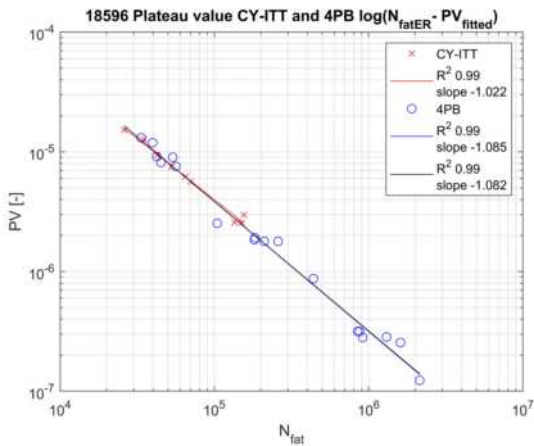


Figure 4.52: Plateau value line 18596

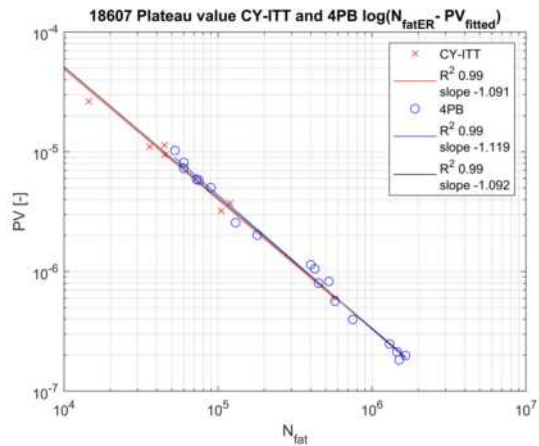


Figure 4.53: Plateau value line 18607

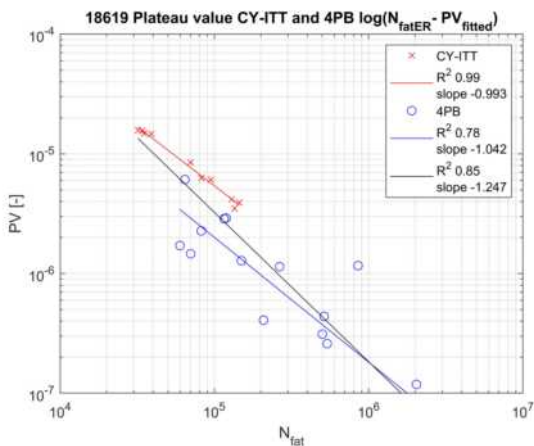


Figure 4.54: Plateau value line 18619

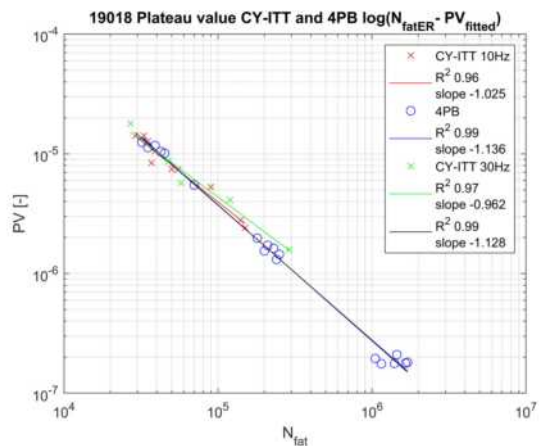


Figure 4.55: Plateau value line 19018

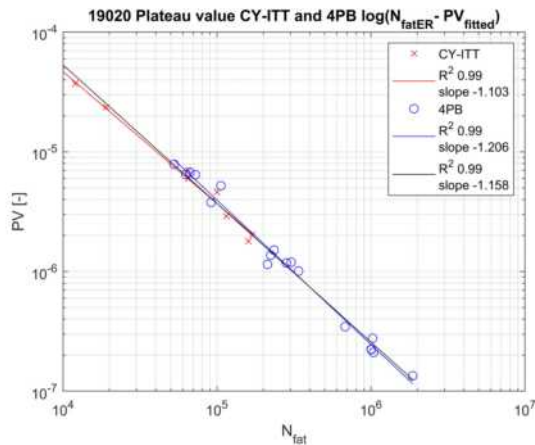


Figure 4.56: Plateau value line 19020

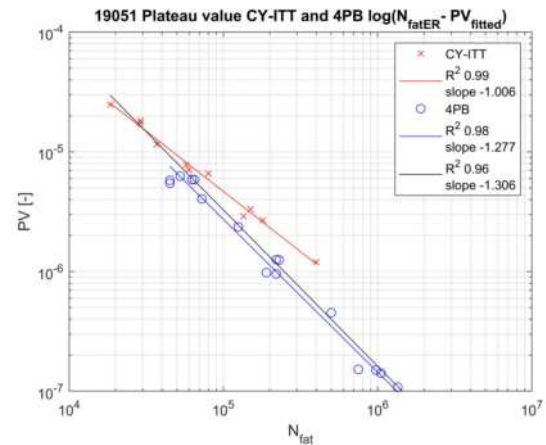


Figure 4.57: Plateau value line 19051

From the previous figures we see that six mixtures perform on a single $PV - N$ relation and six mixtures show a shift behaviour between the 4PB and the CY-ITT. The shifted mixtures are: 18501, 18502, 18523, 18531, 18619 and 19051. The shift occurs on a parallel plane where the CY-ITT results are consistently higher. There is an almost constant shift and slope difference between the CY-ITT and 4PB PV results. The exception of this is mixture 19051, where the CY-ITT is significantly less sloped compared to the 4PB. From the mixtures that have a shift the CY-ITT is above the 4PB. This is the opposite of the found dissipated energy slope in figure 4.42, where the 4PB does describe a higher rate of dissipated energy per load cycle. The normalisation with DE_n degrade that difference to almost zero, as shown in figures 4.46 till 4.57.

As half of the mixtures perform in the single $\log(PV - N_{fat})$ relation and the other half not, considering the different mixture compositions, there is no distinct relation with the mixture design. The differences or similarities are discussed below:

PR content

The amount of PR had a negative influence on the traditional 4PB results in Chapter 3. For the CY-ITT it however improved the fatigue life significant to the 4PB for two mixtures. For the 4PB PR content is causing a larger scatter en lower R-squared values. The same is not true for the RDEC method. Mixtures 19020 and 19051, both with around 50% PR, don't show more scatter than mixtures without PR. Only mixture 18619 with the high amount of 85% PR is scattered. The PR also does not explain the shift between the CY-ITT, as 19051 and 19020 both have large PR content and the one is shifted and the other not.

Temperature

The temperature does not influence the RDEC method. With the single mixture 18609 performed at different temperatures for the CY-ITT and 4PB. Where the CY-ITT is performed on 10°C and 4PB on the standard temperature. As the mixture also contains PMB, the RDEC is not influenced by both factors.

Test equipment

Three different test setups were used for the experiments. Given in appendix A. The differences found between the mixtures and the used specific test setups do not correlate with the 6 mixtures that fall on the same PV line.

Test frequency

Mixtures 18590 and 19018 were tested on different frequencies. As the CY-ITT with mixture 18590 was completely performed on 30 Hz and mixture 19018 partly, they show a good fit with the 4PB. For mixture 19018 with CY-ITT both on 10 and 30 Hz the overall fit between the different frequencies is good. From this we state that the RDEC method with these methods applied is frequency independent.

Field cored

The CY-ITT from mixture 18523 was lab en field prepared with 50% foam bitumen. The PV line is shifted between the 4PB and CY-ITT, however this is not the case for mixture 18596 which also contains foam bitumen. In that mixture the PV line is a single line between both test setups. The field and prepared specimen show a good correlation between them on the PV line. The traditional fatigue line in Chapter 3 didn't show this behaviour. From that we could say that the method maybe be useful for the relation between field and laboratory.

Overall there is no distinct mixture type or test setup explanation available why the different mixtures do or do not fit on the PV line. The explanation should be sought again in the found relation between the N_{fat} and the PV . Where the N_{fat} is rigidly directly related to the number of load repetition and the dissipated energy curve. The calculated PV is however more susceptible to variation. The applied fitting and normalisation is highly dependent on the dissipated energy and the slope of the curves. This dependence is set by the differences found between figures 4.42 and 4.46. The slope of the dissipated energy and the found PV values differ significant and the set normalisation shifts both 4PB and CY-ITT together. The slightest error in the applied fitting or disturbance during testing can alter the outcome of the test.

To state the high susceptibility of the Plateau Value, the result with a PV_{mean} is given in figure 4.58 for mixture 19020. The PV mean is the average of the 10 RDEC values before N_{fatER} . It acts as a comparison for the established fitting principle through the dissipated energy to find PV. It also acted as the reason for needing the fitted method in the first place. From the PV_{mean} result in figure 4.58 the amount of scatter and the low R-squared result shows this clearly. The comparison can be made with figure 4.55, where the R-squared value was 0.99. The fact that both CY-ITT and 4PB are still on the same line is coincidence and is not consistent for other mixtures.

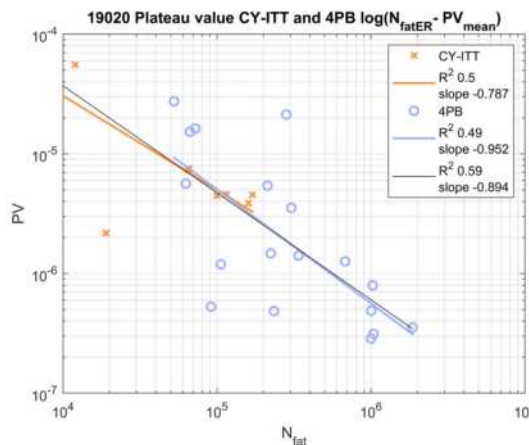


Figure 4.58: Plateau value line 19020

The applied fitting method and established of the PV through the fitting method and the susceptibility of the slope $x(1)$ leads to extraordinary high R-squared values. Meaning that the overall fit is excellent. The only exception is mixture 18619. The rest of the mixtures show an R-squared value of 0.98. Even the shifted mixtures show both for the individual CY-ITT and 4PB high R-squared values. This high fit with the normal amount of scatter can therefore only be explained through the applied fitting function. Thereby making the method of finding PV highly dependent on this fitting equation.

To conclude the results found in figures 4.46 till 4.57, Is the RDEC method loading mode independent? With half the results show a perfect correlation and with the other half not it is not directly a confirmed theory. From this results two possible explanations and possible relations are explored in the next sections. First, all mixtures are plotted together to find the uniqueness of the RDEC method. Second the influence of the mode of loading on the same specimen size, more precise: Force controlled loading mode on 4PB specimen. Third, the influence of the specimens shape. This by a displacement controlled fatigue test on an uni-axial shaped sample. Fourth, The influence of the density of different

made samples. This to discuss the applicability of the method from field to lab comparison and distinction.

4.6.2. All mixtures

The previous results from each individual mixture on 4PB are compared in figure 4.59 on page 79. The difference shown between the mixtures is almost nil. The PMB modified bitumen mixture 18607 falls on the same line as the 18501. Most mixtures are clustered together on this line. Only the mixtures with higher PR content showing more scatter do diverge from this single relation. These are 18523, 18619 and 19051. A remark can be placed in stating that higher performing mixtures are somehow situated lower on this single line, 19051 as an example. However this is illogical if you regard that the applied strain function is normalised by that same strain function. All with the goal to create a load, temperature, frequency independent method. This is also confirmed by the original paper of Shen & Carpenter. [Shen and Carpenter, 2007] Resulting that it is also asphalt concrete mixture property independent.

If you compare the 4PB results with the results of the CY-ITT $\log(N_{fat} - PV)$ in figure 4.60 this previous behaviour is more explicitly visible. The CY-ITT has due it's almost linear increase of strain amplitude a very steady and good fitting for finding the PV value. With this the deviating behaviour from the 4PB, again small variances in $x(1)$, is vanished and the RDEC method comes to it's full theoretical potential. Resulting in the single function on the $\log(N_{fat} - PV)$. Independent of temperature, frequency and asphalt concrete mixture properties. However as shown in the previous section the modes of loading are significantly different with the differences found in the measured slopes. The influence of the mode of loading is studied in the next section.

Take note that the previous mentioned influence of the permanent deformation on the CY-ITT fatigue tests from Chapter 3 that could possible be interfering with the fatigue results does not show in figure 4.60. Although assumed trivial at the center in Chapter 2, the mixture unique properties could still manifest itself. However with the RDEC method this is none distinctive between mixtures. If you would compare it directly to the 4PB from the previous section, the possible large shift of the two high stiffness and permanent deformation resistance mixtures could be an explaining for this case. If that would be true however the 4PB coupled CY-ITT $PV - N_{fat}$ is none existent.

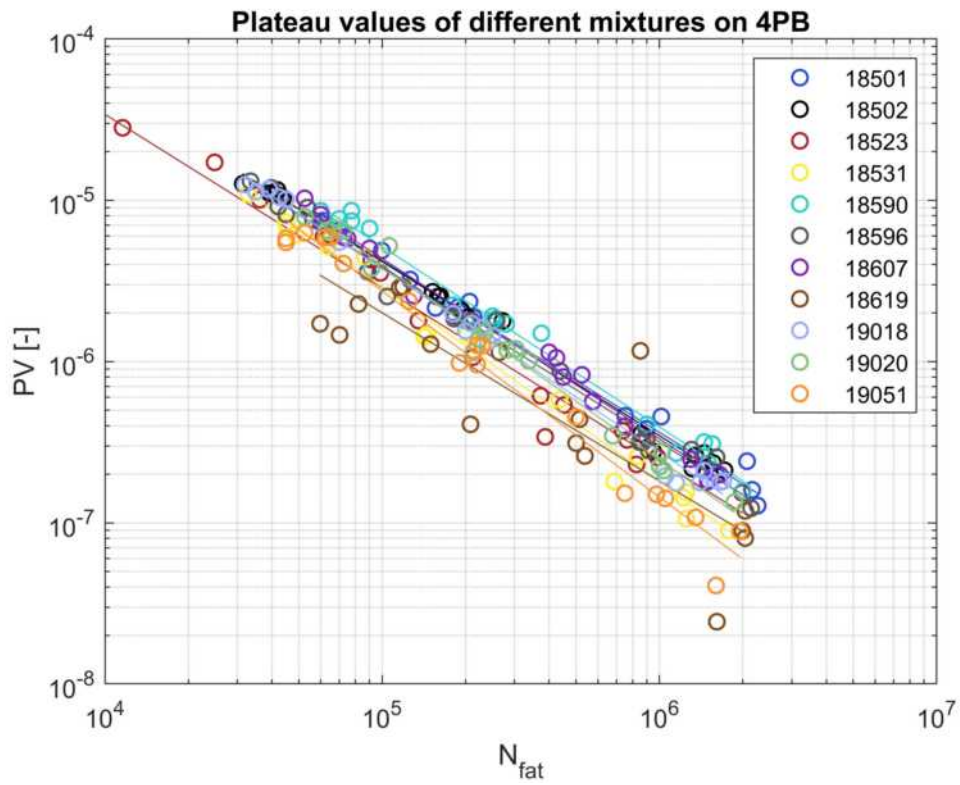


Figure 4.59: Plateau values for different mixtures on 4PB

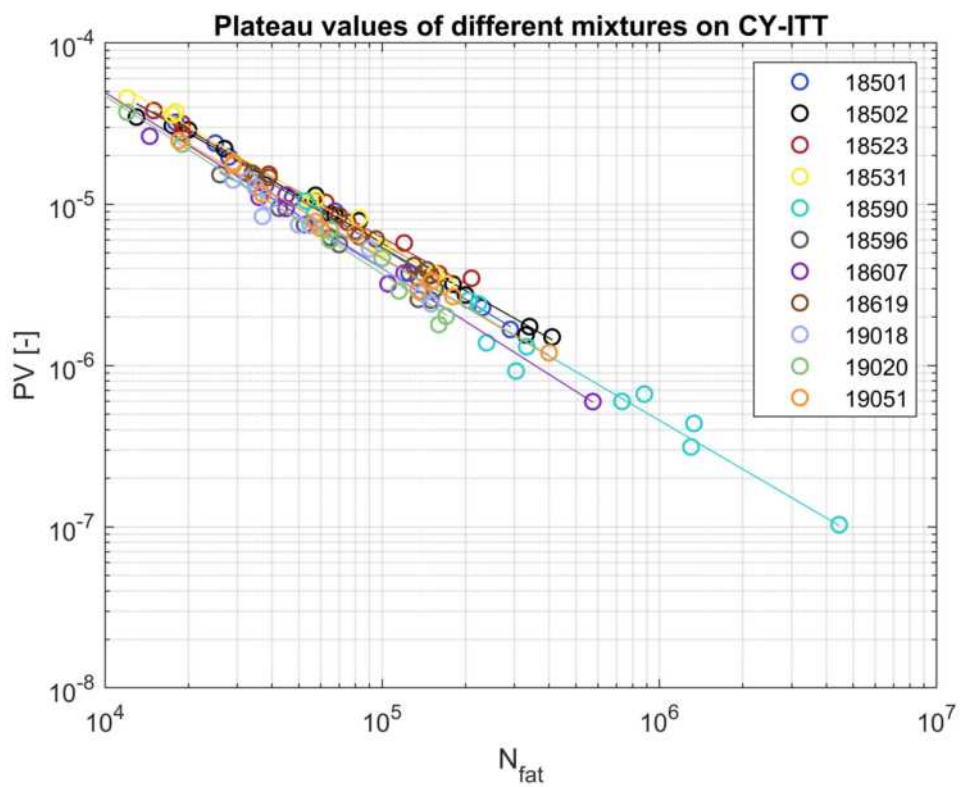


Figure 4.60: Plateau values for different mixtures on CY-ITT

4.7. 4PB force controlled

From the previous section we concluded that the plateau value lines are not a consistent single coherent line. To study the influence of the mode of loading on the fatigue life development, fatigue type test data was searched from previous research performed at the TU Delft and then apply the development methodology of RDEC on that test data. This would save the need to perform own testing and with that time. Li performed in the PhD thesis: *Asphalt mixture fatigue testing, influence of test type and specimen size*, a series of fatigue tests at 5°C at 10 Hz on both displacement and force control.[Li, 2013]. The data was the only one available, but was limited in use to make good conclusions on the influence of force control and the difference found between the two modes of loading.

From those results, an own experiment on force controlled 4PB was carried out. To get a good first impression of the general behaviour, testing conditions and adjustments needed for a stress controlled 4PB test, a total of 21 beams from project 18619 were laid to rest for 3 months after being tested on fatigue life at the laboratory of KWS. Testing was performed at department of Civil Engineering at the TU Delft. The choice to test at the TU Delft was done on the base of the unpredictability of the force controlled test on the testing equipment and the possibility of damaging it. This resulted that not the standard Zwick-Roell or MTS equipment and software could not be used. With the software at the TU Delft outdated and outperforming the wishes to perform the research, there was first the need of updating the software, which took the time of eventually performing the force controlled 4PB test on freshly cut specimen specially prepared for this type test.

The testing was performed on the own constructed equipment of the TU Delft. Because of the nature of a force controlled 4PB test constant monitoring was needed. A beam under flexural displacement mode of loading always have the same amplitude displacement. With that also a constant neutral line. From the initial condition the own weight of the beam is compensated by applying a small constant upward force. A force controlled test applies a certain force amplitude, with that a constant neutral line does not exist. This only exist if both sides are equally stiff and the mass of the beam is exactly compensated. This practically never happens, resulting that the beam has a tendency to deform to a certain side during testing. This can be compensated by adjusting manually the mean applied force or set point during testing. This compensation is mostly needed after the initial few thousand load repetitions. After which an equilibrium between the two outer edges is established. These adjustments also mean that the applied force is not a true sinusoidal signal but an haversine signal. The resulting displacement signal is then as close as possible to the sinusoidal displacement and no mean deviations for the deflections are being observed.

In this section the results are first presented with the Stiffness Repetition failure method on both the work of Li as on project 18619 for the force controlled stiffness curves. Confirming the method can be also applied on force controlled 4PB specimen. Following that the Energy Ratio failure method is applied with the fitting method on the dissipated energy to find the accurate PV on the RDEC curves. All type test results can be found in appendix C and D.

4.7.1. Stiffness Repetition on 4PB force controlled

The method of using the stiffness repetition as a good failure criteria is showed in section 2.4. This failure criteria can also be applied on a force controlled test. In figure 4.61 and 4.62 two examples are shown of 18619TU of the results for using the Stiffness Repetition method on force controlled 4PB testing. As shown the method proves a very coherent and strong result in finding the tipping point of the Stiffness and with that the failure of the specimen in fatigue. If the failure method of 50 % reduction of Stiffness was used the tipping point was clearly past and the specimen was already failing. So the Stiffness Repetition method proves that it also works for force controlled 4PB testing. Take note that the curious increase of the stiffness we saw at the CY-ITT also happens with the 4PB force controlled testing. The reason now can't be compaction wise as there is no constant force applied. The exact reason why this increase happens is unknown to the author. This disturbance will however be the reason again for the initial phase of the corresponding RDEC curve. The remainder of the results of the 18619TU project can be found in appendix D.

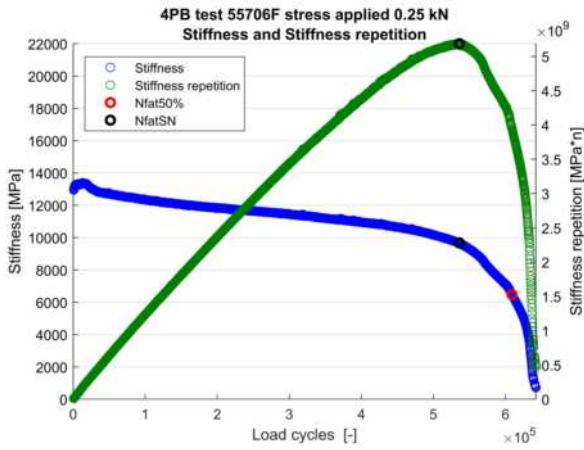


Figure 4.61: Stiffness and Stiffness Repetition, test 55706 force controlled

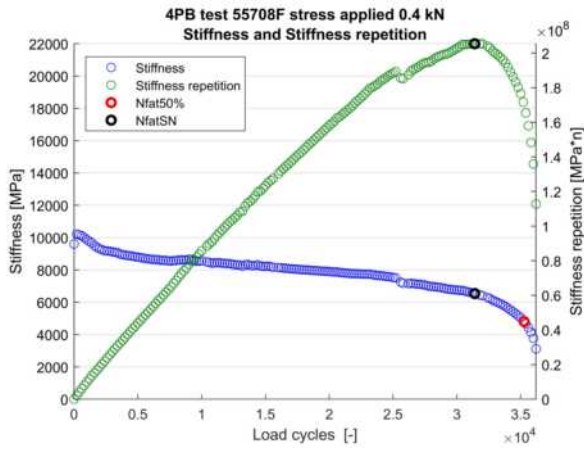


Figure 4.62: Stiffness and Stiffness repetition, test 55708 displacement controlled

Li's work that was used as the initial database, performed a displacement and force controlled testing, but on 5°C. In total 7 force controlled tests and 6 displacement controlled 4PB tests were performed. The results can also be tested and seen if the Stiffness Repetition failure criteria works for lower temperatures. For both force and displacement control one example is shown for the results in figure 4.63 and 4.64. Both figures show a relative high stiffness values, but this is due the low temperature. It also shows the failure criteria N_{fatSN} works for lower temperatures. The remainder of the test results can be found in appendix C.

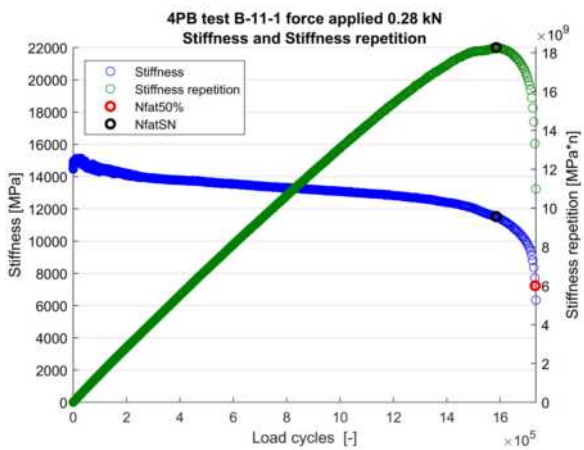


Figure 4.63: Stiffness and Stiffness Repetition of test B-11-1 force controlled

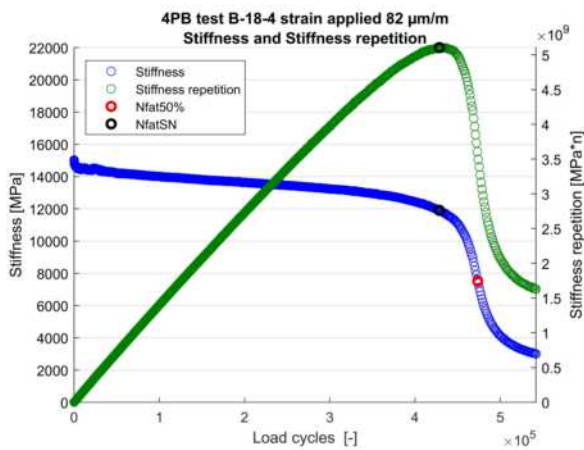


Figure 4.64: Stiffness and Stiffness Repetition of test B-18-4 displacement controlled

4.7.2. RDEC result

For the RDEC and dissipated energy we use the Stiffness Repetition method instead of the Energy Ratio. The reason is that the used capturing technique wasn't accurate enough to determine a steady phase angle through a combined FFT and fitting approach of each individual capture. From Section 4.3.2 we concluded that the overall results don't vary much between both methods and the phase angle stabilises the found result. In this case however the phase angle destabilized the found N_{fat} . Using the method presented in Section 2.3.3 of fitting a linear regression line on the dissipated energy curve and using the proved method of $SN = S_i \cdot N_i$ and we can construct the $\log(N_{fatSN} - PV)$ relationship. First the results for the phase angle, dissipated energy and the RDEC are given from the works of Li, followed by project 18619.

4.7.2.1. Li results

The same two type test are used to present in figure 4.65 and 4.67 the development of the phase angle and dissipated energy against the number of load cycles. Where in the first figure the energy dissipation of a force controlled test is given and in the second figure, the displacement controlled test. The strange thing that occurs in comparison to other displacement controlled type test, is that the dissipated energy follows an upwards slope instead of the downward slope in the B-18-4 test. This shows that the influence of the small increment of the phase angle is larger than the decrease of the applied force over time. Not all displacement controlled test show this behaviour, but B-18-4 is also not the only test. The calculated PV values are shown in figure 4.66 and 4.68. The same scattering visible in the dissipated energy occurs in the RDEC values and especially in figure 4.67 is the scattering numerous, but the overall increase is visible. This is not the case in figure 4.66. There is a none clear visible development of the RDEC and only scattering. The remaining worked out results based of Li can be found in appendix C

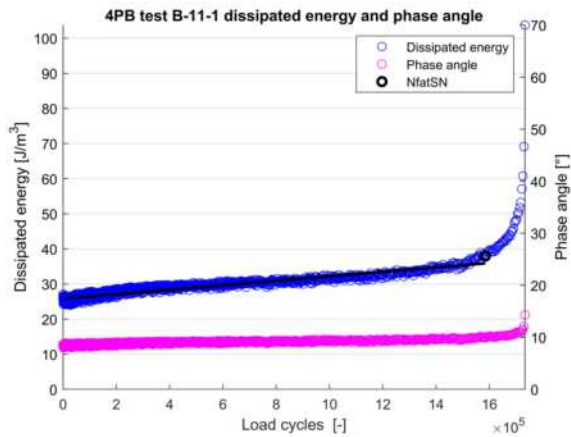


Figure 4.65: Phase angle and dissipated energy B-11-1 force controlled

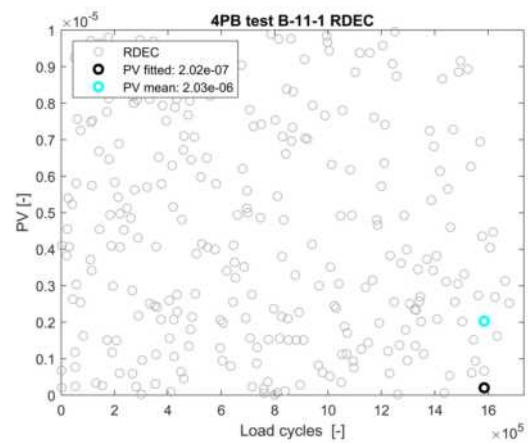


Figure 4.66: RDEC B-11-1

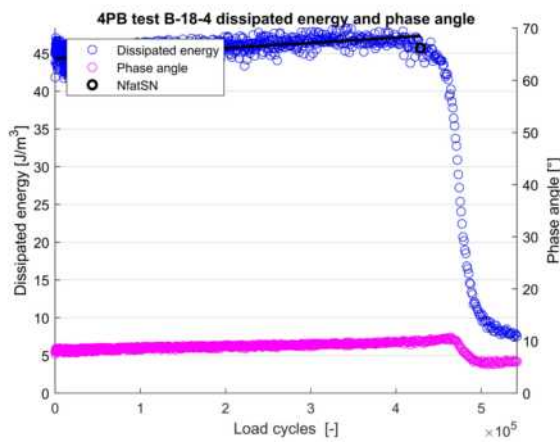


Figure 4.67: Phase angle and dissipated energy B-18-4 displacement controlled

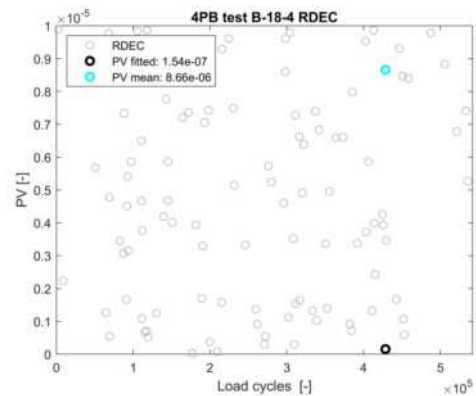


Figure 4.68: RDEC B-18-4

In figure 4.69 the result of both the displacement and force controlled 4PB test is given. From the results it is visible that the displacement controlled test has a very irregular result due the fact that the measured slope of the energy dissipated was sometime upwards.

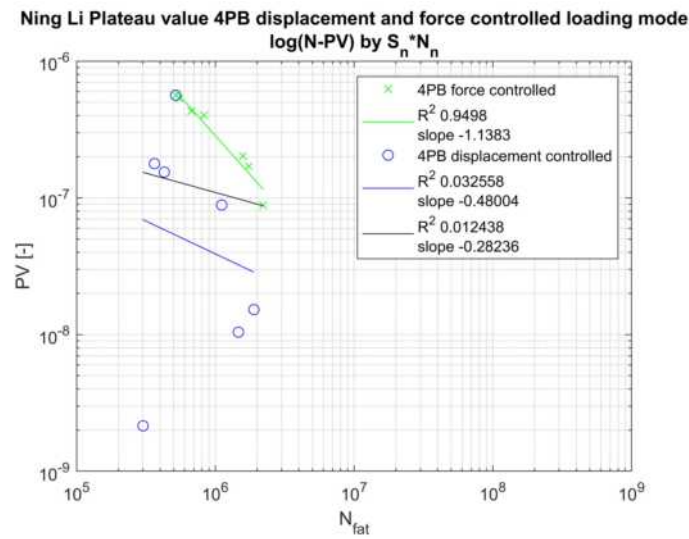


Figure 4.69: Plateau values from N. Li force and displacement controlled

As a result of the unclear Plateau Value results of the displacement controlled fatigue test there is a need for a full own fatigue test. This preferably on a same mixture with more prismatic beam samples and on 20°C. Beams from project 18619 were chosen to perform the tests, which are presented in the next section.

4.7.2.2. 18619 results

Performing the 4PB tests at the TU Delft gave a lot of problems and the limitations of the test equipment came to bear when the results were worked out. The measured phase angle gave a lot of scattering and was not always correct or had to be adapted to be of use in the final result. Switching between the best results given by a Fast Fourier Transform or a sinusoidal fitting method. The IPC 4PB test equipment was checked with an aluminium test beam which gave the result of 0° . In figure 4.70 we see the phase angle and the energy dissipation for test 55706. From it's result it is clear that the failure point presented in figure 4.61 works for the result of the dissipated energy on a force controlled loading mode. In figure 4.71 we see the calculated Plateau Values for the same fatigue test. The theoretical PV curve is visible for the latter part of the test and the failure point PV fitted has a good fit on this curve. The presented point PV mean does not represent in any way a good estimate of the PV values on the presented curve.

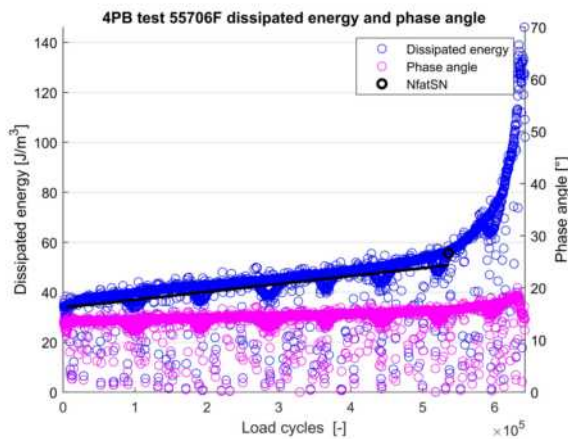


Figure 4.70: Phase angle and dissipated energy 55706

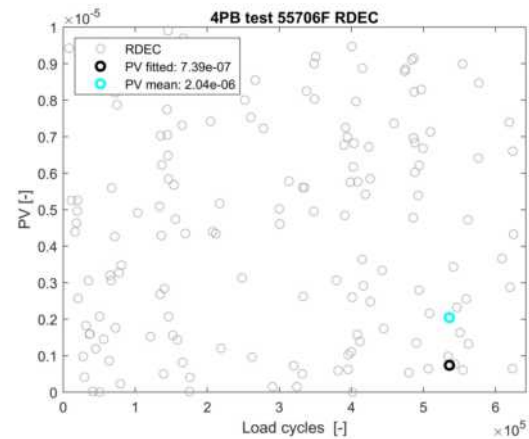


Figure 4.71: RDEC 55706

It is shown in the previous figure that a good PV curve can be visible for a force controlled test. This only happened for 2 of the in total 11 presented fatigue tests. In figure 4.73 a more general result of the RDEC is given. Again a lot of scattering and no clear visible theoretical PV curve. This against the expectations that the given increase of dissipated energy in figure 4.72 is enough to offset the RDEC in a significant way. Through this inconsistent behaviour of the RDEC method

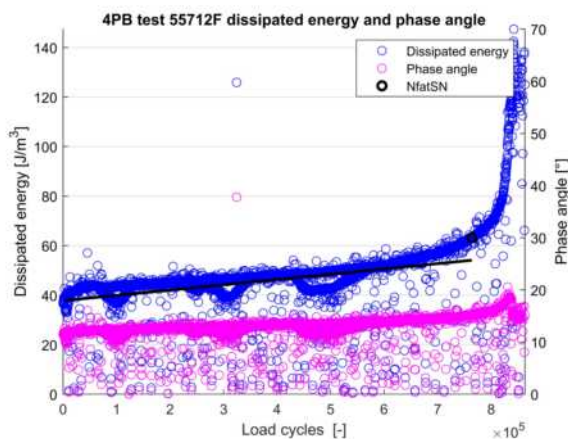


Figure 4.72: Phase angle and dissipated energy 55712

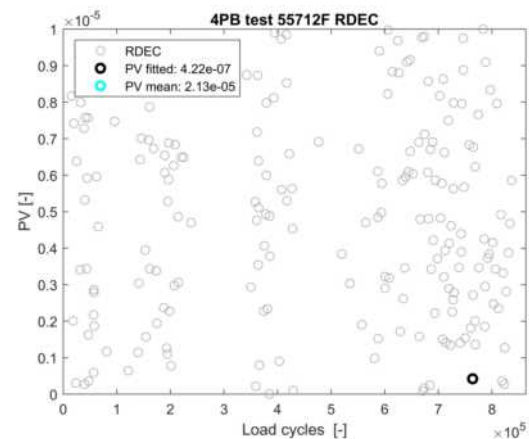


Figure 4.73: RDEC 55712

From figure 4.74 we see that the overall behaviour of the mode of loading is in overall correspondence with the results showed between the 4PB on displacement control and the CY-ITT on force control. The Plateau Values of a force controlled test is higher than that of a displacement controlled test. The overall slope of the force controlled test on the PV line lower than that of a displacement controlled

test. Both behaviours are also the case with the CY-ITT force controlled testing. However it should be noted that the PR content created a lot of scatter in both final PV results and the mixture used was the worst of all the mixtures tested in this thesis.

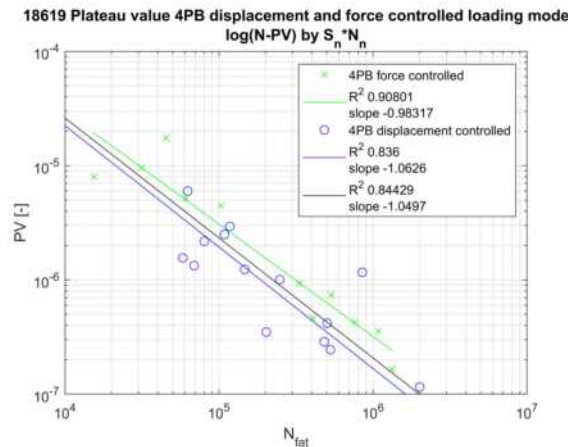


Figure 4.74: Plateau values for 18619 force and displacement controlled

The remark that can be placed with the results is that the beams were reused after already been tested in a fatigue setup. This resulted in breaking the beams quite fast after the test started. Due to the nature of the 4PB test with the maximum strain occurring in the outer fiber, turning the beams 90 degrees, would mean an almost untested part of the beam would be loaded to the maximum applied stress. Given that the PV is a normalized number describing the derivative of the dissipated energy, the important part is the stable region of dissipated energy to describe this part. The only influence that cannot be ignored, is that instead of testing perpendicular to the direction of compaction, the sample is now tested parallel. This influence should be considered, but would not explain solely the difference shown between displacement and force control loading mode.

For a total comparison for the mixtures 18619 in test setup and loading mode, the CY-ITT is added in figure 4.75. It shows that the overall slopes of the force controlled tests are in the same range, but the differences are small. The CY-ITT PV results are higher than that of both 4PB tests. From the results visible we conclude that there is still a difference in the PV values between the two different loading modes and further testing on a stable mixture on 4PB force controlled is recommended.

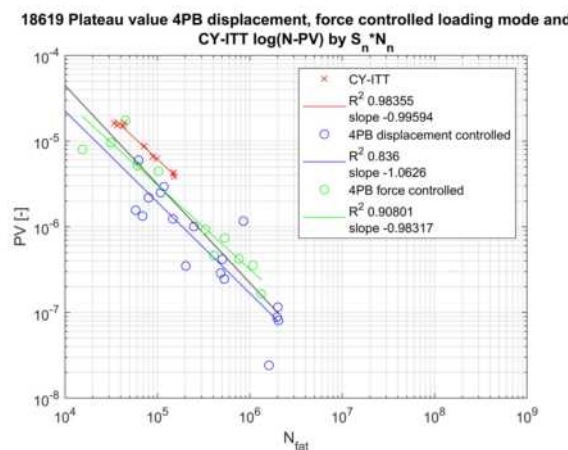


Figure 4.75: Plateau values for 18619 4PB force and displacement controlled and CY-ITT force controlled loading modes

4.8. Uni-axial displacement controlled

To study the influence of the shape of the specimen on the fatigue behaviour, a mixture fatigue test on a uni-axial setup is performed. This is called the uni-axial tensile compression fatigue test (UTCF test). The 4PB beam has the highest stresses and strains at the edges and the CY-ITT has an assumed highest strain levels at the center. Both test don't have a constant uniform surface on where the the fatigue relation studied is performed. A uni-axial fatigue test provides a cylindrical shape specimen with a constant area over the height of the specimen. Performing a dynamical fatigue test on this specimen creates a test that can both imitate the tensile compression behaviour of the 4PB in displacement control mode as well the constant compression state in the force controlled loading mode of the CY-ITT. For a complete research both loading modes should be performed to make a full analysis, but due time restrictions only one loading mode fatigue test is performed. Resulting from the conclusion that the RDEC is load mode dependent from the 4PB force controlled test in the previous section. The choice is made to perform the uni-axial test in a displacement control mode. This will allow to make a conclusion that the RDEC method is maybe shape independent and the CY-ITT test could be modified to a displacement control fatigue test.

The required shape of the specimen and specific test setup needed, led to conducting the fatigue test at the laboratory of the TU Delft. The specimen size of 150 mm in height and 100 mm in diameter required a gyro compactor instead of a plate segmented compactor to compact the specimen to the corresponding density of the reference mixture. The mixture chosen was the same as for the tests of project 18590. This mixture was chosen for his high stable behaviour and good correlating test results in both the CY-ITT and 4PB. Second there was no PR in this mixture, making the results more consistent with the first conducted type tests. While both 4PB and CY-ITT are performed on 30 Hz, the UTCF test were conducted on 10 Hz after considering the high vibrations influence on the rig used to hold the LVDT's. From project 19018 we concluded that frequency does not influence the RDEC slope position. A further complete description of the sample preparation, test setup and procedure, measuring software and all test results are given in annex E.

In total 13 samples were prepared and 11 displacement controlled fatigue tests are performed on different strain levels. The same failure criteria based on the Stiffness repetition principle is applied on the traditional strain fatigue results. For the $\log(PV - N)$ relation the Energy Ratio is applied as the set N_{Fat} . Although both methods do not differ significantly again. The RDEC is calculated based on the same fitting method from section 4.3.2.

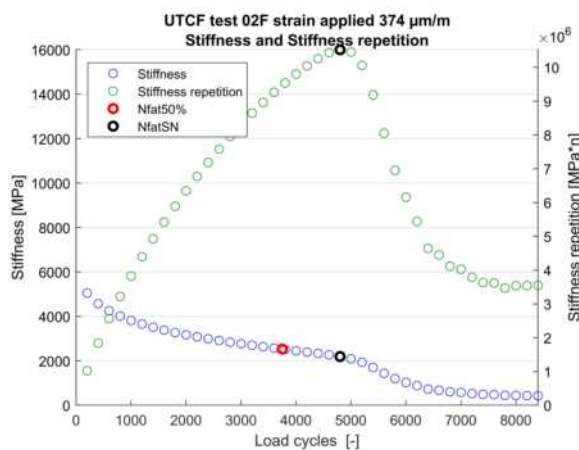


Figure 4.76: Stiffness and Stiffness ratio P02

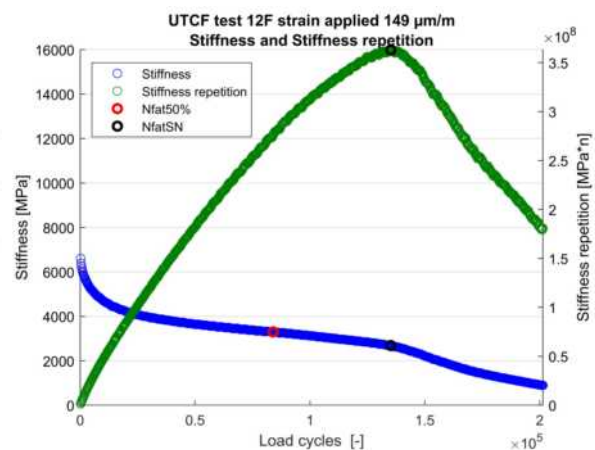


Figure 4.77: Stiffness and Stiffness ratio P02

4.8.1. Stiffness Repetition failure criteria

The UTCF test on displacement control mode leads to the characteristic S shaped curve of the Stiffness which is comparable to the results of a 4PB test. In figure 4.76 and 4.77 two results are shown of a short and long conducted fatigue test. The stiffness curve shows the exact same behaviour as a 4PB

displacement controlled test. The curve is also never a straight line, but consist of two exponential curves that form a S-curve together with an undefined turning point in the middle. This principle holds for the short high strain level tests as well for the long low strain level tests.

In these previous figures 4.76 and 4.77, the Stiffness Repetition failure criteria is also shown with for comparison the traditional $N_{fat50\%}$. It is clear that the method of finding the tilting point before the rapid decrease of stiffness also works for the UTCF tests. The $N_{fat50\%}$ reduction gives a failure that is to early compared to the number of load cycles remaining before the rapid decrease. The remaining other 9 result for the stiffness graphs can be found in annex E. These graphs all support the Stiffness Repetition method as a good and consistent definition of failure for fatigue testing.

4.8.2. RDEC result

Using the result that N_{fatSN} works as failure definition for the Stiffness. We apply the Energy Ratio as the failure for the dissipated energy. The phase angle was measured more precise in these experiments, allowing it's application. It is now used to see if it also holds as a failure definition for the dissipated energy and respectfully the RDEC.

In figure 4.78 the phase angle and dissipated energy are given. The dissipated energy is calculated through the general equation. Both failure criteria methods are found on the same load cycle. The showed phase angle is very consistent. In contrast to the measured phase angle of a generic 4PB beam test, there is no initial small increase at the start or larger increase at failure. The measurements are either way accurate or flawed by the way the tests are conducted. This is further discussed in detail in annex E. It is remarkable to see a same measured phase angle range for both the 4PB on force control mode and this UTCF test. Both tests are conducted by the same controller and measurement software. While the one is performed on a 30 Hz frequency, the UTCF is performed on 10 Hz, which should lead to a difference in phase angle, not the least the difference in mixtures used.

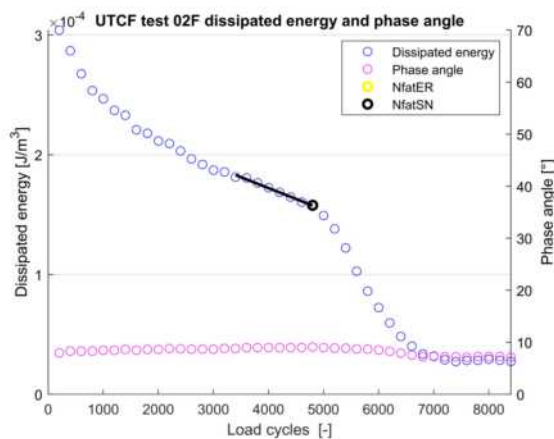


Figure 4.78: Phase angle and dissipated energy P02

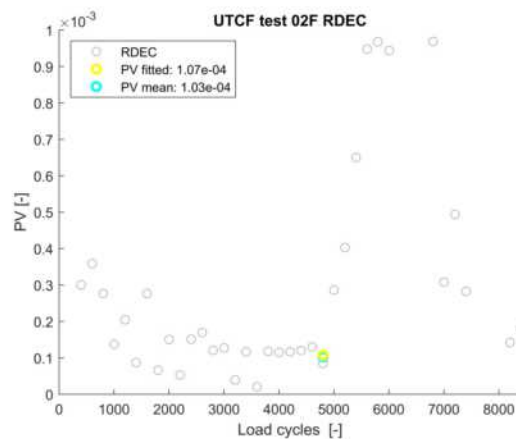


Figure 4.79: RDEC P02

In figure 4.79 the calculated PV is given associated to to the dissipated energy of figure 4.78. The characteristic bathtub shape is visible and the fitted PV is in line with the surrounding data points. In figure 4.80 and 4.81 test sample number 12 is shown. This test was a long fatigue test at a lower strain level. Due to increasing number of data points, although a stable phase angle, the scattering cloud is much more present then in a short high strain test. Also due the low strain level applied, the dissipated energy decreases much slower, resulting in a harder to visualise fatigue failure in the RDEC graph. Both failure criteria are again much the same in figure 4.80.

If we combine the results of all the tests from the UTCF and combine them with the results obtained from the CY-ITT and 4PB from project 18590, we get the following result in figure 4.82. From the results presented in Section 4.6 for mixture 18590 we saw that the CY-ITT and 4PB already collapsed on the same $PV - N$ relation. Figure 4.82 shows that the $\log(N - PV)$ relation is on a single line for all 3 different test setups. For both methods the same failure criteria and PV calculations are used. While the

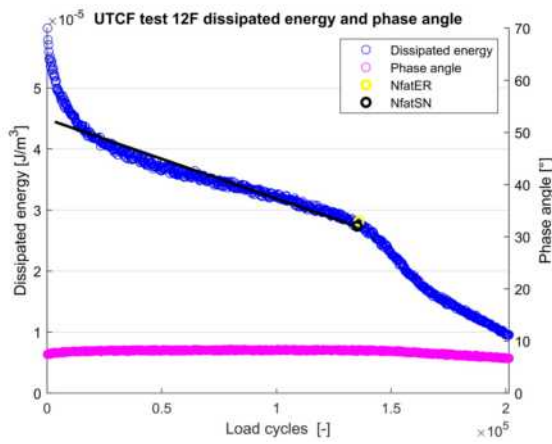


Figure 4.80: Phase angle and dissipated energy P12

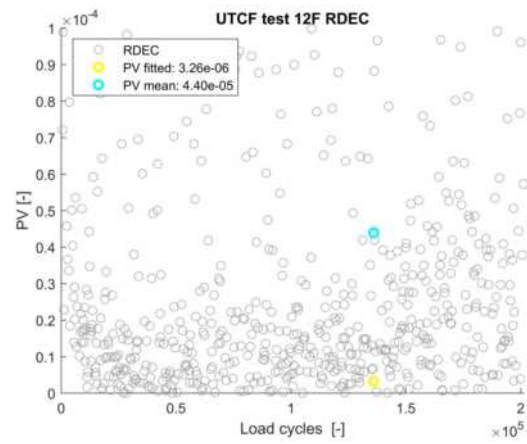


Figure 4.81: RDEC P12

test frequency and specimen shape differ, the resulting Plateau Value vs the number of load repetitions at failure is a united coherent relation. Meaning that the normalised rate of dissipated energy per loading cycle for a certain number of load repetitions at failure is an independent and interchangeable relation between specimen size in a displacement controlled fatigue test.

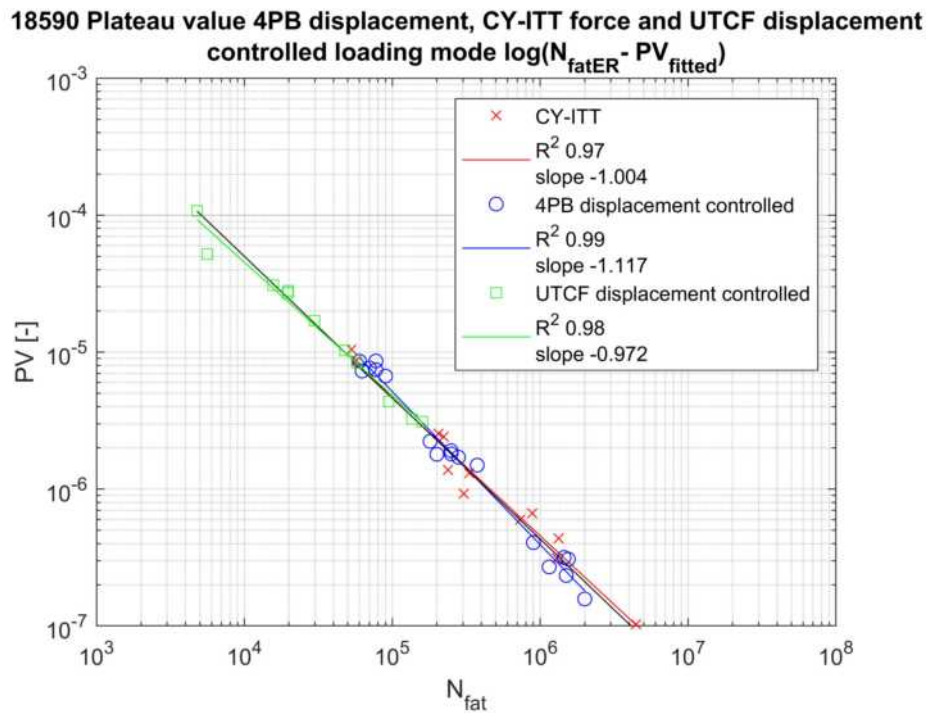


Figure 4.82: Plateau values for 18590 4PB, UTCF displacement and CY-ITT force controlled loading modes

4.9. Influence of mass density on RDEC

The compacted density of a constructed asphalt layer is one of the key factors in validation of the applied asphalt concrete layer. It influences all functional properties of the asphalt layer [Oosterhout, 2018]. In practise it is often set a minimum percentage of reached density to approve the road by authorities [RAW, 2015]. As mentioned before the RDEC method could possible be used to functional verify the differences between road and lab produced specimen. As stated in section 4.6 the different mixtures do not influence the log(N-PV) relation. But the density could still be a influence factor on

the dissipated energy. That is why in this section the influence of different densities is discussed with the RDEC method.

Mixture 18619 is prepared on a targeted 97%, 100% and 103% mass density, with 0% PR. The reason for the 0% is for the negative influence on scatter of PR as seen in Chapter 3 and the already compacted state of the used broken, but still partial intact PR. Setting the desired 100% mass density at 2375 kg/m^3 . The mass density of the samples is reached by the degree of compaction in percentages. The real averaged measured mass density of the prepared samples is given in table 4.5. For all three levels the targeted density was not exactly reached. Especially the over compacted prepared plate. The first prepared plate was disregarded due the high amount of cracks. The second plate was set at a lower compaction rate. Reaching an average of 101.5%. This resulted in fewer number samples available and only the high and low strain levels were tested.

Table 4.5: Mixture 18619 density's.

Target	Reached density [kg/m^3]	Reached percentage
97%	2316	97.5%
100%	2356	99.2%
103%	2410	101.5%

The traditional fatigue result with the stiffness repetition method is given in figure 4.83. Where the 103% mass density fatigue line clearly is situated above the under compacted other two fatigue lines. The density has an overall positive influence on the fatigue life, set with an unspecified limit. The reason is that overcompaction of specimen leads to macro cracking at the preparation state, resulting that fatigue testing is no longer possible, due the high cracking damage.

In figure 4.84 the results are shown with the applied fitting method and the N_{fatER} as the set failure criteria. The found Plateau Values through the RDEC method are again independent from each other. Resulting in the same single log(PV-N) relation found in the previous sections. From that we can conclude that the RDEC method is also independent and or indifferent to the degree of compaction.

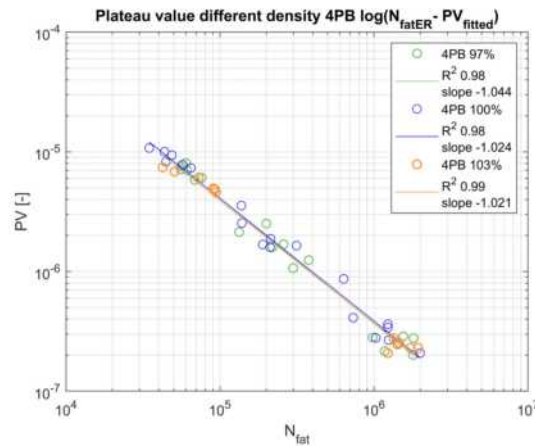
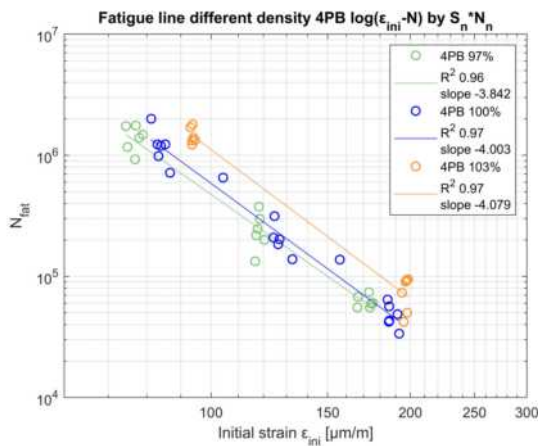


Figure 4.83: Fatigue line mixture 18619 different density's

Figure 4.84: Plateau Value line mixture 18619 different density's

4.10. Conclusion

In this chapter the results and significance of the Ratio of Dissipated Energy Change were given. In short the following conclusions can be summarised from the individual sections:

- The measured phase angle is an important variable. Fluctuations or measurement errors make the dissipated energy and resulting RDEC results completely useless.

- The RDEC method is not influenced by the specimen size or the used static parameters in the given equation. It is solely dependent on the slope of the measured force and displacement.
- The amount of RDEC scatter found in all test results is abundantly inconsistent. It makes the application of an average or other visual methods of establishing N_{fat} and PV not feasible.
- The dependence of the RDEC curve on the dissipated energy course and with a consistent phase angle, the dependence on the stiffness curve was proven. Resulting that the failure set by the RDEC curve is dependent on the failure point on a stiffness curve.
- The failure criteria of Stiffness Repetition of Chapter 3 proved itself in finding the tilting point of the dissipated energy curve. Setting it as a consistent bitumen type and loading rate independent failure criteria.
- The failure criteria, Energy Ratio proofed itself nearly always consistent with the Stiffness Repetition failure criteria. The method combined with a good measured phase angle is however more stable than the Stiffness Repetition. Making it the preferred method for the failure criteria if the final fatigue parameter is based on the dissipated energy curve.
- The application of a fitting method directly on the assumed linear part of the dissipated energy curve proves itself a consistent and promising method. The result is a dissipated energy slope parameter $x(1)$ which is mixture unique.
- The statistical method was not applicable with the current set of required linear fitting equations and boundary conditions.
- The theoretical dissipated energy curves for CY-ITT and 4PB validated the the concept of the applied fitting line. The result is due the non-linear development however lower than the theoretical expected value.
- The overall results from the fitting method combined with the Energy Ratio failure criteria are above expectations. Creating $\log(PV - N)$ relations with overall R-squared values above 0.98.
- From the 12 used mixtures 6 are a perfect fit between the CY-ITT and 4PB. The other 6 mixtures are shifted slightly with the CY-ITT above the 4PB. Only 1 mixture had significantly different slopes between the CY-ITT and 4PB.
- The RDEC is independent of the test frequency.
- The RDEC is probably independent of test temperature, however the phase angle is not, making the method on lower temperatures unstable.
- The RDEC is independent of mixture type, making it a none distinctive relation in identifying different mixtures.
- The RDEC is independent of the stress strain relation between different size samples.
- The RDEC is independent of the mass density of a mixture tested under the same mode of loading.

The conclusions drawn from this chapter are highly dependent on the assumed and applied method of linear fitting. The established slope parameter $x(1)$ is thereby the crucial and essential parameter. The other calculated RDEC values are of no significance in this applied method as the amount of scatter prevent any consistent analysis.

From the previous statements it becomes clear that the 'Ratio' part of the RDEC is confirmed. The application of a ratio based method on the dissipated energy makes it a trivial relation for the study of fatigue and materials. There is a none distinct single $PV - N_{fat}$ relation in which every unique aspect of an asphalt concrete mixture dissolves. Making it therefore possible to relate the CY-ITT and 4PB, but further a non practical meaningless solution as a validation between a constructed work and the laboratory conducted fatigue test.

5

Results VECD

This chapter presents the results that follow from the theory of the Viscous Elastic Continuum Damage (VECD) model discussed in section 2.3.4. The main presented variables will be the total released pseudo energy W_c^R and the derivative or rate of dissipated pseudo energy G^R . These will be related to the previous established N_{fat} on log log scale. The failure criteria is set by the Stiffness Repetition method. The first Section will discuss the general behaviour of the method. Section 5.2 will present the relation for the two executed force controlled 4PB project as a confirmation of the theory in Section 2.3.4. In Section 5.3 the linear elastic frequency dependence is discussed followed with the VECD method on the CY-ITT and 4PB for different mixtures. In Section 5.4 the conclusion is given from the presented VECD results.

5.1. General behaviour

In dynamic fatigue testing the VECD method is based on the linearization of the Hysteresis loop. Instead of calculating the area inside the loop, the vector of F is calculated. The equation was given in Chapter 2 in equation 2.27. In where F is based on the pseudostrain. The pseudostrain is the strain amplitude at N_i multiplied by the found stiffness at the frequency sweep. The total released pseudostrain energy is a function given by equation 2.34. The equation describes the change of F to the undamaged state of the sample. The triangle area created between F and the undamaged state of the sample is therefore W_c^R . This was depicted in figure 2.22. The G^R is then stated as the rate of dissipated pseudostrain energy.

In this section the linearization of the strain is primarily discussed. As it is the main assumption of the VECD on dynamical testing. In figure 5.1 the stress pseudostrain linearization is given for a 4PB sample. The same sample 55003F from mixture 19018 as in figure 4.8 is used. Two different vectors F are given at load repetition $n = 100$ and at the failure criteria set at $n = 1.150.000$. The resulting triangle is the set total released pseudostrain energy. As the 4PB is loaded in tensile and compression the pseudostrain is positive and negative. As assumed only the tensile part acts as fatigue damage and only the positive triangle is used for W_c^R .

The CY-ITT VECD vector F is given in figure 5.2. Sample 55202F from mixture 19018 is used. The sample is in a constant tensile state at the center, resulting that the vector is only given positive for the double pseudostrain amplitude. Take note that at the force controlled loading mode the pseudostrain increases, while at the displacement controlled mode the stress decreases. Both modes of loading results in a triangular increasing shape.

From figure 5.1 and 5.2 the assumptions that the F is linear is reached by using only the maximum of the strain and stress amplitudes. Disregarding the measured phase angle. As the stress is declining during a 4PB test, the vector F becomes smaller and this change of the vector is due the fatigue damage in the sample. All viscous related properties are omitted and this simplification made for the dynamic testing can be highly criticized. In this chapter we hold on to the assumed linearization for

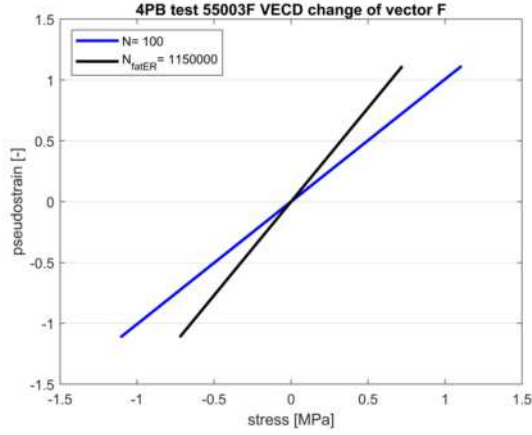


Figure 5.1: 19018 4PB, change of vector F

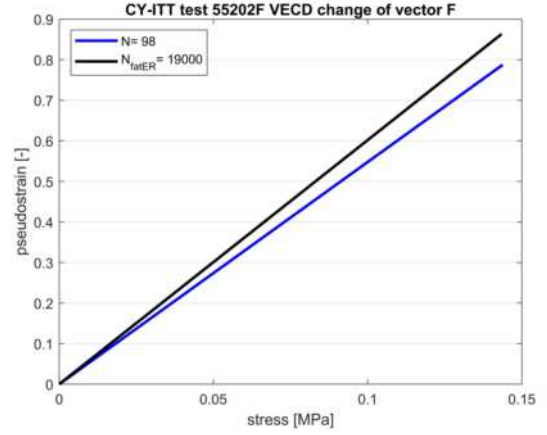


Figure 5.2: 19020 CY-ITT, change of vector F

the dynamical fatigue testing made by [Underwood et al., 2010].

As the method is only dependent on the vector F we will discuss in the next section the general results of the total released pseudo strain energy and the resulting rate of change.

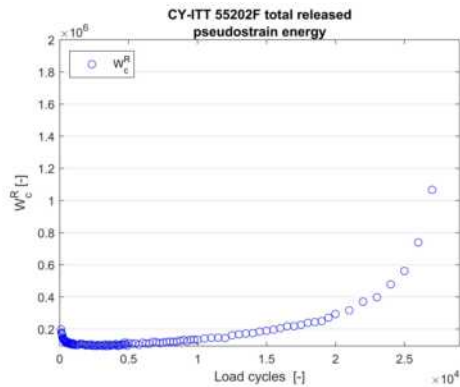
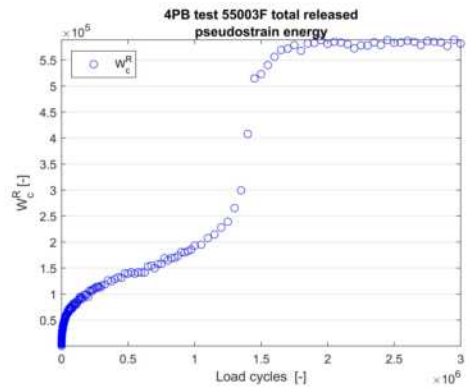
5.2. General VECD results

In Section 5.1 the applied VECD method was discussed. In this section the general results of the resulting W_c^R is presented. It is followed by the application of the previous established Stiffness Repetition failure method on this curve and see if it can be applied. Final is the determination of the rate of pseudostrain energy G^R . The latter is discussed with three different methods.

5.2.1. Total released pseudostrain energy W_c^R

The total released pseudostrain energy over the number of load repetition is a positive function. Otherwise there would be energy added to the specimen. This last phenomena is the case with the CY-ITT. With the first compaction stage of the sample and the increase of stiffness, the released pseudostrain energy is declining and can become negative. Energy delivered by the dynamical force to the sample is partly or completely used for the compaction of the sample instead of fatigue damage. This can be seen in figure 5.3. The W_c^R is however shifted positive for the determination of G^R in section 5.2.3 later.

The general W_c^R behaviour for CY-ITT follows the inverse general behaviour of the stiffness curve from Chapter 3. This is the result of the general fatigue damage describing the natural logarithm curve. Which is clearly depicted in figure 5.3. As the summation part of the W_c^R is only influenced by the steepness of the increase.

Figure 5.3: W_c^R 19020 test 55202FFigure 5.4: W_c^R 19018 test 55003F

The same inverse behaviour from the stiffness curve is also true for the 4PB test in figure 5.4. The summation of the decrease of vector F results in a similar inverse natural logarithm curve. The reached constant phase after the sudden increase is related to the phase were the beam is failed in fatigue. The stiffness is reduced to almost zero and so is the force applied to the sample. The added pseudostrain energy related to fatigue is therefor also zero and the W_c^R has reached a maximum. The two depicted sample examples are the general result that all asphalt concrete samples follow. The variation is found in the size and slope of the established curve. The same as in the dissipated energy from Chapter 4.

5.2.2. Failure Criteria

From the previous subsection we saw the general results of the W_c^R . In this part we discuss the previous established fatigue failure criteria on the W_c^R curve. The Stiffness Repetition method is applied instead of the Energy Ratio method. As the summed pseudostrain energy function is only dependent on the measured strain en stress amplitude. The influence of the phase angle is left out, so the relation at failure should be dependent on the stiffness curve. The latter is shown between figure 5.5 and figure 5.6. The stiffness and stiffness failure criteria N_{fatSN} is given in the first for the 4PB. It can be directly related to W_c^R in figure 5.6.

Zhang, as the main contributor to the utilised literature in this chapter, used a different failure criteria [Zhang and Kim, 2012]. Zhang employed a similar approach as the statistical method applied by Telman. A same linear fitted function was utilised in which the certain threshold was set to determine N_{fat} when the curve deflected from that fitted linear line. As proven in Chapter 3 the Stiffness Repetition method is not far from those results and this method will be used.

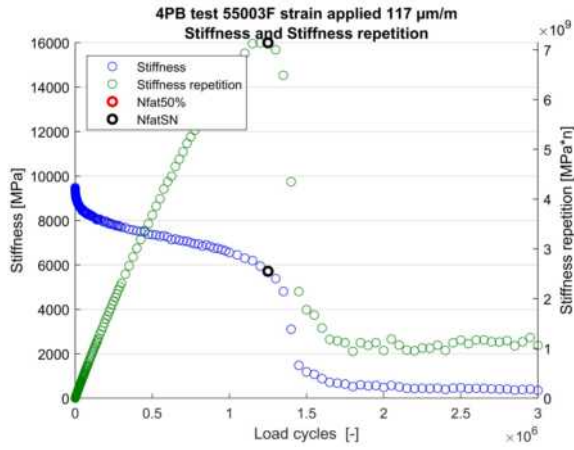


Figure 5.5: Stiffness and stiffness Repetition 19018 test 55003F

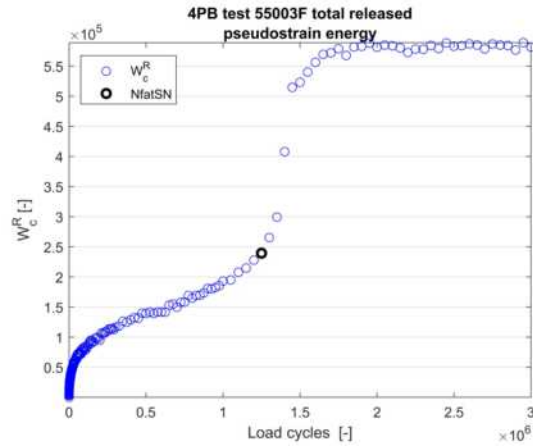


Figure 5.6: W_c^R 19018 test 55003F

In figure 5.7 and 5.8 the CY-ITT results are given. A drawback from the exponential function comes forth. As the fatigue damage exponential grows of the number of load repetitions, the summation of the pseudostrain energy increase in twofold. Resulting that the linear first increase before N_{fatSN} is graphically difficult to observe. This can be circumnavigated by leaving out certain measurement points, but then the exponential behaviour is neglected. As stated in Chapter 4 the difference found between the Stiffness Repetition and Energy Ratio was small. The N_{fatSN} is therefor the set failure criteria with the pseudostrain energy. The N_{fatER} is however showed for comparison in the remainder graphs found in appendix B. In the next subsection the rate of the W_c^R curve and its determination is discussed.

5.2.3. Rate of pseudostrain energy G^R

The G^R is stated as the rate of the pseudostrain energy. It can be therefore be stated as the first derivative of the pseudostrain energy. The rate is calculated through equation 5.1 in Chapter 2. It is comparable to the $x(1)$ parameter of 4, although here perfectly linearized and dependent on the estab-

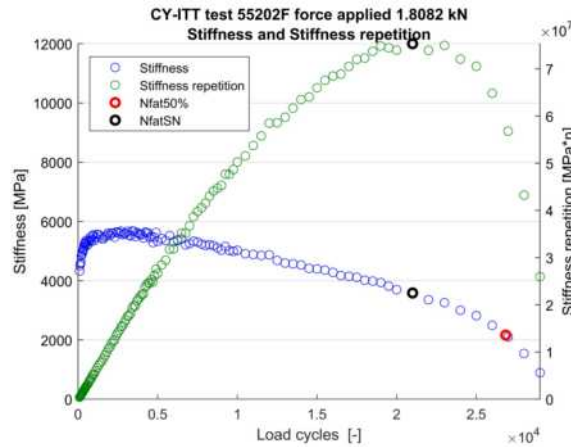


Figure 5.7: Stiffness and Stiffness Repetition 19020 test 55202F

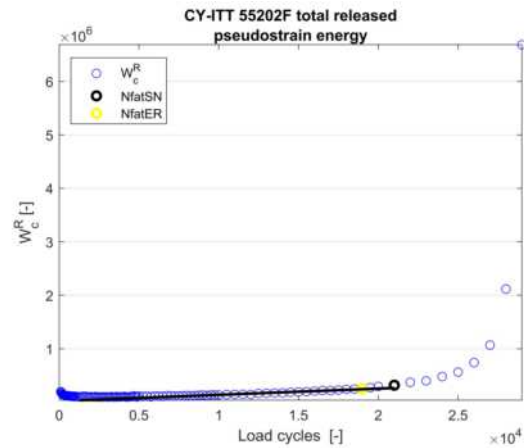


Figure 5.8: W_c^R 19020 test 55202F

lished stiffness of the frequency sweep. It was stated that this parameter G^R is a load independent, but mixture dependent parameter in the log-log relation with the N_{fat} . That is why this VECD relation is explored as a possible distinctive relation for the CY-ITT and 4PB. In combination with the found N_{fat} from the Stiffness Repetition, we can use three different methods to establish the rate of pseudostrain energy G^R at failure.

First the same method as finding the Plateau Value through fitting a linear line to the assumed linear section of W_c^R . This linear line is created by the assumption that after a certain number of load repetitions, the steady phase of the W_c^R starts. The number of load repetitions after the first phase is dependent on the duration of the test in the 4PB and the initial settling for the CY-ITT. The right boundary is then set by the N_{fat} minus 5 data points, this to limit the influence of the already started incline part of the W_c^R . This method is called G^R fitted.

Second, we could calculate the G^R at failure through the equation 2.35 set by Sabouri Sabouri and Kim [2014]. Called G^R calc. For ease given here again as equation 5.1 This method integrates the area under the W_c^R curve, with the boundaries zero and N_{fat} . Divided by the N_{fat} squared. Resulting in the G^R at failure. The surface under the W_c^R is decisive so the overall W_c^R curve has to be positive. With the initial increase of stiffness of the CY-ITT the W_c^R becomes negative, resulting that equation 5.1 no longer holds. Therefore the needed shift of the CY-ITT result to ensure that all W_c^R values are positive.

$$G_r = \frac{\int_0^{N_{fat}} W_c^R}{N_{fat}^2} \quad (5.1)$$

The final method uses the average value of the 10 data points of G^R before the N_{fat} . Called G^R mean. This method is previous applied on the RDEC values. While this last method is heavily dependent on the amount of scattering, it gives a good indication how much scattering there is. It is also a good comparison in the divergence of the calculated and fitted method from the real measured values. Furthermore it is an indication of how much the N_{fat} does diverge from the steady phase. The latter is the case when N_{fat} is much further calculated in the curved turning point than the linear fitting method would agree upon.

Results from all three methods are given in all rate the G^R figures. For the previous samples the G^R is given in figures 5.9 and 5.10. The overall shape of the two figures show again a bathtub type shape. Where the initial G^R reduction of the CY-ITT in figure 5.9 is again the result of the initial increase of the stiffness. The scattering found for the CY-ITT in this method prevents an accurate determination of N_{fat} or G^R . The outcome of the three methods to find G^R are not significantly different and in table 5.1 the full CY-ITT G^R are given with the magnitude of difference between the three methods.

In previous figure 5.8 the fitted method was showed on the W_c^R curve to establish G^R fitted.

The 4PB in figure 5.10 give the same comparable behaviour as the RDEC method. The N_{fatSN} is established to the end of the the steady state phase of the pseudostrain energy. The scattering is severe and the G^R cannot be determined by the graph. The G^R is not normalised so the found values are dependent on the fatigue behaviour of the mixture, resulting in a distinct G^R graph per mixture. The three methods don't differ much in the established G^R and for the full mixture 19018 the G^R values are given in table 5.2.

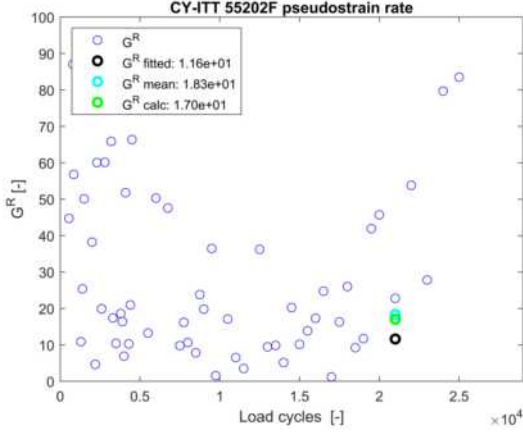


Figure 5.9: G^R 19020 test 55202F

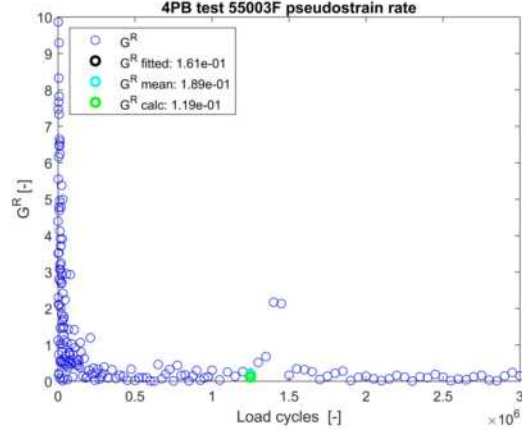


Figure 5.10: G^R 19018 test 55003FF

In table 5.1 the CY-ITT results are given for mixture 19020. The three different G^R methods are compared and the magnitude between the different methods are given. The strain is displayed as a measure of a short or long fatigue test. The differences found between the fitted and calculation method is quite large. As both methods are directly based on the W_c^R curve a smaller difference was expected. The fitted method is however consistent smaller in G^R value. The G^R mean is inconsistent from the G^R calc. Proving again that the scatter of a rate based method is unable to produce a consistent result.

Table 5.1: Mixture 19020 CY-ITT G^R

Sample	ε_{ini}	G^R fitted	ΔG^R	G^R calc	ΔG^R	G^R mean
55202F	115	11,63	-1,5	17,03	-1,1	18,34
55203F	57	0,41	-1,9	0,79	13,5	0,06
55204F	66	1,20	-1,1	1,30	1,2	1,05
55205F	44	0,14	-1,6	0,23	-1,3	0,29
55206F	67	1,00	-1,4	1,43	2,0	0,71
55207F	128	27,05	-1,5	39,35	1,8	21,28
55208F	48	0,13	-2,1	0,26	-1,6	0,42
55209F	137	23,78	-1,6	37,43	-1,4	53,30
55210F	48	0,21	-1,7	0,36	-1,0	0,38

Table 5.2 presents the 4PB results for mixture 19018. The distinct and important difference with the CY-ITT is that the magnitude between the G^R fitted and G^R calc is not consistent. The fitted method results for the longer fatigue test in a higher G^R value and for the short tests a lower value. Resulting in a change of slope on the log-log scale relation with the N_{fat} . The shift between both methods is relative small with the largest difference of 1.4. Again the G^R mean does show a large scatter compared with the G^R calc method. It is both positive as negative scattered around the calculated method. The remainder of the results and other corresponding graphs from this mixture result and other mixtures can be found in appendix B.

Table 5.2: Mixture 19018 4PB G^R

Sample	ε_{ini}	G^R fitted	ΔG^R	G^R calc	ΔG^R	G^R mean
54987F	225	12,21	-1,1	13,45	3,3	4,03
54990F	184	3,63	1,1	3,25	-1,3	4,31
55018F	114	0,15	1,4	0,11	-1,2	0,14
55005F	169	2,10	1,1	1,95	-2,3	4,57
55992F	261	28,77	-1,2	34,50	1,8	18,73
55003F	117	0,16	1,4	0,12	-1,6	0,19
55007F	175	2,45	1,1	2,23	1,1	1,94
55004F	260	34,52	-1,3	44,89	1,5	30,59
55006F	114	0,13	1,3	0,10	-1,7	0,18
55012F	173	2,18	1,1	1,96	9,1	0,22
55008F	261	27,48	-1,2	33,03	1,4	24,43
55014F	115	0,17	1,3	0,14	-2,1	0,30
55017F	175	2,75	1,1	2,51	1,4	1,86
55013F	261	33,43	-1,2	39,35	-1,0	40,66
55016F	115	0,15	1,4	0,11	-1,9	0,22
55009F	174	2,77	1,1	2,50	1,3	1,88
55015F	262	32,92	-1,2	40,00	1,6	25,01
55993F	114	0,14	1,4	0,10	-2,1	0,20

From the tables it is not proven which method proves consistent or a better represented of most accurate G^R value. In the next section the two force controlled test performed on the 4PB are used to find the most accurate method.

5.3. 4PB force controlled

To follow a logical path in proving the concept of VECD on CY-ITT and 4PB, we first look at 4PB displacement and force controlled fatigue test. The initial VECD results were analysed using Li's test results with the calculation method of Sabouri. These looked promising enough to use in this thesis and will be discussed first.

5.3.1. Li results

As in chapter 3 we can use the results from the 4PB fatigue tests that Li performed for his thesis. These tests were all performed on 10 Hz and at 5°C. Performed both on a force & displacement controlled loading mode. In figure 5.11 we see the W_c^R for a displacement controlled test and below that in 5.13 the same curve for a force controlled test.

Due the nature of how the total released pseudostrain energy is calculated the curve will positively cumulative upwards during the fatigue test. For a stress controlled test this line will be so good as linear, following the mirrored stiffness curve. Resulting from a constant stress and a slowly increasing strain amplitude. For the displacement controlled test this will be again two natural logarithm curves, mirrored from the stiffness curve.

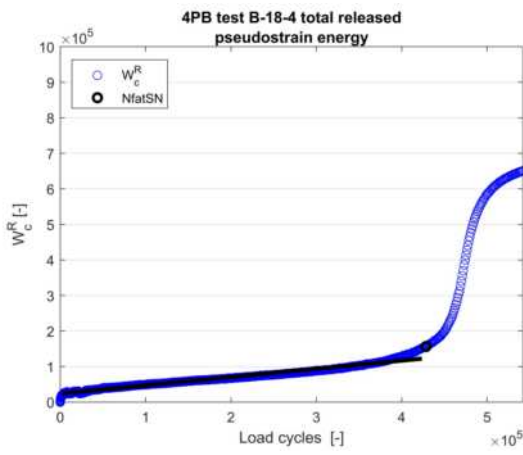


Figure 5.11: Total released pseudo strain energy B-18-4 displacement controlled

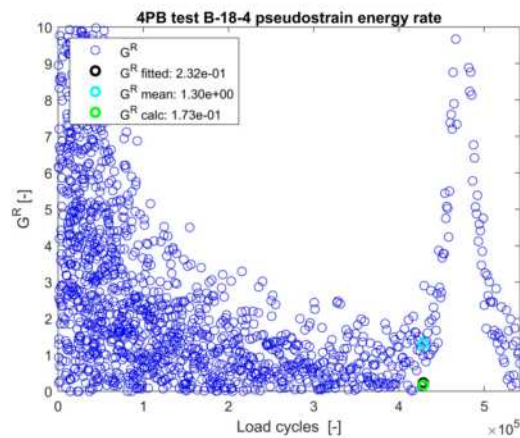


Figure 5.12: G^R B-18-4

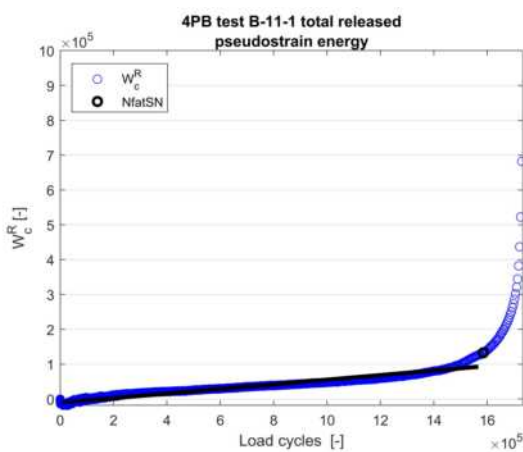


Figure 5.13: Total released pseudo strain energy B-11-1 force controlled

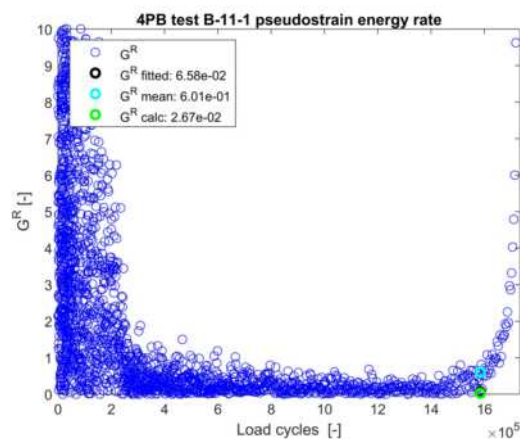


Figure 5.14: G^R B-11-1

In the figures next to them the respective G^R are given for both test. The overall curve that reflects the rate of released pseudostrain energy is visible and interpretable despite the scatter. The three calculated G^R values are given and show a good correlation. The first remark is place with the G^R mean value found. This is overall higher, which is logically if the G^R graph is compared with the W_c^R . It can be clearly seen that the N_{fat} is already in the incline area of the curve. Resulting in a higher rate around N_{fat} .

The second remark is the comparison between the fitted and the calculated G^R . For the six displacement controlled tests the fitted value is on average twice as high as the calculated value. For the seven force controlled samples the fitted G^R values are on average 2.3 times higher than the calculated G^R . This difference can be explained that both methods have their previous discussed disadvantages.

A log log scale graph can be composed from the individual fatigue test results. Resulting in a linear relation between the different results on which, through the R-squared method, a best fit line can be constructed. A higher R-squared is a better cohesion between individual test results. From the 4PB works of Li the following two figures are constructed for the 4PB on force and displacement controlled loading mode. Given the number of load repetitions at failure, determined by the Stiffness Repetition, vs the rate of released pseudostrain energy. The general layout is with force controlled loading mode in red and the displacement controlled in blue. The overall fitted linear function between the two types of loading modes is given in black. The remaining results from each fatigue test are given in appendix C.

Given in figure 5.15 is the method where G^R is calculated by equation 5.1 from Sabouri. The overall result, especially for the displacement controlled loading mode is with a high amount of scatter, resulting in a R-squared with a very low coefficient. This inconsistent result from the displacement controlled test gives the impression that the method gives a good correlation between the modes of loading. With both the displacement and force control measurements on both side of the overall fitted function represented in black in the figure. However the overall R-squared value of 0.77 is still very low.

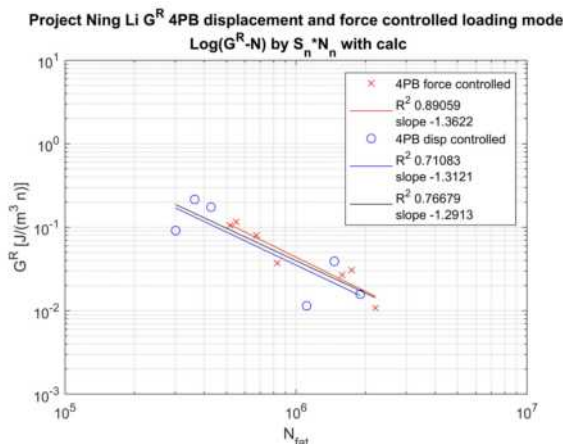


Figure 5.15: G^R calc from Li force and displacement controlled

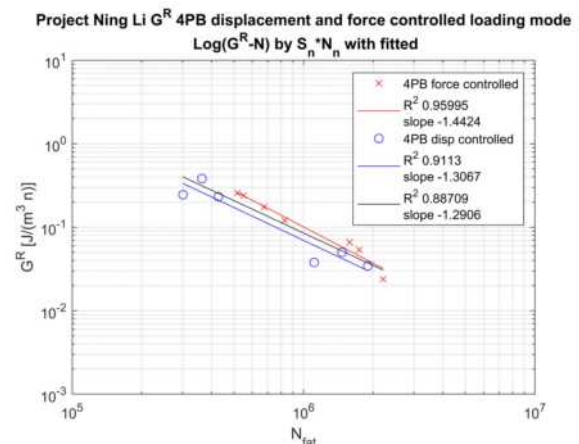


Figure 5.16: G^R fitted from Li force and displacement controlled

In figure 5.16 the result of G^R by the method of fitting on the W_c^R curve is given. The overall result is shifted vertically around a average factor of 2. The scattering is way lower compared to the calculating method. Resulting in a R-squared for the displacement controlled 4PB of 0.91 instead of 0.71. The other result from that reduce scatter is that the individual displacement and force controlled results are more packed together. Given a distinct difference between the two applied loading modes.

For both figures the slopes of the force and displacement controlled loading modes are given. For the fitted method in figure 5.16 the slopes are close to parallel. With the slope of the force controlled loading mode being a bit steeper than the displacement controlled loading mode. The calculation method however shows an almost parallel behaviour in the measured slope between the loading modes. Take

note that the application of the force controlled test performed by Li were not applicable in the final $\log(PV - N_{fat})$ relation in Chapter 4. This because of the sensitivity of the phase angle at the low temperature at which the tests were performed. This temperature sensitivity behaviour is obliterated with the VECD method.

The latter difference between the slopes is studied more broadly by using the 4PB results of mixture 18619TU. This project was also performed both on force and displacement control loading modes with more samples and a standard 20°C temperature.

5.3.2. 18619TU results

Using again the results from the displacement controlled 4PB carried out at the central laboratory of KWS and the force controlled 4PB at the TU Delft. We can make the same comparisons between these two loading modes as in the previous section.

Both modes of loading are executed at 20°C and at 30 Hz. Again as mentioned before, the beams in the force controlled loading tests were turned 90° after 3 months of rest after being used previously for the displacement controlled fatigue test. The E_{LVE} is set through the average value of all frequency sweeps at 30 Hz. Given at 14272 MPa. The average sample deviation is determined by the DMR and results in correction factor between the samples own frequency sweep and the averaged found for the Master-curve.

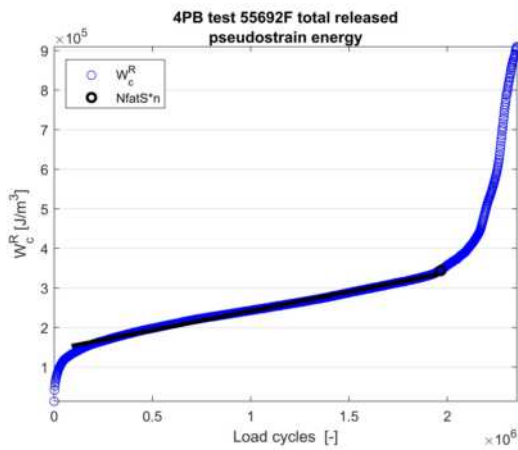


Figure 5.17: Total released pseudo strain energy 55692 displacement controlled

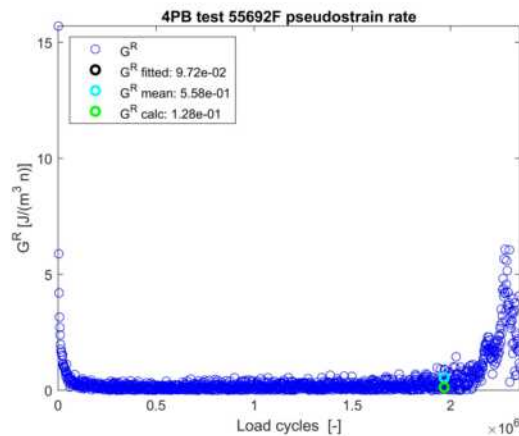


Figure 5.18: G^R 55692

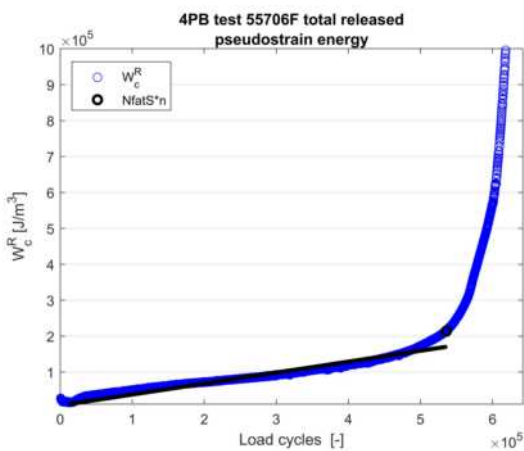


Figure 5.19: Total released pseudo strain energy 55706 force controlled

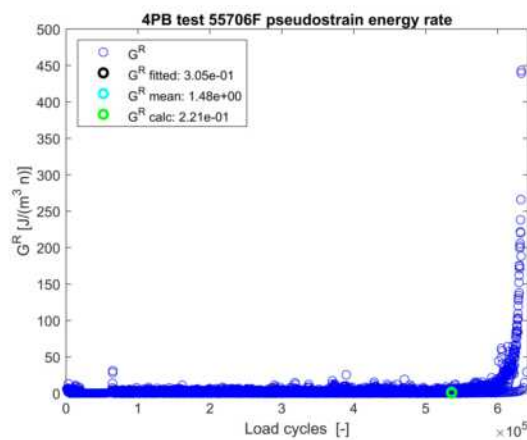


Figure 5.20: G^R 55706

From figure 5.17 the W_c^R curve for a displacement control test is shown. The overall behaviour is similar to the tests performed on 10 Hz and 5°C. The same coherent behaviour is shown for the force controlled loading mode in figure 5.19. With the remaining results for each individual fatigue test are given in appendix D.

From each individual result we can summarize for displacement control 4PB as well as for force controlled 4PB that the Stiffness Repetition failure criteria is an overall good failure criteria if used on the W_c^R curve. As shown previously the determined failure point is on the turning point of the stiffness curve, resulting that it is also mirrored on the turning point of the W_c^R curve. This relation between a stiffness curve and the total released pseudostrain energy curve is set through the strain amplitude relation. Disregarding any relation with the phase angle on the dissipated energy. Because of this theoretical application without the phase angle, the Stiffness Repetition fatigue criteria holds for the 4PB force controlled W_c^R curve.

In figures 5.18 and 5.20 the results are given for the G^R curves of the displacement and force controlled loading modes. Especially for the force controlled 4PB tests the general behaviour is hard to capture due the fast increment of the displacement amplitude at failure. Resulting in a larger scale on the y-axis to capture this. The calculated G^R values for all displacement controlled tests are on average 1.17 larger than for the fitted method. For the force controlled loading mode the calculated G^R are 1.27 higher than the fitted method. This is the opposite of the results from Li, where the fitted G^R values on both modes of loading were much higher.

Given in figure 5.21 is the method where the G^R is calculated by the given Sabouri equation. With more samples the overall behaviour can be more defined and given more substantiation. The method provides quite a good R-squared for the displacement controlled results. The force controlled does still have quite a lot of scatter, this is however to be expected from the different test setup, the amount of PR and the reuse of the samples.

In figure 5.22 the result with the fitted method is shown. The scattering is higher for both the force as the displacement controlled results. Resulting in a lower R-squared value overall.

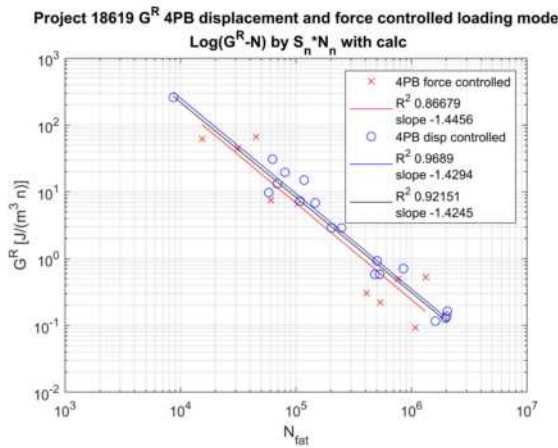


Figure 5.21: G^R calc from 18619 force and displacement controlled

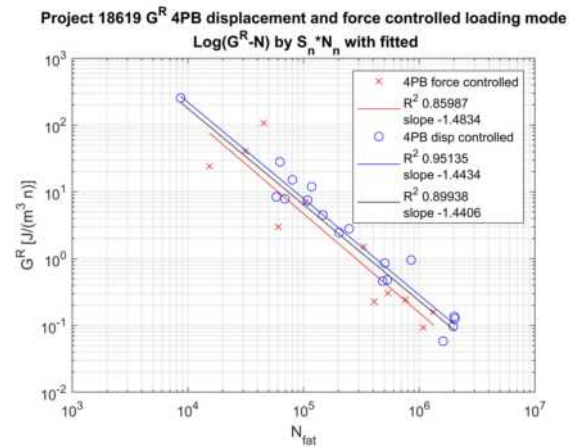


Figure 5.22: G^R fitted from 18619 force and displacement controlled

5.3.3. Conclusion

In this section the results for the 4PB in different loading modes were compared. The following conclusions are made: The VECD method is applicable on both 4PB displacement as force controlled loading modes. The set failure criteria by using the Stiffness Repetition can be applied and result in a consistent failure point. Different methods to determine G^R are discussed and the calculation method gave the best G^R results for both modes of loading. The found G^R between the two different mixtures are unique and are temperature dependent.

5.4. VECD shift hypothesis

Chapter 4 showed the mixture unique and different magnitudes of the slope of dissipated energy. Asphalt concrete is frequency dependent on the measured stiffness during linear frequency sweep testing and during fatigue testing. The linearization of the fatigue in the VECD method through parameter E_{LVE} , leads to the established of a frequency shift factor that is directly related to the found results of the frequency sweep. In other words, fatigue testing on a certain frequency can be shifted with the E_{LVE} from the frequency sweep to another frequency and find the same $\log(N_{fatSN} - G_{calc}^R)$ line.

The main assumption and hypothesis is therefor stated as follows: The $\log(N_{fatSN} - G_{calc}^R)$ fatigue relation is frequency dependent and can through the parameter E_{LVE} be shifted to another performed fatigue frequency test. Time was limited to completely validate this statement, during this already broad research. The recommendation is made to further research this in a different specific study. In the next subsection the results leading this assumption are given.

Mixture 19018 on the CY-ITT was performed on two different frequencies. Given in figure 5.23 is the found G^R relation to the number of load cycles at failure. There is a distinct shift visible between the two frequencies. The E_{LVE} for the 30 Hz is given at 11260 MPa and for 10 Hz at 8617 MPa by figure 3.12 from the frequency sweep. G^R is a rate and not a ratio dependent method, resulting that E_{LVE} does influence the rate of the pseudostrain energy. In figure 5.24 is the result given if the 30 Hz performed tests are recalculated with the 10 Hz assumed linear stiffness. The result is a single line describing the rate of the pseudostrain energy function.

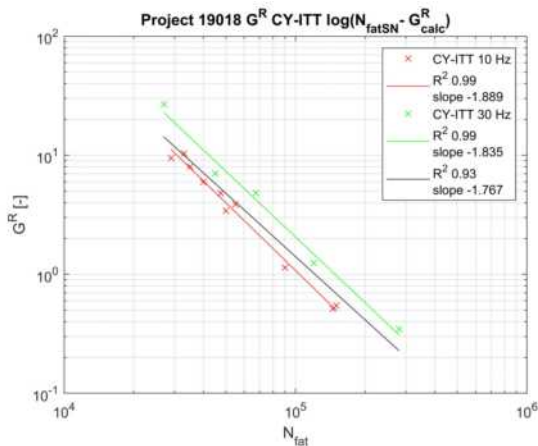


Figure 5.23: G^R line 19018 CY-ITT on 10 and 30 Hz.

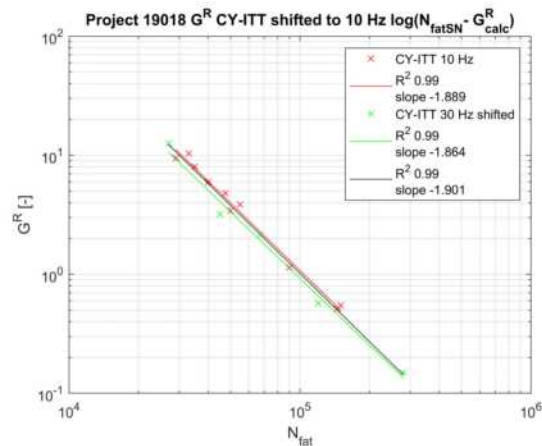


Figure 5.24: G^R line 19018 CY-ITT shifted to 10 Hz.

As mentioned only a single project was performed on two fatigue frequencies. The tests were furthermore only conducted on CY-ITT and not on 4PB to establish a scientific backing of the statement. More research should be conducted to validate the statement. In the next subsection we discuss the impact on the fatigue relation between the CY-ITT and 4PB. Both on the original G_R and the hypothesised shifted line.

5.5. Mixture Results

In this section the CY-ITT force controlled and 4PB displacement controlled fatigue results with the $\log(N_{fatSN} - G_{calc}^R)$ relation are presented and discussed. First the individual mixture results are presented. Starting with the same frequency performed mixture 18590. It is followed with the different mixtures in a single graph to determine the uniqueness of the $\log(N_{fatSN} - G_{calc}^R)$ relation.

5.5.1. Individual $G^R - N_{fatSN}$ Results

Mixture 18590 was performed in its entirety on 30 Hz so the discussed shift factor does not play a role on these results. In figure 5.25 the result is given for the 4PB and CY-ITT on 30 Hz. The results is a shifted line that is not perfect parallel. The measured fitted slope parameters of 2 and 1.65 in figure 5.25 show a to large difference. However the perfect parallel behaviour can occur as shown for the latter mixture 19020 in figure 5.27. The remaining shift factor between both fatigue line in mixture 18590 is of a magnitude 6.

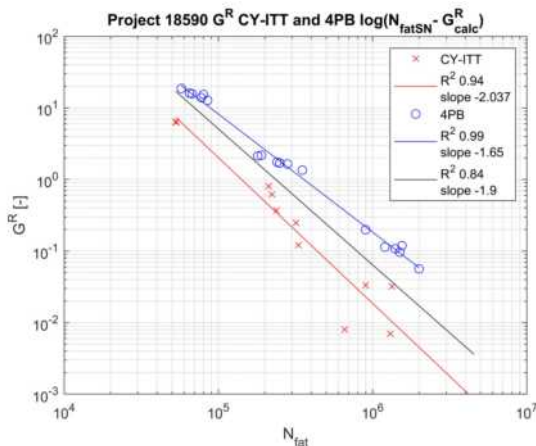


Figure 5.25: G^R line 18590

The CY-ITT rate of pseudostrain energy is significantly smaller than that of the 4PB in figure 4.78. Interpreting that the amount of pseudostrain energy over the number of load repetitions is smaller than that of a 4PB test. A explanation is given by the calculated small strains at the center of the CY-ITT sample. The pseudostrain and therefore the pseudostrain energy rate is related to measured strain by equation 2.28. A small strain relates directly to a small G^R . Although the found E_{LVE} of the CY-ITT is on average 18% higher than the 4PB, the measured strains of the 4PB are a factor 3 higher. Resulting in a definite difference in the found pseudostrain rate.

For completeness the difference with en without the E_{LVE} shift is given for mixture 19020. In figure 5.26 the CY-ITT E_{LVE} on 10 Hz is 6256 MPa. The 4PB is given at 30 Hz at 7886 MPa. In figure 5.27 the shift over the frequency sweep is applied on the CY-ITT from 10 to 30 Hz with E_{LVE} at 8453 MPa.

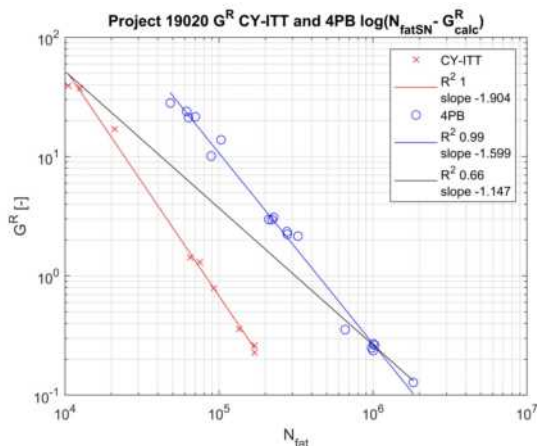


Figure 5.26: G^R line 19020

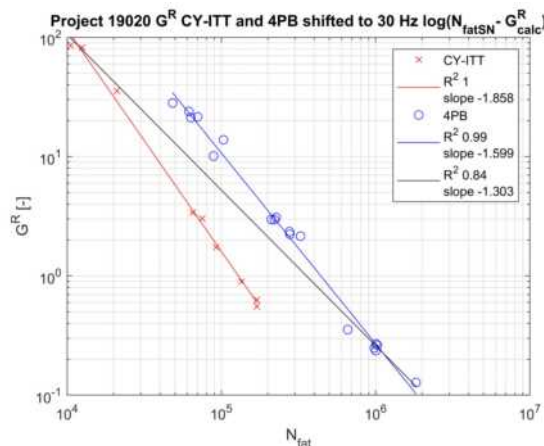


Figure 5.27: G^R line 19020 CY-ITT shifted to 30 Hz.

The none shifted result of G^R in figure 5.26 results in a distinctive shift. Shifted with E_{LVE} in figure 5.27, the fatigue lines are brought more closer, resulting in an almost perfect parallel behaviour. However the found difference between both lines is still around a factor 6 for G^R .

Results for mixture 18501 is given in figures 5.28 and 5.29. The final shifted line is again in the same magnitude different between the CY-ITT and 4PB. However if the CY-ITT is shifted through the linear stiffness of E_{LVE} , the slope of the CY-ITT decreases towards the 4PB fatigue line. A constant shift factor applied after the G^R is therefore not an option as that does not change the slope of G^R .

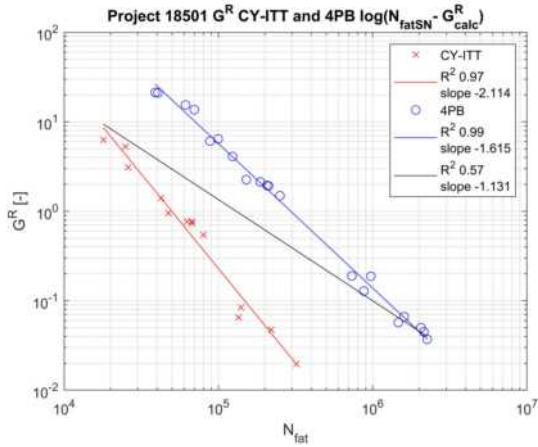


Figure 5.28: G^R line 18501

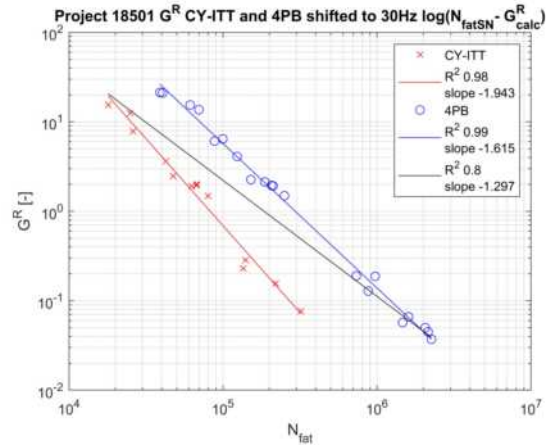


Figure 5.29: G^R line 18501 CY-ITT shifted to 30 Hz.

A third and final example is given with mixture 19051. The mixture is composed of a modified type bitumen which resulted in a high stiffness and high fatigue life from Chapter 3. The result is given in figure 5.30 for the original CY-ITT 4PB G^R relation and the shifted result in figure 5.31. The LVE for the CY-ITT at 10 Hz is given at 10180 MPa and the 4PB at 30 Hz at 11150 MPa. The resulting leftover gap between both lines in the shifted result of figure 5.31 has a magnitude of around 4. Proving that a constant none mixture related shift factor is not applicable.

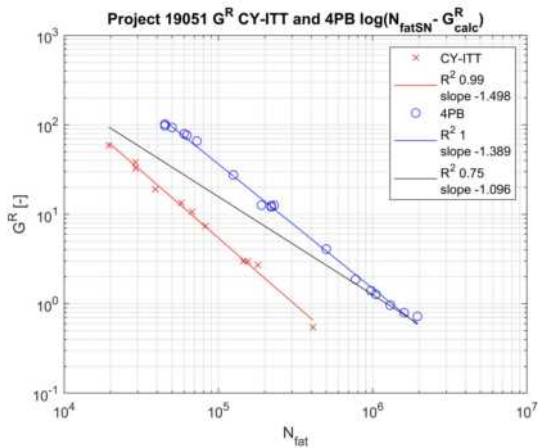


Figure 5.30: G^R line 19051

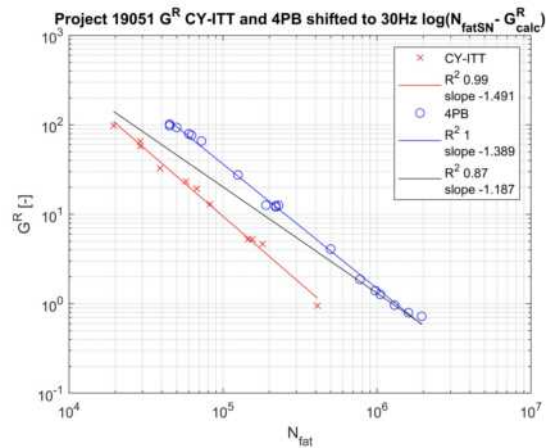


Figure 5.31: G^R line 19051 CY-ITT shifted to 30 Hz.

The shift hypothesis applied to the 4PB would result in a similar behaviour as in the previous figures. The shift would take place from 30Hz to 10 Hz, resulting in a downwards shift of the 4PB G^R fatigue line. The resulting difference between both line was found to be comparable with the shift applied on the CY-ITT.

The previous results all showed a considerable gap between the CY-ITT and 4PB. Another distinction was made in the values found for G^R . Mixture 19051 is considerable higher for both CY-ITT and 4PB than mixtures 18501 and 19020. The overall results between the different mixtures is given and discussed in the next section.

5.5.2. All mixtures

5.5.2.1. 4PB

The previous results, given and non given from each individual mixture on 4PB are compared in figure 5.32. All results are given at the 30 Hz standard test frequency and calculated through the mixtures corresponding E_{LVE} . The overall differences between the mixtures is not great. Were the traditional fatigue life relation with the strain gives a good distinction between mixtures, the result in figure 5.32 does not. Mixture 19051 stands out with its special modification. Together with the standard PMB mixture 18619. The high stiffness related, but low traditional fatigue life mixture of 18607 is relatively high compared to the other mixtures. Suggesting that the E_{LVE} has a significant influence on the overall outcome of the $\log(N_{fatSN} - G^R)$ graph.

Analysing the results it comes forth that most mixtures describe the same rate of pseudostrain energy. Most mixtures already show this same fatigue relation in the traditional relation in figure 3.42. The scale is however set greater in figure 5.32 compacting the bunch together. The bunch mixtures are all made with the same type of bitumen. The VECD method therefore presents a similar way of defining the better performing mixtures in fatigue.

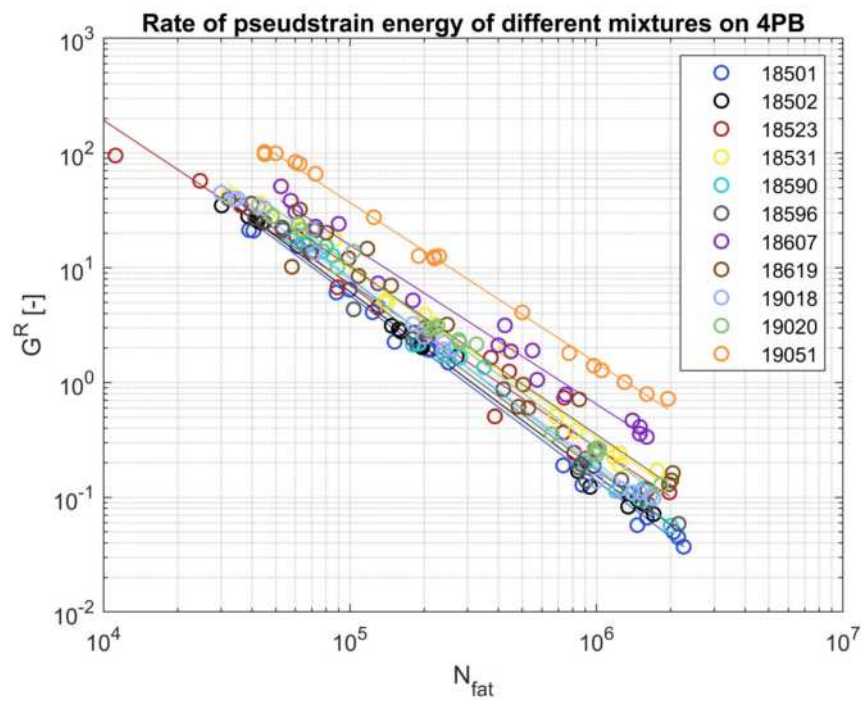
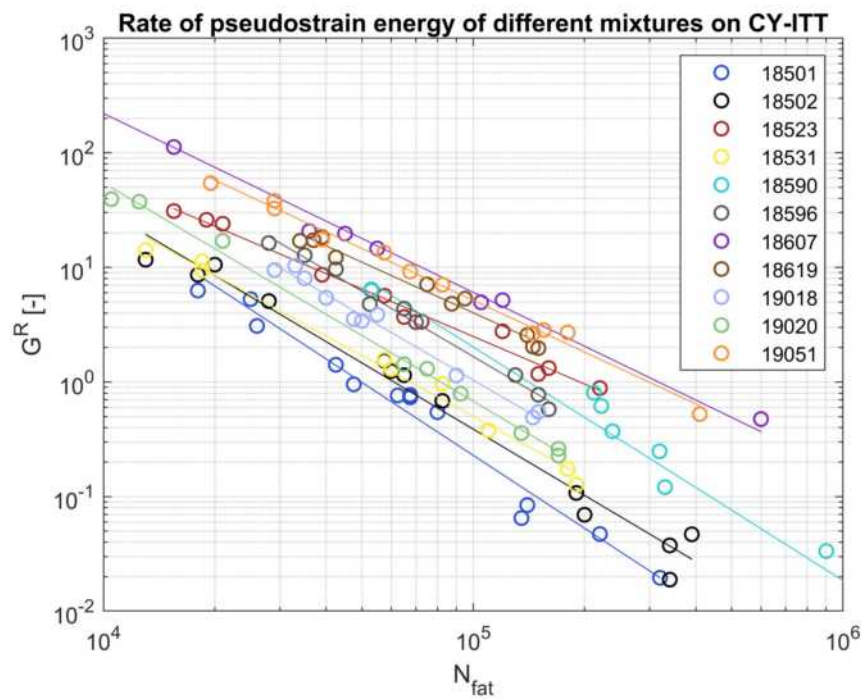
5.5.2.2. CY-ITT

In figure 5.33 the pseudostrain rates are given for the different mixtures performed on the CY-ITT. All mixtures are given at their tested temperature and frequencies. Two remarks to the presented mixtures, mixture 18607 was performed on a lower temperature and 18590 was performed on 30 Hz. They are therefore not directly comparable to the other mixtures. 18590 can be shifted downwards to the 10 Hz frequencies as stated in Section 5.4. The temperature dependence or shift was not established, but mixtures 18607 is likely to be shifted lower, as lower temperatures influence the stiffness positively during fatigue testing.

The results are spread out more compared to the 4PB. Resulting that the overall found G^R values deviates more on a CY-ITT test setup compared to the 4PB. This can be explained partly for the high variability that is found for the stiffness values during the frequency sweep. As cored samples have no defined test direction, turning a specimen can give a difference in stiffness of 10%, see appendix B. This would result in a shift on the G^R as it is dependent on E_{LVE} . The influence of this variability of the measured stiffness during frequency sweep testing is a recommendation for a future research project. Another explanation is the initial compaction of the sample. This results that the W_c^R curve drops below zero if not shifted. This practical problem and resulting shift is not taken into account when the VECD theory for the CY-ITT was formed in 2. The result is that the W_c^R curve does not describe truthfully the inverse stiffness curve. Taken into account that each mixture is different in its ability to resist permanent deformation. The method therefore does not longer describe only fatigue damage but becomes subjected to the initial permanent deformation. The influence of this part is hard to study as all specimen show this behavior in some degree.

A remarks is placed on the none confirmation the $\log(N_{fatSN} - G^R)$ provides on the CY-ITT. Where the 4PB provides a concurring result with the previous results made in the traditional and RDEC results. The CY-ITT results add only more uncertainly and other parameters that are not controllable during a force controlled fatigue test.

The $\log(N_{fatSN} - G^R)$ proved to be stiffness related and the G^R relation to the number of load cycles till failure did not provide the linking behaviour sought in this thesis. The chapter is concluded in the next section.

Figure 5.32: G^R line for different mixtures on 4PBFigure 5.33: G^R line for different mixtures on CY-ITT

5.6. Conclusion

In this chapter the results were given of the application of the VECD method on the CY-ITT and 4PB fatigue test. The method is established through the increase of the triangle formed by the pseudostiffness vector F . Disregarding the influence of the phase angle. It resulted in a method that gives the rate over the summation of this pseudostiffness. Making it dependent on the inverse relation to the actual measured stiffness. Directly endorsing that that the failure criteria is set by the stiffness dependent Stiffness Repetition method.

The calculated G^R resulted in the same scattered behaviour as the RDEC and follows the same bathtub shape. The scatter prevented a feasible determination of the G^R . The actual rate of the pseudostrain energy G^R was therefore determined with three different methods. The stated calculation method proved to be the most coherent. The resulting fatigue relation of $\log(N_{fatSN} - G^R)$ proved to be mixture and loading mode independent for the two 4PB fatigue projects.

The stated frequency shift hypothesis was partly proven for the CY-ITT setup. Stating that the G^R fatigue line can be shifted over the frequency domain related to the frequency sweep. However the shifted and non shifted G^R fatigue line between the CY-ITT and 4PB didn't form a single coherent line. The fatigue $\log(N_{fatSN} - G^R)$ relation provided by the VECD method is therefore stated as sample size and or stress strain distribution dependent.

Sub-question 5 and 6 for the VECD can therefore be shortly summarized that the VECD is a mixture unique rate dependent fatigue relation that cannot couple the CY-ITT and the 4PB. The critical influence parameters found are the G^R and the relation to the N_{fatSN} . It is therefore recommended to investigate the full C-S relation on both the 4PB and CY-ITT.

6

Conclusions and recommendations

In this research an answer was sought to the following question:

How and can the energy methods be applied in coupling the 4PB and CY-ITT fatigue tests?

In this chapter the conclusions and recommendations of the research program are described. Section 6.1 contains the conclusions directly related to the research questions and a separate section on the research and testing itself. It is followed by the recommendations in Section 6.2.

6.1. Conclusions to the research question

6.1.1. Main research question

The objective of this research was formed to find a mixture unique relation to couple the 4PB and CY-ITT fatigue test results. The method to find that relation was sought in using two energy models, leading to the research question stating if the energy methods could be applied in establishing that relation. From this research it came forth that the first used energy method of 'Ratio of Dissipated Energy Change (RDEC) can with reservation be used for that coupling. However it will loose each individual mixture uniqueness characteristic in the process, making it unable to identify different mixtures on their fatigue life. The Viscous-Elastic Continuum Damage model (VECD) used with the derived relation of the pseudo strain energy rate and number of cycles before failure, could not establish a coupled relation between the CY-ITT and 4PB fatigue tests.

6.1.2. Sub-questions

1. How are the 4PB and CY-ITT fatigue tests characterized and what are their differences?

In Section 2.2 the fatigue test are described in detail. The differences between the fatigue tests are given in table 2.1. The 4PB beam fatigue test is based on a beam with a constant moment at the inner clamps, resulting in a assumed cyclic linear envelope at both outer edges. Controlled by a set displacement that is held constant over the number of load repetitions the amount of force needed for this displacement decreases. The CY-ITT has a cylindrical shaped specimen under a cyclic, always compression, force tested that results in an exponentially increase of the displacement amplitude. The maximum amount of horizontal stress and strain is set by the bi-axial stress-strain formulation at the center of the specimen.

The most significant difference is the shape of the specimen. That results in two other significant differences. Namely the mode of loading and the stress-strain distribution. The other differences found are derived from these.

2. What are the main energy methods currently found in pavement engineering literature and how are they described

The two most described energy methods in literature are those of the Ratio of Dissipated Energy Change

(RDEC) and the Viscous-Elastic Continuum Damage (VECD). These are described in detail in Section 2.3. The main concept of the RDEC is that it is based on the change of the hysteresis loop over the number of load repetitions. This change is then normalised by the same hysteresis loop. Resulting in this Ratio based method on dissipated energy change. The derived method of the VECD applied in this thesis is based on the rate of the pseudo energy density function or G^R . Not the C-S damage relation. This method utilises the linearization of the dissipated energy change by the pseudostiffness. Creating a method that is based on the summation of the change of the pseudostiffness. Taking the rate of that change versus the number of load repetitions is the final overall fatigue line relationship.

3. Which failure criteria method applied to both modes of loading describes the specimen failure point the most accurate?

A repetition based methodology proved to be the most accurate, in which the Stiffness Repetition method came forth as the most accurate method to describe the loss of stiffness tilting point for both the 4PB and CY-ITT. This Stiffness Repetition method is based on the original Energy Ratio failure criteria described in Section 2.4. It was proven in Section 3.3.1 to be applicable to the 4PB displacement controlled fatigue test. The Stiffness Repetition is the same method as the current failure criteria of the CY-ITT, only renamed for clear indication. As for the dissipated energy curve, the failure was set by the more stable, through the phase angle, method of the original Energy Ratio. This can be found in Section 4.3.1 in table 4.1

4. How can the energy methods be applied to the different properties and specimen shapes of both fatigue tests?

This is discussed in Section 2.3.2 for the RDEC and in 2.3.4 for the VECD. Both energy models are directly applicable to the 4PB fatigue results through the stated formulas. For the CY-ITT however with a constant compression state and the assumed failure from fatigue at the center of the specimen, a factor of 2 was formulated for the dissipated energy, see equation 2.12, by the constant compression and peak-peak measurement values on the hysteresis loop. The CY-ITT fatigue results through the VECD method is stated to be dependent on the full force amplitude as given in figure 2.25, in Section 2.3.4.

5. What are the critical influence parameters of each of the two applied energy methods on the resulting fatigue line?

For the RDEC these are the fitted dissipated energy slope $x(1)$ parameter, which if normalised result to the Plateau Value and the cycles till failure set by the criteria N_{fatER} . The fitting function on the dissipated energy curve can be found in Section 4.3.3 and the importance of the parameter $x(1)$ is discussed in Section 4.5. For the VECD these are the rate of the pseudo strain energy density function G^R and the failure criteria by N_{fatSN} . G^R is established through equation 5.1 and has the preference over a fitting equation as discussed in Section 5.2.3. The N_{fatSN} is used over the N_{fatSN} failure criteria as the VECD is not related to the phase angle.

6. Is the resulting fatigue life parameter unique and useful in comparing and coupling the different fatigue tests?

No. For the RDEC method figure 4.59 was established for all 4PB mixtures and proved that mixture uniqueness disappears with the Ratio aspect of the method. This was also confirmed with the application of 'a same mixture, different density's and traditional fatigue life' in Section 4.9. Here there was no distinct difference to be found with the RDEC method. So although the different fatigue test are coupled, see also Section 4.8 for the Uni-axial fatigue test conformation of that, the RDEC method is not useful. The VECD method is found to be mixture unique, see figure 5.32. It is however through the rate of pseudo energy density equation vs cycles till failure, not succeeded in coupling the CY-ITT and 4PB fatigue test, see figure 5.26 in Section 5.5.1.

7. How do the two energy methods differ from one another when applied?

Both energy methods are foremost based on the linear increasing (CY-ITT) and decreasing (4PB) assumed phase 2, see figure 2.1, of a fatigue curve and the rate of this change. Where the RDEC method uses this rate with a normalisation part in its equation, the VECD uses the linearization of the dissipated energy by the linear stiffness, resulting in a rate based equation of the stiffness curve, see Section

5.1. The greatest difference is therefore found in the Ratio and Rate aspects of both methods. It is unproven in this thesis, but highly probable that if the G^R is normalised like the RDEC, a similar result can be found.

6.1.3. Research related conclusions

During the research some aspects are found that are worth mentioning here at the end:

A. Stiffness results CY-ITT-4PB

The frequency sweep proved that the CY-ITT has on average a 18% higher stiffness value at 8 Hz than the 4PB. The measured phase angle is on average the same at 8 Hz. For the different mixtures, there is no constant coherent parallel behaviour between the CY-ITT and 4PB over the set frequencies, see the figures in Section 3.2.3. Setting the requirement that a possible shift factor in fatigue testing should be related in magnitude to the found frequency sweep results. The calculated stiffness and phase angle are opposites of each other.

B. Traditional fatigue failure criteria 4PB

The traditional fatigue criteria set by the 50% reduction in stiffness for the 4PB was replaced by the Stiffness Repetition method in this thesis. Section 3.3.1 discusses this in detail as the 50% reduction of stiffness tends to overshoot the tilting point at low strain ranges. At high strain ranges the failure is often defined too early. The established failure by the Stiffness Repetition method determines the failure consistent on the tilting point. The resulting $\log(\varepsilon_{ini} - N_{fatSN})$ relation however leads to a decline of the slope of the fatigue line.

C. Traditional fatigue life 4PB vs CY-ITT and the influence of permanent deformation

Although the CY-ITT in its calculations compensate for the measured permanent horizontal displacement for the strain value, see Section 2.2.2 and figure 2.10, the influence of the permanent deformation on fatigue life itself should not be neglected. From figure 3.43, where the CY-ITT fatigue life is given, mixtures with high permanent deformation resistance perform better than their beam counterparts on 4PB in figure 3.42. It should therefore be considered if the CY-ITT is a 'true' tensile failure fatigue test and not partly influenced by other mixture properties.

D. Shifting isotherms of rate based fatigue line by frequency sweep results

In Section 5.4 the possible shifting of a fatigue line relation with the frequency sweep result was used for the G^R established fatigue line between different frequencies. Meaning that there could be a possible connection between the stiffness obtained during the frequency sweep and the resulting rate of a fatigue test at different frequencies.

E. Final remarks

The core concept of both energy methods is the rate of the increase or decrease of the measured force and displacement respectfully. To find this parameter it is assumed there is a stable second phase, which due load dependence, is found to be never really stable, see Section 4.4. The rates itself cannot be determined directly due the huge amount of scatter, Section 4.6. A linear line is applied on a natural logarithm curve in the assumed stable phase to determine this rate. As a final conclusion it can be stated that both methods at their current research state, with the high dependence on the different assumptions, are not to be used outside the current experimental state in determining the fatigue life of asphalt concrete.

6.2. Recommendations

This section provides recommendations for further research on the topics discussed in this thesis.

1. RDEC

With the outcome of this research, indicating the loss of each unique mixture characteristic, an application to the practical Functional Verification program and other research related to the direct RDEC method should be disregarded or approached cautiously.

2. VECD

Although the applied rate of G^R was not successful in coupling the CY-ITT and 4PB fatigue test, a solution can possibly be sought in the full C-S relation of the VECD. In this research mentioned in Section 2.3.4. Here the relation is based on two different parameters, releasing its dependence on the number of load repetitions N . This theory is already applied on the DSR as the LAS test.

3. CY-ITT

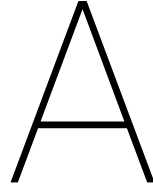
The CY-ITT test setup is used heavily in this thesis, however some basic functionalities are not completely understood. First is the measurement accuracy, heavily debated, although data results show a clear sinusoidal wave, see figure 4.3, it can be checked with higher accurate strain gauges to eliminate further discussions. Second, the influence of permanent deformation, vertical as well horizontally, on the fatigue life. It's possible influence on the measured fatigue life could be significant and misleading our current interpretations of the results. Third, The use of a CY-ITT test setup that can be displacement controlled. This can possibly be achieved by using a very stiff frame around the cylindrical sample that pushes the sample to its original position after each load cycle, eliminating the permanent deformation.

Bibliography

- A. Abedali. Predicting complex shear modulus using artificial neural networks. *Journal of Civil Engineering and Construction Technology.*, 2015.
- M. Abojaradeh and W. Witzak. Validation of initial and failure stiffness definitions in flexure fatigue test for hot-mix asphalt. *ASTM Journal of Testing and Evaluation*, 35:95–102, 2007.
- G. Airey, D. Presti, and A. Subhy. New simplified approach for obtaining a reliable plateau value in fatigue analysis of bituminous materials. *Engineering Failure Analysis*, 2017.
- G. Al-Khateeb and K. Ghuzlan. The combined effect of loading frequency, temperature, and stress level on the fatigue life of asphalt paving mixtures using the idt test configuration. *International Journal of Fatigue*, 59:254–261, 2014.
- H. Benedetto, D. Perraton, and R. Toehara. Ability of the classical fatigue criterion to be associated with macro-crack growth. *Materials and Structures/Materiaux et Constructions*, 2015.
- S. Carpenter. Perpetual pavement: Laboratory validation. *57th Annual Ohio Transportation Engineering Conference*, 2003.
- S. Carpenter and K. Ghuzlan. Energy-derived damage-based failure criterion for fatigue testing. *Transportation Research Record*, 1723,TRB, 2001.
- S. Carpenter and M. Jansen. Fatigue behavior under new aircraft loading conditions. *Proceedings of Aircraft Pavement Technology in the Midst of change*, pages 259–271, 1997.
- S. Carpenter, K. Ghuzlan, and S. Shen. Fatigue endurance limit for highway and airport pavements. in transportation research. *TRBh Board, No. 1832 Engineering Conference*, pages 131–138, volume = 1832, quality = 0, 2003.
- civil uminho. 4pb platform. URL <http://www.civil.uminho.pt/4pb/>. Online accessed 10 May 2020.
- A. Cocurullo, G. Airey, A. Collop, and C Sangiorgi. Indirect tensile versus two-point bending fatigue testing. *Transport Proceedings of the Institution of Civil Engineers*, 161-4:207–220, 2008.
- CROW. Crow oia, a. URL <https://www.crow.nl/thema-s/infratechniek/asfaltverharding/oia>. Online accessed 1 May 2020.
- CROW. Crow asfalt-impuls, b. URL <https://www.crow.nl/asfalt-impuls>. Online accessed 20 February 2020.
- W. Dijk van and H. Moreaud. The fatigue of bitumen and bituminous mixes. *3th International Conference on Structural Design of Asphalt Pavements (ISAP)*, 1, 1975.
- W. Dijk van and W. Visser. The energy approach to fatigue for pavement design. *Association of Asphalt Paving Technologists (AAPT)*, 46:1–41, 1977.
- S. Dijkhuis. Fatigue and healing of asphalt mortar. *Master Thesis*, 2016.
- R. Ebe. Software package for asphalt testing: Cyclic indirect tension tests (citt) according to al sp asphalt 09. 2012. doi: BRA3.958121.10.
- L. Francken and C. Clauwaert. Characterization and structural assessment of bound materials for flexible road structures. *Proceedings of the Sixth ICSDAP*, pages 130–144, 1987.
- FGSV Forschungsgesellschaft für Strassen-und Verkehrswesen. Arbeitsanleitung zur bestimmung des steifigkeits- und ermüdungsverhaltens von asphalten mit dem spaltzug-schwellversuch als eingangsgrosse in die demensionierung al-sp-asphalt 09. *FGSV 430*, 2009.

- J. Grenfell. Experimental characterisation of fatigue damage in foamed bitumen stabilised materials using dissipated energy approach. *Construction and Building Materials*, 216:1–10, 2019.
- F. Haddadi and H. Hosseini. Validation of a simplified method in viscoelastic continuum damage (vecd) model developed for flexural mode of loading. *Construction and Building Materials*, 95:892–897, 2015.
- G. Hondros. Evaluation of poisons ratio and the modulus of materials of a low tensile resistance by the brazilian (indirect tensile) test with particular reference to concrete. *Austr. J. Appl. Sci. 10(3): 243-268.*, 1959.
- P. Hopman and A. Pronk. Energy dissipation: The leading factor in fatigue, highway research, sharing the benefits. *Proc. Conf. of the United States Strategic Highway Research Program, Institution of Civil Engineers*, pages 255–267, 1991.
- P. Hopman, P. Kunst, and A. Pronk. A renewed interpretation method for fatigue measurement, verification of miner’s rule. *4th Eurobitume Symposium*, 1:557–561, 1989.
- I. Isailovi, A. Cannone, M. Falchetto, and P. Wistuba. Energy dissipation in asphalt mixtures observed in different cyclic stress-controlled fatigue tests. *RILEM*, 8:693–703, 2016.
- J. Kim and C. Koh. Development of a predictive system for estimating fatigue life of asphalt mixtures using the indirect tensile test. *Journal of transportation engineering*, 138:12, 2012.
- Y. Kim and H. Lee. Viscoelastic constitutive model for asphalt concrete under cyclic loading. *Journal of Engineering Mechanics*, 124:1, 1996.
- Y. Kim, H. Wen, and J. Daniel. Fatigue performance evaluation of westrack asphalt mixtures using viscoelastic continuum damage approach. *FHWA/NC/2002-004*, 2002.
- M. Kutay and M. Lanotte. Viscoelastic continuum damage (vecd) models for cracking problems in asphalt mixtures. *International Journal of Pavement Engineering*, 19:3:231–242, 2017.
- L. Lee. Application of the viscoelastic continuum damage mechanics to asphalt mixtures under indirect tensile load. *Journal of Engineering Mechanics*, 141:5, 2015.
- N. Li. Asphalt mixture fatigue testing. *PhD thesis Technical University Delft*, 2013.
- R. Lytton, Y. Zhang, X. Luo, and R. Luo. Indirect tensile versus two-point bending fatigue testing. *Advances in Asphalt Materials*, pages 243–272, 2015.
- L. Mello, K. Kaloush, and M. Farias. Application of continuum damage theory for flexural fatigue tests. *2nd Workshop on Four Point Bending*, 2009.
- L. Mello, M. Farbrias, and K. Kaloush. Damage theory applied to flexural fatigue tests on conventional and asphalt rubber hot mixes. *Road Materials and Pavement Design*, 11:681–700, 2010.
- E. Oosterhout. Influence of mass density on functional asphalt properties. *Unpublished*, 2018.
- S. Park, R. Kim, and R. Shapery. viscoelastic continuum damage model and its application to uniaxial behavior of asphalt concrete. *Mechanics of Materials*, 24:4:241–255, 1996.
- N. Poeran, M. Mohamad, and B. Sluer. Analyse van vermoeingsgedrag met methode shen & carpenter. *CROW infradagen*, 2016.
- A. Pronk. Temperature increase in an asphalt beam during fatigue, theory and practice. *CROW infradagen*, 1996.
- A. Pronk. Theory of the four point dynamic bending test. *Dienst Weg- en Waterbouwkunde (DWW)*, 2002.
- A. Pronk. Collaborative study with 4pb devices in europe round robin test with three reference beams - annex a. 2009. doi: <http://www.civil.uminho.pt/4pb/beam.htm>.

- A. Pronk. Why the product of the beam stiffness modulus times nk makes sense for an objective determination of the fatigue life in 4pb tests. *Unpublished*, 2019.
- G. Rowe. Performance of asphalt mixtures in the trapezoidal fatigue test. *Euro-Bitumen Conference Barcelona, Spain*, 1993.
- G. Rowe and M. Boulding. Improved techniques to evaluate the fatigue resistance of asphalt mixtures. *Association of Asphalt Paving Technologist*, pages 754–763, 2000.
- M. Sabouri and Y. Kim. Development of a failure criterion for asphalt mixtures under different modes of fatigue loading. *Journal of the Transportation Research Board*, 2447:117–125, 2014. doi: 10.3141/2447-13.
- R. Schapery. Correspondence principles and a generalized j-integral for large deformation and fracture analysis of viscoelastic media. *International Journal of Fracture*, 25:195–223, 1984.
- S. Shen and S. Carpenter. Dissipated energy concepts for hma performance: fatigue and healing,. *Department of Civil and Environmental Engineering, University of Illinois, Urbana (IL)*, 2007.
- B. Sluer and J. Stigter. Functioneel verifiëren asfaltverhardingen. *CROW infradagen*, 2014.
- J. Telman. Verificatie rdec methodiek voor karakterisering asfaltvermoeiing. *Waardenburg*, 2017.
- F. Tolman, B. Sluer, and N. Poeran. Het energiebeginsel voor vermoeiing van asfalt. *CROW infradagen*, 2018.
- B. Underwood, M. Gudatti, and Y. Kim. Improved calculation method of damage parameter in viscoelastic continuum damage model. *International Journal of Pavement Engineering*, 11:354–366, 2010.
- A Wöhler. Wöhler’s experiments on the strength of metals. *Engineering*. 4, 4:160–161, 1867.
- J. Zhang and Y Kim. Development of failure criteria for asphalt concrete mixtures under fatigue loading. *Master thesis*, 2012.



Mixture details

A.1. Overview

In this appendix an overview is given for all mixtures used in the different projects. Even the later left out mixtures of 18529 and 18592. The two mixtures data are available, but not analysed in full for the validation of the energy methods. In table A.1 the rough mixture composition is given for the different fatigue test projects. Added in comparison to table 3.1 in chapter 3 are the machines on which the fatigue test is performed. These can be the Zwick, MTS-86 or the MTS-07. In the case the raw datafiles were available this is indicated by the term 'fitted'. The projects with the raw data and the own developed fitting scripts were compared and the differences found between the FFT method, applied by the controller of the MTS and Zwick machines and the own developed fitting script through a haversine function were found insignificant.

Table A.1: Mixture overview including test setup.

Projectnumber	Mixture	PEN-grade	PR [%]	CY-ITT performed on	4PB performed on
18501	AC 11 Surf	50/70	30	MTS-07	MTS-86
18502	AC 11 Surf	40/60	0	MTS-07	MTS-86
18523	AC 16 Base	30/45 Foam	50	MTS-07	MTS-86
18529	AC 11 Surf	70/100	0	MTS-07	Zwick
18531	AC 8 Surf	70/100 Red	0	MTS-07	MTS-86
18590	AC 16 Surf	40/60	0	MTS-07-fitted	Zwick
18592	AC 11 Surf	40/60	10	MTS-07-fitted	MTS-86
18593	AC 8 Surf	40/60	0	Zwick-fitted	Zwick
18596	AC 11 Surf	30/45 Foam	40	Zwick-fitted	MTS-86
18607	AC 11 Surf	PMB	0	Zwick-fitted	Zwick
18619	AC 16 Base	40/60	85	MTS-07-fitted	MTS-07-fitted
19018	AC 11 Top	40/60	0	Zwick-fitted	Zwick-fitted
19020	AC 11 Top	-	55	Zwick-fitted	MTS-07-fitted
19051	AC 8 Surf	-	50	MTS-07-fitted	Zwick-fitted

- Project 18523, From a road construction project with the same mixture a number of samples are cored. These are compared with the samples prepared in the laboratory.
- Project 18590, the complete CY-ITT is executed at 30Hz.
- Project 18590TU, 150x100 mm gyrator compacted and subsequently cored samples are prepared at the TU Delft from this mixture to be tested on uni-axial fatigue. Tests were performed at 10 Hz on a displacement controlled loading mode.
- Project 18590TU4PB, 4PB test force controlled. A new batch of 18 4PB beams are made special for a force controlled 4PB fatigue test. Due time restrictions the test were not conducted.

- Project 18619TU, the same samples as 18619 were reused to be tested on force controlled loading mode. The beams have been laid to rest for 3 months and turned 90° to minimize the influence from the previous fatigue test. This was a test before special new beams were made.
- Project 18619, Conducted with 0% PR content on three different degrees of compaction to study the practical aspects of distinctive compaction with the RDEC method.
- Project 18607, the CY-ITT is performed at 10 °C and the 4PB at the standard 20°C. This is because the low stiffness of this PMB modified mixture.
- Project 19018, The CY-ITT of this project was partly done on 30 Hz and 10 Hz loading frequency. This project was actually performed on CY-ITT before the CY-ITT of 18590. This to study the difference between the 10 Hz and 30 Hz on the same mixture.

During the testing phase of the 4PB force controlled a lot of setbacks were encountered. This resulted in a lot of time wasted on software adaptations and modifications which shouldn't be necessary. The result was that in the time frame of the research the special prepared beams for this part were left out, so project 18590TU4PB was cancelled. At this moment only the results of Li and the reused beams of 18619 are available for the 4PB force controlled loading mode. In which the beams for Li were tested on 5 °C and the 18619 are reused beams. This gives of course some discussion on the validity of the results. However in both chapter 4 and 5 it shows that the results holds.

A.2. Test remarks

During testing and analyzing the results a lot of remarks were being placed. These can be over the general behaviour of a mixture as for a single specific test result.

Table A.2: Mixture and test remarks overview.

Project number	Deviations and remarks
18501	4PB & CY-ITT both performed good on N_{fatSN} , but too short for high strain ranges.
18502	4PB & CY-ITT both performed good on N_{fatSN} , but too short for high strain range.
18523	8 field cores are available, do not perform in line as the lab mixtures on traditional fatigue .
18529	-Left out, data available-
18531	4PB & CY-ITT both performed good on Nfat
18590	CY-ITT performed on 30 Hz. Both CY-ITT & 4PB show very good results
18590TU	11 samples Uni-axial test performed on displacement control 10Hz
18592	-Left out, data available-
18593	All test were conducted with extra test time
18596	4PB & CY-ITT both performed good on Nfat. On CY-ITT RDEC is little to none visibly
18607	4PB op 20°C en CY-ITT op 10°, both performed good on Nfat
18619	Nfat performed bad on 4PB & CY-ITT, also RDEC is visible, very bad R^2 on fatigue.
18619TU	Beams reused after 3 months of healing turned 90° clockwise tested on stress control
19018	CY-ITT 5 samples on 30 Hz, 11 samples on 10 Hz. Both long test, RDEC visible
19020	4PB & CY-ITT both performed good on determining Nfat
19051	Some 4PB tests were terminated to early to determine N_{fat} . CY-ITT results are determined good.

B

Results mixtures KWS

In this appendix the results of the fatigue tests per mixture are given. These are split between the 4PB and CY-ITT results. This completes the main thesis and gives insight in all the fatigue test results that are used in the main body of this thesis. The basis is formed by the 4PB and CY-ITT tables. For each mixture, 4PB and CY-ITT three fatigue test result are shown graphically at a low, medium and long test duration.

For each result the Stiffness and Stiffness Repetition failure method is given in a single figure. Both $N_{fat50\%}$ and N_{fatSN} are given. The second figure gives the RDEC result, given with the values of PV fitted and mean at N_{fatER} . The row below gives in the third figure the dissipated energy and phase angle. Here the N_{fatSN} and N_{fatER} are given, the fitted line is the parameter $x(1)$. The fourth figure depicts the W_c^R with the fitted line with N_{fatSN} and N_{fatER} . The fifth figure gives the G^R at N_{fatSN} with the three applied methods of fitted, calc and mean values of G^R .

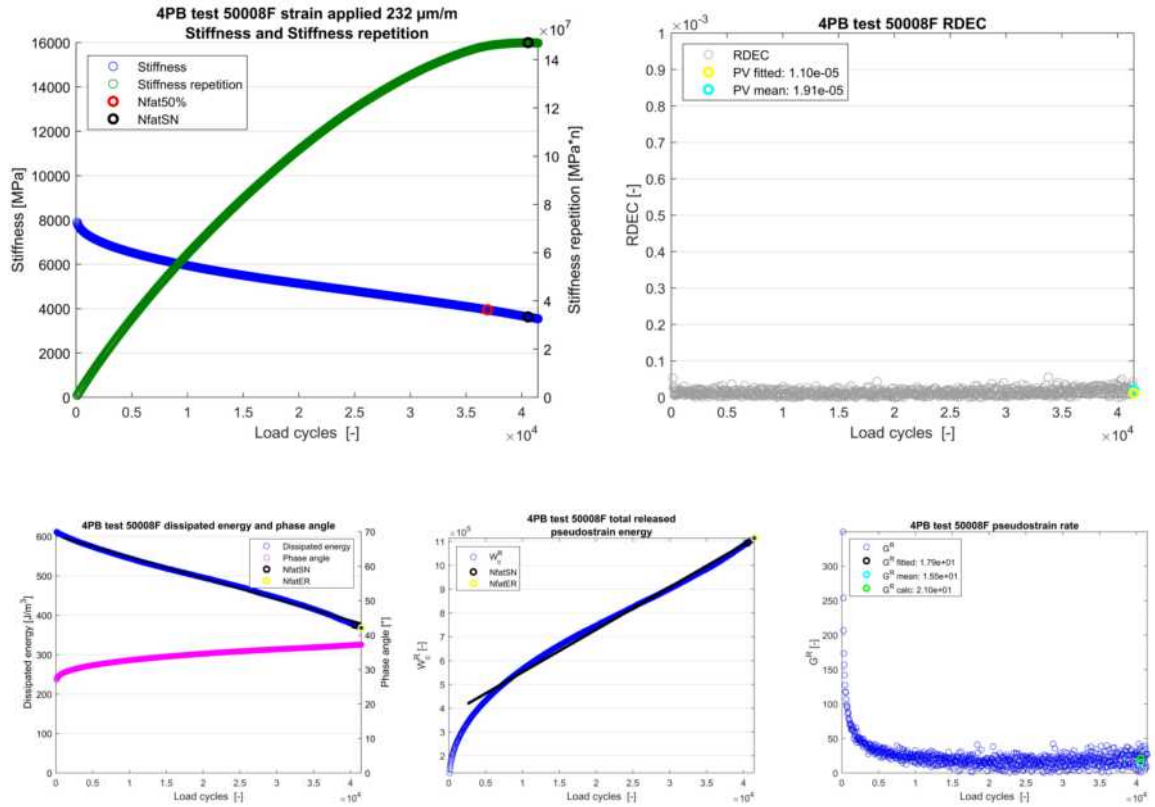
The published fatigue results in this thesis and the remaining left out results are property of the company Koninklijke Wegengbouw Stevin. Usage and publication of the original fatigue test data without permission of the author is not allowed. For research purposes the full digital fatigue data collection can be distributed through the original author. The author can be reached through: renestegeman@gmail.com.

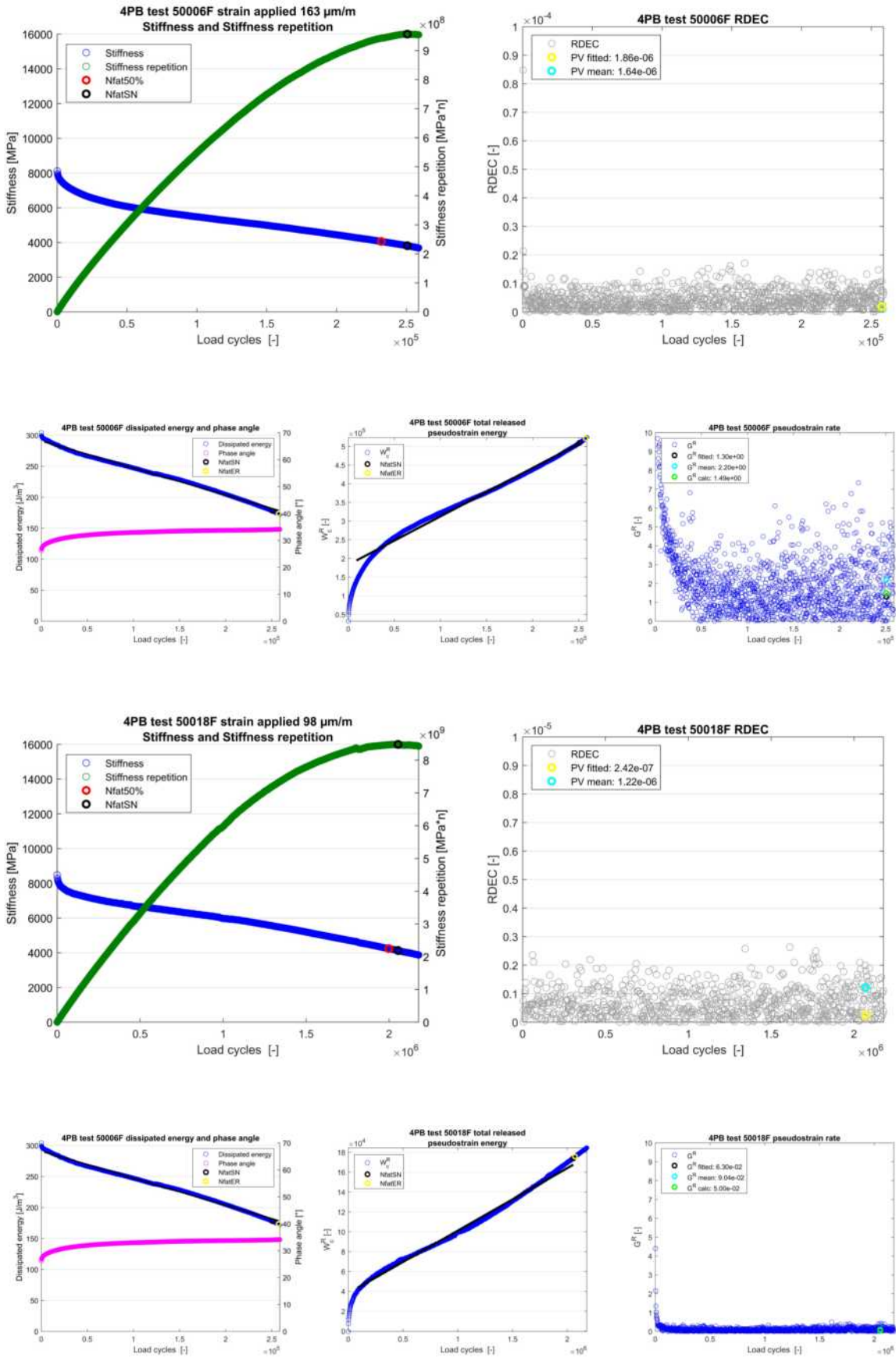
B.1. 18501 results

B.1.1. 4PB

Table B.1: Mixture 18501 4PB results

Sample	Strain applied ε_{ini} [$\mu\text{m}/\text{m}$]	$N_{fat50\%}$	N_{fatSN}	N_{fatER}	$x(1)$	PV fitted (* 10^{-6})	PV mean (* 10^{-6})	ΔPV	G_{calc}^R
50003F	187	120657	123577	126096	-1,01E-03	3,27	6,77	-2,1	4,10
50004F	202	83850	99637	99637	-1,75E-03	4,87	6,86	-1,4	6,44
50005F	116	924269	973870	1015269	-5,84E-05	0,47	0,08	6,2	0,19
50006F	163	232045	250652	257492	-4,36E-04	1,86	1,64	1,1	1,49
50007F	108	946709	876673	896472	-4,26E-05	0,39	0,70	-1,8	0,13
50008F	232	36924	40558	41453	-5,36E-03	11,03	19,12	-1,7	21,04
50012F	98	2533288	2257231	2260831	-1,12E-05	0,13	0,81	-6,4	0,04
50013F	234	37072	38967	40111	-5,38E-03	11,15	20,94	-1,9	21,33
50014F	170	212423	211778	214118	-4,75E-04	1,88	0,00	703,1	1,92
50015F	97	1602401	1465254	1494053	-1,67E-05	0,19	0,23	-1,2	0,06
50016F	189	92147	88113	88653	-1,18E-03	3,63	7,98	-2,2	6,09
50017F	167	158724	151655	155795	-5,91E-04	2,22	8,92	-4,0	2,26
50018F	98	1997757	2053832	2070031	-2,03E-05	0,24	1,22	-5,0	0,05
50021F	169	180671	187111	187651	-5,57E-04	2,17	1,87	1,2	2,13
50022F	233	50220	61191	61141	-3,53E-03	7,47	1,76	4,2	15,44
50023F	103	1757899	1602047	1607447	-1,93E-05	0,20	0,20	-1,0	0,07
50024F	233	60652	69704	69903	-3,07E-03	6,50	11,79	-1,8	13,66
50025F	114	789898	732676	752476	-5,66E-05	0,47	1,67	-3,5	0,19
50026F	168	186938	206553	206553	-5,85E-04	2,35	2,82	-1,2	1,95
50027F	101	2340511	2145629	2160029	-1,46E-05	0,16	0,32	-2,0	0,04

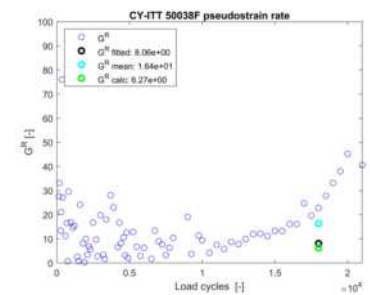
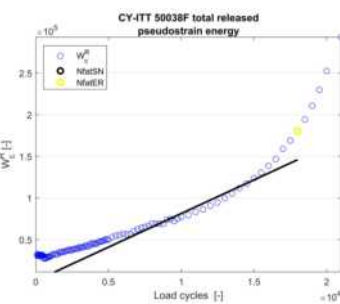
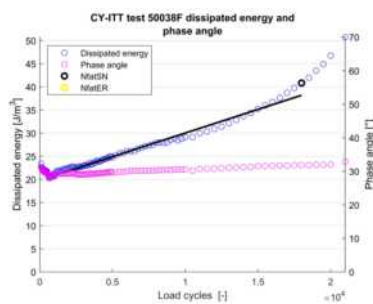
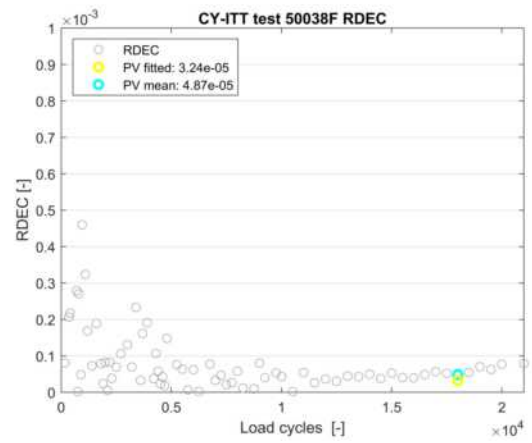
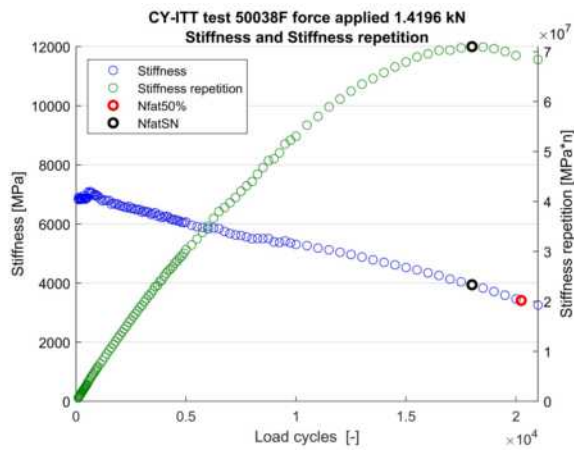


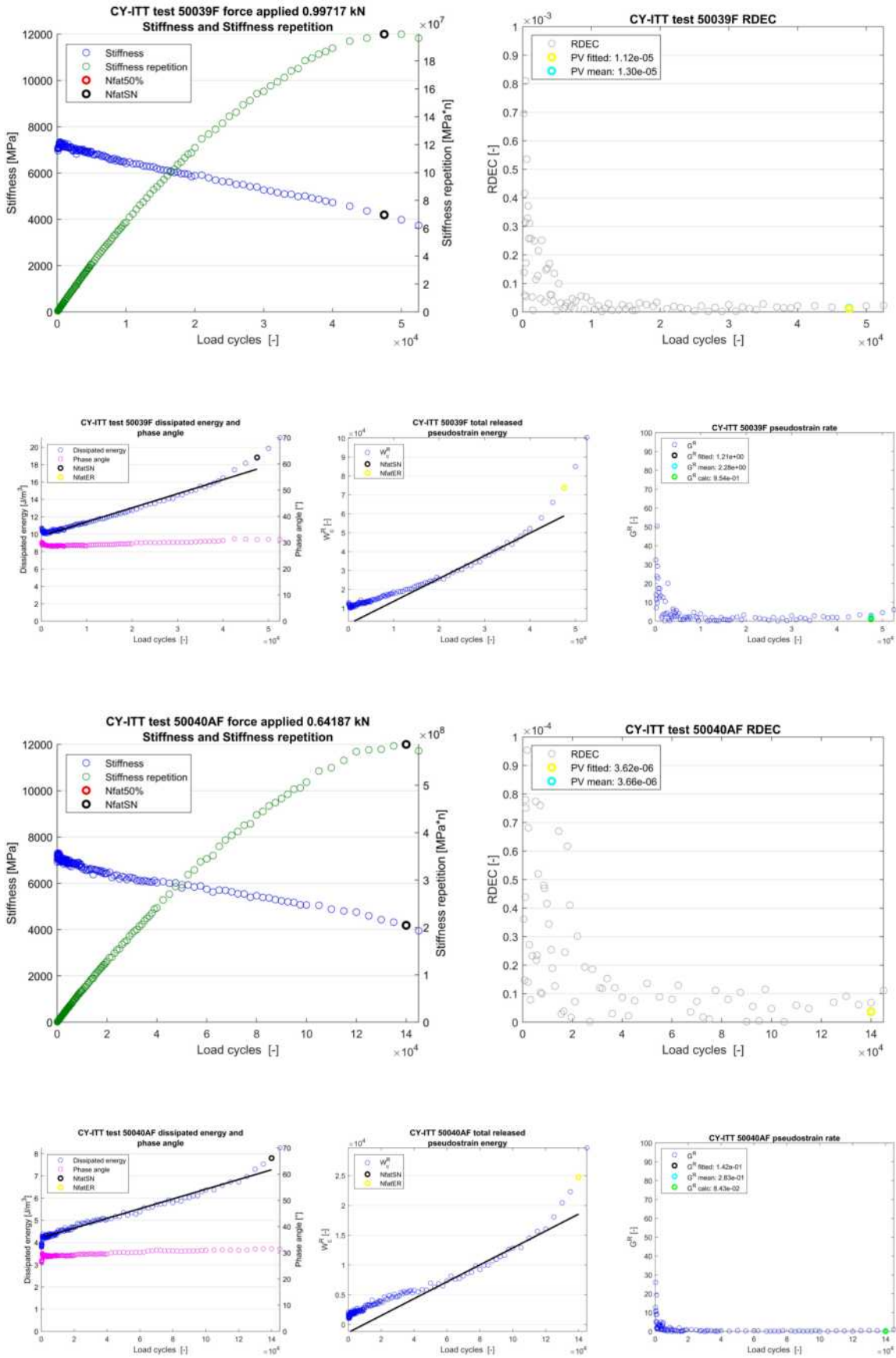


B.1.2. CY-ITT

Table B.2: Mixture 18501 CY-ITT results

Sample	Strain n=100 ϵ_{ini} [$\mu\text{m}/\text{m}$]	$N_{fat50\%}$	N_{fatSN}	N_{fatER}	$x(1)$	PV fitted (*10 ⁻⁶)	PV mean (*10 ⁻⁶)	ΔPV	G_{calc}^R
50031F	55	-	26000	28000	4,76E-04	19,26	19,20	1,0	3,09
50032F	42	-	67500	67500	1,33E-04	8,61	5,37	1,6	0,73
50033F	25	-	21998	22998	1,16E-05	2,24	0,14	16,3	0,05
50034F	47	-	42500	38000	2,31E-04	14,50	11,66	1,2	1,41
50035F	26	-	134999	124999	1,83E-05	3,93	3,78	1,0	0,06
50036F	44	-	67499	67499	1,39E-04	9,04	10,66	-1,2	0,77
50037F	23	-	31995	28996	7,00E-06	1,78	1,56	1,1	0,02
50038F	62	20236	18000	18000	1,02E-03	32,36	48,71	-1,5	6,27
50039F	43	-	47500	47500	1,62E-04	11,20	12,95	-1,2	0,95
50040AF	27	-	139999	139999	2,19E-05	3,62	3,66	-1,0	0,08
50040BF	40	64815	62500	62500	1,48E-04	10,15	15,37	-1,5	0,76
50040CF	64	26770	25000	25000	7,82E-04	23,94	37,57	-1,6	5,28
50040F	42	-	79999	79999	9,32E-05	6,83	2,91	2,3	0,54



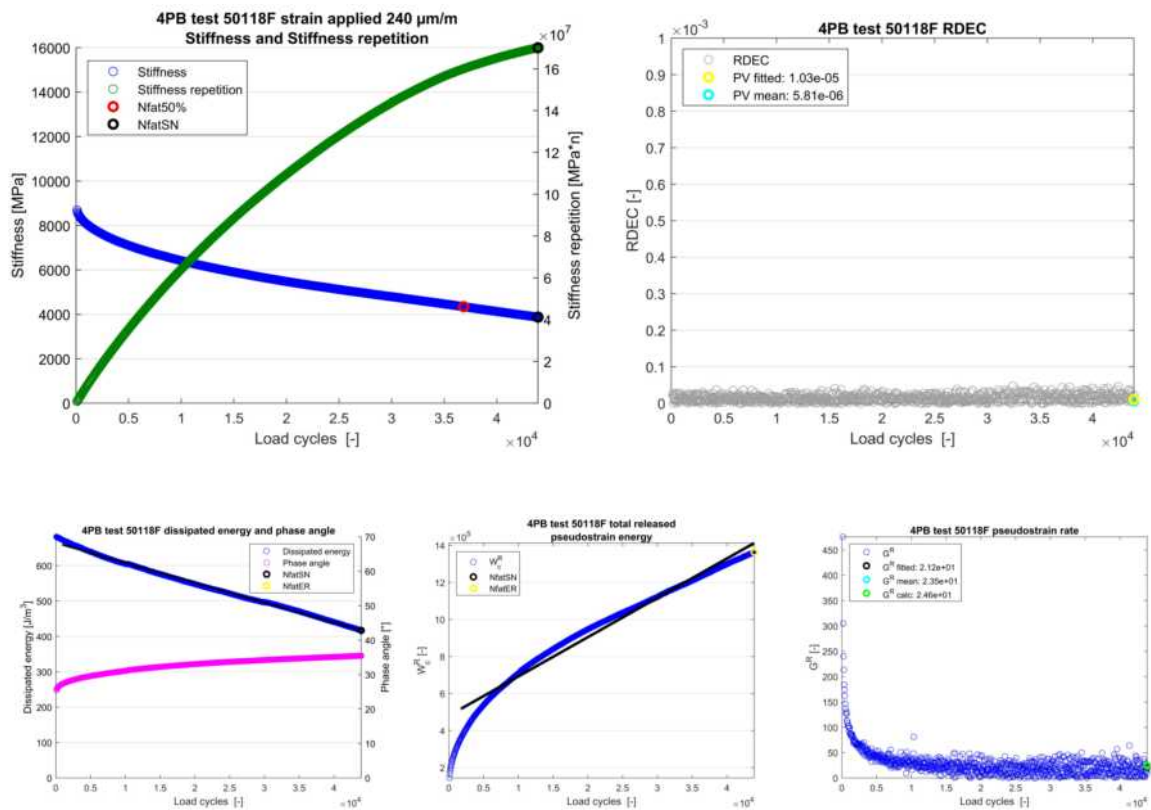


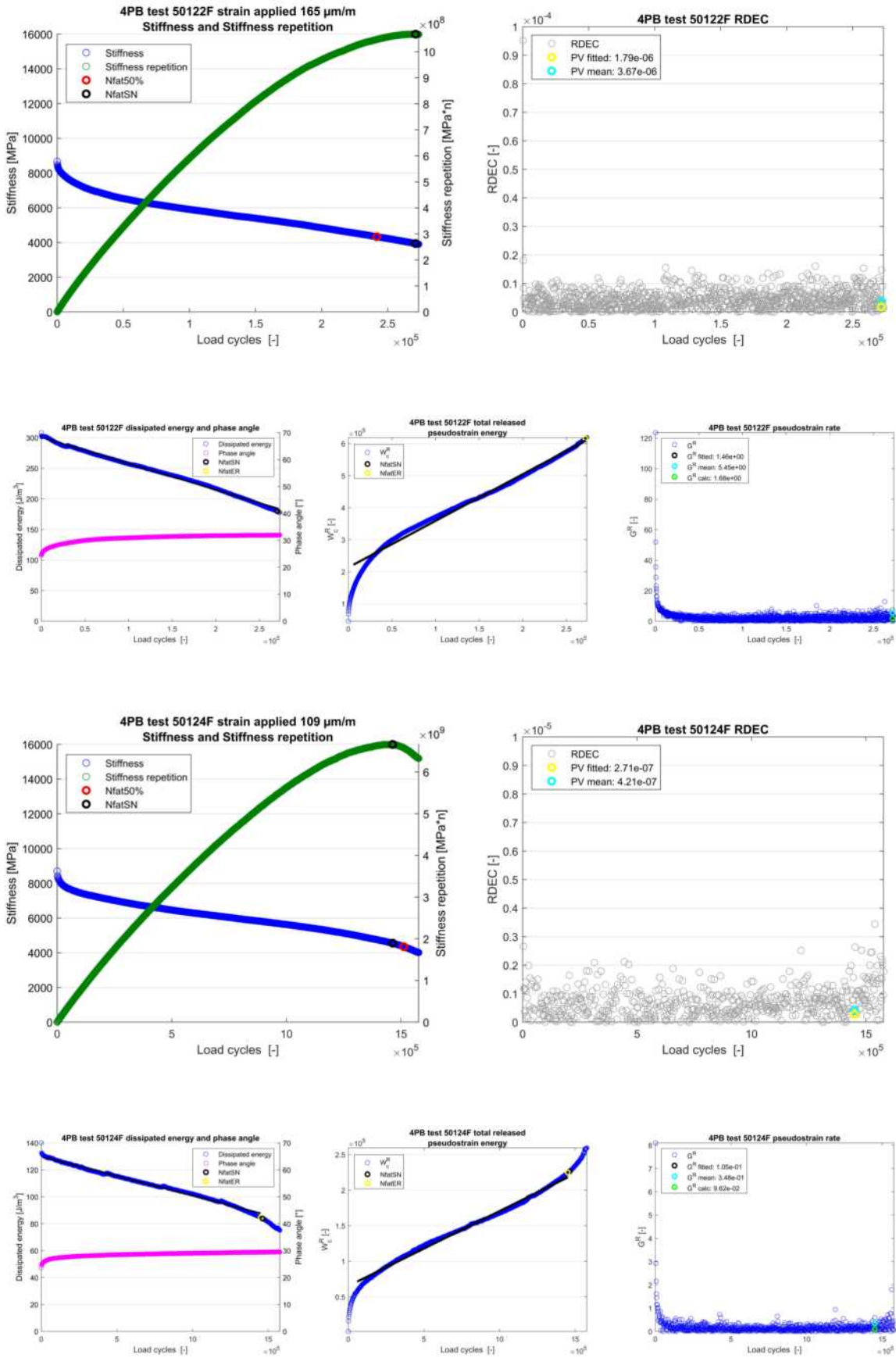
B.2. 18502 results

B.2.1. 4PB

Table B.3: Mixture 18502 4PB results

Sample	Strain applied ε_{ini} [$\mu\text{m}/\text{m}$]	$N_{fat50\%}$	N_{fatSN}	N_{fatER}	$x(1)$	PV fitted (* 10^{-6})	PV mean (* 10^{-6})	ΔPV	G_{calc}^R
50104F	246	35463	41870	41870	-6,33E-03	11,58	0,66	17,5	26,12
50105F	177	146899	147695	152015	-7,69E-04	2,70	4,45	-1,6	3,12
50106F	104	1636617	1540850	1560650	-2,38E-05	0,24	0,06	4,1	0,09
50107F	171	154191	157771	158491	-6,82E-04	2,52	5,32	-2,1	2,91
50108F	104	1021992	941470	950470	-2,91E-05	0,28	0,17	1,7	0,12
50109F	245	36364	42541	42640	-5,87E-03	10,52	13,91	-1,3	27,32
50112F	109	1412665	1350056	1346456	-2,96E-05	0,26	0,61	-2,4	0,11
50113F	104	1465788	1344653	1314054	-2,25E-05	0,22	0,34	-1,6	0,08
50114F	245	36012	38606	39206	-5,96E-03	11,05	15,66	-1,4	28,13
50115F	165	204585	196112	203132	-4,58E-04	1,88	1,34	1,4	2,03
50116F	104	1823814	1704642	1717241	-2,11E-05	0,21	0,02	9,4	0,07
50117F	165	192827	194129	193050	-5,27E-04	2,07	0,17	12,1	2,10
50118F	240	36844	43913	43913	-5,63E-03	10,33	5,81	1,8	24,61
50122F	165	241629	270987	271707	-4,30E-04	1,79	3,67	-2,1	1,68
50123F	246	30432	30182	31424	-7,29E-03	12,64	27,04	-2,1	34,89
50124F	109	1512515	1463452	1450852	-2,90E-05	0,27	0,42	-1,6	0,10
50125F	240	37896	42264	42911	-5,42E-03	10,63	26,40	-2,5	25,52
50126F	109	921202	840673	858672	-4,05E-05	0,36	0,77	-2,2	0,17
50127F	170	158740	160839	161919	-6,70E-04	2,54	1,41	1,8	2,79

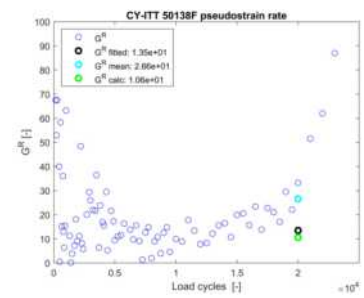
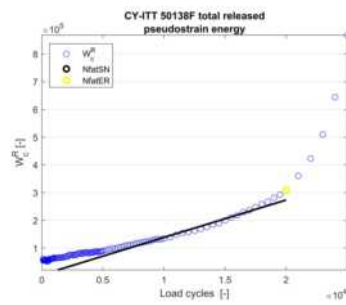
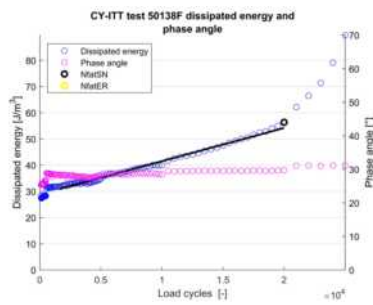
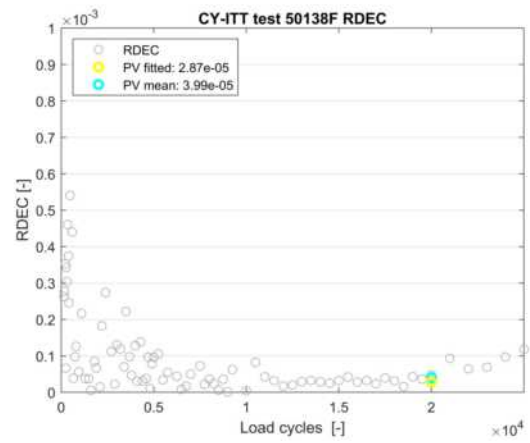
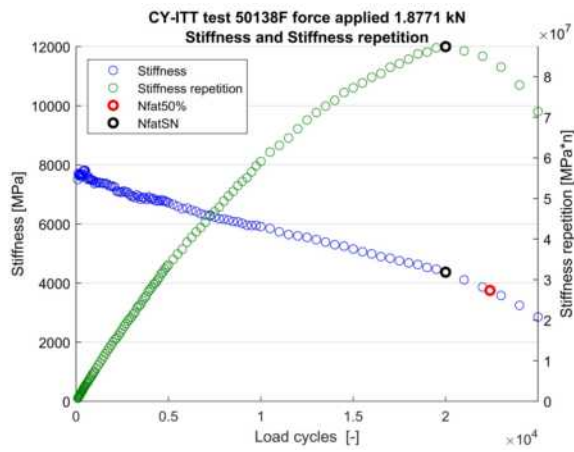


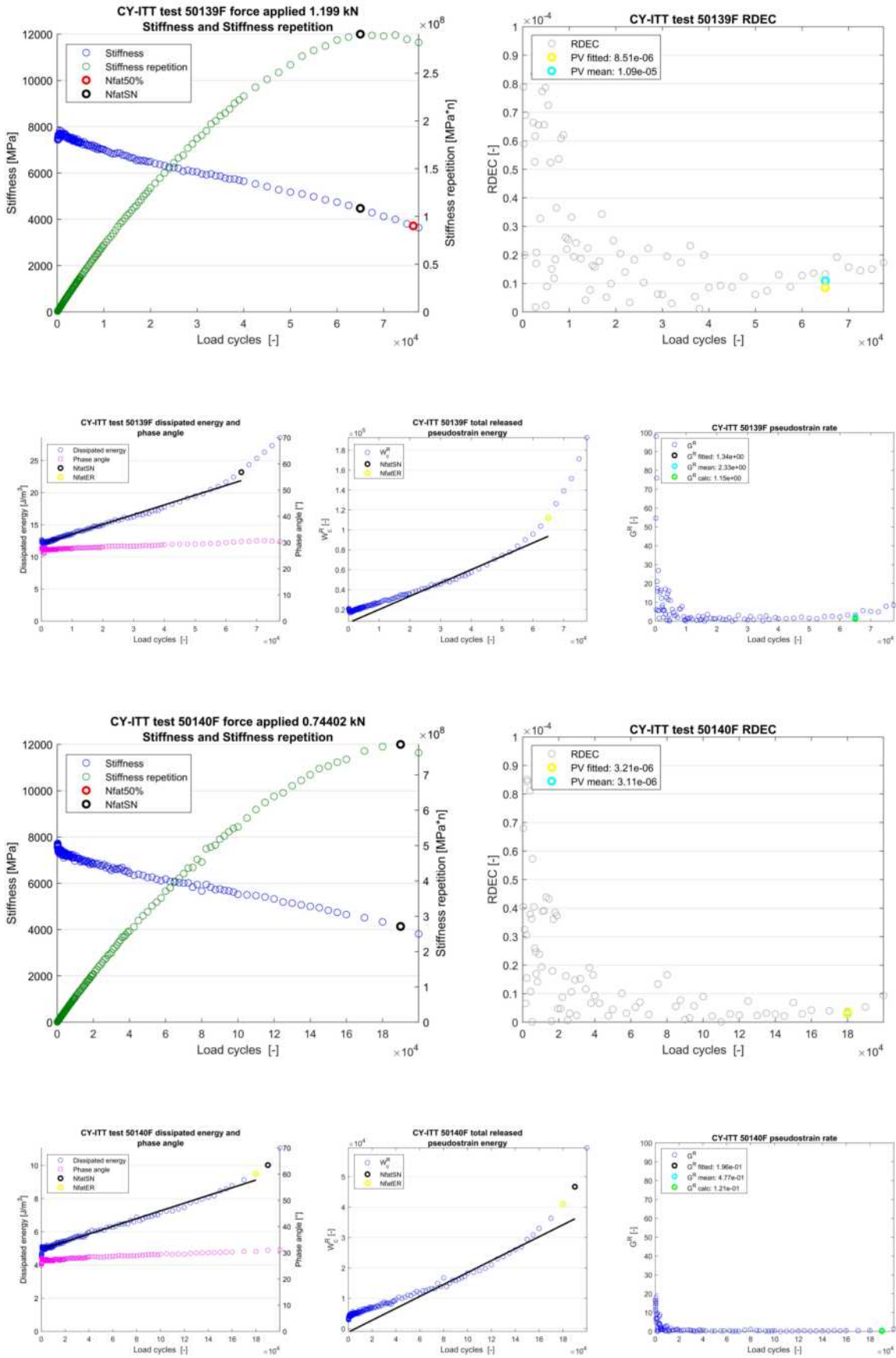


B.2.2. CY-ITT

Table B.4: Mixture 18502 CY-ITT results

Sample	Strain $n=100$ ε_{ini} [$\mu\text{m}/\text{m}$]	$N_{fat50\%}$	N_{fatSN}	N_{fatER}	$x(1)$	PV fitted (* 10^{-6})	PV mean (* 10^{-6})	ΔPV	G_{calc}^R
50130F	22	-	339993	329994	6,27E-06	1,54	0,67	2,3	0,02
50131F	46	64783	57500	57500	2,00E-04	11,09	23,25	-2,1	1,53
50132F	64	20367	18000	17500	1,19E-03	31,64	44,55	-1,4	9,06
50133F	27	-	199999	199999	1,42E-05	2,68	3,88	-1,5	0,07
50134F	39	86680	82499	82499	1,18E-04	7,84	8,08	-1,0	0,68
50135F	60	28922	28000	27000	8,02E-04	22,52	17,52	1,3	5,46
50136F	43	-	59999	67499	1,41E-04	7,88	8,03	-1,0	1,00
50137F	24	-	339994	339994	9,85E-06	1,76	0,10	16,9	0,04
50138F	71	22402	20000	20000	1,27E-03	28,71	39,91	-1,4	10,56
50139F	46	76350	64999	64999	1,52E-04	8,51	10,90	-1,3	1,15
50140F	29	-	189999	180000	2,32E-05	3,21	3,11	1,0	0,12
50141BF	25	-	389992	409991	9,98E-06	1,50	2,01	-1,3	0,04
50141F	66	15598	13000	13000	1,39E-03	34,81	40,81	-1,2	11,66



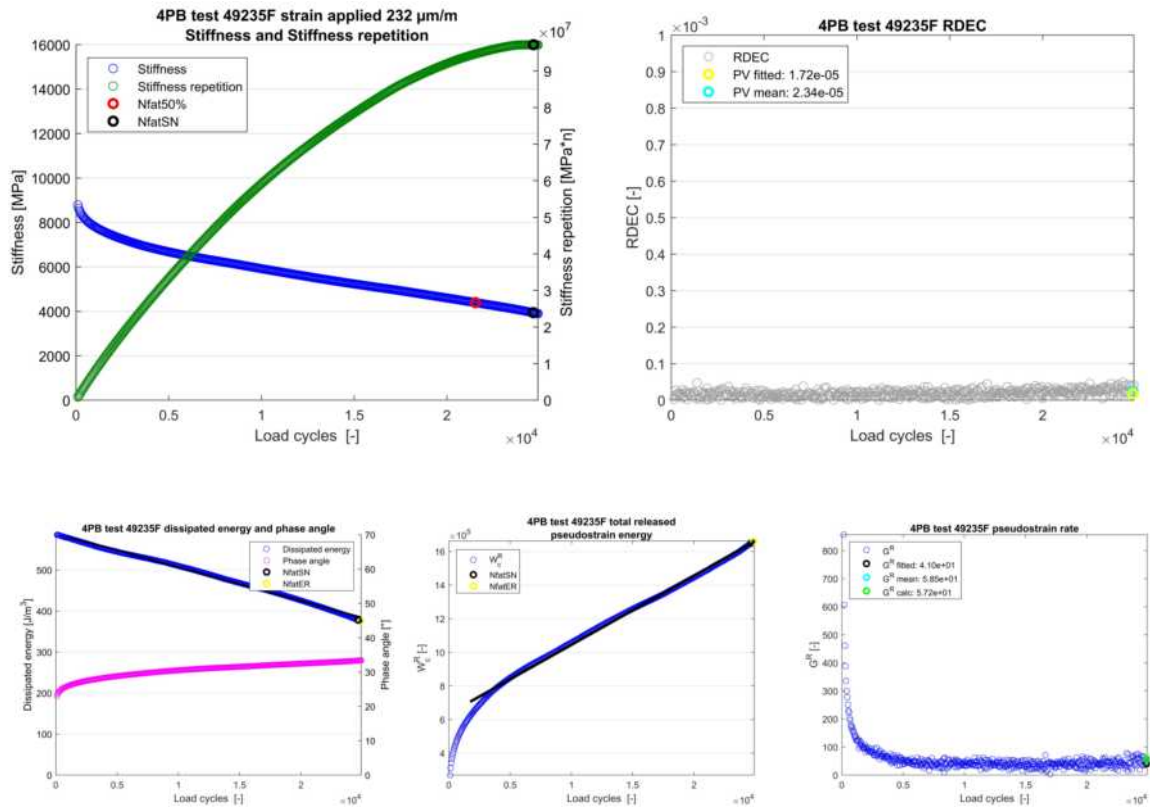


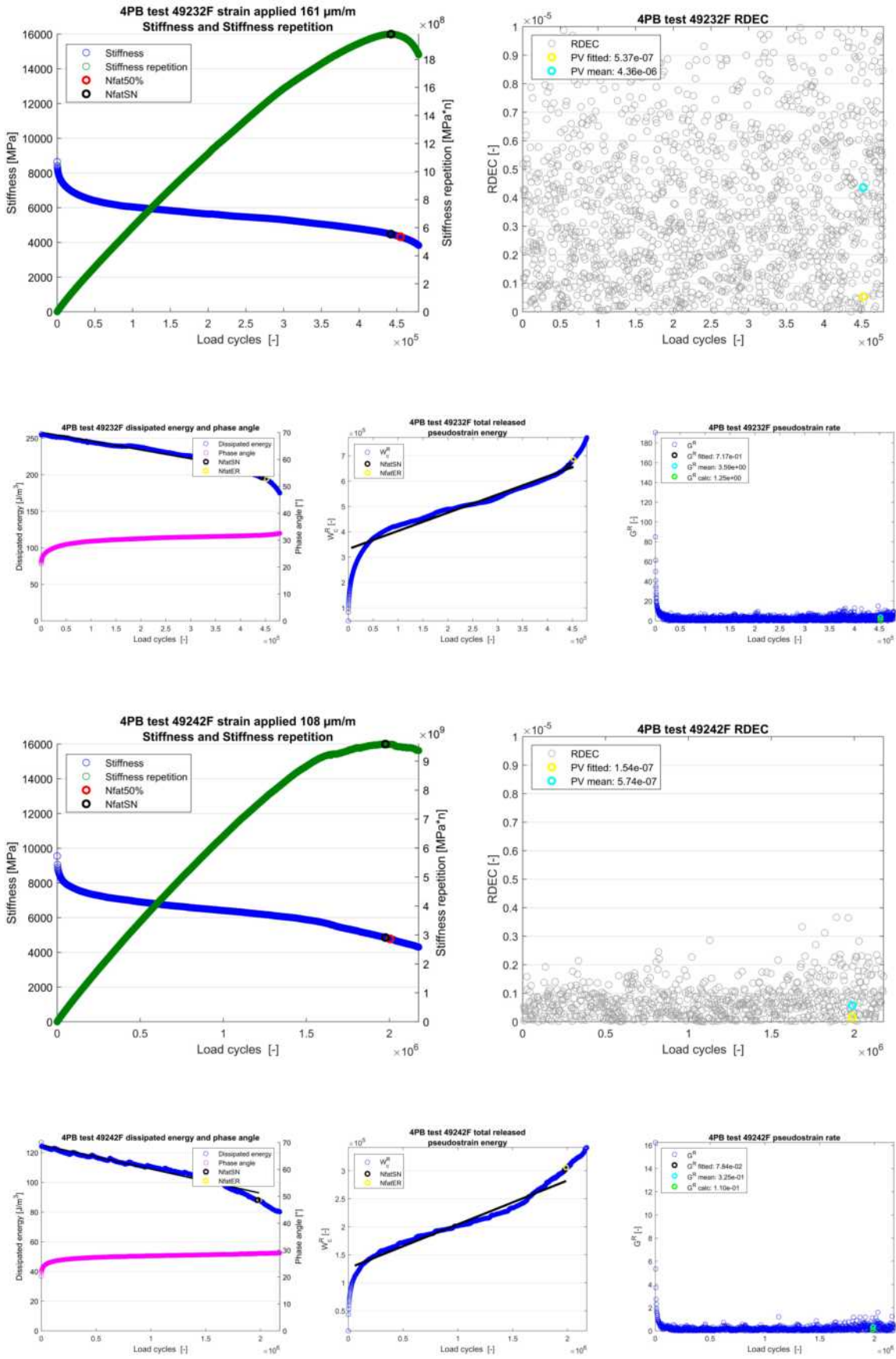
B.3. 18523 results

B.3.1. 4PB

Table B.5: Mixture 18523 4PB results

Sample	Strain applied ϵ_{ini} [$\mu\text{m}/\text{m}$]	$N_{fat50\%}$	N_{fatSN}	N_{fatER}	$x(1)$	PV fitted ($\times 10^{-6}$)	PV mean ($\times 10^{-6}$)	ΔPV	G_{calc}^R
49231F	119	1030773	984670	984670	-3,28E-05	0,25	0,90	-3,5	0,26
49232F	161	454792	442185	452086	-1,21E-04	0,54	4,36	-8,1	1,25
49233F	306	8487	7806	7905	-2,65E-02	31,21	71,50	-2,3	308,14
49234F	166	217805	208896	212316	-2,64E-04	1,06	1,70	-1,6	2,80
49235F	232	21541	24661	24860	-8,19E-03	17,16	23,38	-1,4	57,22
49236F	119	791485	734477	765076	-4,39E-05	0,33	0,83	-2,5	0,37
49241F	219	32117	36086	36185	-4,43E-03	10,07	27,54	-2,7	34,91
49242F	108	2004763	1976440	1987239	-1,63E-05	0,15	0,57	-3,7	0,11
49243F	163	139967	130056	135096	-4,55E-04	1,79	2,19	-1,2	4,55
49244F	215	12034	11183	11580	-1,28E-02	28,10	55,91	-2,0	95,10
49245F	161	83006	89018	91357	-9,68E-04	4,27	0,45	9,4	6,76
49246F	109	891212	811875	826275	-2,66E-05	0,23	1,19	-5,2	0,24
49250F	154	731224	740074	737014	-8,33E-05	0,37	0,25	1,5	0,74
49251F	207	80704	98636	98486	-1,33E-03	3,54	10,80	-3,0	12,09
49252F	207	53051	60536	61386	-2,45E-03	5,94	1,80	3,3	18,84
49253F	113	432155	387087	387087	-4,26E-05	0,34	1,05	-3,1	0,51
49254F	105	954681	901872	900072	-3,38E-05	0,33	0,48	-1,4	0,22
49255F	159	348457	372692	372692	-1,64E-04	0,61	3,77	-6,1	1,65





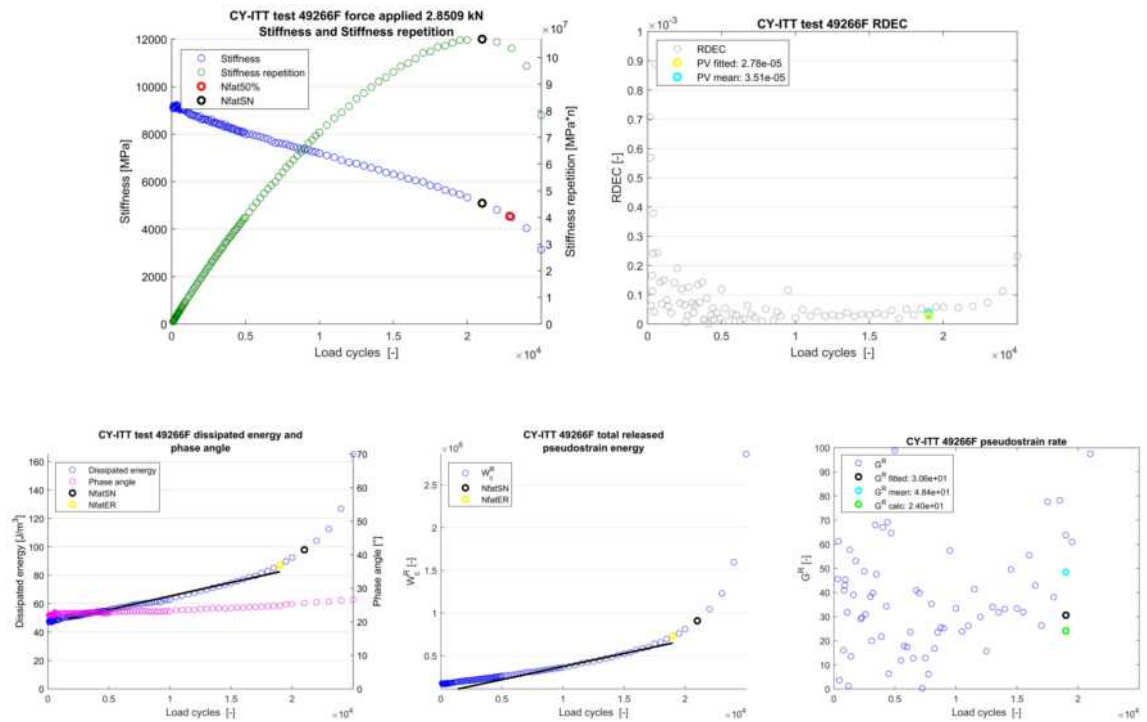
B.3.2. CY-ITT

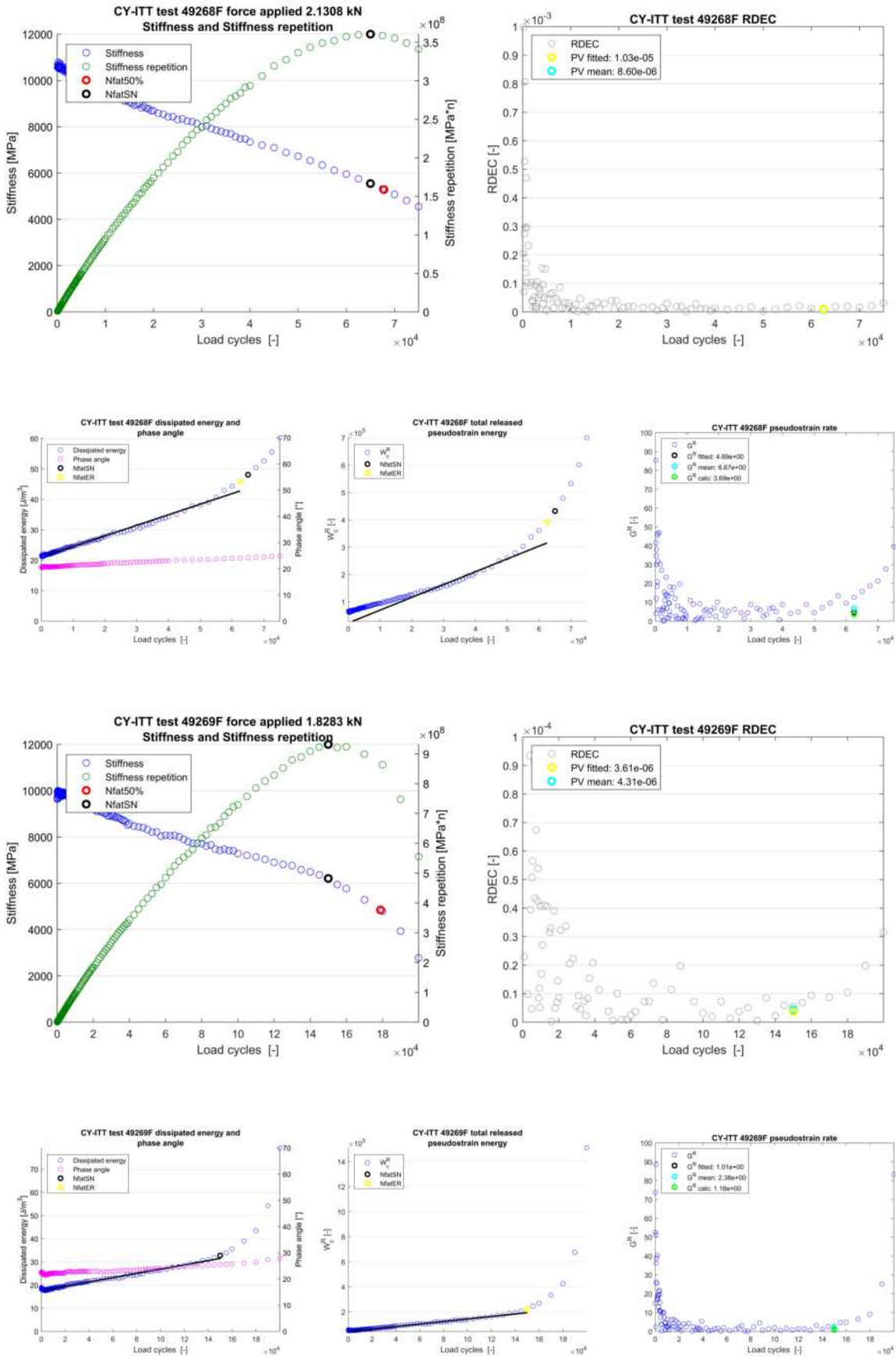
Table B.6: Mixture 18523 laboratory CY-ITT results

Sample	Strain $n=100$ ε_{ini} [$\mu\text{m}/\text{m}$]	$N_{fat50\%}$	N_{fatSN}	N_{fatER}	$x(1)$	PV fitted (* 10^{-6})	PV mean (* 10^{-6})	ΔPV	G_{calc}^R
49258F	54	222493	219998	209999	9,23E-05	3,47	3,55	-1,0	0,88
49259F	69	62896	57500	57500	4,70E-04	10,58	7,98	1,3	5,66
49260F	87	16946	15500	15000	2,68E-03	38,08	50,26	-1,3	30,98
49261F	84	21143	19000	19000	2,26E-03	31,55	43,00	-1,4	26,00
49262F	69	-	120000	120000	2,63E-04	5,75	7,35	-1,3	2,77
49264F	60	82698	72499	74999	2,64E-04	7,73	8,05	-1,0	3,36
49266F	92	22865	21000	19000	1,91E-03	27,80	35,13	-1,3	24,03
49267F	71	44113	38999	38999	7,40E-04	15,31	7,31	2,1	8,62
49268F	59	67795	64999	62500	3,47E-04	10,27	8,60	1,2	3,69
49269F	54	178920	149998	149998	9,21E-05	3,61	4,31	-1,2	1,18
49270F	53	167644	159998	159998	1,11E-04	3,70	1,91	1,9	1,32

Table B.7: Mixture 18523 field CY-ITT results

Sample	Strain $n=100$ ε_{ini} [$\mu\text{m}/\text{m}$]	$N_{fat50\%}$	N_{fatSN}	N_{fatER}	$x(1)$	PV fitted (* 10^6)	PV mean (* 10^6)	ΔPV	G_{calc}^R
49508F	72	37641	35000	35000	9,32E-04	19,98	23,43	-1,2	9,07
49510F	84	17024	15000	14500	3,02E-03	37,43	52,47	-1,4	25,78
49511F	113	6869	6500	6250	1,23E-02	90,83	125,96	-1,4	124,85
49512F	32	435947	409991	409991	1,05E-05	0,96	0,82	1,2	0,09
49513F	51	-	110000	115000	1,67E-04	5,83	6,53	-1,1	1,41
49514F	54	112340	100002	100002	1,51E-04	5,62	9,13	-1,6	1,59
49515F	59	89319	84999	84999	2,81E-04	7,56	7,11	1,1	2,45
49516F	122	6129	6000	6000	1,66E-02	120,60	172,89	-1,4	173,24



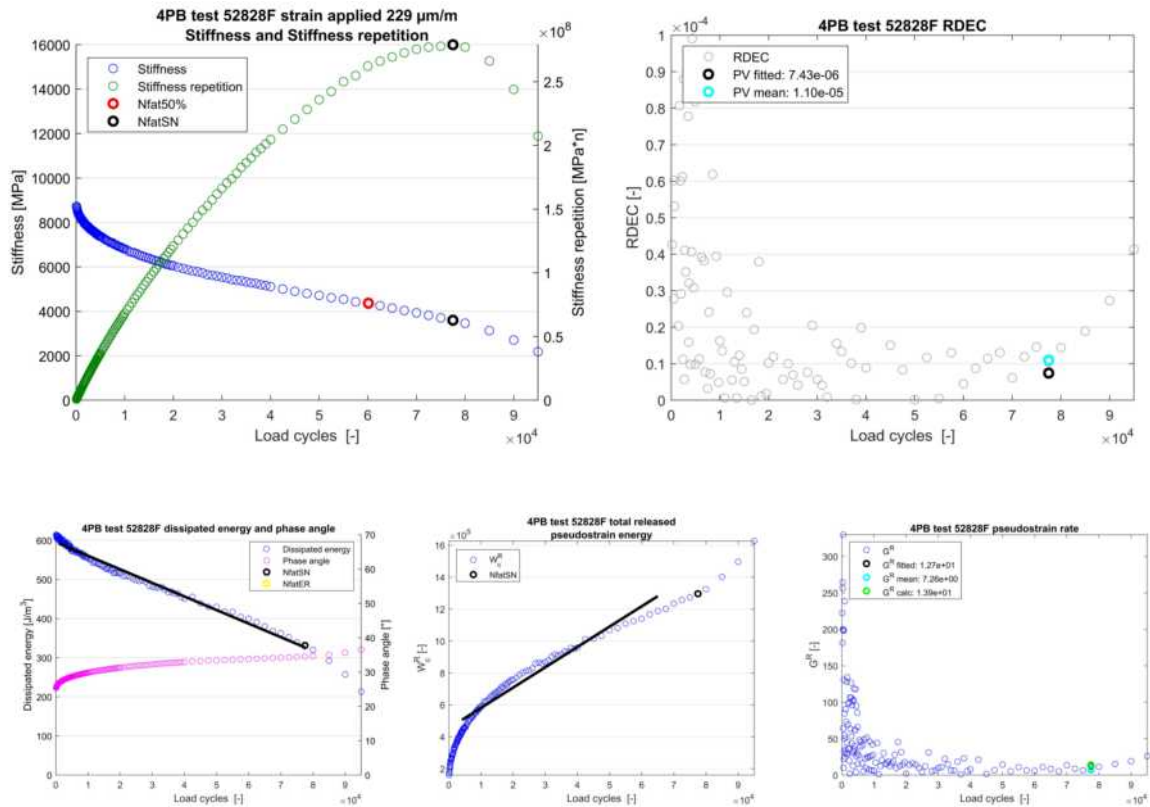


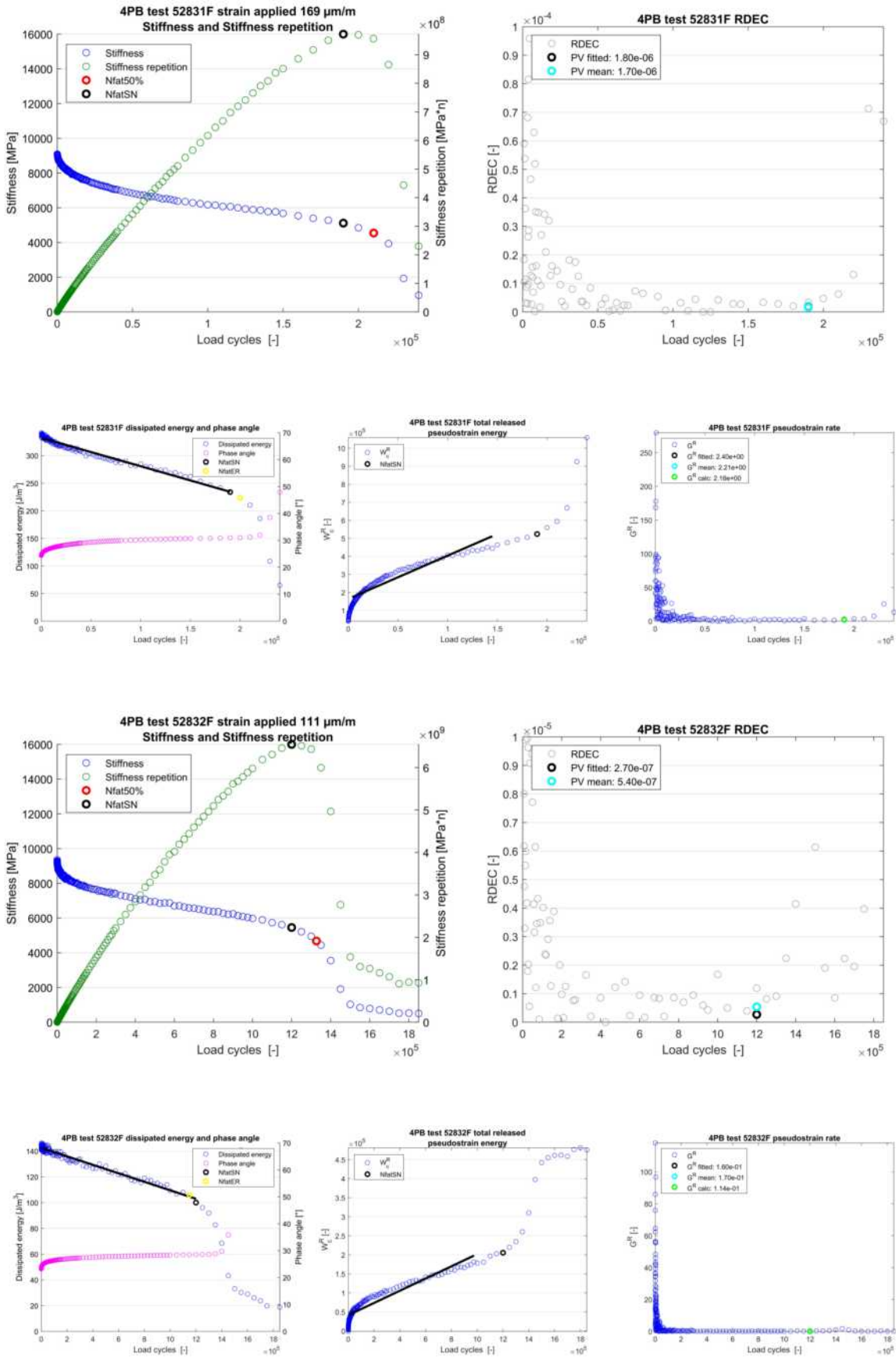
B.4. 18590 results

B.4.1. 4PB

Table B.8: Mixture 18590 4PB results

Sample	Strain applied ε_{ini} [$\mu\text{m}/\text{m}$]	$N_{fat50\%}$	N_{fatSN}	N_{fatER}	$x(1)$	PV fitted ($\times 10^{-6}$)	PV mean ($\times 10^{-6}$)	ΔPV	G_{calc}^R
52829F	162	233164	240000	250000	-4,79E-04	1,91	2,26	-1,2	1,75
52828F	229	60122	77500	77500	-3,47E-03	7,43	11,04	-1,5	13,92
52830F	102	2225500	2000000	2000000	-1,62E-05	0,16	0,12	1,3	0,06
52831F	169	210163	190000	200000	-5,15E-04	1,80	1,70	1,1	2,18
52834F	234	56569	67500	70000	-3,87E-03	7,66	6,42	1,2	15,75
52838F	233	65761	85000	90000	-3,23E-03	6,69	6,61	1,0	12,77
52832F	111	1326911	1200000	1150000	-3,30E-05	0,27	0,54	-2,0	0,11
52841F	168	268131	280000	280000	-4,41E-04	1,71	2,28	-1,3	1,65
52842F	236	51896	80000	77500	-4,02E-03	8,62	9,00	-1,0	15,44
52847F	235	59242	65000	62500	-3,52E-03	7,28	12,69	-1,7	16,03
52837F	112	1617422	1500000	1500000	-2,70E-05	0,23	0,24	-1,0	0,10
52839F	169	190222	180000	180000	-6,01E-04	2,23	3,21	-1,4	2,14
52846F	169	248230	250000	250000	-4,73E-04	1,81	1,55	1,2	1,70
52840F	111	1437031	1400000	1450000	-3,62E-05	0,32	0,64	-2,0	0,11
52851F	168	324917	350000	375000	-3,76E-04	1,50	1,34	1,1	1,36
52849F	235	51275	57500	60000	-4,27E-03	8,59	6,24	1,4	18,74
52848F	114	1599869	1550000	1550000	-3,73E-05	0,31	0,28	1,1	0,12
52850F	120	954359	900000	900000	-5,67E-05	0,41	0,14	2,9	0,20

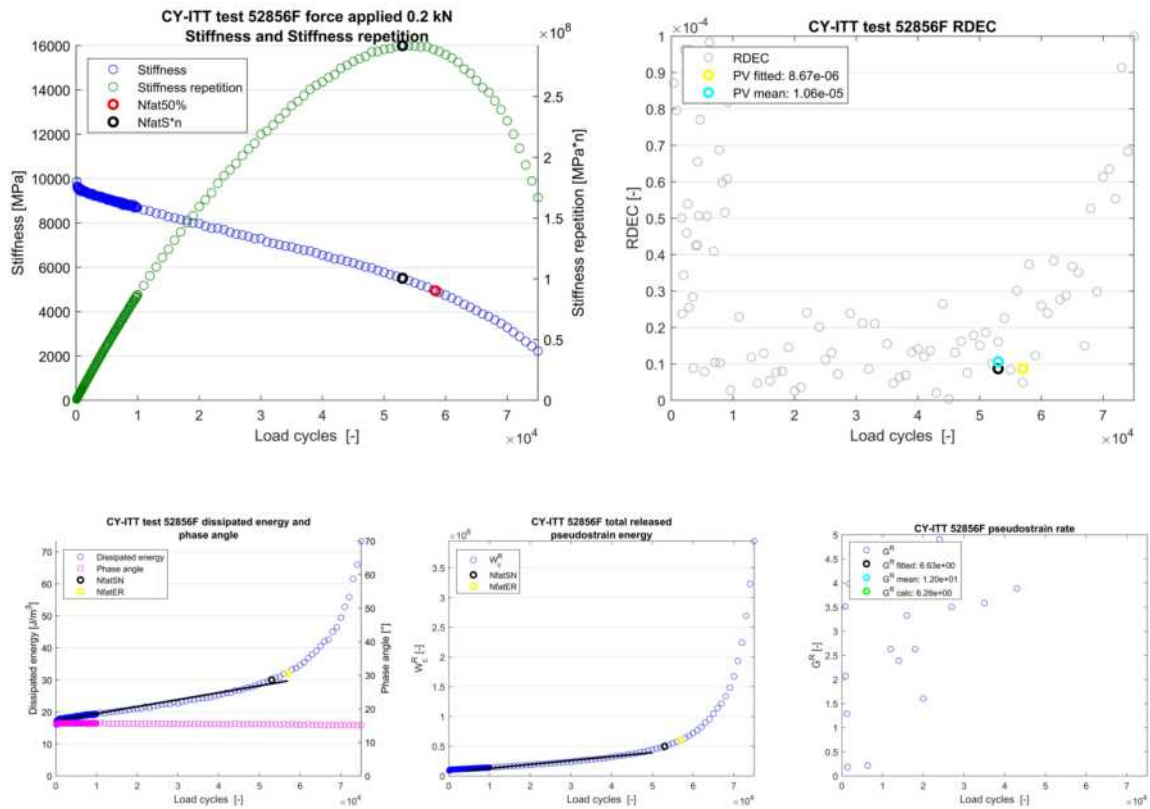


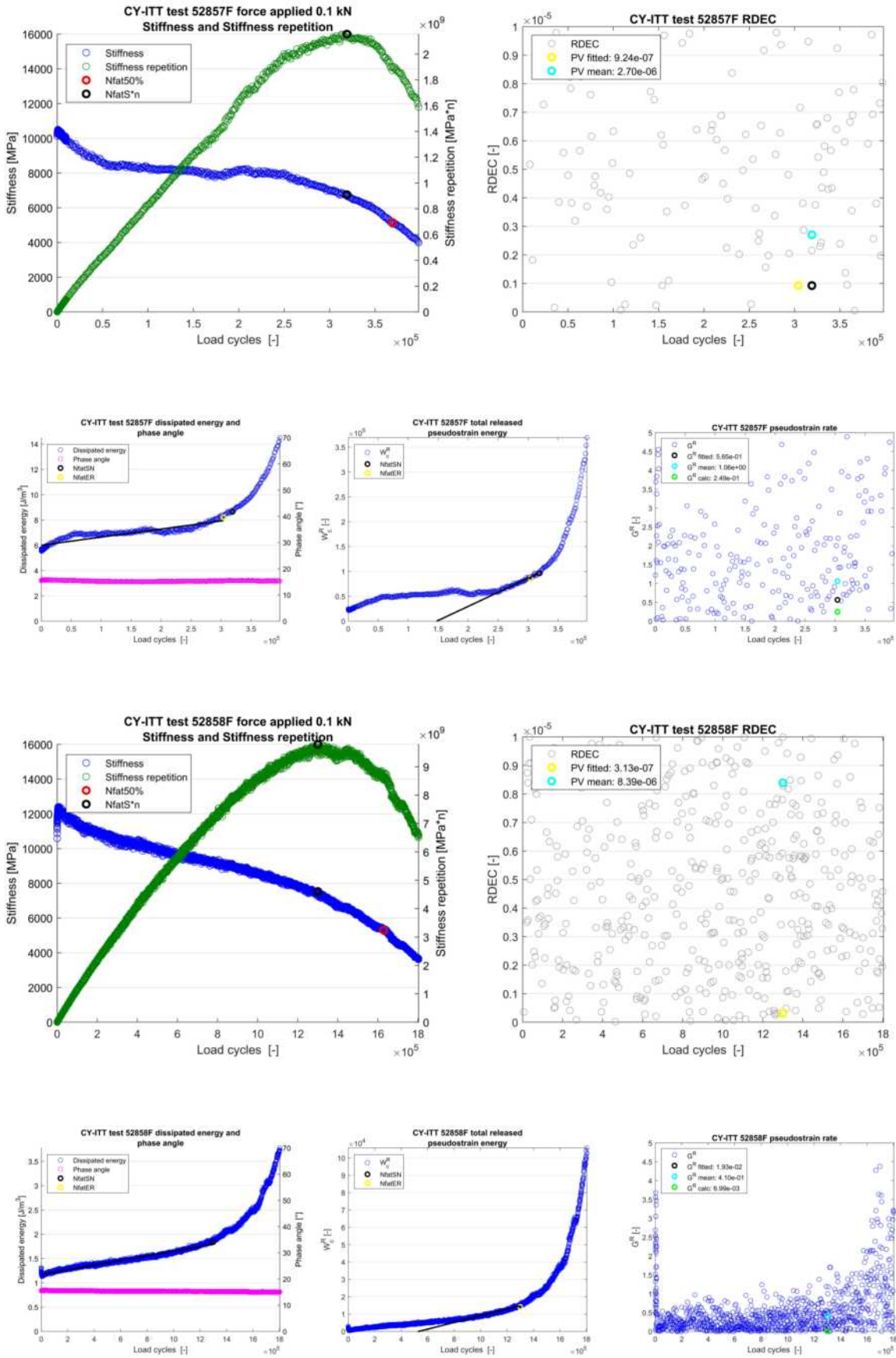


B.4.2. CY-ITT

Table B.9: Mixture 18590 CY-ITT results

Sample	Strain $n=100$ ε_{ini} [$\mu m/m$]	$N_{fat50\%}$	N_{fatSN}	N_{fatER}	$x(1)$	PV fitted (*10 ⁻⁶)	PV mean (*10 ⁻⁶)	ΔPV	G_{calc}^R
52854F	36	-	238001	238001	1,24E-05	1,38	3,80	-2,7	0,37
52855F	17	798510	659002	733002	1,44E-06	0,60	15,15	-25,3	0,01
52856F	64	58382	53002	57002	2,17E-04	8,67	10,58	-1,2	6,28
52857F	35	369314	319002	304002	6,40E-06	0,92	2,70	-2,9	0,25
52858F	16	1628571	1300002	1300002	4,75E-07	0,31	8,39	-26,9	0,01
52859F	62	58576	53002	53002	2,55E-04	10,45	16,90	-1,6	6,42
52860F	41	240617	222002	222002	2,27E-05	2,41	1,74	1,4	0,62
52861F	14	-	4527002	4447002	1,36E-07	0,10	13,57	-131,7	0,00
R2F	42	250291	212001	205001	3,24E-05	2,53	2,36	1,1	0,81
R3F	20	1070726	901001	882001	2,09E-06	0,66	3,30	-5,0	0,03
R4F	32	-	330002	332002	8,85E-06	1,31	8,29	-6,3	0,12
R6F	24	-	1332001	1332001	1,54E-06	0,44	10,61	-24,3	0,03



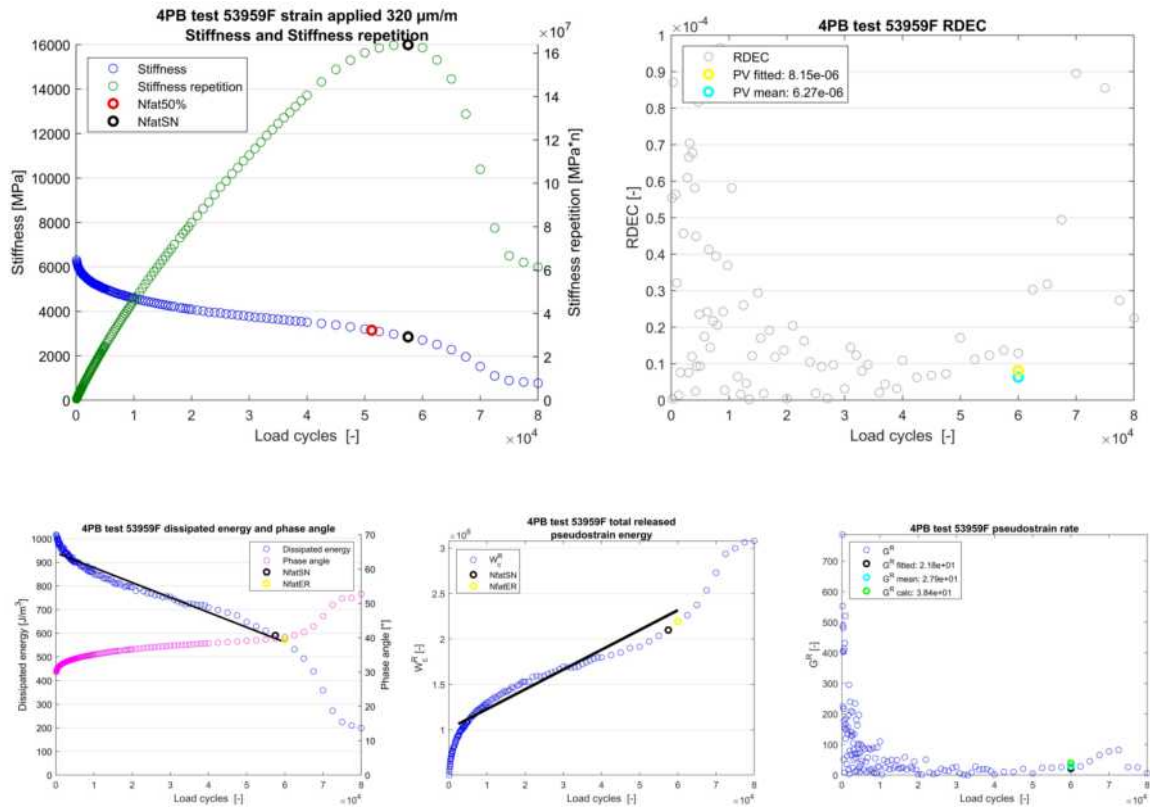


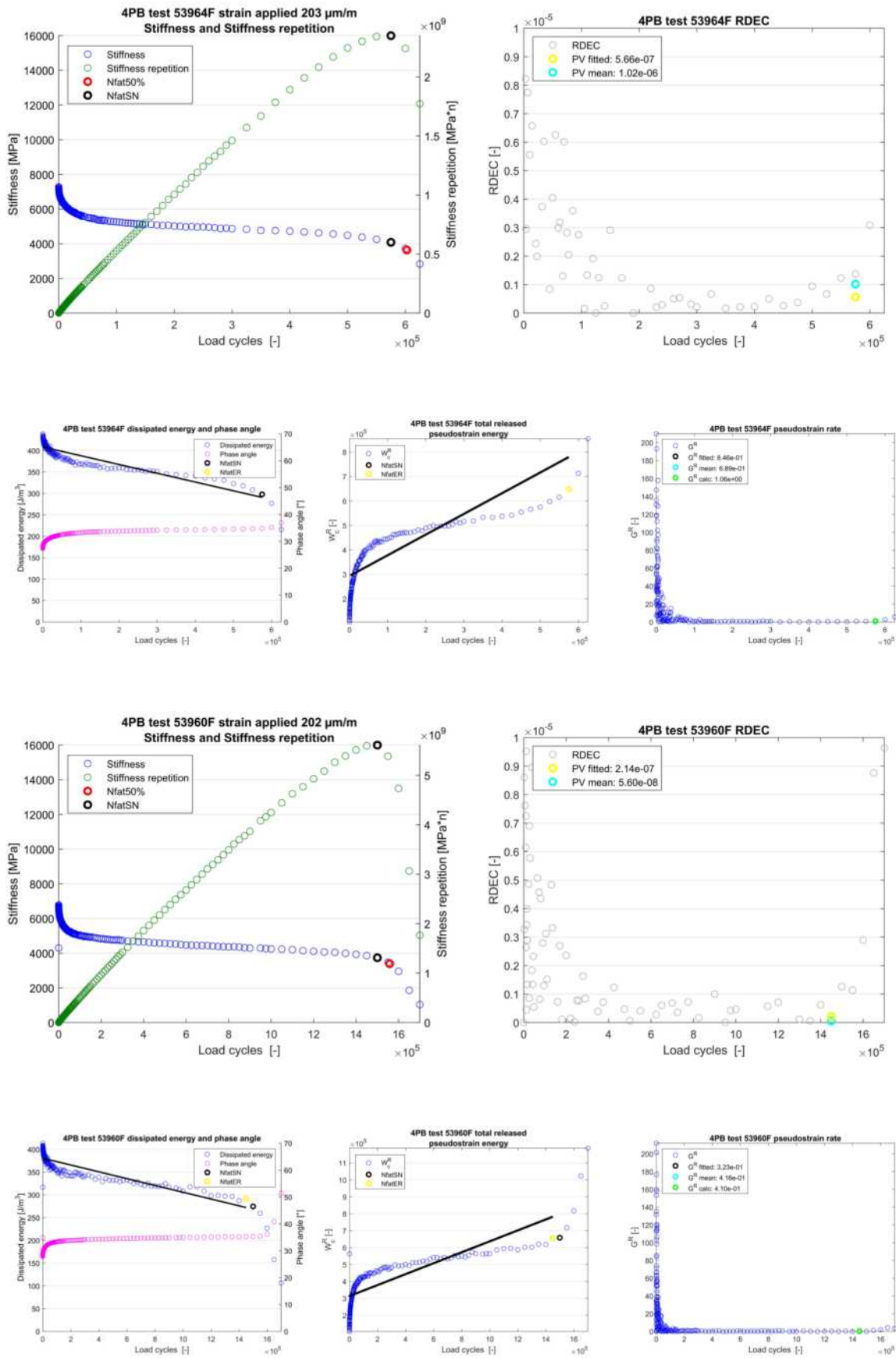
B.5. 18607 results

B.5.1. 4PB

Table B.10: Mixture 18607 4PB results

Sample	Strain applied ε_{ini} [$\mu\text{m}/\text{m}$]	$N_{fat50\%}$	N_{fatSN}	N_{fatER}	$x(1)$	PV fitted ($\cdot 10^{-6}$)	PV mean ($\cdot 10^{-6}$)	ΔPV	G_{calc}^R
53940F	283	66261	72500	72500	-3,95E-03	5,90	5,28	1,1	21,34
53941F	221	364823	400000	400000	-4,74E-04	1,14	1,31	-1,1	2,11
53943F	240	134762	130000	130000	-1,33E-03	2,56	0,83	3,1	7,31
53944F	186	1671995	1600000	1650000	-6,19E-05	0,20	0,06	3,3	0,34
53945F	291	64907	72500	75000	-4,00E-03	5,79	8,25	-1,4	22,81
53948F	350	35251	52500	52500	-1,09E-02	10,27	6,84	1,5	51,21
53949F	197	-	1500000	1500000	-7,03E-05	0,18	0,26	-1,4	0,36
53951F	230	469802	450000	450000	-3,93E-04	0,80	1,89	-2,4	1,87
53953F	239	182052	180000	180000	-1,14E-03	2,01	2,63	-1,3	5,20
53954F	308	55928	60000	60000	-6,58E-03	7,28	4,37	1,7	30,81
53955F	200	805800	750000	750000	-1,65E-04	0,40	0,29	1,4	0,79
53958F	242	525031	550000	525000	-3,86E-04	0,83	1,39	-1,7	1,90
53959F	320	51203	57500	60000	-6,30E-03	8,15	6,27	1,3	38,44
53960F	202	1557785	1500000	1450000	-7,46E-05	0,21	0,06	3,8	0,41
53961F	322	82525	90000	90000	-4,05E-03	5,02	2,82	1,8	24,14
53962F	208	1456587	1400000	1300000	-9,27E-05	0,25	0,14	1,7	0,47
53963F	262	409712	425000	425000	-5,90E-04	1,05	0,28	3,8	3,15
53964F	203	602605	575000	575000	-2,05E-04	0,57	1,02	-1,8	1,06

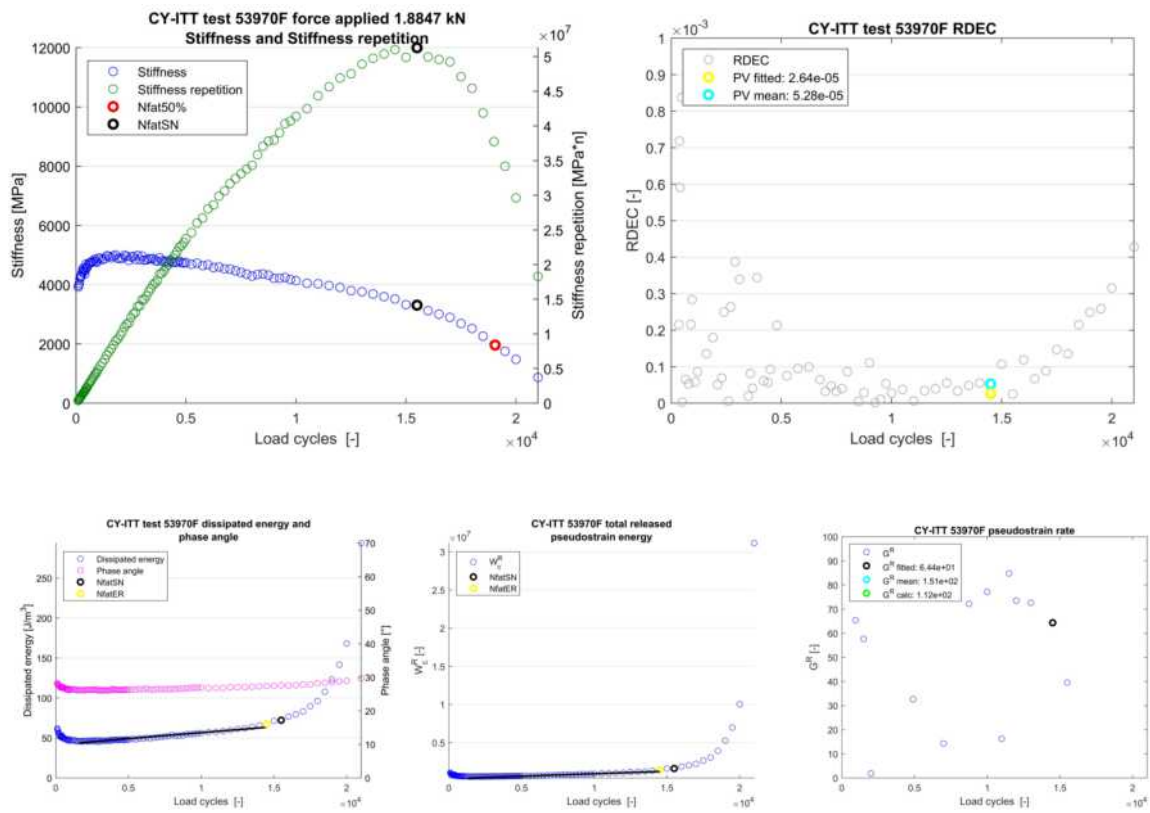


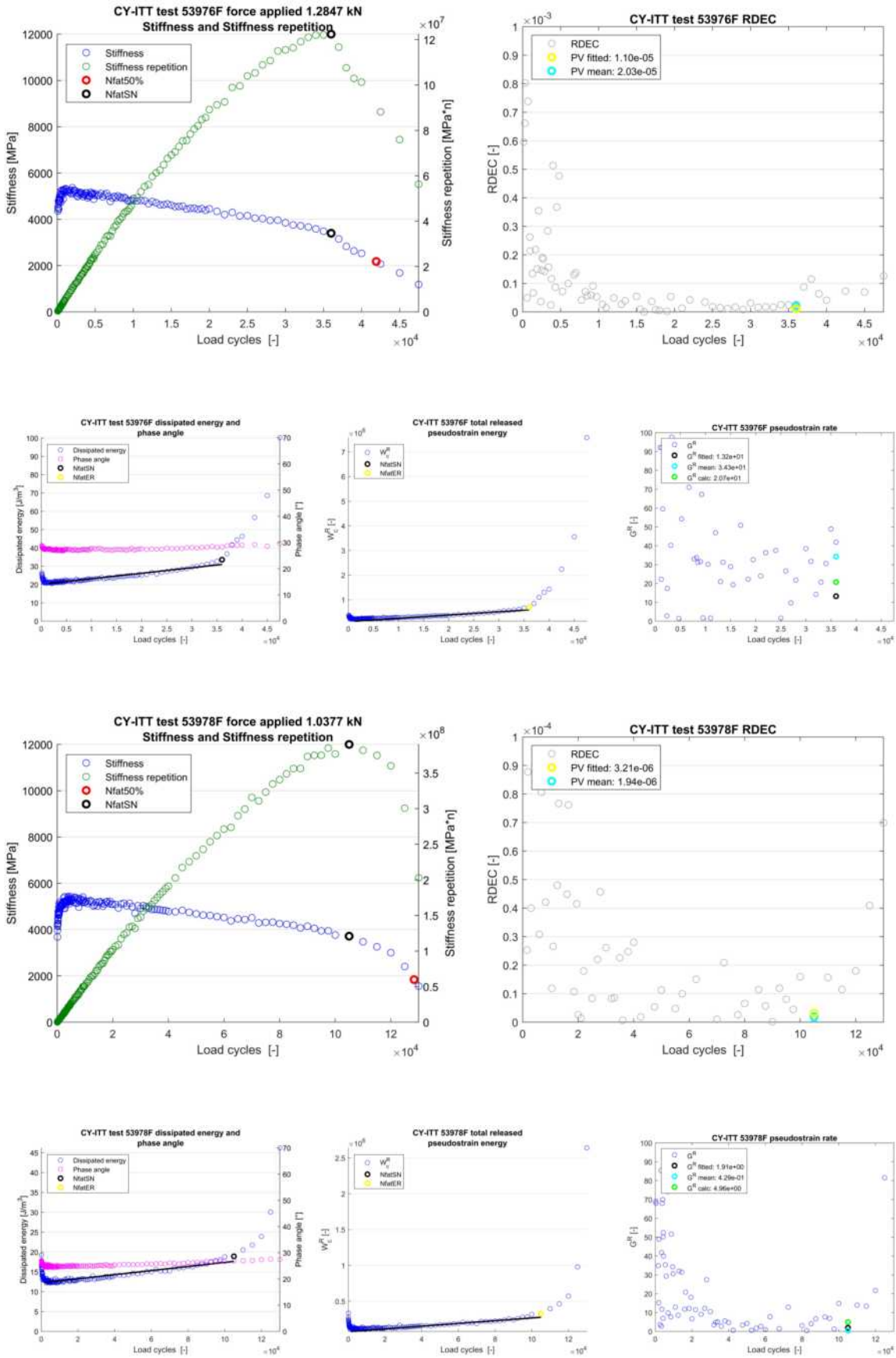


B.5.2. CY-ITT

Table B.11: Mixture 18607 CY-ITT results

Sample	Strain $n=100$ ε_{ini} [$\mu\text{m}/\text{m}$]	$N_{fat50\%}$	N_{fatSN}	N_{fatER}	$x(1)$	PV fitted (* 10^{-6})	PV mean (* 10^{-6})	ΔPV	G_{calc}^R
53968F	219	4085	3100	3100	2,56E-02	170,61	320,64	-1,9	1978,57
53969F	54	-	600000	575000	6,11E-06	0,60	0,16	3,8	0,48
53970F	131	19053	15500	14500	1,50E-03	26,40	52,77	-2,0	112,17
53976F	82	41926	36000	36000	3,01E-04	11,04	20,33	-1,8	20,73
53978F	73	128345	105000	105000	5,14E-05	3,21	1,94	1,7	4,96
53983F	75	144336	120000	120000	6,86E-05	3,74	2,91	1,3	5,18
53984F	111	8841	8500	8500	6,44E-03	73,71	1,49	49,3	244,88
53985F	93	62702	55000	45000	2,53E-04	9,41	11,68	-1,2	14,62
53987F	89	-	45000	45000	3,31E-04	11,36	7,73	1,5	19,70



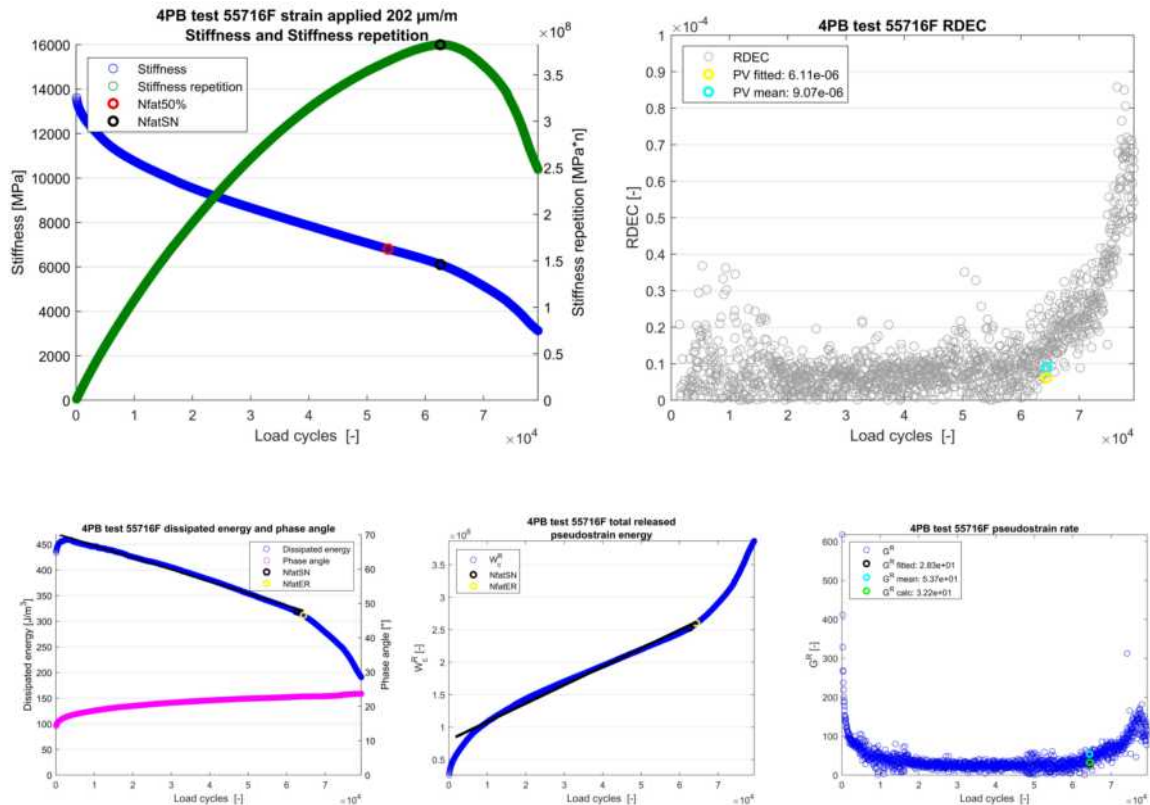


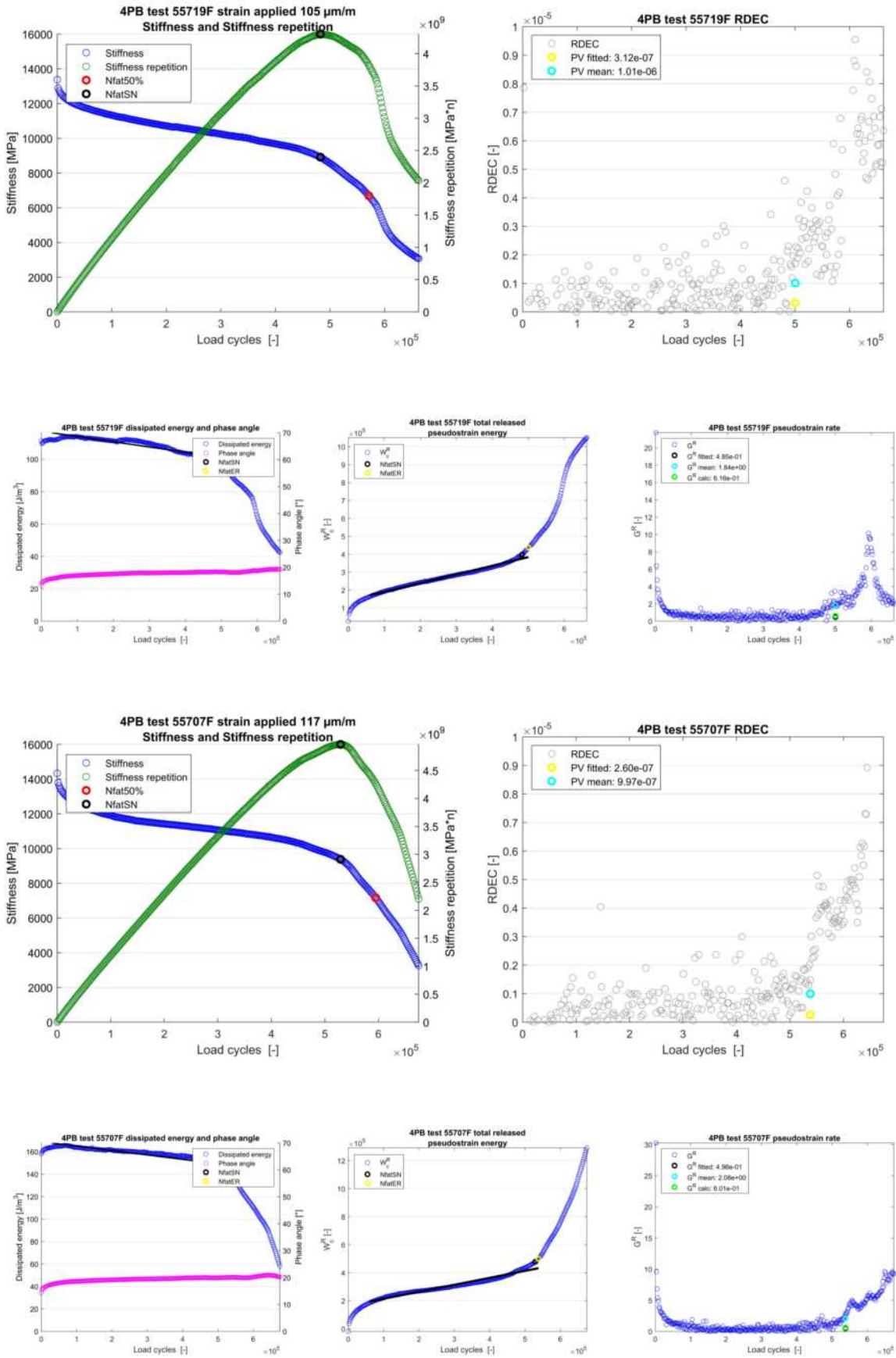
B.6. 18619 results

B.6.1. 4PB

Table B.12: Mixture 18619 4PB results

Sample	Strain applied ε_{ini} [$\mu\text{m}/\text{m}$]	$N_{fat50\%}$	N_{fatSN}	N_{fatER}	$x(1)$	PV fitted ($\cdot 10^{-6}$)	PV mean ($\cdot 10^{-6}$)	ΔPV	G_{calc}^R
55692F	100	2218808	1967454	1989054	-9,99E-06	0,09	0,59	-6,6	0,13
55697F	113	2278751	2041251	2037651	-1,13E-05	0,08	0,34	-4,3	0,16
55698F	148	268154	247851	264608	-2,43E-04	1,14	1,31	-1,1	3,20
55703F	160	158054	146768	149471	-3,62E-04	1,28	1,14	1,1	7,01
55705F	198	109829	117534	115682	-1,19E-03	2,87	55,39	-19,3	14,69
55704F	128	560939	504088	514888	-7,58E-05	0,44	0,73	-1,7	0,96
55705F	161	77741	68930	70192	-4,16E-04	1,46	9,42	-6,4	13,58
55709F	156	118027	108390	119021	-6,27E-04	2,91	3,70	-1,3	8,49
55707F	117	594926	529288	538287	-3,93E-05	0,26	1,00	-3,8	0,60
55708F	149	229423	202986	208212	-9,02E-05	0,41	1,97	-4,8	3,02
55714F	199	85042	80170	82123	-9,62E-04	2,27	6,06	-2,7	20,22
55713F	150	67769	58119	59741	-4,16E-04	1,71	12,46	-7,3	10,19
55716F	202	53600	62592	64395	-2,33E-03	6,11	9,07	-1,5	32,20
55715F	103	2197220	2010654	2039454	-1,33E-05	0,12	2,73	-23,0	0,14
55719F	105	571234	482489	500489	-3,25E-05	0,31	1,01	-3,2	0,62
55718F	98	1625149	1609262	1611062	-2,46E-06	0,02	0,48	-19,7	0,12
55717F	105	339180	851480	853280	-9,81E-05	1,16	0,14	8,4	0,71

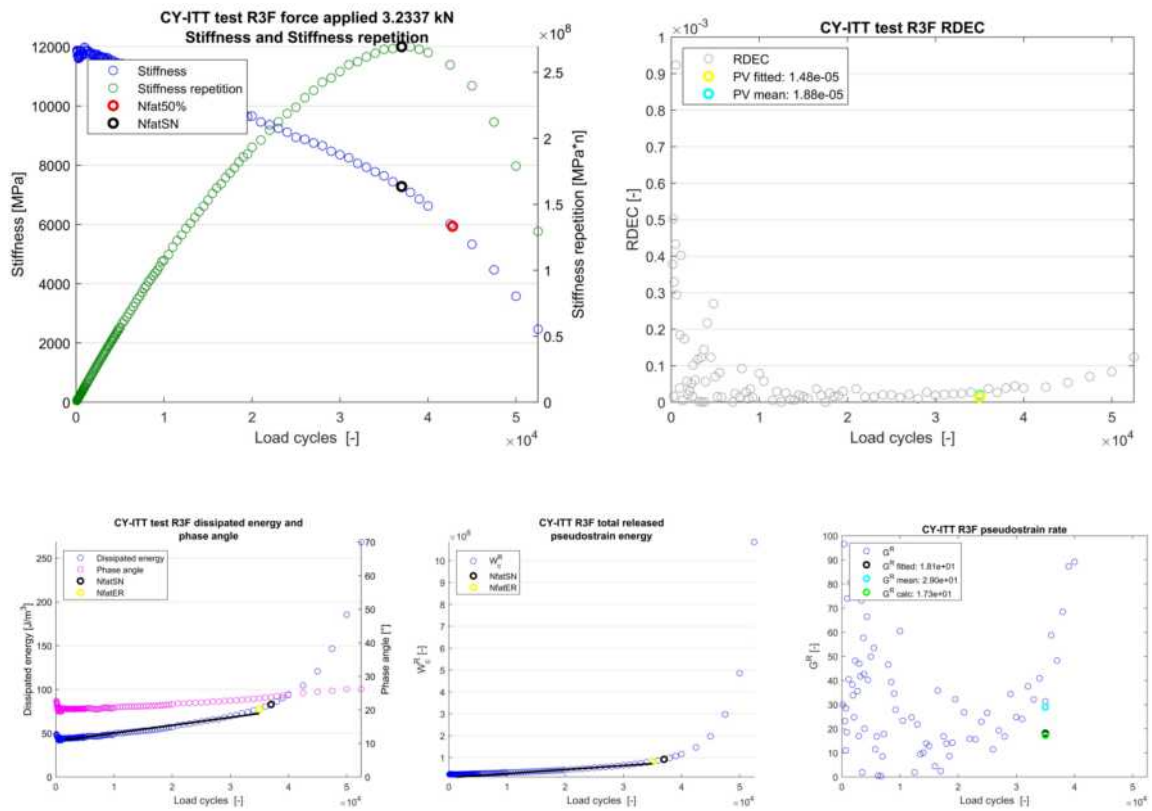


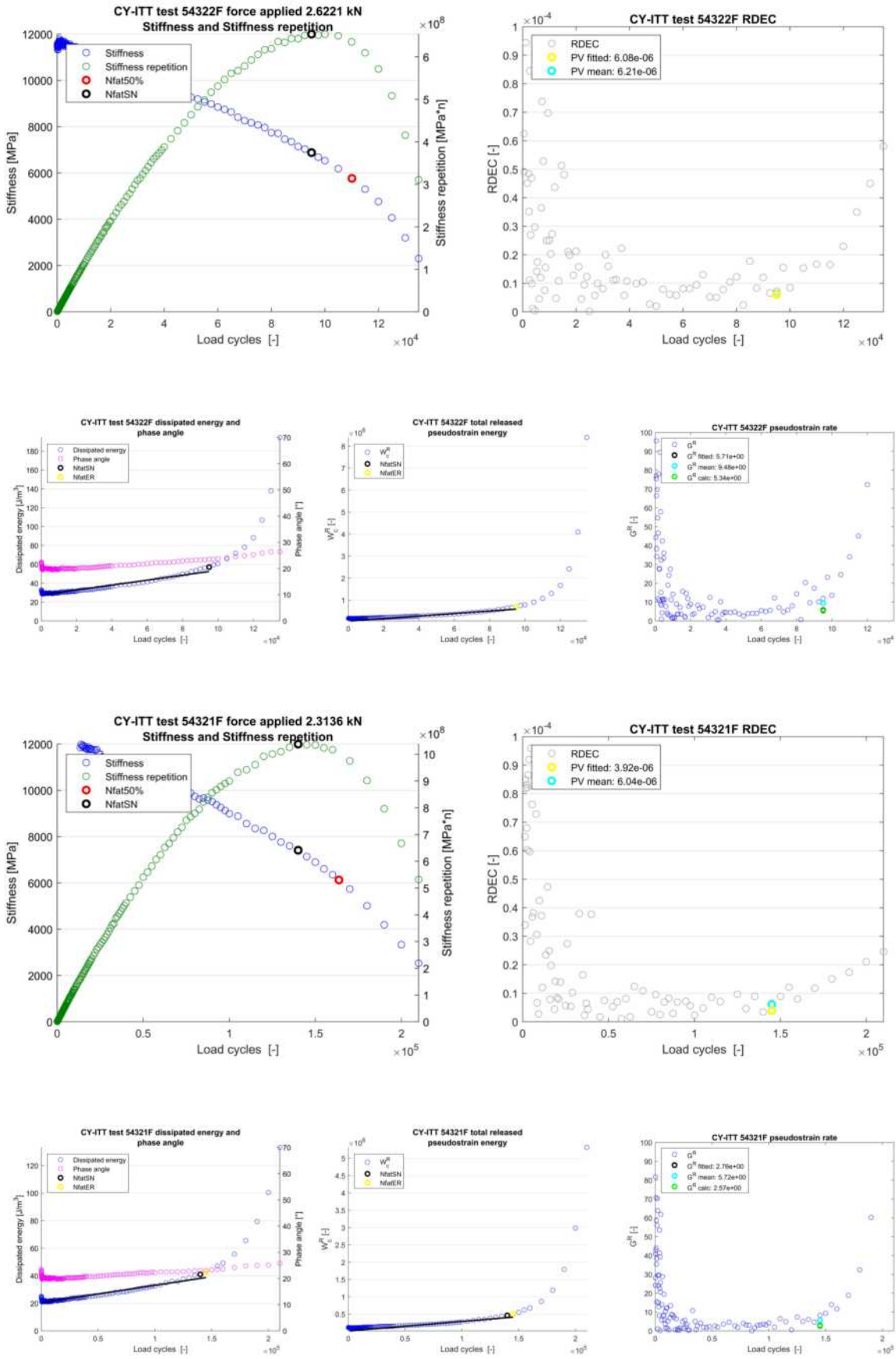


B.6.2. CY-ITT

Table B.13: Mixture 18619 CY-ITT results

Sample	Strain $n=100$ ε_{ini} [$\mu\text{m}/\text{m}$]	$N_{fat50\%}$	N_{fatSN}	N_{fatER}	$x(1)$	PV fitted (* 10^{-6})	PV mean (* 10^{-6})	ΔPV	G_{calc}^R
54319F	80	45426	42500	34000	9,08E-04	15,54	20,05	-1,3	12,20
54316F	71	81993	74999	69999	3,89E-04	8,48	10,10	-1,2	7,11
54317F	58	165403	150000	130000	1,31E-04	4,17	4,21	-1,0	1,97
54320F	58	174224	145000	135000	1,07E-04	3,49	8,03	-2,3	2,04
54321F	56	163686	140000	145000	1,26E-04	3,92	6,04	-1,5	2,57
54322F	67	110087	94998	94998	2,62E-04	6,08	6,21	-1,0	5,34
R3F	81	42781	36999	35000	9,04E-04	14,84	18,81	-1,3	17,27
R4F	78	38796	34000	32000	9,27E-04	15,77	23,37	-1,5	17,04
R5F	81	45861	38999	38999	9,38E-04	14,65	17,71	-1,2	18,41
R7F	66	101639	87498	82499	2,52E-04	6,30	7,09	-1,1	4,82



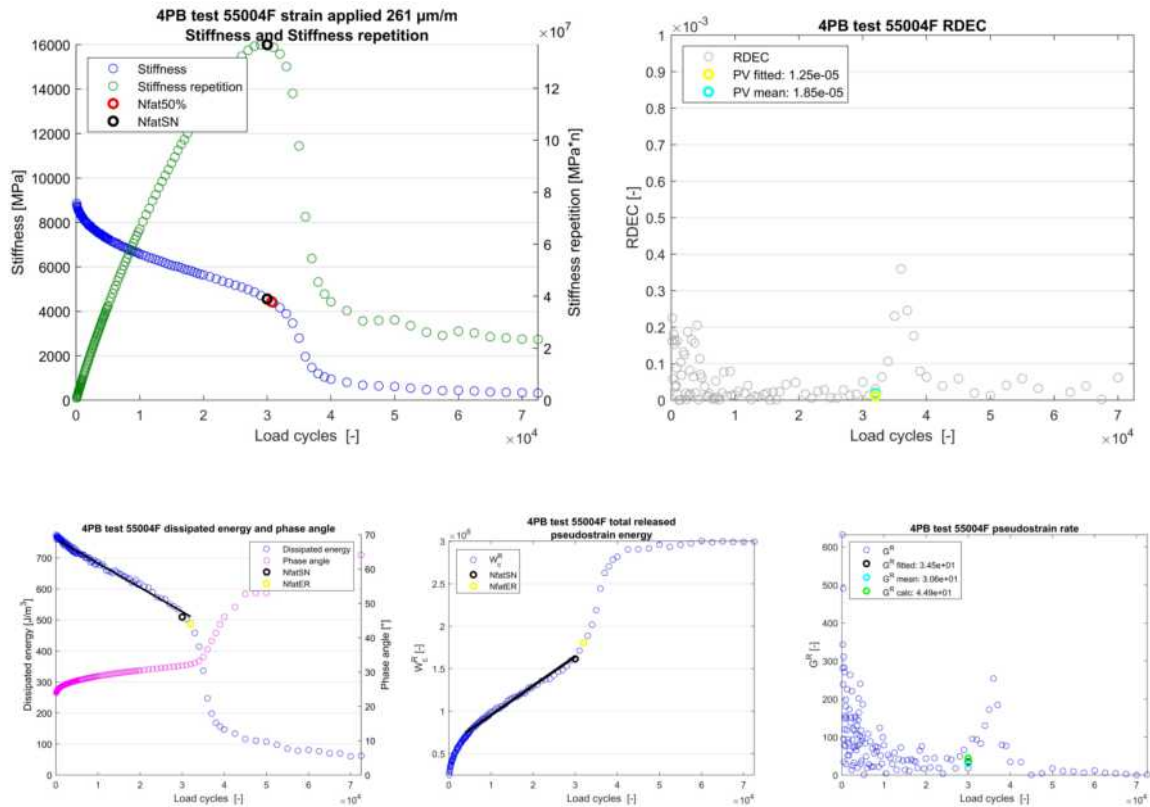


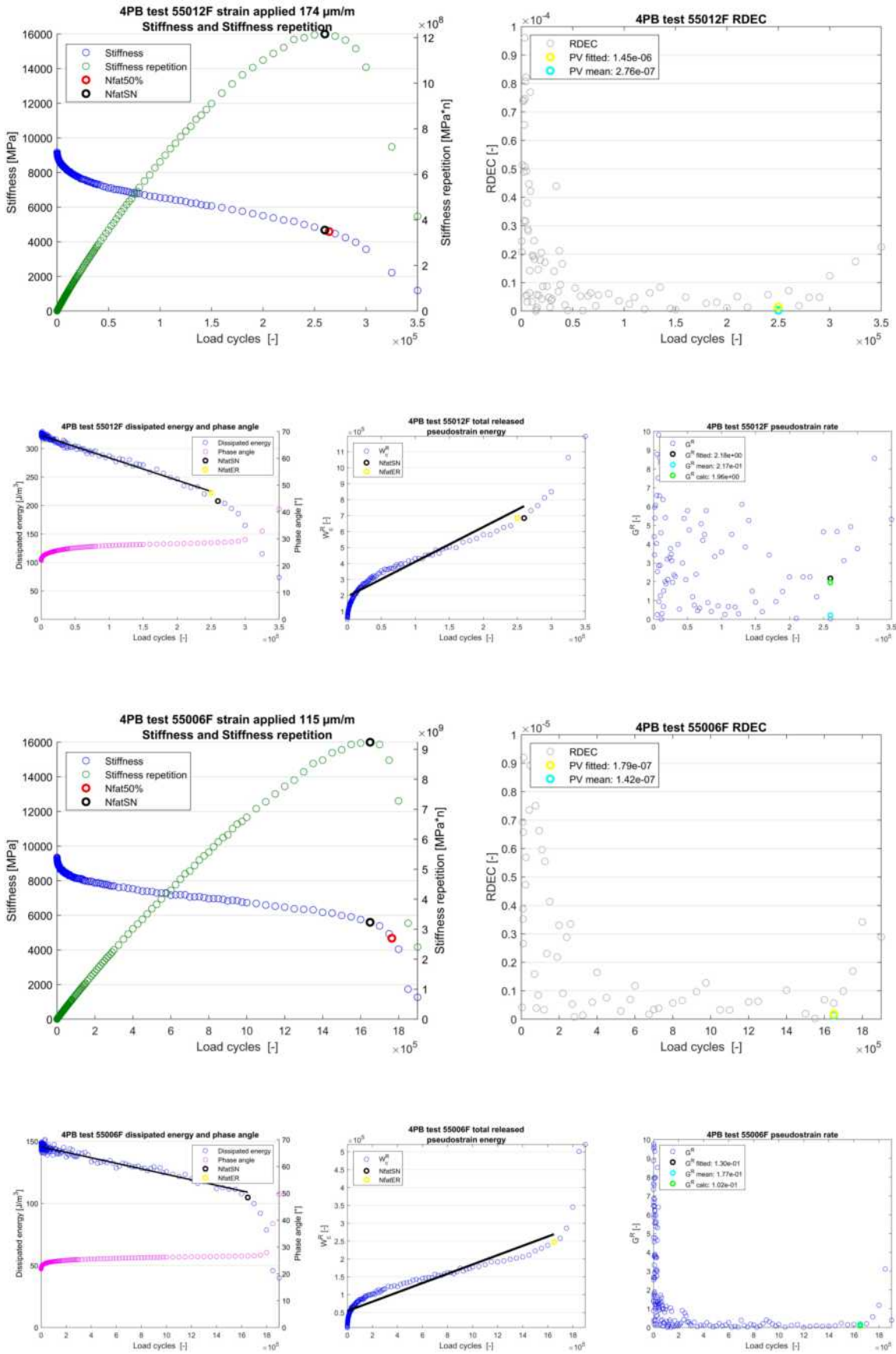
B.7. 19018 results

B.7.1. 4PB

Table B.14: Mixture 19018 4PB results

Sample	Strain applied ε_{ini} [$\mu\text{m}/\text{m}$]	$N_{fat50\%}$	N_{fatSN}	N_{fatER}	$x(1)$	PV fitted ($\cdot 10^{-6}$)	PV mean ($\cdot 10^{-6}$)	ΔPV	G_{calc}^R
54987F	225	71827	72500	70000	-2,48E-03	5,50	6,86	-1,2	13,45
54990F	184	184340	180000	180000	-6,25E-04	1,98	2,52	-1,3	3,25
55018F	115	1562490	1400000	1450000	-2,67E-05	0,21	0,57	-2,7	0,11
55005F	169	258905	240000	240000	-3,55E-04	1,31	1,35	-1,0	1,95
55992F	262	38542	42500	42500	-6,51E-03	10,44	22,11	-2,1	34,50
55003F	117	-	1250000	1150000	-2,34E-05	0,18	0,71	-4,0	0,12
55007F	176	239816	240000	230000	-4,61E-04	1,63	1,87	-1,2	2,23
55004F	261	30703	30000	32000	-7,82E-03	12,49	18,46	-1,5	44,89
55006F	115	1764515	1650000	1650000	-2,22E-05	0,18	0,14	1,3	0,10
55012F	174	264144	260000	250000	-3,94E-04	1,45	0,28	5,3	1,96
55008F	261	40793	45000	45000	-6,18E-03	10,12	14,35	-1,4	33,03
55014F	116	1132466	1000000	1050000	-2,49E-05	0,20	1,37	-7,0	0,14
55017F	176	217329	200000	200000	-4,58E-04	1,55	5,01	-3,2	2,51
55013F	261	34872	34000	39000	-7,23E-03	11,73	18,50	-1,6	39,35
55016F	116	1606073	1500000	1400000	-2,33E-05	0,18	0,03	6,3	0,11
55009F	175	212760	200000	210000	-4,88E-04	1,72	1,60	1,1	2,50
55015F	262	34214	35000	35000	-7,00E-03	11,30	20,65	-1,8	40,00
55993F	115	1808149	1700000	1700000	-2,26E-05	0,18	0,20	-1,1	0,10





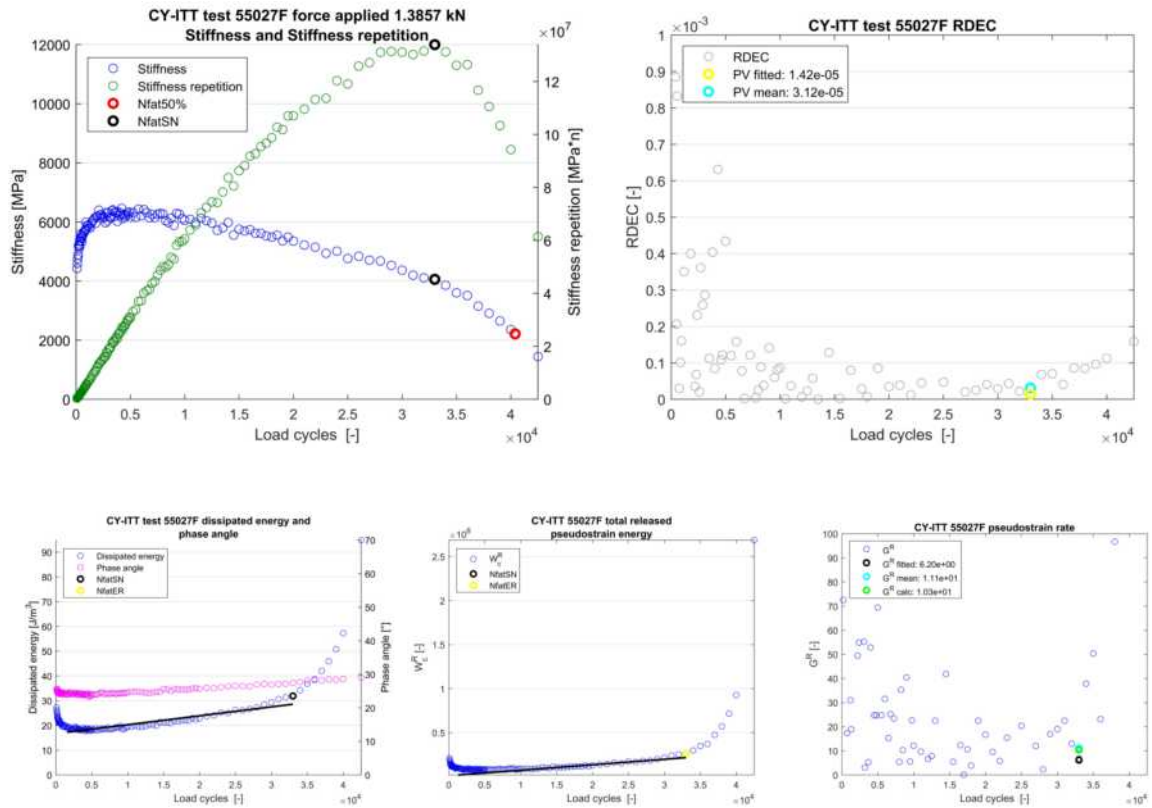
B.7.2. CY-ITT

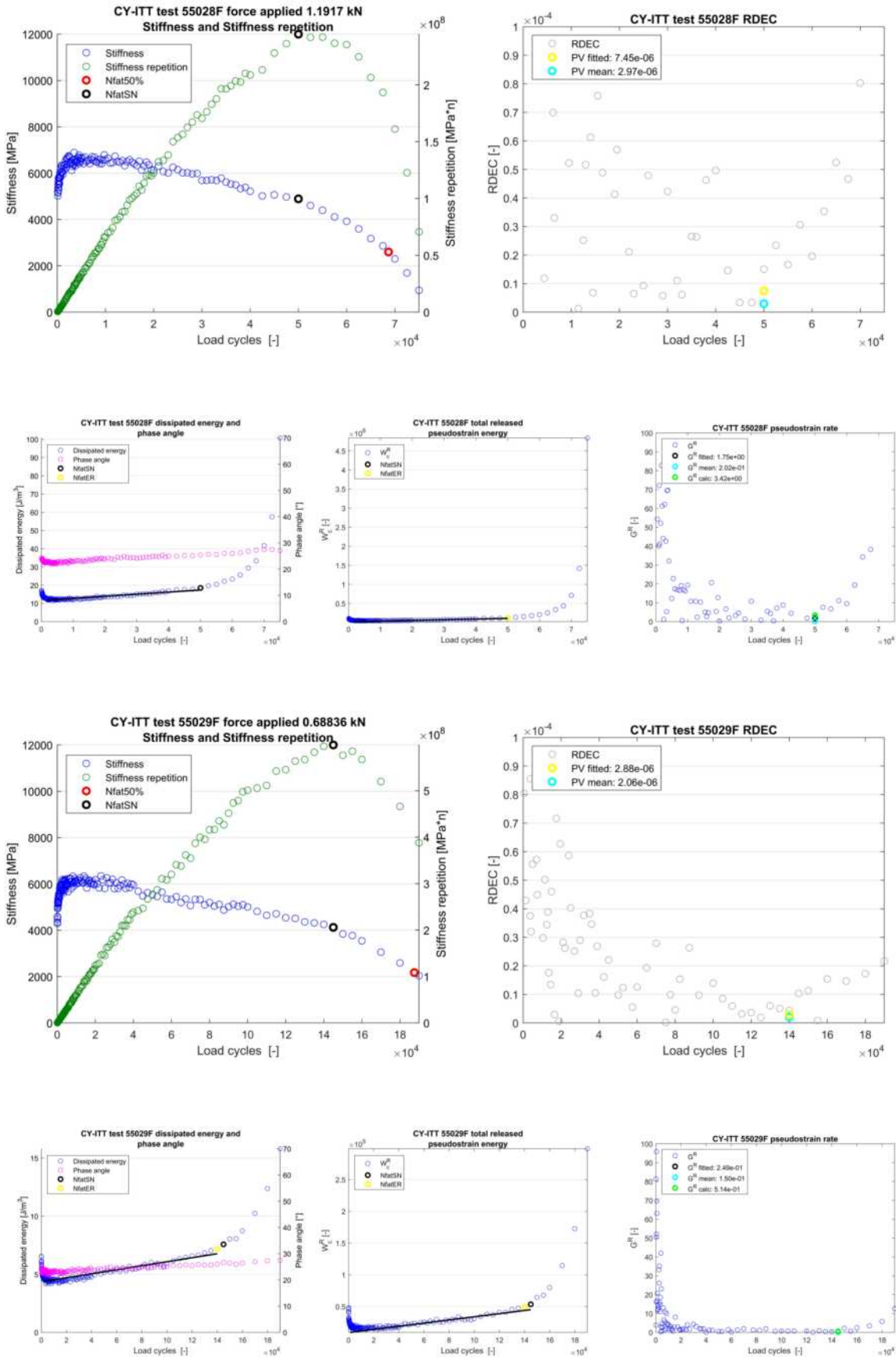
Table B.15: Mixture 19018 30 Hz CY-ITT results

Sample	Strain $n=100$ ϵ_{ini} [$\mu\text{m}/\text{m}$]	$N_{fat50\%}$	N_{fatSN}	N_{fatER}	$x(1)$	PV fitted (* 10^{-6})	PV mean (* 10^{-6})	ΔPV	G_{calc}^R
55020F	95	35989	27000	27000	7,54E-04	17,91	3,50	5,1	26,85
55021F	64	82764	67500	57500	1,31E-04	6,89	6,76	1,0	4,83
55022F	35	-	280000	290000	8,64E-06	1,54	2,16	-1,4	0,35
55023F	63	69198	45000	47500	1,65E-04	8,33	17,95	-2,2	7,04
55024F	40	156369	120000	120000	3,70E-05	4,12	15,09	-3,7	1,24

Table B.16: Mixture 19018 10 Hz CY-ITT results

Sample	Strain $n=100$ ϵ_{ini} [$\mu\text{m}/\text{m}$]	$N_{fat50\%}$	N_{fatSN}	N_{fatER}	$x(1)$	PV fitted (* 10^6)	PV mean (* 10^6)	ΔPV	G_{calc}^R
55025F	47	119937	90000	90000	4,32E-05	5,29	2,03	2,6	1,14
55026F	69	68538	55000	55000	1,29E-04	7,40	15,20	-2,1	3,87
55027F	83	40396	33000	33000	3,60E-04	14,18	31,22	-2,2	10,34
55028F	66	68684	50000	50000	1,16E-04	7,45	2,97	2,5	3,42
55029F	43	187550	145000	140000	1,73E-05	2,88	2,06	1,4	0,51
55030F	76	-	35000	35000	2,96E-04	12,78	15,43	-1,2	8,03
55030bF	79	39626	29000	29000	3,17E-04	14,13	37,32	-2,6	9,48
55030cF	74	52387	40000	37000	1,70E-04	9,96	9,58	1,0	5,95
55030dF	45	192277	150000	150000	1,49E-05	2,41	2,08	1,2	0,55
55030eF	68	55977	47500	39000	1,95E-04	12,82	22,91	-1,8	4,81



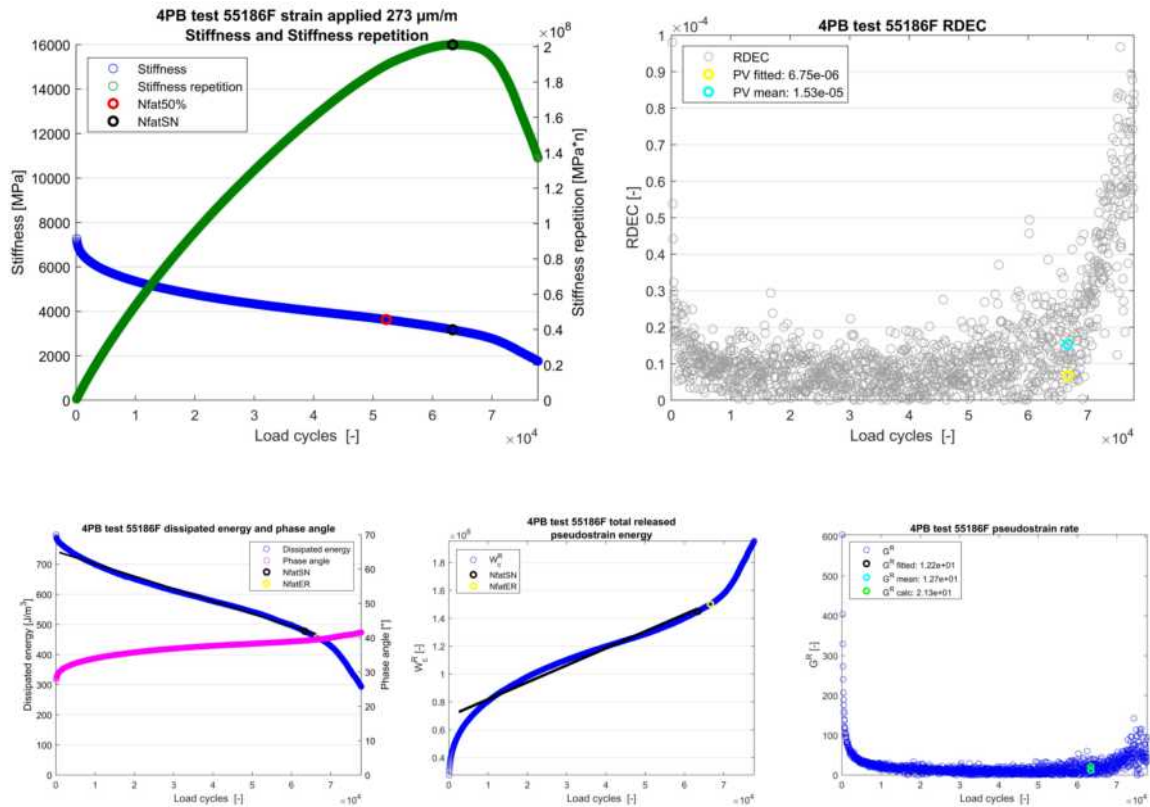


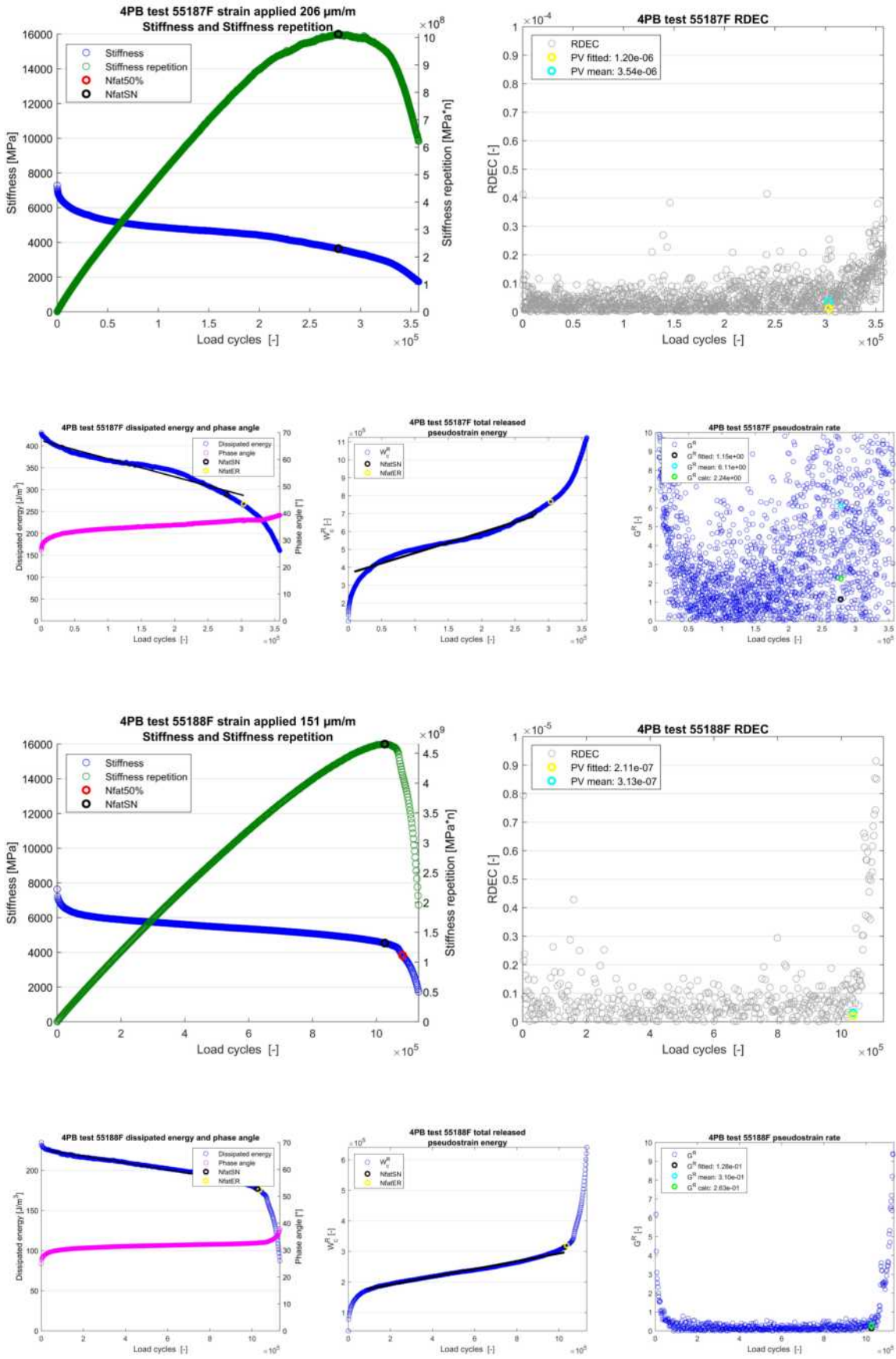
B.8. 19020 results

B.8.1. 4PB

Table B.17: Mixture 19020 4PB results

Sample	Strain applied ϵ_{ini} [$\mu\text{m}/\text{m}$]	$N_{fat50\%}$	N_{fatSN}	N_{fatER}	$x(1)$	PV fitted ($\cdot 10^{-6}$)	PV mean ($\cdot 10^{-6}$)	ΔPV	G_{calc}^R
55176F	238	87361	88935	91490	-1,87E-03	3,78	0,53	7,1	10,12
55177F	206	221972	220372	223255	-5,17E-04	1,37	1,47	-1,1	2,96
55179F	207	221294	210372	212895	-4,13E-04	1,15	5,43	-4,7	2,97
55180F	146	1116344	1000877	1000877	-4,24E-05	0,22	0,29	-1,3	0,24
55181F	268	55281	103106	105910	-3,02E-03	5,21	1,19	4,4	13,83
55182F	151	1083075	1006277	1004477	-4,44E-05	0,22	0,49	-2,2	0,27
55185F	145	1983238	1825257	1863056	-2,33E-05	0,13	0,35	-2,6	0,13
55186F	273	52204	63392	66647	-4,15E-03	6,75	15,32	-2,3	21,26
55187F	206	277978	278124	303529	-4,13E-04	1,20	3,54	-3,0	2,24
55188F	151	1082265	1026076	1036875	-4,23E-05	0,21	0,31	-1,5	0,26
55189F	206	273474	276138	282084	-4,19E-04	1,18	21,29	-18,0	2,35
55190F	282	52931	70258	72311	-4,10E-03	6,44	16,29	-2,5	21,57
55194F	213	220768	226588	234516	-5,70E-04	1,51	0,49	3,1	3,10
55195F	282	45150	48271	52576	-4,98E-03	7,89	27,49	-3,5	28,18
55196F	151	1079738	981077	1024276	-5,18E-05	0,28	0,79	-2,9	0,25
55197F	289	53064	61644	62695	-4,22E-03	6,47	5,65	1,1	23,95
55198F	151	730593	658885	678684	-6,77E-05	0,35	1,27	-3,7	0,35
55199F	212	311811	325687	338300	-3,62E-04	1,01	1,41	-1,4	2,16

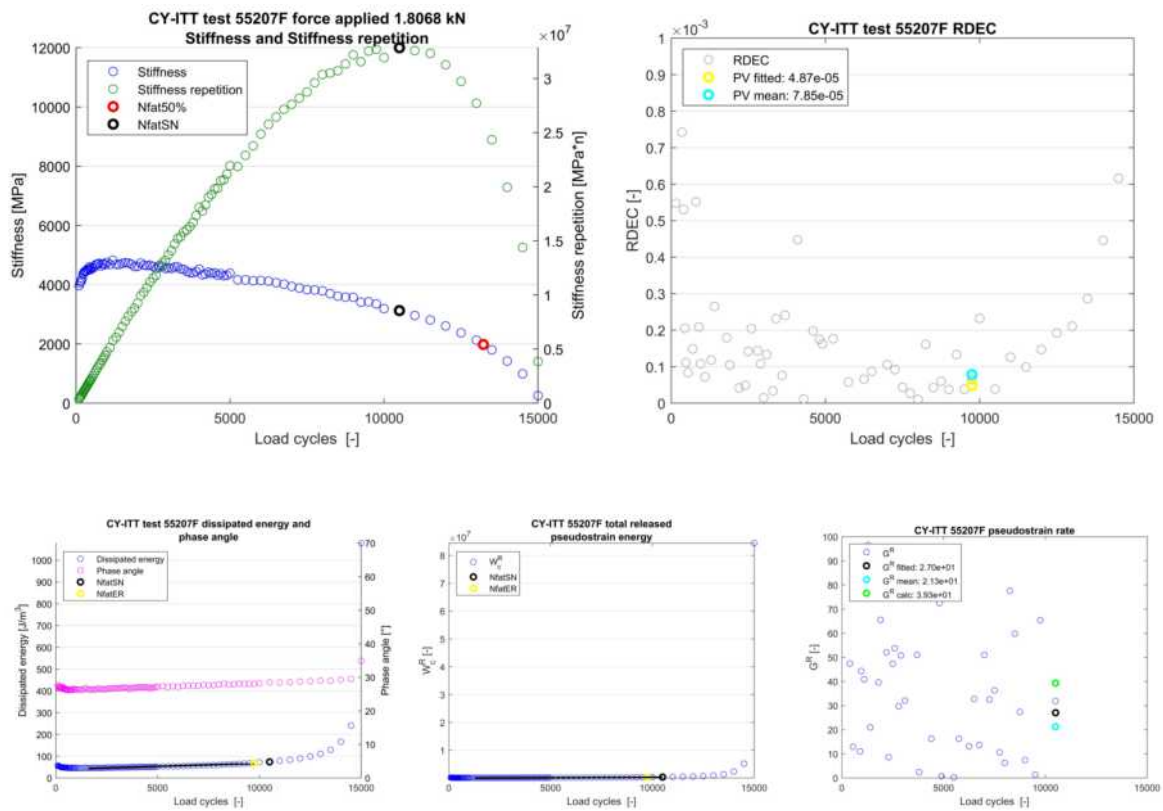


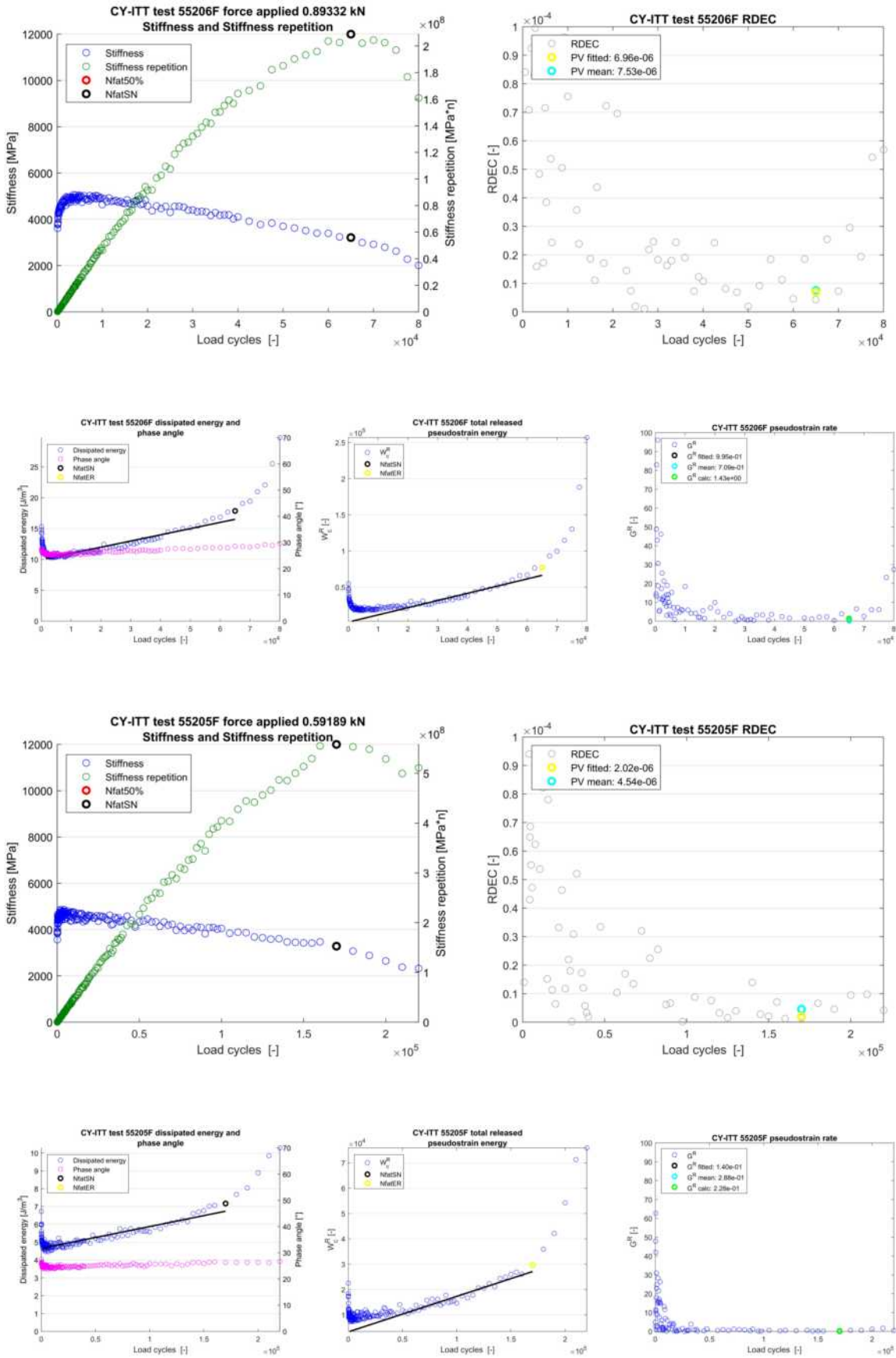


B.8.2. CY-ITT

Table B.18: Mixture 19020 CY-ITT results

Sample	Strain $n=100$ ε_{ini} [$\mu\text{m}/\text{m}$]	$N_{fat50\%}$	N_{fatSN}	N_{fatER}	$x(1)$	PV fitted (* 10^{-6})	PV mean (* 10^{-6})	ΔPV	G_{calc}^R
55202F	115	26846	21000	19000	1,20E-03	25,54	2,18	11,7	17,03
55203F	57	125177	92500	100000	5,41E-05	4,39	4,46	-1,0	0,79
55204F	66	86559	75000	65000	1,05E-04	7,09	7,32	-1,0	1,30
55205F	44	-	170000	170000	1,23E-05	2,02	4,54	-2,2	0,23
55206F	67	-	65000	65000	1,01E-04	6,96	7,53	-1,1	1,43
55207F	128	13227	10500	9750	2,78E-03	48,72	78,49	-1,6	39,35
55208F	48	217892	170000	160000	1,15E-05	1,87	3,85	-2,1	0,26
55209F	137	15527	12500	12000	2,50E-03	39,30	55,55	-1,4	37,43
55210F	48	-	135000	115000	2,48E-05	3,33	4,60	-1,4	0,36



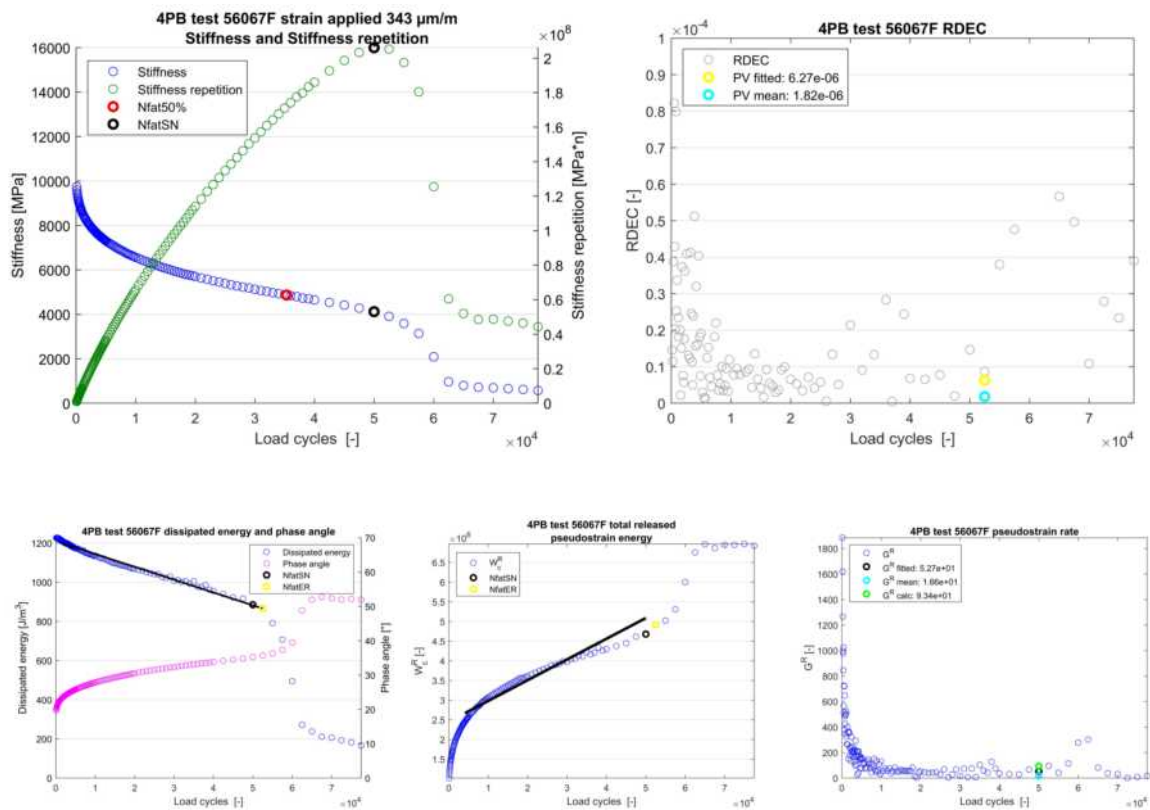


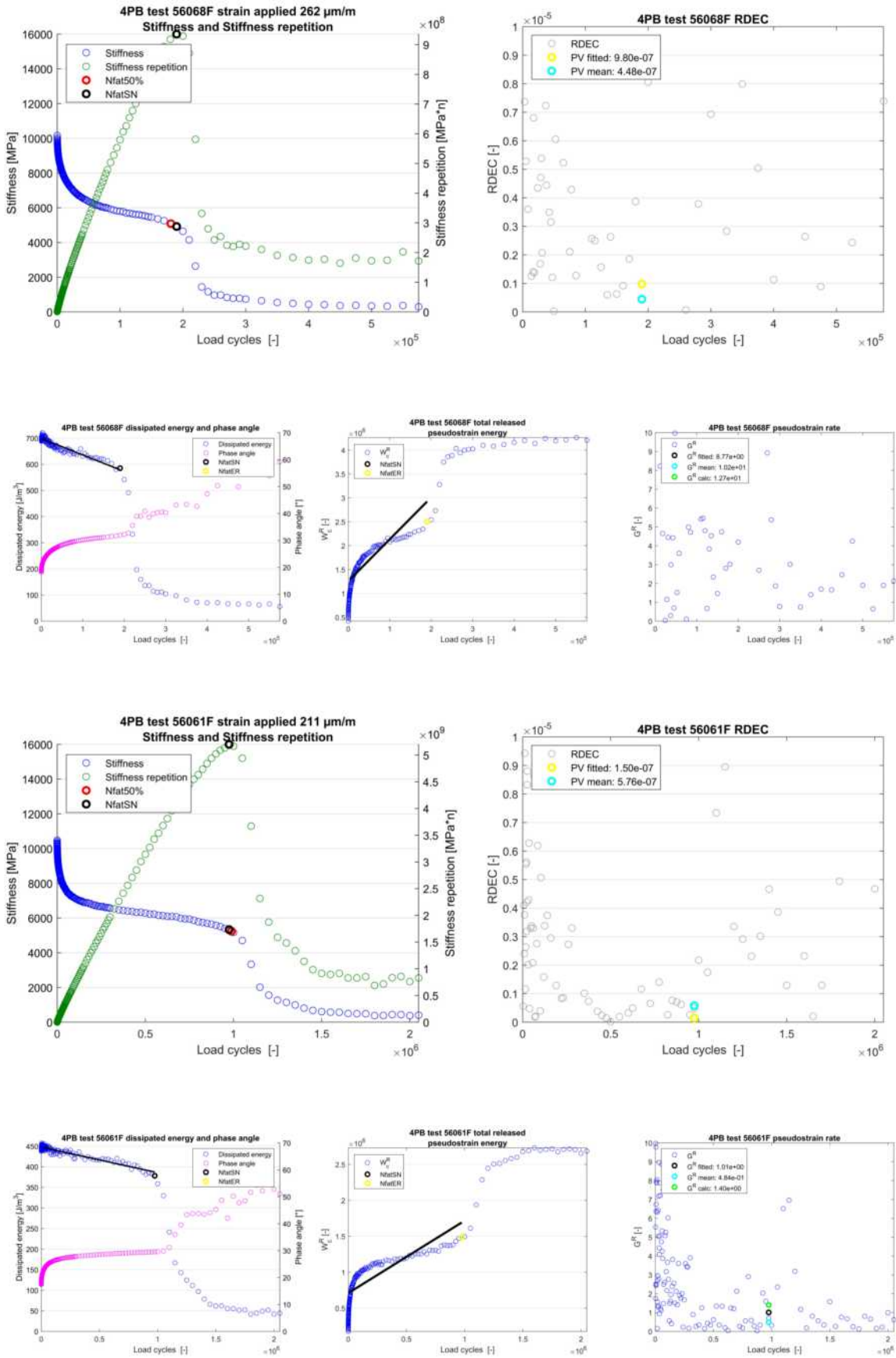
B.9. 19051 results

B.9.1. 4PB

Table B.19: Mixture 19051 4PB results

Sample	Strain applied ε_{ini} [$\mu\text{m}/\text{m}$]	$N_{fat50\%}$	N_{fatSN}	N_{fatER}	$x(1)$	PV fitted ($\cdot 10^{-6}$)	PV mean ($\cdot 10^{-6}$)	ΔPV	G_{calc}^R
56048F	300	115753	125000	125000	-1,92E-03	2,37	3,78	-1,6	27,55
56051F	243	495141	500000	500000	-2,48E-04	0,45	0,84	-1,8	4,09
56057F	344	40107	45000	45000	-5,98E-03	5,47	4,72	1,2	101,93
56056F	343	40963	60000	62500	-5,90E-03	5,89	15,41	-2,6	79,37
56049F	273	203121	220000	220000	-8,77E-04	1,26	1,34	-1,1	12,47
56058F	218	799147	775000	750000	-6,88E-05	0,15	0,04	4,3	1,87
56052F	275	199751	230000	230000	-8,89E-04	1,25	0,23	5,4	12,62
56059F	345	41264	62500	65000	-5,94E-03	5,85	8,48	-1,4	76,66
56067F	344	35325	50000	52500	-6,54E-03	6,27	1,82	3,4	93,44
56066F	274	209616	220000	220000	-6,39E-04	0,96	1,27	-1,3	12,05
56069F	342	43852	72500	72500	-4,32E-03	4,05	1,73	2,3	65,97
56061F	211	988684	975000	975000	-6,18E-05	0,15	0,58	-3,8	1,40
56068F	262	180945	190000	190000	-6,33E-04	0,98	0,45	2,2	12,67
56070F	202	1339009	1300000	1350000	-4,03E-05	0,11	0,86	-7,9	0,96
56091F	203	1597681	1600000	1600000	-1,51E-05	0,04	0,59	-14,3	0,79
56060F	340	39892	45000	45000	-6,05E-03	5,79	1,80	3,2	97,67
56053F	209	2001926	1950000	1950000	-3,60E-05	0,09	0,41	-4,6	0,72
56055F	209	1042325	1050000	1050000	-5,61E-05	0,14	0,41	-2,9	1,28

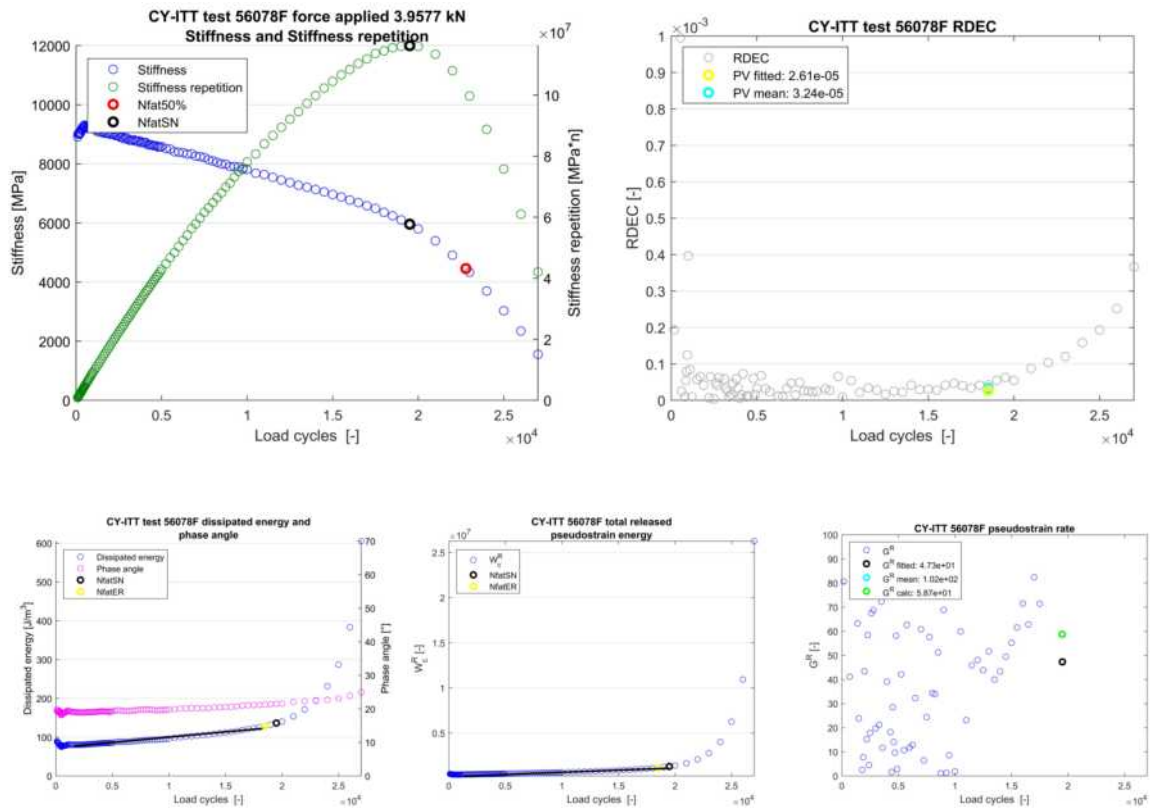


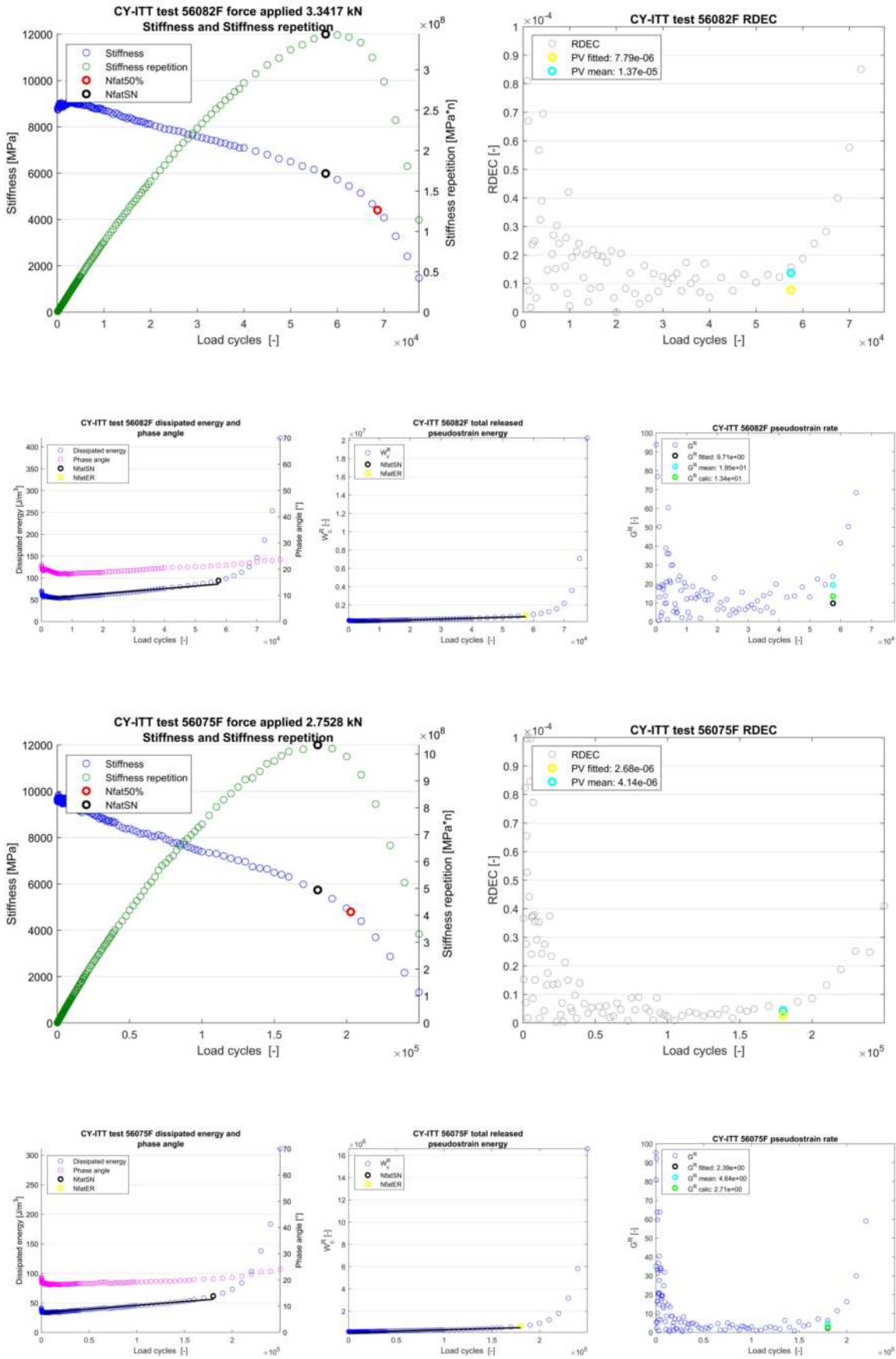


B.9.2. CY-ITT

Table B.20: Mixture 19051 CY-ITT results

Sample	Strain $n=100$ ε_{ini} [$\mu\text{m}/\text{m}$]	$N_{fat50\%}$	N_{fatSN}	N_{fatER}	$x(1)$	PV fitted (* 10^{-6})	PV mean (* 10^{-6})	ΔPV	G_{calc}^R
56073F	60	476731	409997	399997	3,02E-05	1,22	1,68	-1,4	0,55
56074F	82	173075	154999	149999	1,54E-04	3,38	5,20	-1,5	2,99
56075F	83	202838	180000	180000	1,29E-04	2,68	4,14	-1,5	2,71
56076F	113	80000	67499	59999	5,84E-04	7,44	6,24	1,2	10,70
56077F	82	164095	145000	135000	1,33E-04	3,08	4,83	-1,6	2,98
56078F	131	22783	19500	18500	2,72E-03	26,09	32,42	-1,2	58,73
56079F	128	33344	29000	29000	1,93E-03	17,46	28,04	-1,6	38,16
56080F	109	45147	38999	36999	9,30E-04	12,19	21,13	-1,7	19,06
56081F	104	100065	82498	79998	4,75E-04	6,70	9,02	-1,3	7,39
56082F	114	68617	57500	57500	5,93E-04	7,79	13,72	-1,8	13,43
56083F	127	33951	29000	29000	1,90E-03	18,22	28,08	-1,5	32,64





C

Results based on works of Li

In this appendix the results are presented using the fatigue tests performed by Li. The results and mixture descriptions can be found in the PhD thesis: *Asphalt mixture fatigue testing, influence of test type and specimen size*. The test results were accessible in the test equipment and used with permission of the operator. As fatigue testing cost valuable time, the use and interpreting previous results on a new method is advisable. The interest of the works lie in the fact that both displacement en force controlled 4PB test were performed. The result were therefore used to establish for both the RDEC and VECD the mode of loading relation.

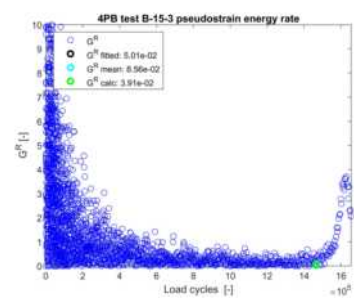
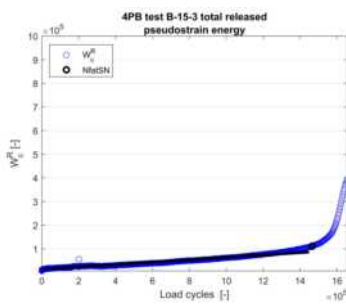
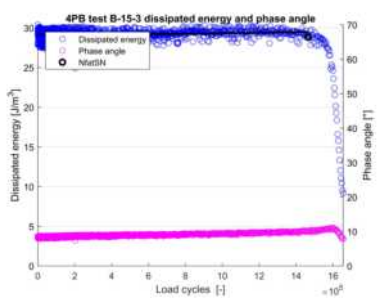
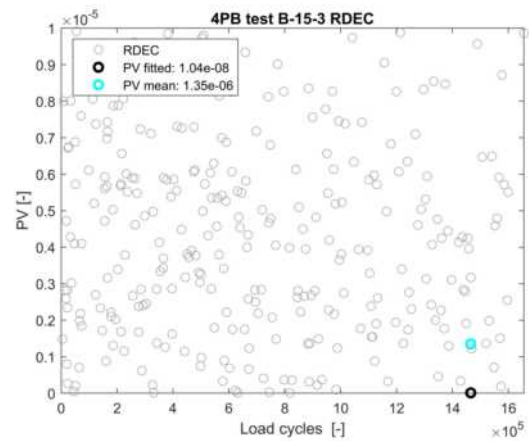
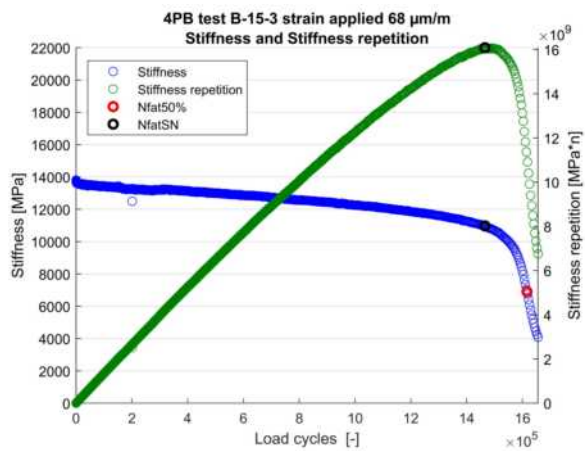
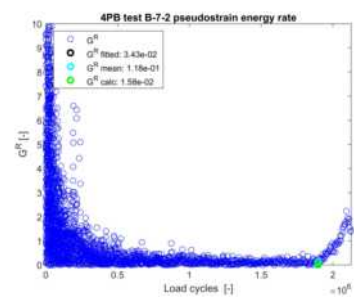
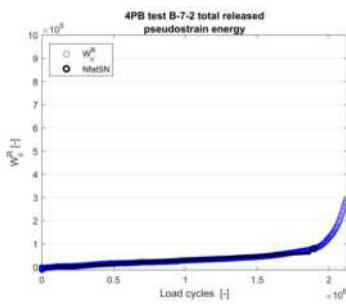
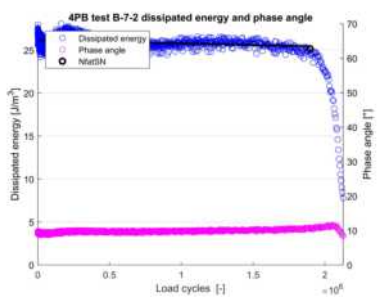
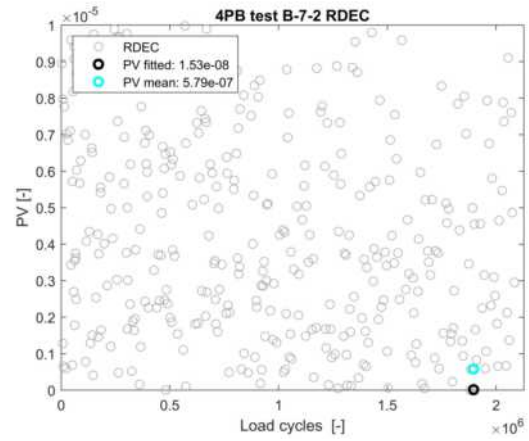
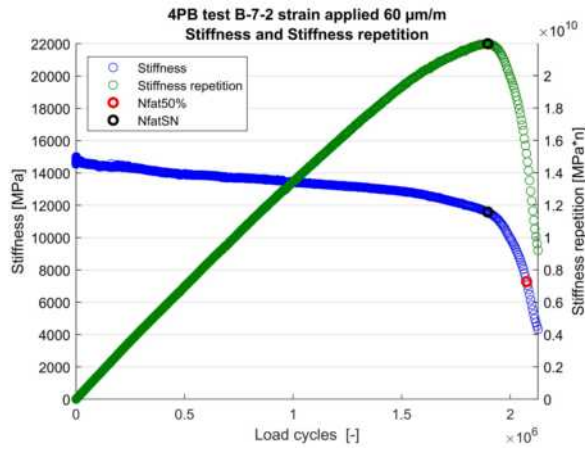
The tests were performed at 5°C at 10 Hz. The test equipment of the TU Delft was used for the experiments. The temperature will be the cause to the deviating behaviour of the dissipated energy. Resulting in the completely ludicrous RDEC results.

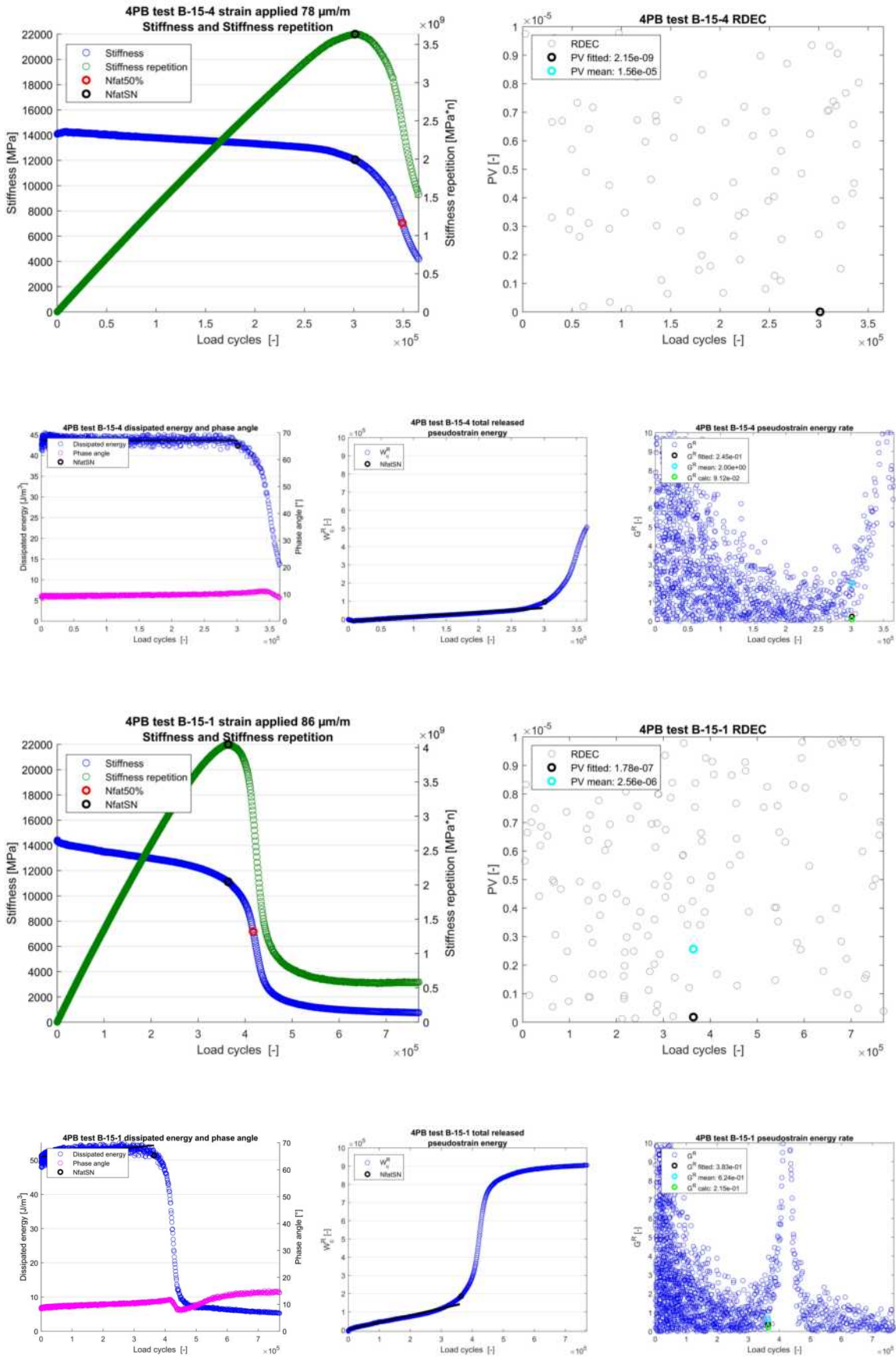
For each result the Stiffness and Stiffness Repetition failure method is given in a single figure. Both $N_{fat50\%}$ and N_{fatSN} are given. The second figure gives the RDEC result, given with the values of PV fitted and mean at N_{fatSN} . The row below gives in the third figure the dissipated energy and phase angle. Here the N_{fatSN} is given, the fitted line is the parameter $x(1)$. The fourth figure depicts the W_c^R with the fitted line with N_{fatSN} . The fifth figure gives the G^R at N_{fatSN} with the three applied methods of fitted, calc and mean values of G^R .

C.1. 4PB strain controlled

Table C.1: Mixture Li strain controlled 4PB results

Sample	Strain applied ε_{ini} [$\mu\text{m}/\text{m}$]	$N_{fat50\%}$	N_{fatSN}	N_{fatER}	$x(1)$	PV fitted (*10 ⁶)	PV mean (*10 ⁶)	ΔPV	G_{calc}^R
B-7-2	60	2075660	1896712	2128148	-3,95E-07	0,02	0,58	-37,9	0,02
B-15-3	68	1616140	1465549	1655775	3,02E-07	0,01	1,35	-129,7	0,04
B-18-1	73	1263000	1111741	1358316	3,28E-06	0,09	7,79	-87,8	0,01
B-15-4	78	349074	301306	364758	9,33E-08	0,00	15,57	-7237,5	0,09
B-18-4	83	473629	428551	542009	7,01E-06	0,15	8,66	-56,1	0,17
B-15-1	86	417151	363921	769138	9,07E-06	0,18	2,56	-14,4	0,21

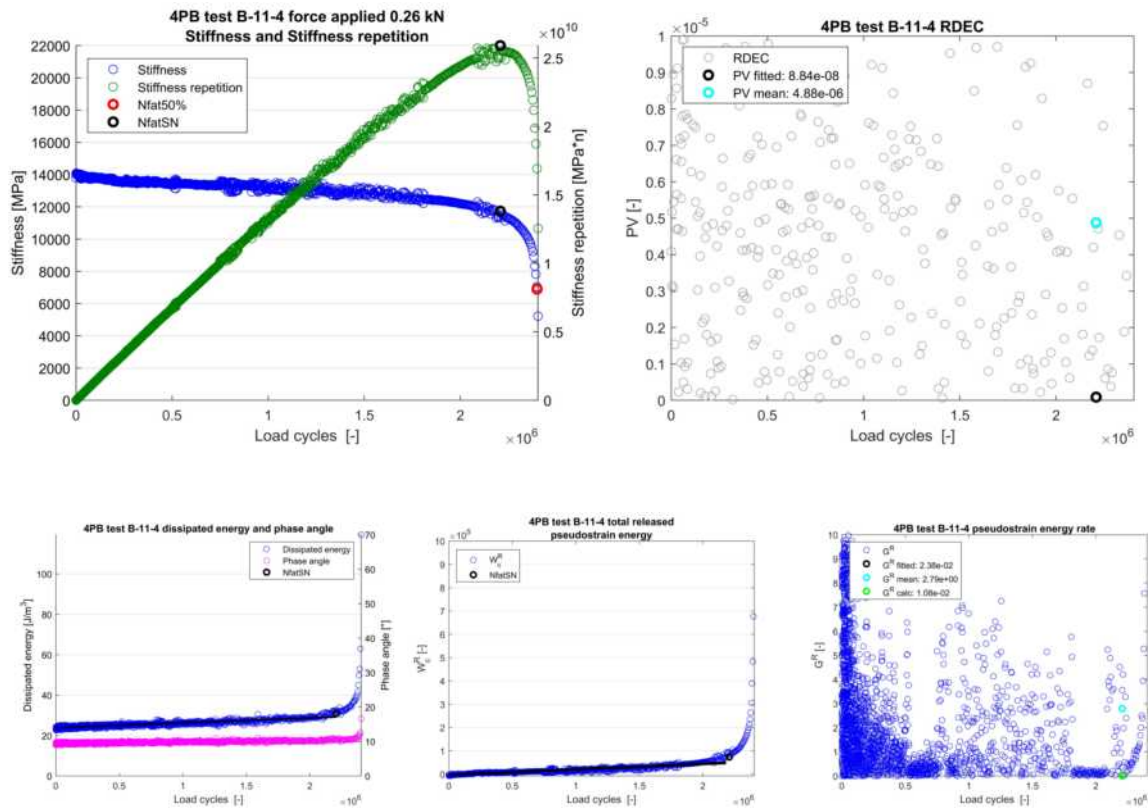


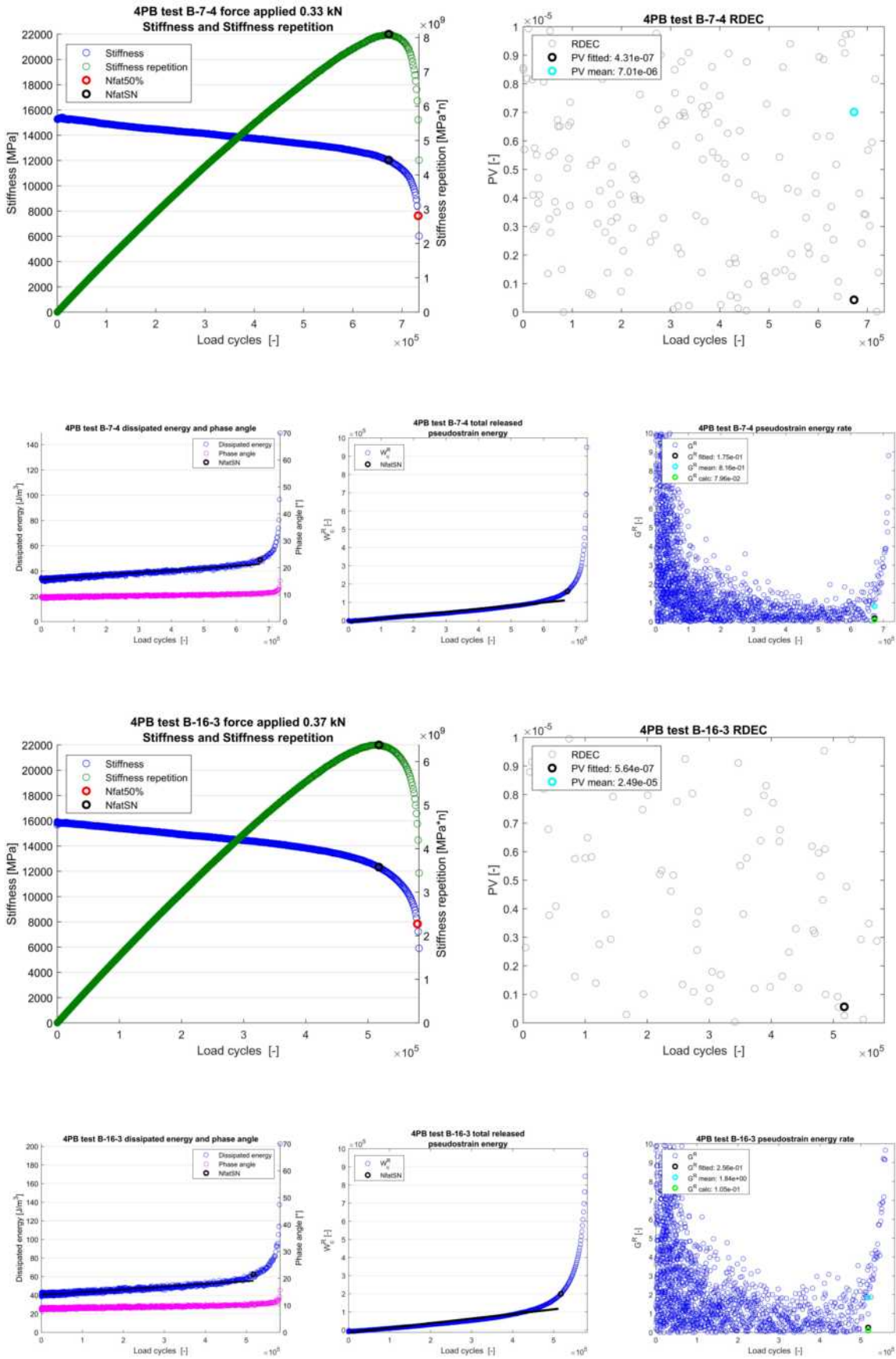


C.2. 4PB stress controlled

Table C.2: Mixture Li stress controlled 4PB results

Sample	Strain $n=100$ ε_{ini} [$\mu m/m$]	$N_{fat50\%}$	N_{fatSN}	N_{fatER}	$x(1)$	PV fitted (* 10^6)	PV mean (* 10^6)	ΔPV	G_{calc}^R
B-11-4	57	2399298	2208008	2098945	2,42E-06	0,09	4,88	-55,2	0,01
B-11-1	63	1731192	1584899	1479112	6,36E-06	0,20	2,03	-10,0	0,03
B-11-2	63	1856882	1741815	1686559	6,03E-06	0,17	0,62	-3,6	0,03
B-7-3	65	-	829854	820360	1,59E-05	0,40	0,23	1,7	0,04
B-7-4	67	732844	672984	645655	1,79E-05	0,43	7,01	-16,3	0,08
B-7-1	68	597208	550808	538272	2,55E-05	0,53	1,12	-2,1	0,12
B-16-3	73	579546	517607	504666	2,92E-05	0,56	24,89	-44,1	0,11





D

Results 18619TU

In this appendix the complete results of the 4PB force controlled testing are presented. A total of 21 test were performed of which 14 where successful. Some samples broke directly after applying the amplitude force or other test circumstances where of deviation that the test wasn't conducted properly. Of these 14, 3 tests showed a significant deviation that they where left out of the final results. This is a common practice because of the inhomogeneity of asphalt samples and the high amount of variation that can exist.

D.1. Stiffness and Stiffness Repetition

In this first section all 11 results are shown for the fatigue test in Stiffness and the results with the Stiffness Repetition method for finding N_{fat} . The measured Stiffness shows a good overall steady decrease over the number of loading cycles corresponding with the increase of the displacement amplitude over time. This actual steady decrease is in general similar to the behaviour of a force controlled CY-ITT Stiffness development we saw in Annex B

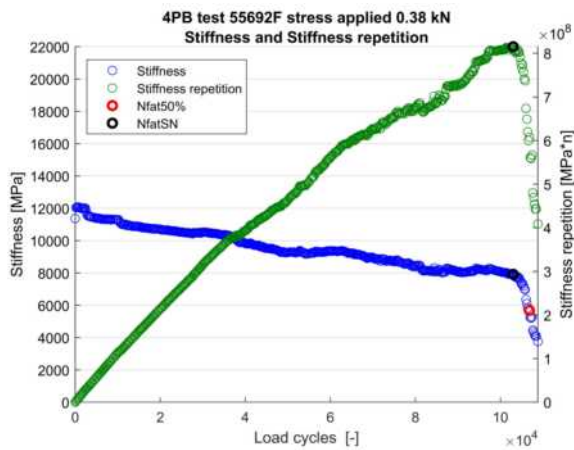


Figure D.1: Stiffness and Stiffness ratio 55692

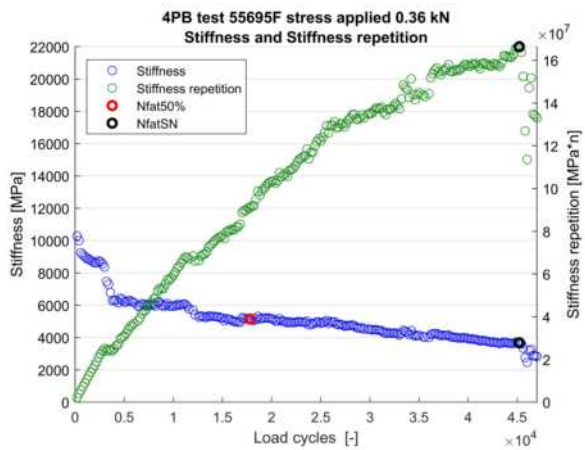


Figure D.2: Stiffness and Stiffness ratio 55695

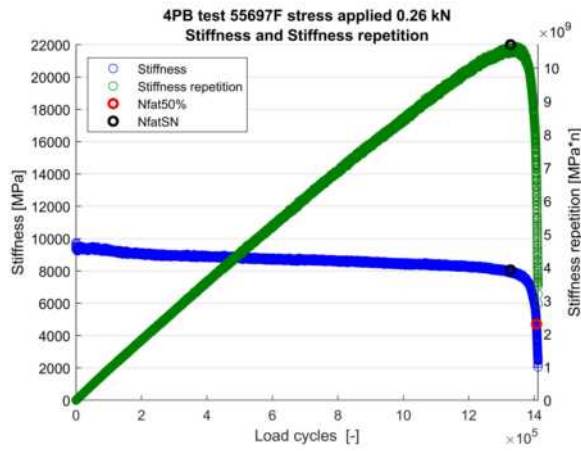


Figure D.3: Stiffness and Stiffness ratio 55697

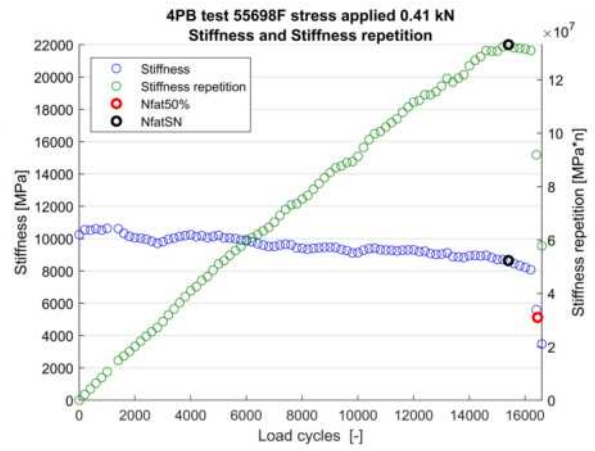


Figure D.4: Stiffness and Stiffness ratio 55698

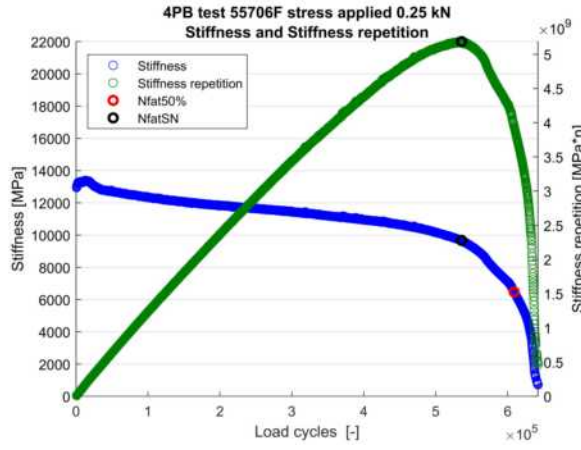


Figure D.5: Stiffness and Stiffness ratio 55706

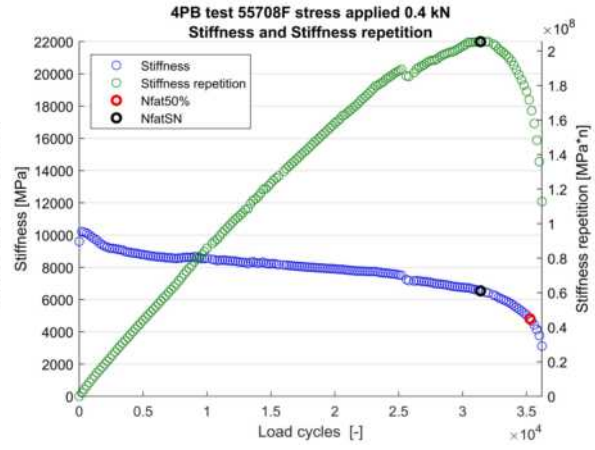


Figure D.6: Stiffness and Stiffness ratio 55708

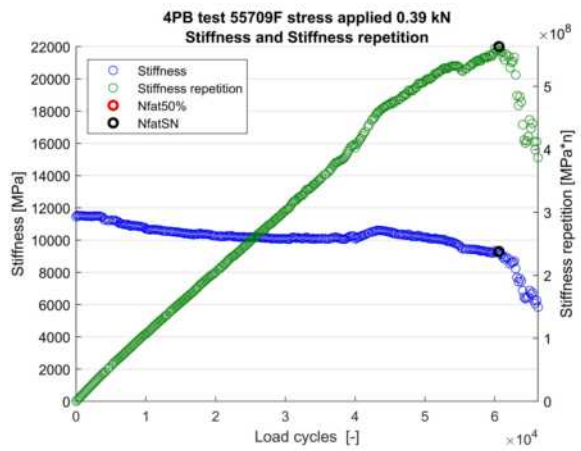


Figure D.7: Stiffness and Stiffness ratio 55709

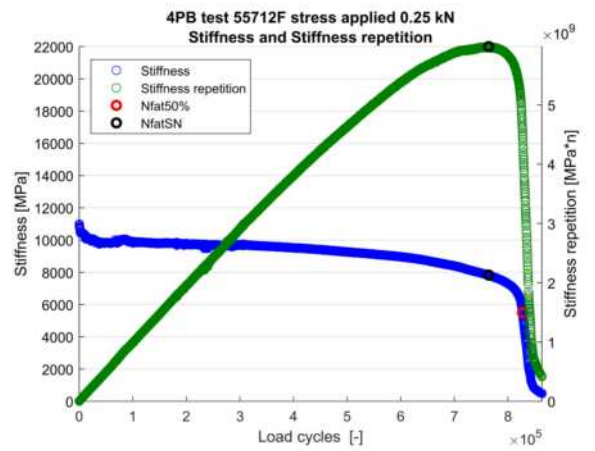


Figure D.8: Stiffness and Stiffness ratio 55712

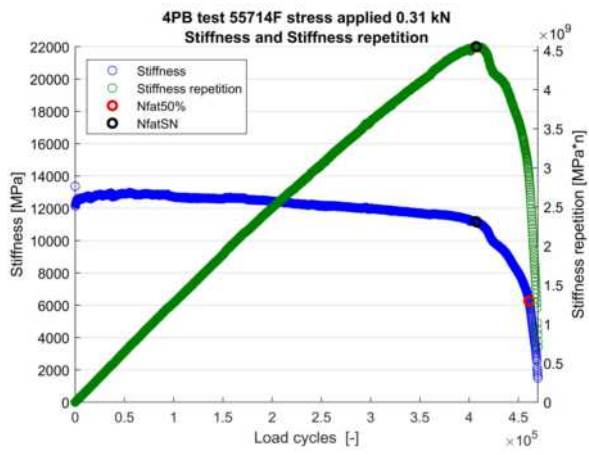


Figure D.9: Stiffness and Stiffness ratio 55712

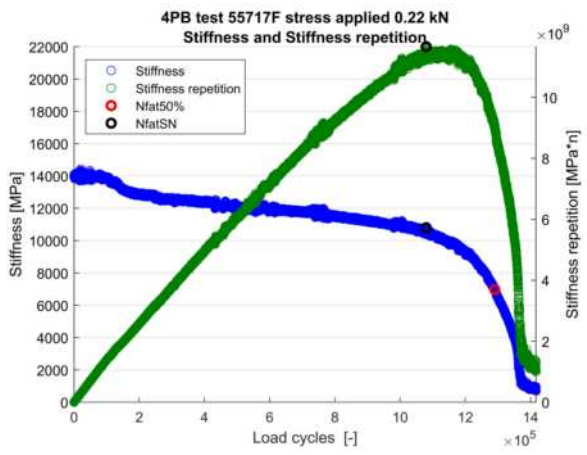


Figure D.10: Stiffness and Stiffness ratio 55717

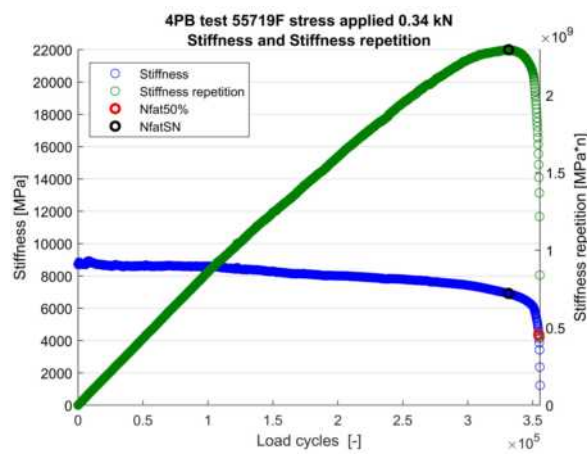


Figure D.11: Stiffness and Stiffness ratio 55719

D.2. Phase angle, dissipated energy and RDEC

In this section the 11 test results of the phase angle, dissipated energy and RDEC are presented. These are combined in 2 figures which are presented side by side. Because the huge fluctuations in the measured phase angle in combination with that phase angle at low angles, gives a complete scattered RDEC. The scattering of the phase angle is explained by the measurement frequency of only 25 point per load cycle. All other test are done with the minimum of 50 points per load repetition. The resulting FFT and or sinusoidal fitting couldn't be consistently used to find a steady phase angle from the measured displacement and force amplitudes. Once again emphasizes the importance of good measurements of the phase angle as in Chapter 4.

The amount of scattering in the phase angle also resulted in setting the failure criteria to the Stiffness Repetition method. As proven in Chapter 4 this is of no significant impact. To see the difference again between the measured RDEC and the fitting method, the PV fitted and the PV mean is given. *PV mean* is the average value of the 10 measurements before failure point N_{fatSN} . Due the huge scattering taking place in the RDEC both values are not always plotted. When reading the graphs, keep in mind that the PV values can also be negative and with the axis set to zero, there is an equal part of PV values on the negative side. PV mean is due that fact calculated of only the positive PV values for a better estimate.

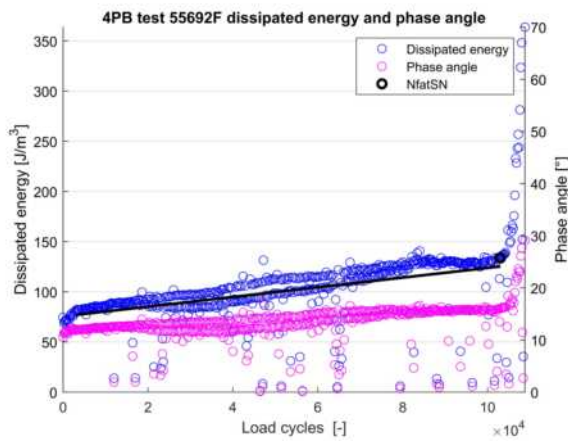


Figure D.12: Phase angle and dissipated energy 55692

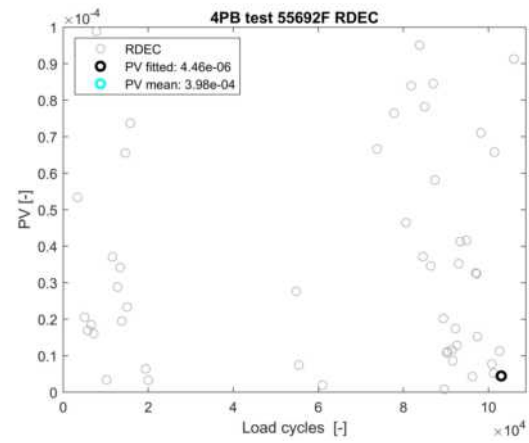


Figure D.13: RDEC 55692

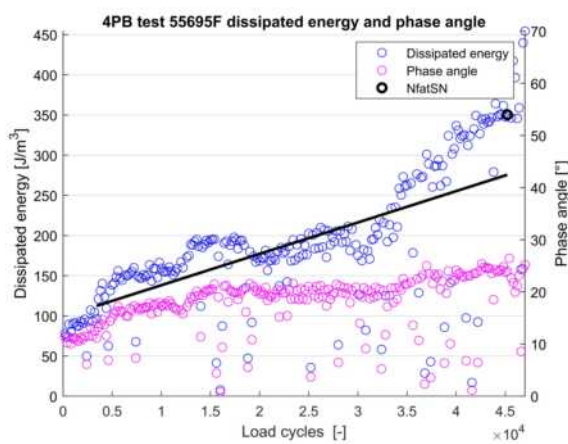


Figure D.14: Phase angle and dissipated energy 55695

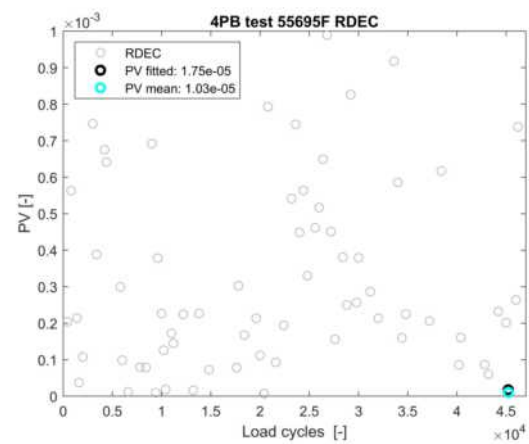


Figure D.15: RDEC 55695

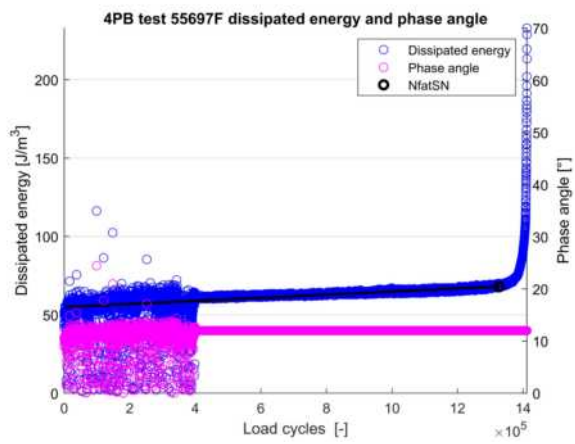


Figure D.16: Phase angle and dissipated energy 55697

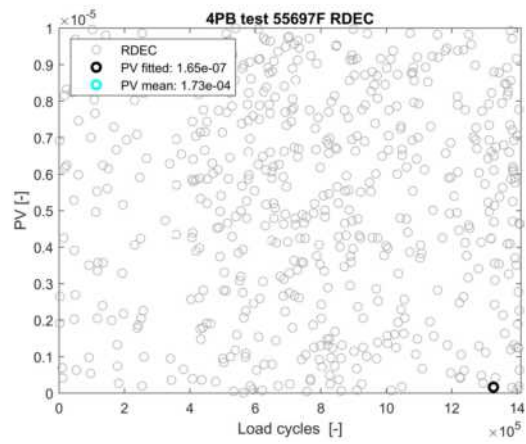


Figure D.17: RDEC 55697

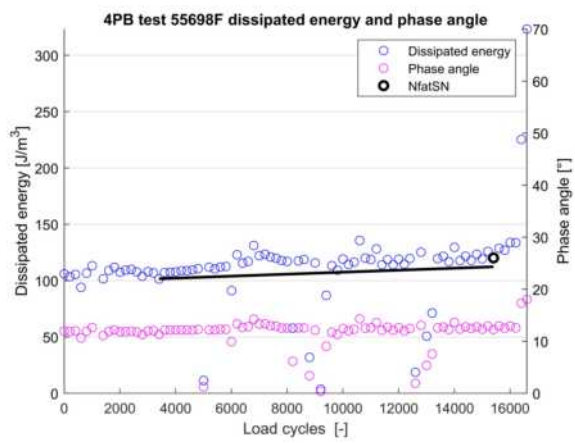


Figure D.18: Phase angle and dissipated energy 55698

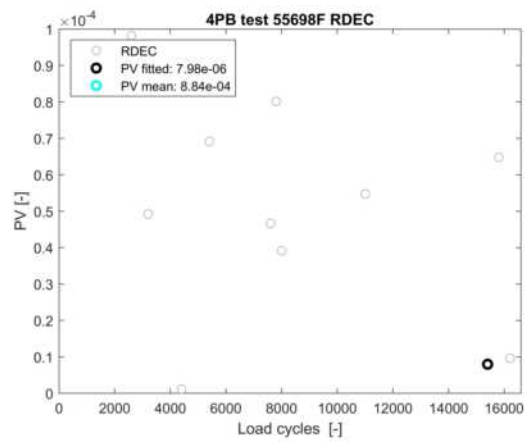


Figure D.19: RDEC 55698

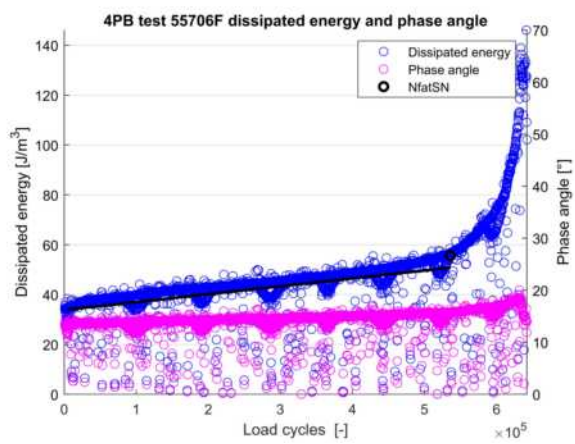


Figure D.20: Phase angle and dissipated energy 55706

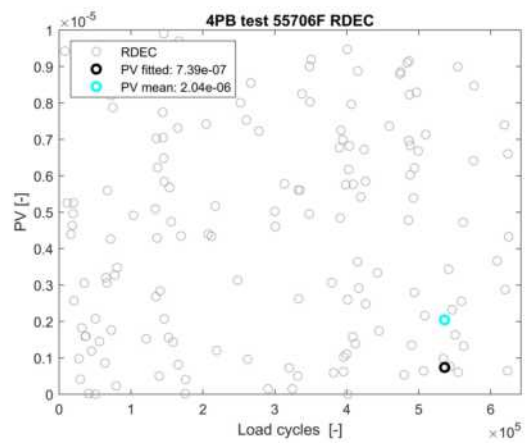


Figure D.21: RDEC 55706

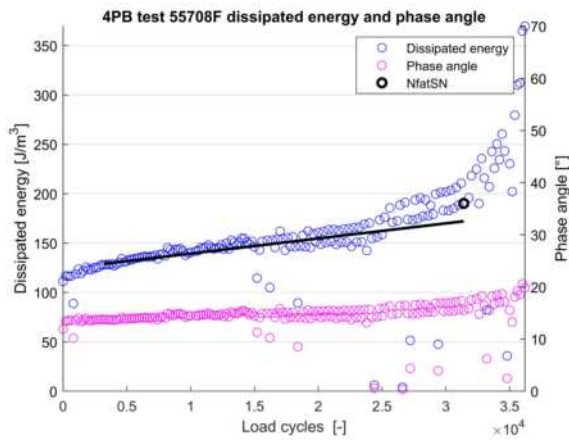


Figure D.22: Phase angle and dissipated energy 55708

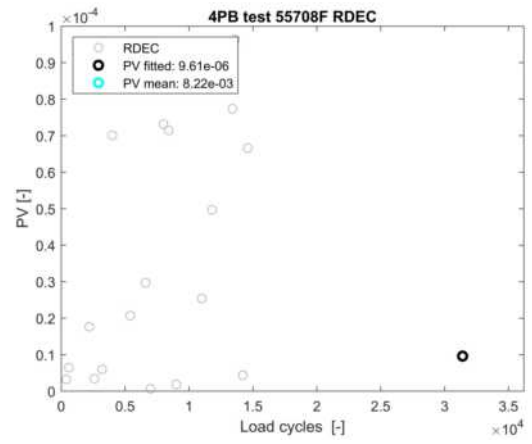


Figure D.23: RDEC 55708

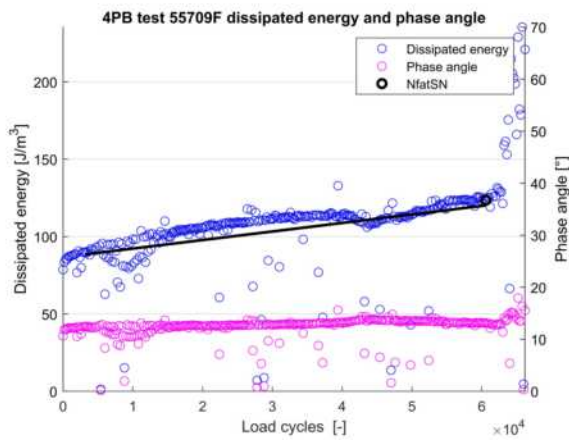


Figure D.24: Phase angle and dissipated energy 55709

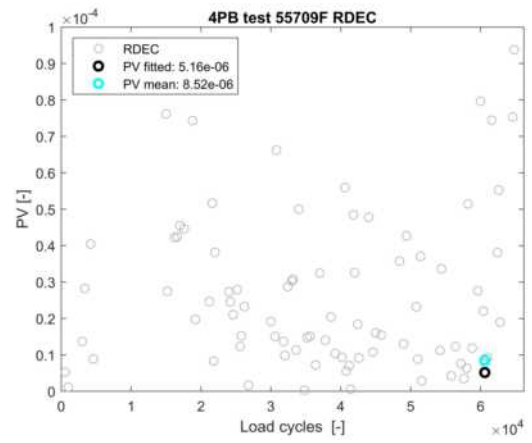


Figure D.25: RDEC 55709

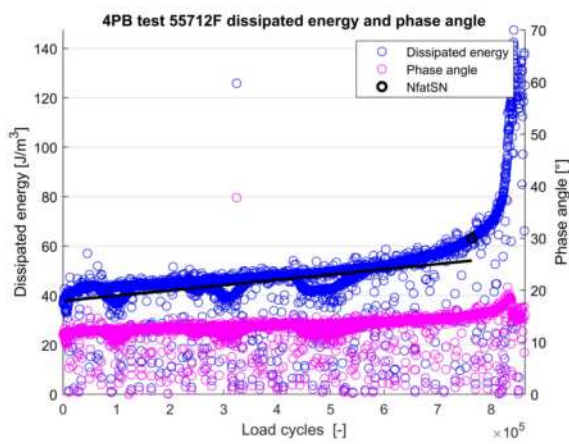


Figure D.26: Phase angle and dissipated energy 55712

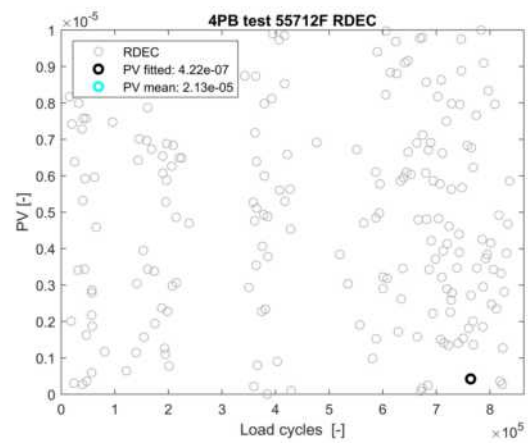


Figure D.27: RDEC 55712

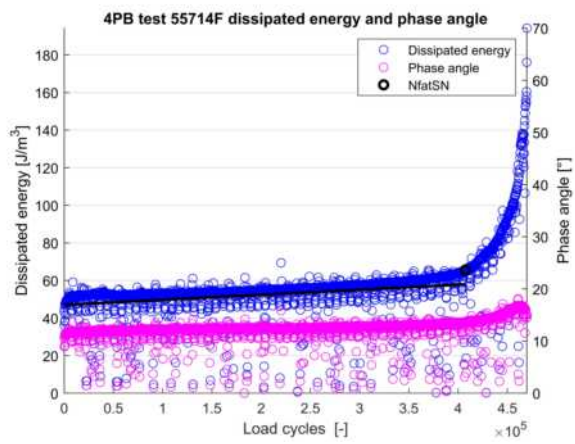


Figure D.28: Phase angle and dissipated energy 55714

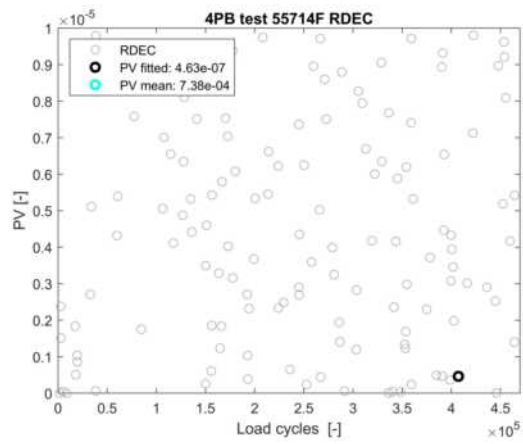


Figure D.29: RDEC 55714

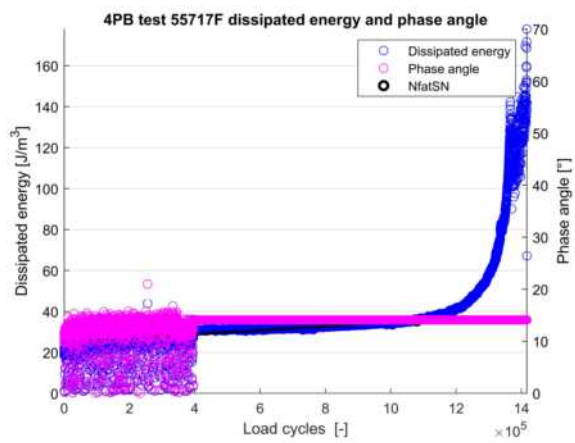


Figure D.30: Phase angle and dissipated energy 55717

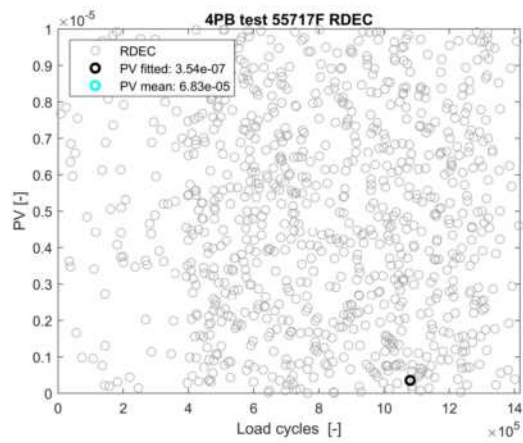


Figure D.31: RDEC 55717

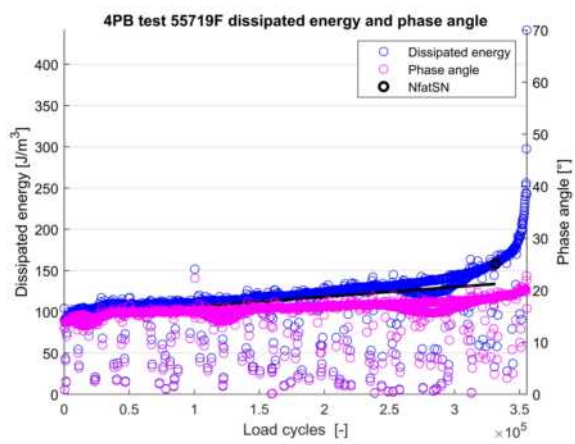


Figure D.32: Phase angle and dissipated energy 55719

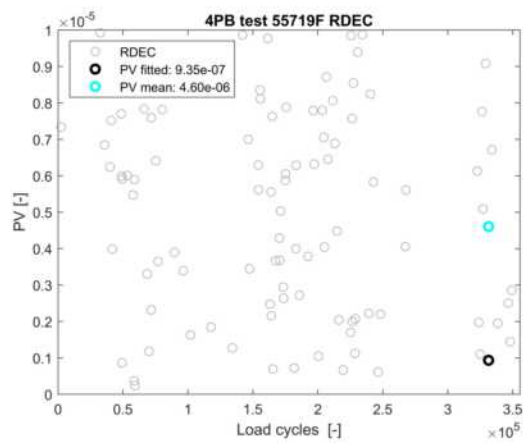


Figure D.33: RDEC 55719

D.3. Table

In table D.1 the previous results are given in a single table. The applied strain, failure criteria SN, the fitted slope of the dissipated energy, the resulting PV fitted, the average found PV at failure and the magnitude differences between them. The magnitude factor is through the roof due the amount of phase angle scatter.

Table D.1: Mixture 18619TU 4PB force controlled results

Sample	Strain applied ε_{ini} [$\mu\text{m}/\text{m}$]	N_{fatSN}	$x(1)$	PV fitted (* 10^6)	PV mean (* 10^6)	ΔPV
55692F	98	103003	4,83E-04	4,46	398,14	-89,3
55695F	128	45204	3,90E-03	17,47	10,28	1,7
55697F	97	1327310	9,95E-06	0,17	173,30	-1047,7
55698F	125	15404	8,85E-04	7,98	883,93	-110,7
55706F	60	536003	3,16E-05	0,74	2,04	-2,8
55708F	127	31404	1,53E-03	9,61	8223,69	-855,4
55709F	107	60603	5,52E-04	5,16	8,52	-1,7
55712F	75	764004	2,14E-05	0,42	21,26	-50,3
55714F	80	407204	2,69E-05	0,46	737,68	-1592,8
55717F	50	1079957	1,02E-05	0,35	68,30	-192,7
55719F	117	331404	1,18E-04	0,93	4,60	-4,9

Uni-axial Tensile Compression test

In this appendix the description, execution and results of the Uni-axial Tensile Compression Fatigue (UTCF) tests in displacement control are given. A total of 11 test were performed of which all test were executed successfully with no large deviations. In total 13 samples were made with the same mixture composition as the 18590 project made at the KWS central laboratory. 2 samples were damaged at the production or sawing stage. The choice for this mixtures was based on the stability and consistent results shown at the time in the 4PB and CY-ITT tests. Due to the unavailability of the gyrator mould size and test equipment needed to perform a UTCF test in Hoogblokland, the tests were performed at the road construction laboratory at the Technical University Delft.

E.1. Specimen preparation

Samples were prepared with the same mixture composition from project 18590 performed in the central laboratory of Hoogblokland. It is a stable surface layer mixture with a normal bitumen Pen-Grade of 40/60 with a content of 5.7 % [m/m]. More detailed information regarding the mixture composition is not available due company's policy. Granulates were prepared per sample and heated to 170 degree Celsius. The mixture was mixed for 3 minutes in a Hobart shear mixer, with adding the bitumen first and gradually adding the amount of filler. The hot loose mix was poured into a mould with size 150 mm in diameter and 200 mm in height and shear compacted in a gyrator to the preferred set height. Two test samples were made in advance to get the right density in overall agreement with the plates made in Hoogblokland. The samples were stored at a controlled climate chamber at 13°C and cored after one week to the preferred diameter of 100 mm. The preferred height of 150 mm was reached by polishing the bottom and top, both sides were reduced by around 10 mm overall. See figure E.1 for an example of a cored and polished sample. Because of the edge effects a gyrator has on a specimen and the distortions it brings in density, it is necessary to remove material from both sides. After coring and polishing the samples were stored again in the climate chamber. After 2 months of storage, due problems with the test equipment, the samples were tested.



Figure E.1: Cored sample with the remaining outer shell

Density of the samples was measured in water described in NEN-EN 12697-6:2012. The average density was 2382 [kg/m³]. The average density of the samples cut from the asphalt plate made for the 4PB fatigue test was 2356 [kg/m³]. This slight deviation was expected between a plate segmented compactor and a gyro shear compactor.

E.2. Test setup

The European norm does not have a standardised description for the uni-axial test setup available under the NEN-EN12697-24:2018 guideline. So the test setup and specimen size were based on the American AASHTO 107-2014 norm. The full title is: 'Determining the Damage Characteristic Curve of Asphalt Mixtures from Direct Tension Cyclic Fatigue Tests'. The only change made from the Norm is increasing the specimen height from 130 to 150 mm.

Tests were performed on the equipment of the TU Delft. It consist of a climate chamber for maintaining a constant temperature. A MTS developed hydraulic actuator was controlled by a Instron 8400 controller. The testing rig was modified to test in tension-compression sinusoidal displacement mode around zero. No tolerance between moving parts were left in the setup. It was equipped with a 50 kN load cell from Lebow due the expected stress. Force and displacement signals were captured and stored with the in house developed MP3 data acquisition program. Displacement was measured, controlled and averaged with 3 +/- 1 mm range LVDT's attached to the sample on 120 degrees rotation separation. Attaching the LVDT's was done in a light frame loaded under a high spring force around the sample. To ensure no rotation or vertical displacement of this frame would take place, it was coated with a high friction substance. The displacement between the top and lower frame was measured over a 100 mm height difference. In figure E.2 a test sample is shown mounted in the test setup.



Figure E.2: Test sample installed in the Uni-axial setup



Figure E.3: Aluminium cap and plastic rings

The specimen are glued with a two component adhesive glue 'X60 Pleximon 801' to an aluminum cap at one side. To ensure no movement of the specimen the other side is glued with force controlled mode applied in the test setup to another aluminum cap. Only breaking the sample would now make it possible to remove it. A first test sample indicated that the specimen can have a tendency to brake at the cap and not in the specimen itself during a fatigue test. Observed was not a failure of the glue, but around the the first few millimeters of bitumen. To ensure a better and more gradually introduction of the forces to the sample, bigger caps (120 diameter instead of 100 mm) and plastic rings of 10 mm in height and width were ordered and used, see figure E.3. Using these plastic rings glued to the cap and sample, a more gradually introduction of the applied force was ensured.

E.3. Test Procedure

The sample is first brought to room temperature for at least 3 hours. It is cleaned, degreased and the top side side is glued. A 4 kg weight is applied for 5 minutes to secure a good adhesion. The sample is attached to the top of the test setup and the actuator is activated in load control with a 40 Newton load to glue the bottom side. The weight of the sample on the load cell of the sample was compensated by using the load control function of the controller. This way it is ensured that the samples endures

no to very little stress due to its own weight in the middle of the specimen. After setting the mode of loading to displacement control the specimen had time to relax at the test temperature of 20°C . First a frequency sweep was conducted at $50\ \mu\text{m}/\text{m}$ for 0.1, 0.2, 0.5, 1, 2, 5, 8, 10, 20 and 30 Hz at the set temperature of 20°C . Only this temperature was tested in accordance with the procedure of the other fatigue tests. After the frequency sweep a certain strain amplitude between 120 and $400\ \mu\text{m}/\text{m}$ at 10 Hz was set. The applied strain signal was a sinusoidal shape with the average close to or zero. This way an Uni-axial Tensile Compression Fatigue test was conducted. After a certain number of load repetitions the sample would break and the test could be aborted. Due the nature of the displacement controlled test the set controller limits would not be triggered. The sinusoidal set displacement signal will continue with only a small force active when the sample is loaded in compression. The tension part will result in a small visible crack. The resulting total movement of the specimen will lead to hearing a clapping sound.

In figure E.4 and 2.6 the resulting crack is shown for 2 different samples. All other 11 samples showed the same cracking pattern. The crack was continuous and through the complete section of the specimen. No sample was cracked at or directly at the mounted measuring frame. After abortion of the fatigue test, the control mode was put in actuator-displacement mode and the crack was made visible.



Figure E.4: Specimen 5 after fatigue testing



Figure E.5: Specimen 10 after fatigue testing

E.4. Measuring software and calculations

Capturing the 4 incoming signals was done with the help of a special script written for the MP3 data acquiring software. Three of these were LVDT displacement and 1 was the force signal. With an interval of 200 load repetitions, 10 repetitions were recorded with 250 Hz. Resulting in 25 points per repetition. Every interval was saved individually and automatically post processed with an own developed Matlab script. This script works through fitting a sinusoidal wave on the measured points. Resulting in an amplitude for the average displacement of the 3 LVDT and a force amplitude. From these two fitted sinusoidal equations the phase angle is calculated through $\Delta t [ms]$ between the peaks of the two equations. An example of the method and result is shown in figure E.6 and E.7. The displacement values can all be negative or as well all be positive in another test. This due the setting of the LVDT's at the start of the test. This can vary per test performed. The state of tension or compression of the sample is determined by the load cell. The strain determined at those points are following the amplitude calculated to the mean of the peak to peak displacement. So only if there is an divergence from zero in the mean force signal, we have to go from a sinusoidal to haversine approach. In the end all variables per 200 load repetitions are saved in a 4 column wide .csv file.

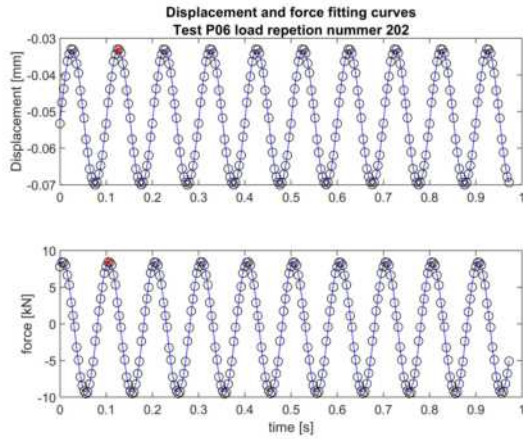


Figure E.6: Example of the fitted curves on the measured data points

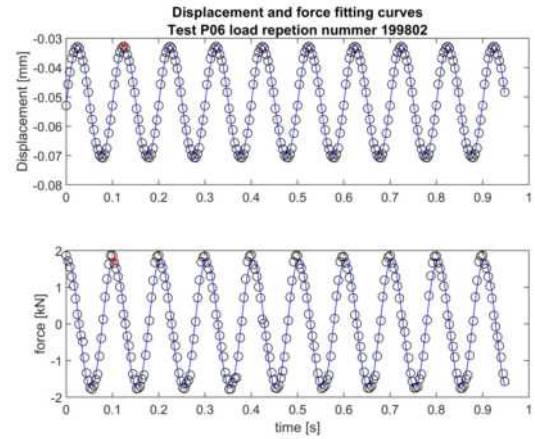


Figure E.7: Example at N 199802 of the fitted curves on the measured data points

For a 50 kN load cell the force signal is still a good sinusoidal function after cracking of the sample. Shown in figure E.7 is the fitting of load repetition 199802. This is after the sample has failed in fatigue. The controlled displacement and resulting force signal is still smooth enough to get an accurate phase angle. This results in steady phase angles values shown in section E.5.2.

Calculations needed for the strain and stress based on these displacement and force amplitudes for every specimen are trivial and are left to the reader. The same basic formulas for stiffness and dissipated energy from chapter 2 are used.

E.5. Results

In this section all results are presented for the UTCF test. This is done for all 11 test by presenting the graphs for the Stiffness, Stiffness Repetition, phase angle, dissipated energy, Energy Ratio and the Plateau Values.

E.5.1. Stiffness and Stiffness ratio

To find N_{fat} the method of stiffness ratio is used for the traditional fatigue relation. Both $N_{fat50\%}$ and N_{fatSN} failure criteria are shown in the following stiffness graphs. In figure E.9 it is visible that test P04 was terminated too quickly.

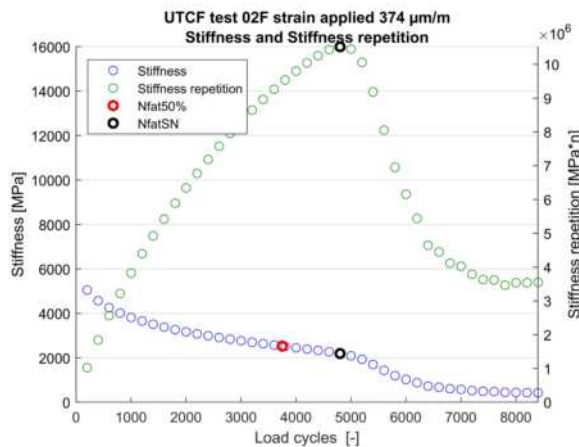


Figure E.8: Stiffness and Stiffness ratio P02

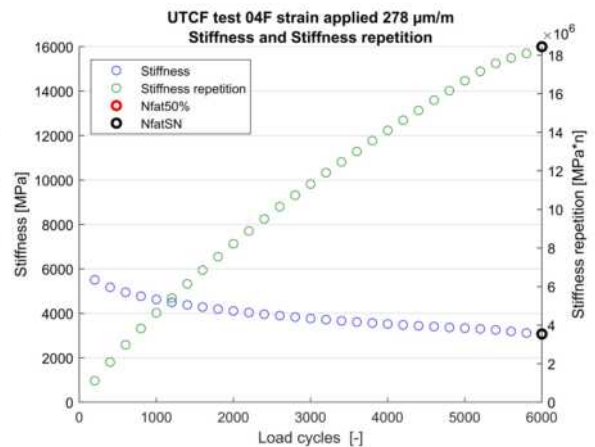


Figure E.9: Stiffness and Stiffness ratio P04

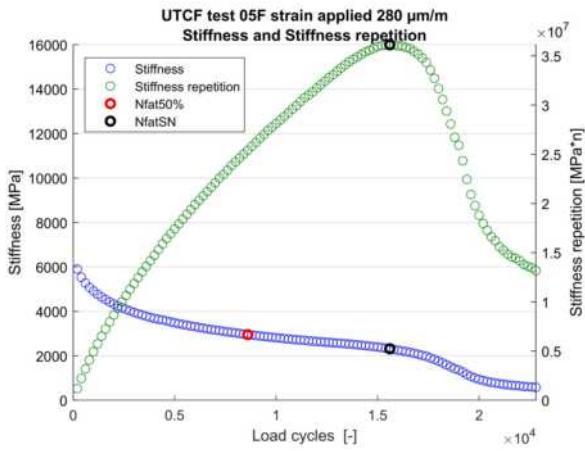


Figure E.10: Stiffness and Stiffness ratio P05

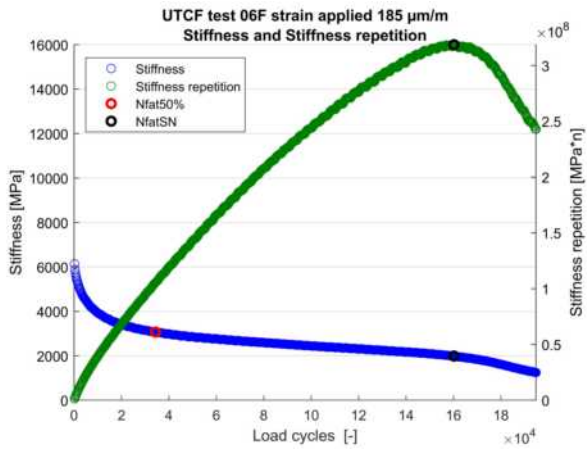


Figure E.11: Stiffness and Stiffness ratio P06

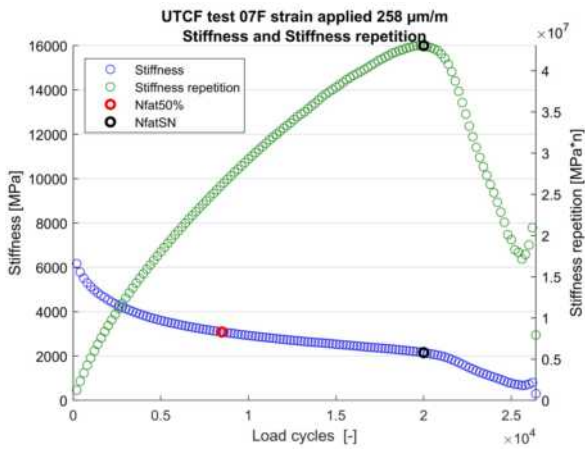


Figure E.12: Stiffness and Stiffness ratio P07

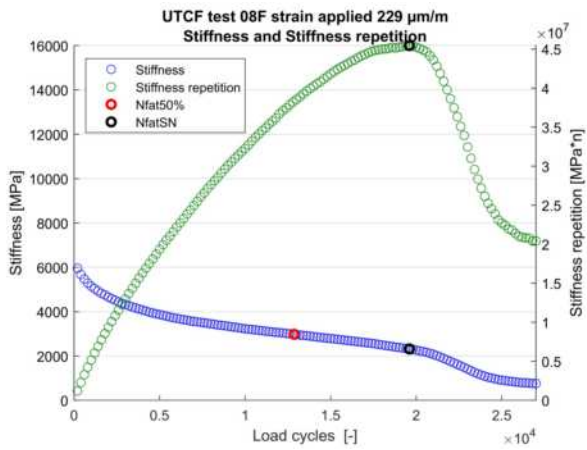


Figure E.13: Stiffness and Stiffness ratio P08

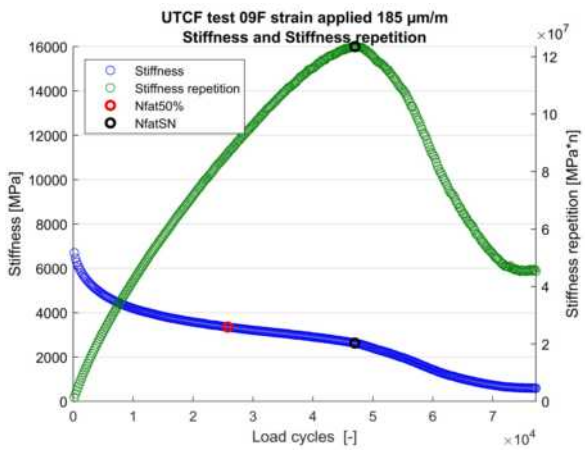


Figure E.14: Stiffness and Stiffness ratio P09

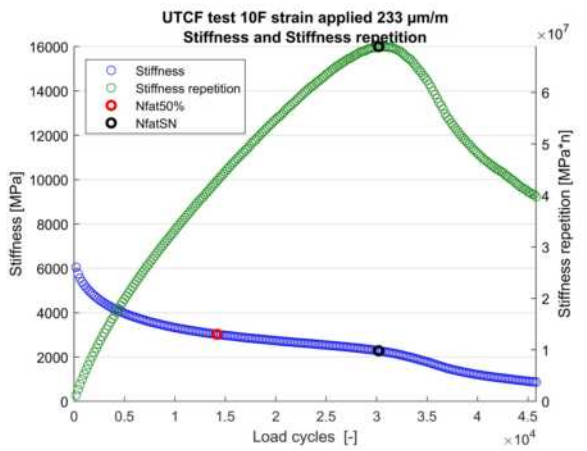


Figure E.15: Stiffness and Stiffness ratio P10

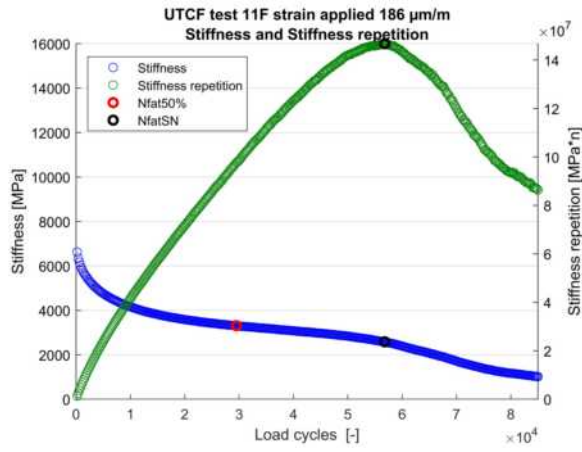


Figure E.16: Stiffness and Stiffness ratio P11

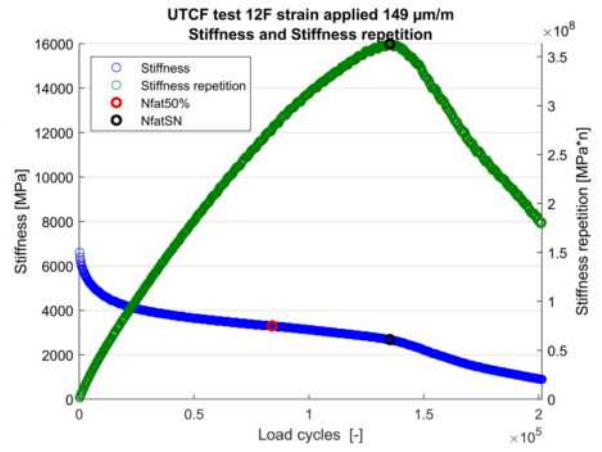


Figure E.17: Stiffness and Stiffness ratio P12

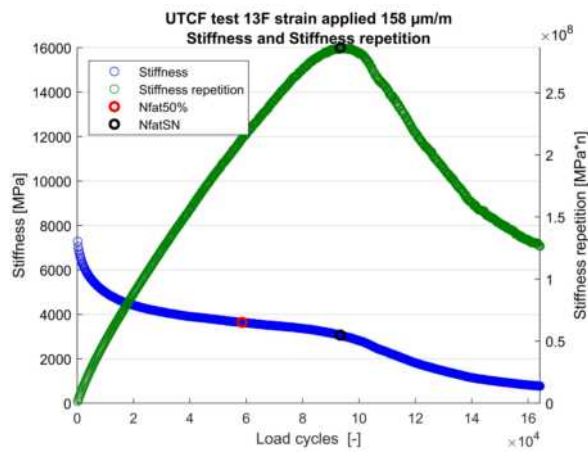


Figure E.18: Stiffness and Stiffness ratio P13

E.5.2. Phase angle, dissipated energy and RDEC

In this section the 11 test results of the phase angle, dissipated energy, failure criteria ER and RDEC are presented. The failure criteria again don't differ significantly as discussed by the 4PB displacement controlled tests. These are combined in 2 figures which are presented side by side. Due to the 10 Hz more data points per load repetition were available. This increased the accuracy and no huge phase angle fluctuations were found as in the 4PB force controlled testing. The same Matlab script was used to set the boundaries of the linearization of the dissipated energy. After a standard of 17 measuring points ($N=3400$) till N_{fatER} . This interval should represent the Plateau Value stage. From this interval on the dissipated energy, the script calculates the Plateau Value. The fitted line is not always perfect as shown in figure E.25. For the medium strain levels it is almost perfect as shown for P05,P07,P08 and P09.

In The RDEC graphs the fitted PV is given as well as the average PV from the five data points before the N_{fat} . This is called the PV mean. For P02, P05,P07,P08,P09,P10 and P11 the RDEC is clearly shown. This is quite an improvement compared to the 4PB force controlled tests. A stable phase angle is the best improvement in this case.

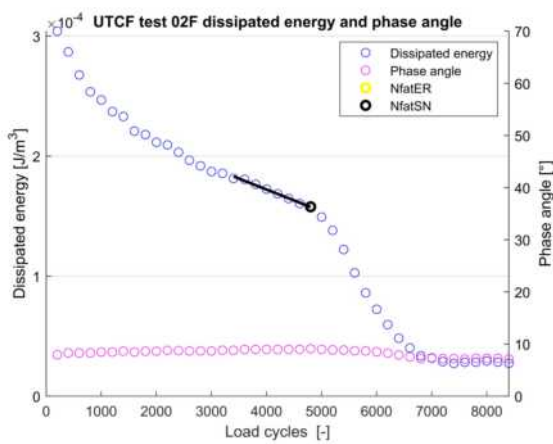


Figure E.19: Phase angle and dissipated energy P02

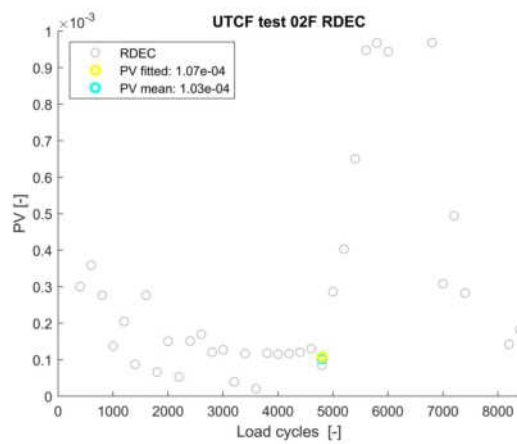


Figure E.20: RDEC P02

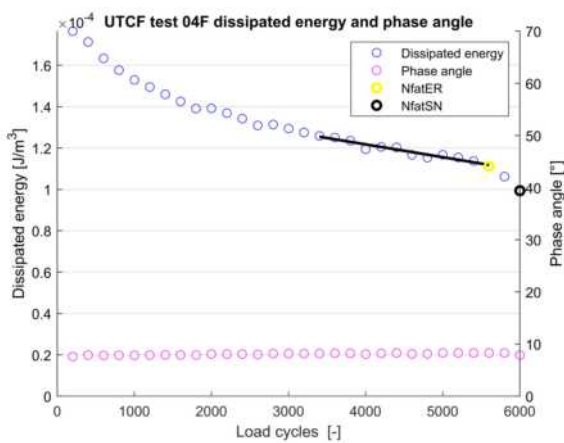


Figure E.21: Phase angle and dissipated energy P04

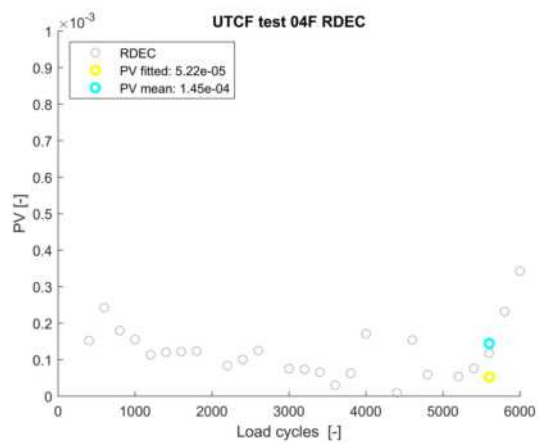


Figure E.22: RDEC P04

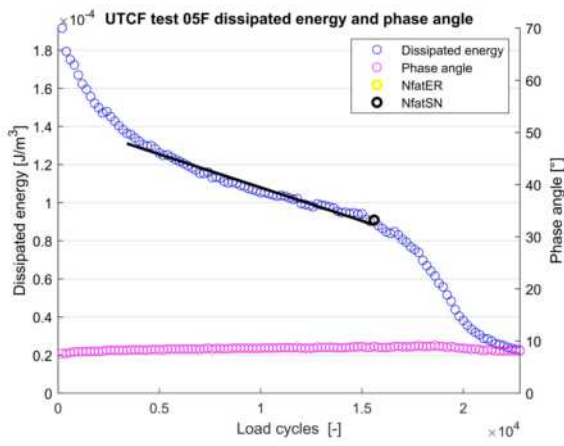


Figure E.23: Phase angle and dissipated energy P05

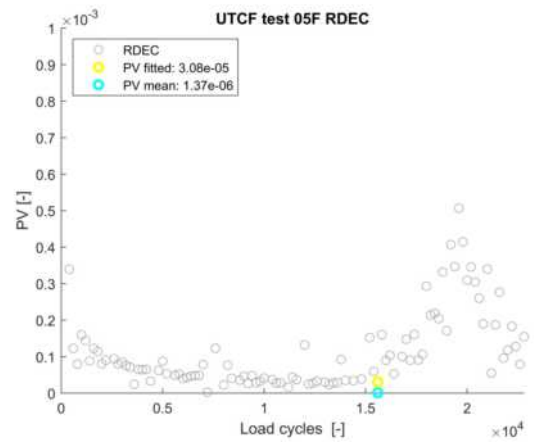


Figure E.24: RDEC P05

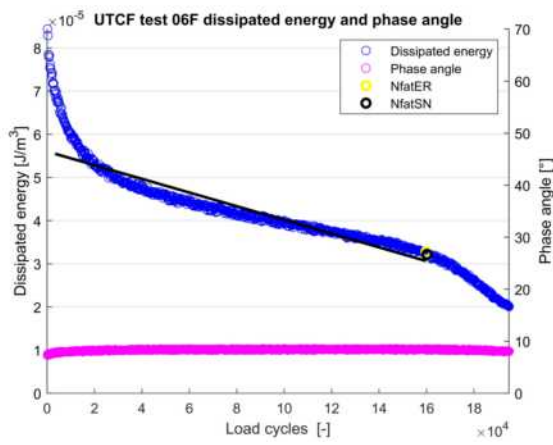


Figure E.25: Phase angle and dissipated energy P06

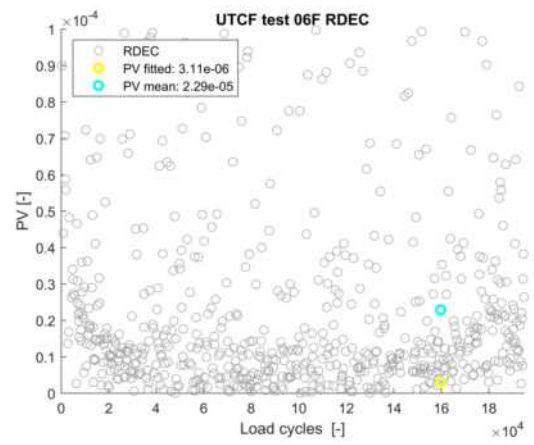


Figure E.26: RDEC P06

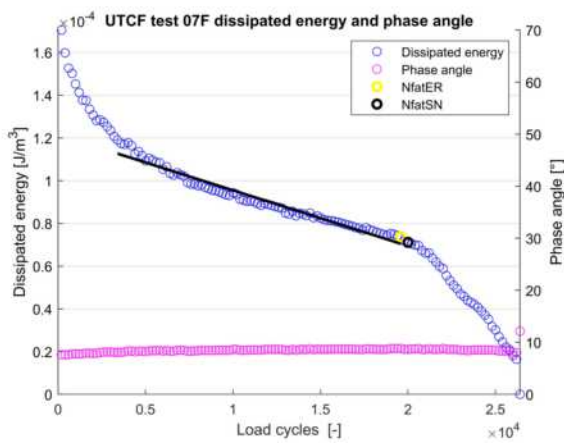


Figure E.27: Phase angle and dissipated energy P07

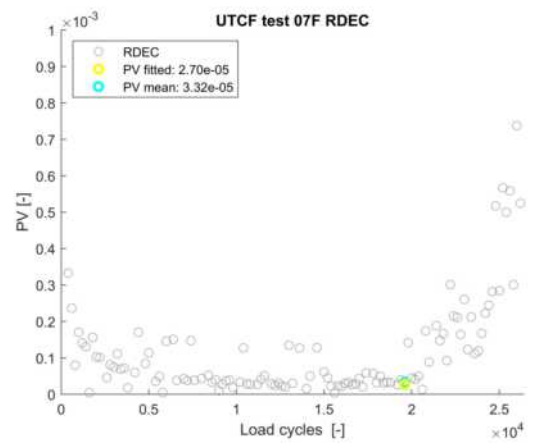


Figure E.28: RDEC P07

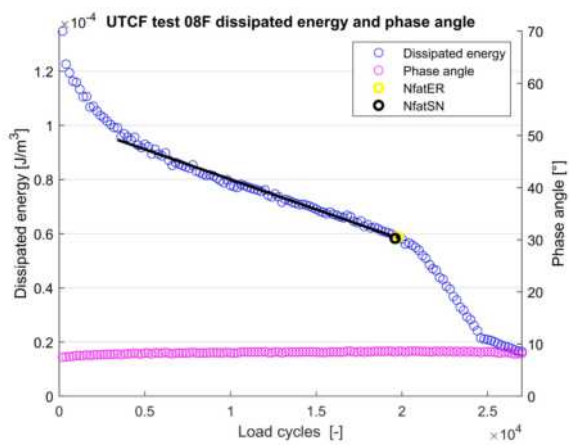


Figure E.29: Phase angle and dissipated energy P08

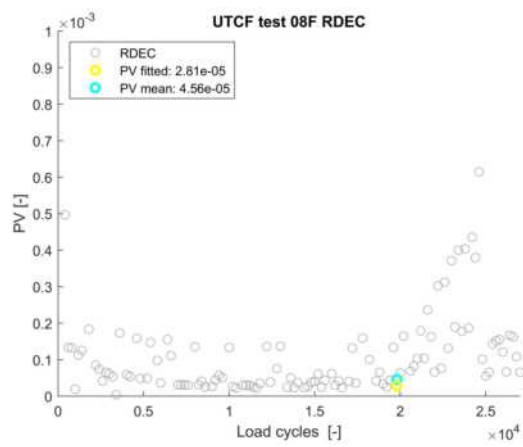


Figure E.30: RDEC P08

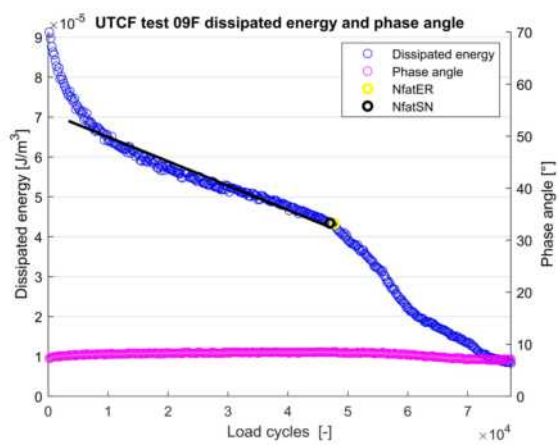


Figure E.31: Phase angle and dissipated energy P09

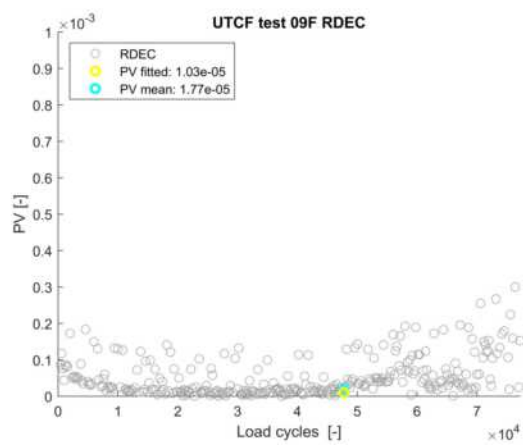


Figure E.32: RDEC P09

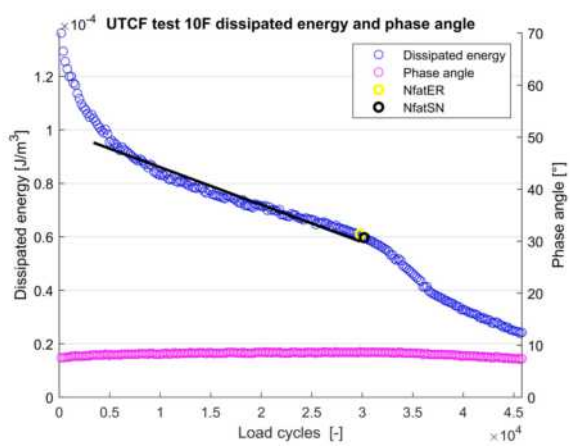


Figure E.33: Phase angle and dissipated energy P10

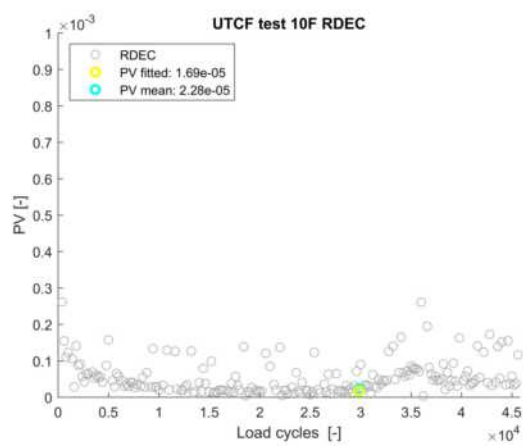


Figure E.34: RDEC P10

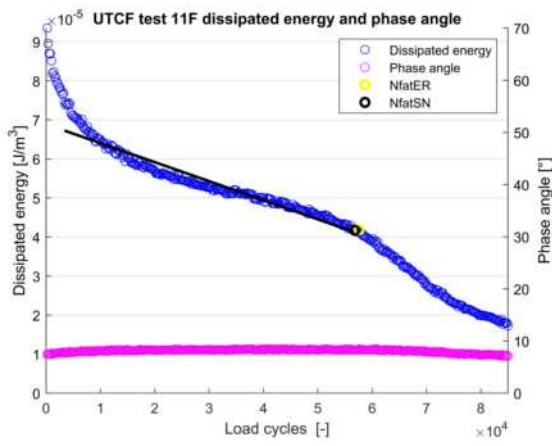


Figure E.35: Phase angle and dissipated energy P11

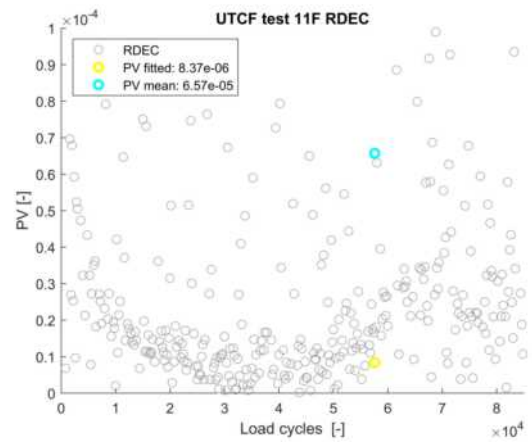


Figure E.36: RDEC P11

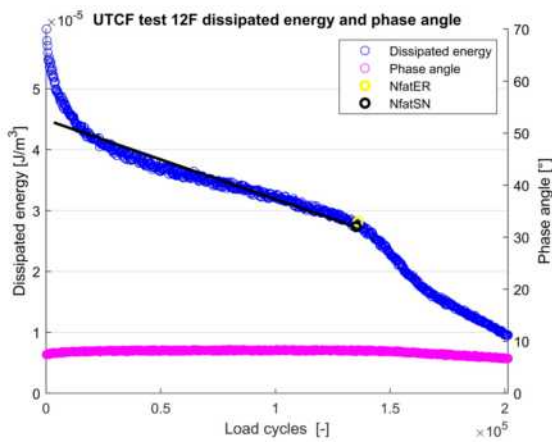


Figure E.37: Phase angle and dissipated energy P12

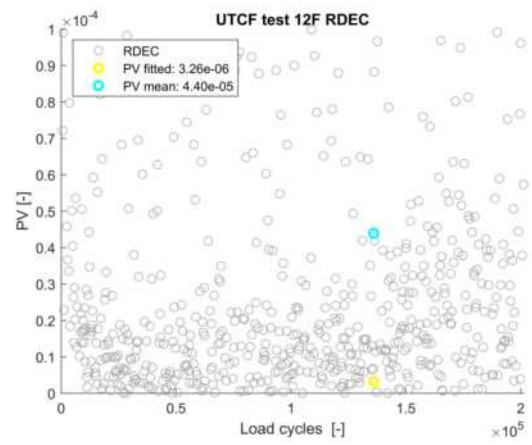


Figure E.38: RDEC P12

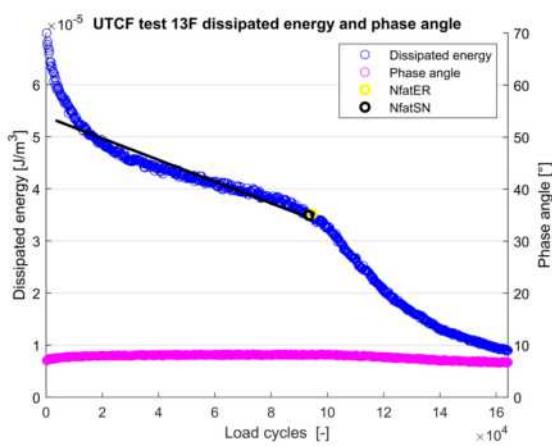


Figure E.39: Phase angle and dissipated energy P13

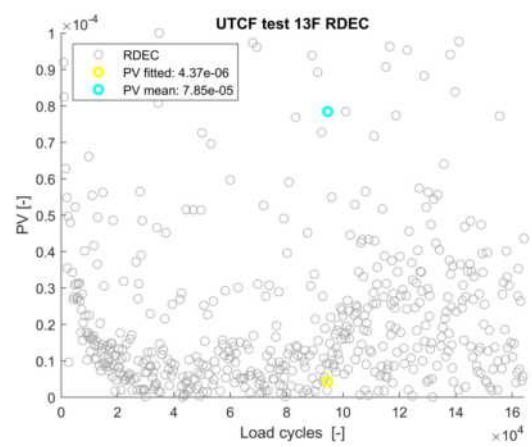


Figure E.40: RDEC P13

E.5.3. Log strain & Log PV

In this subsection the results for the number of load repetitions and the strain on a log-log scale are given in figure E.41. Despite the overall good performance during testing and the steady findings of N_{fat} with the Stiffness ratio method, the least squared error is a bit low at 0.87. Especially compared with the found error of 0.98 for the 4PB test with the same mixture in figure 3.35. The relation for the Plateau Value versus the number of load repetitions are given in figure E.42. A better correlation is found, but this is logical with the RDEC method as explained in chapter 4.

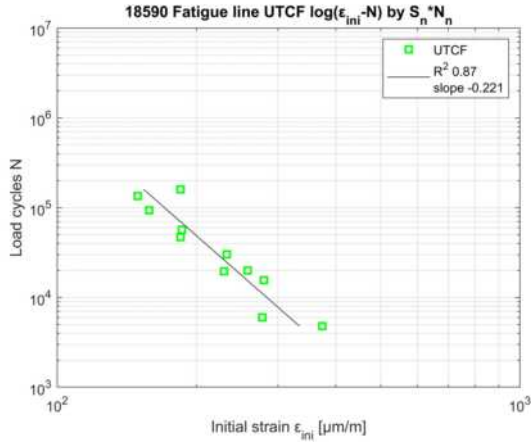


Figure E.41: Fatigue line 18590 UTCF

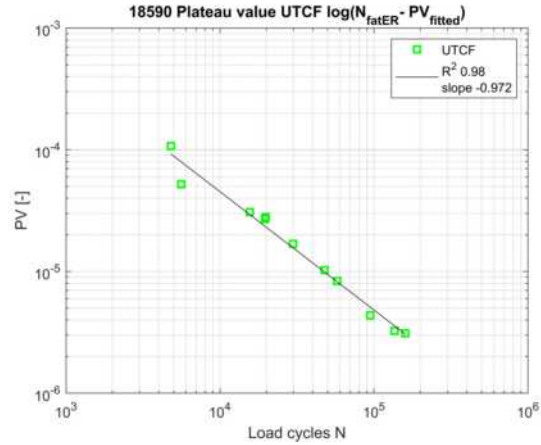


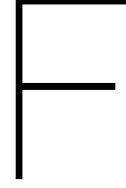
Figure E.42: Plateau value line 18590 UTCF

E.5.4. Table

In table E.1 all the previous results are given in a single table. The applied strain, the different failure criteria, the fitted slope of the dissipated energy, the resulting PV fitted, the average found PV at failure and the magnitude differences between them.

Table E.1: Mixture 18590 UTCF results

Sample	Strain applied ϵ_{ini} [$\mu\text{m}/\text{m}$]	$N_{fat50\%}$	N_{fatSN}	N_{fatER}	$x(1)$	PV fitted ($\cdot 10^6$)	PV mean ($\cdot 10^6$)	ΔPV
02F	374	3750	4802	4802	-1,82E-08	107,38	102,82	1,0
04F	278	-	6002	5602	-6,19E-09	52,21	144,63	-2,8
05F	280	8604	15602	15602	-3,50E-09	30,78	1,37	22,5
06F	185	34351	160202	159802	-1,59E-10	3,11	22,91	-7,4
07F	258	8488	20002	19602	-2,61E-09	27,01	33,20	-1,2
08F	230	12862	19602	19802	-2,22E-09	28,09	45,61	-1,6
09F	185	25795	47002	47802	-6,10E-10	10,29	17,67	-1,7
10F	233	14181	30202	29802	-1,40E-09	16,91	22,78	-1,3
11F	186	29491	56802	57602	-4,87E-10	8,37	65,70	-7,9
12F	149	84003	135202	136002	-1,30E-10	3,26	43,96	-13,5
13F	158	58524	93402	94602	-2,08E-10	4,37	78,47	-18,0



Statistical method

In this appendix a statistical method is discussed to establish a relation between the N_{fat} and the resulting PV. The method itself in this research gave unsatisfactory and incomplete results. It is therefore placed in the appendixes of the research. As the statistical method is till now the only approach in linking the CY-ITT and 4PB through the RDEC method it is an important method to include.

The statistical method is build on the concept of a fitting method in establishing the PV through the dissipated energy with a fitted line. Now the fitted line is ended not by the repetition method, but when the dissipated energy curve deviates from the applied statistical curve.

The method employed here is based on the works by Telman [2017]. It is used in this thesis on the different mixtures to validate and discuss the statistical method. Telman discusses three potential options to find a correlation $\log(N - PV)$ relationship between the CY-ITT and 4PB. The statistical fitting method discussed in chapter 4.3 of the paper [Telman, 2017], is till now the only method that showed a clear correlation between the logarithmic PV-N relation for both the CY-ITT and 4PB. It also agrees with the statements made by Pronk / Hopman that the N_{fat} can be determined when the Dissipated Energy Ratio curve defects by the stated linear line that can be developed by this method. This method will therefore be explained, discussed and validated on the own performed fatigue tests.

Theory

The method utilised is based on the values of the Dissipated Energy itself and not the calculated RDEC. This to avoid the use of absolute values for RDEC and the huge spread of RDEC overall [Telman, 2017]. The goal is to find the second phase of the characteristic RDEC curve in which the PV is constant or slightly sloped over the number of load repetitions. This is what Telman calls the 'exponential' part of the DE curve. Which is positive for the CY-ITT and negative for the 4PB. We rewrite equation F.1 through equation F.2 to equation F.3 to find the exponential dissipated energy curve [Telman, 2017].

$$PV = \frac{DE_{n+1} - DE_n}{DE_n} \quad (F.1)$$

$$DE_{n+1} = DE_n \cdot (PV + 1) \quad (F.2)$$

$$DE_n = DE_o \cdot (PV + 1)^n \quad (F.3)$$

In which PV is the estimated fitted value of the dissipated energy. Because PV is almost always very small $PV < 10^{-4}$ the exponential function will be close to linear. The first part of the dissipated energy is a none exponential part, so the function does not start at $N = 0$, but a latter point so the fitting equation becomes:

$$Y = DE_o \cdot R^{n-n_o} \quad (F.4)$$

To find PV, we use equation F.4 and fit this over the exponential part of the dissipated energy curve. To calculate PV now we use $PV = R - 1$. To find N_{fat} , we use the highest value of N were this equation

still fits. The latter part is done by means of a statistical analysis. It is done by the following iterative approach:

1. Find the exponential part of the DE-curve and take a certain amount of points n
2. Fit $Y = b \cdot R^n$ in which $b = DE_0 \cdot R^{-n_0}$
3. note R and find standard deviation s_{rest}
4. Set the condition, if true ad point, repeat for below and above the starting point.
5. When the condition returns as false the PV is calculated and Nfat is set as the average of the highest n true for the set conditions and the successive load n .

The condition for the upper level is set through:

$$|DE_{up} - Y_{pred}| < t_{n-2} \cdot \sqrt{s_{rest}^2 + s_{pred}^2} \quad (F.5)$$

where: Y_{pred} = Predicted DE value by the fitting equation
 t_{n-2} = Two sided 95% value for the $n-2$ degrees of freedom

This method is applied to two mixtures, called 252 and 938. And results for the CY-ITT and 4PB in a single line correlation presented in figure F.1 for mixture 252. Mixture 938 showed the same single line correlation between the CY-ITT and 4PB and can be found in the original paper.

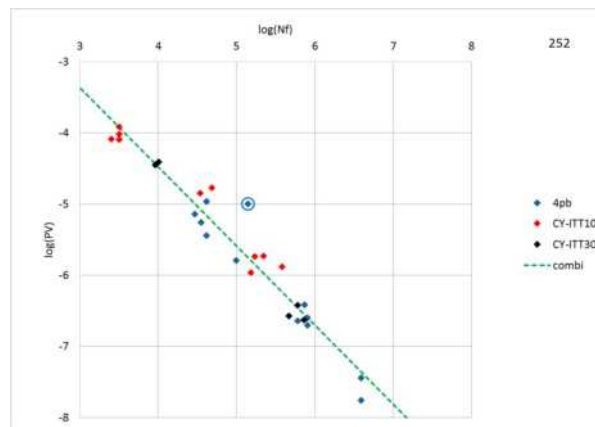


Figure F.1: Plateau Value J.Telman exponential statistical method on mixture 252 [Telman, 2017]

It is very clear from figure F.1 that this statistical method gives a solution that shows a clear correlation between the 4PB and CY-ITT. The drawback is that the results aren't discussed any further in detail or that the founded Plateau Values are plotted back on the original dissipated energy graphs shown in the appendix of the paper [Telman, 2017]. This will lead to the following discussing about the presented results of this statistical method.

Discussion

The original founded values of the published work for mixture 252 in the appendix tables are plotted over the values presented in figure F.1. The values from the tables in appendix 1 are in agreement with the presented result of the individual fatigue test of the CY-ITT and 4PB found in appendix 2 from the paper [Telman, 2017]. Figure F.2 is the result of this comparison between the presented statistical method and the published Nf_{micro} and corresponding PV values.

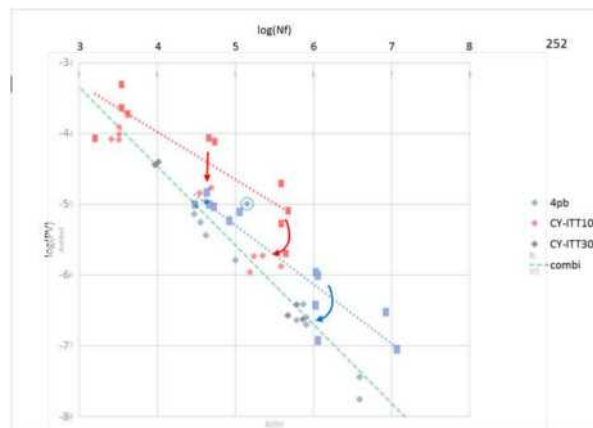


Figure F.2: Plateau Value mixture 252, Table vs statistical method

In the figure the squared block upper markers are the values from the tables. In red the CY-ITT values are given and in blue the values of the 4PB. The values from the statistical method are presented by the original tilted blocks. It is more than clear that a huge shift has occurred for both fatigue tests. The values for both CY-ITT and 4PB have decreased in PV and for the N_{fat} . Some measurement point have shifted almost a log block down, which is a factor 10 in value! For the N_{fat} this can be understandable for given that the previous method used in the tables gave maybe a too high N_{fat} . It would for understanding and completeness good to see how this shifted N_{fat} would relate on the corresponding stiffness graph. The large decrease of at least a factor 5 of the overall PV values for both fatigue test could be better documented. It can be the case that the predicted exponential function to find PV in in equation F.4 is a more accurate way of finding an overall average of PV.

From the first section of Chapter 4 where the three main variables are discussed, we can clearly see that the dissipated energy of the CY-ITT follows always a almost linear straight line till failure of the sample. The complete curve can be described by a the natural logarithm curve. The 4PB is actually never a clear straight line or a line that is almost linear as stated by Telman at low RDEC values. 4PB dissipated energy curves always follows a double mirrored shape natural logarithm curve. In the next section the method is worked out.

Results

The applied method of finding a statistical method with a non-linear equation as set by equation F.4 is not directly possible on a standard 4PB dissipated energy curve. As the equation is set by the a formulation that does not correlate with a mirrored inverse natural logarithm curve that the 4PB describes in the latter half. We find here the same problem as Carpenter with neglecting the turning point in a displacement controlled 4PB fatigue curve. For the CY-ITT the formulation can hold and follows the overall dissipated energy curve.

The problem that arises is the set linear equation on the dissipated energy curve fails quite fast. Given the fact that the set standard deviation can only be set by a linear fitting equation and the 95% confidence boundary condition falls too fast outside the real dissipated energy curve. Resulting that the method in the current state can not directly be applied to the dissipated energy curve.

The meager result can however be further development in a future study. In which more time and resources are available to develop a statistical approach in finding the N_{fat} . It will act as a recommendation to develop and discuss this method in more detail with the original author.

G

Matlab code

In this appendix the generic matlab code used in this thesis is given. The main formula's and formulations are presented for validation and transparency of the found results. Each fatigue test has it own main script that is partially presented here with the main formulations.

G.1. 4PB

The matlab code used and presented here for the 4PB starts after the initial automated part. That part took care of the numerous results used for the thesis and the automatic coupling between specimen dimensions, fatigue results (fitted or direct results) and frequency sweep results. These are quite ingenious and kept with the author. The results from this the shown script are stored in columns and or tables and are used in other more graphically focused matlab script for presenting and analysing the results.

```
1      %%--- Calculations ---%%
2      L = length(data(:, (4*i-3)))-sum(isnan(data(:, (4*i-3))));
3      Lr = [Lr;L];
4      L_min = round(mean(Lr));
5      N=data(1:L,4*i-3);
6      phirad = data(1:L,4*i-2)*pi()/180;          %phi in radians by pi/180
7      phir = 180/pi*phirad;
8      epsilon = (0.5*12*data(1:L,4*i)*hoogte)/(3*a^2-4*a^2);          %0.5 factor ...
9      %for peak to peak value and not amplitude
10     epsilon_r = [epsilon_r; (epsilon(5,1)*10^6)];
11     sigma = (0.5*3*data(1:L,4*i-1)*a)/(breedte*hoogte^2);          %0.5 factor for peak ...
12     %to peak value and not amplitude
13     Smix = sigma./epsilon;
14     DE = pi()*epsilon.*sigma.*sin(phirad)*10^6 ;          %J/m^3
15
16     %%--- VECD ---%%
17     DMR = E_finger/E_LVE;          %Ratio between frequency sweep and mastercurve ...
18     %established stiffness
19     e_pseudo = epsilon*(E_LVE);          %4PB half is in tensile so only the amplitude
20     F_pseudo = (sigma)./(epsilon*E_LVE*DMR);
21     Wcr = 0.5*(1-F_pseudo).*e_pseudo.^2*10^6;          %J/m3
22     DMRr = [DMRr;DMR];
23
24     for k=1:(L-1)
25         RDEC = -(DE((k+1)) - DE(k))/(N(k+1)-N(k))*DE(k+1); %minus because negative ...
26         %dissipated energy slope
27         RDECr = [RDECr;RDEC];
28
29         %VECD
30         G_r = (Wcr((k+1)) - Wcr(k))/(N(k+1)-N(k));
31         G_rr = [G_rrr;abs(G_r)];
32     end
33
34     %%--- Failure Criteria ---%%
```

```

31 S50 = Smix(1,:)/2;
32 I1 = find(abs(Smix - S50) < 1000);
33 TF = isempty(I1);
34 if TF == 1
35     I1 = [1;2]
36     display( 'Geen Nfat50 ');
37 end
38
39 N1=N(I1);
40 M1=Smix(I1);
41 Nfat50 = interp1(M1, N1, S50, 'linear ');
42 Nfat50r=[Nfat50r;Nfat50];
43
44 SN=N.*Smix;
45 [Smax,I2] = max(SN);
46 NfatSN = N(I2);
47 NfatSNr = [NfatSNr;NfatSN];
48 M2=Smix(I2);
49 M3=sigma(I2);
50 DEN = (N.*DE)/DE(1);
51 [DENmax,I4] = max(DEN);
52 NfatDEN = N(I4);
53 NfatDENr = [NfatDENr;NfatDEN];
54
55
56 %%--- RDEC ---%%
57 xdata = N(17:I4,1); %17 is around N=1000
58 myfun = @(x,xdata) xdata.*x(1)+x(2);
59 x0 = [0.1; 0.01];
60 [x] = lsqcurvefit(myfun,x0,xdata,DE(17:I4,1));
61
62 PV = abs(x(1)/(DE(1)));
63 PVde = abs(x(1)/(mean([DE(17,1);DE(I4,1)]))); % (mean([DE(17,1);DE(I2,1)]))
64 PVder = [PVder;PVde];
65 PVcor = abs(x(1));
66 Gradient = x(1);
67 Gradientr = [Gradientr;Gradient];
68 PVmean = abs(mean([RDECr(I4-11);RDECr(I4-1)]))
69 PVr = [PVr;PV];
70 PV50 = -(1-(1+100/Nfat50)^x(1))/100;
71 PV50r = [PV50r;PV50];
72 PVmeanr = [PVmeanr;PVmean];
73 Smixr = [Smixr;Smix(1)];
74
75 %%--- VECD ---%%
76 Ngr = N(1:I2) ;
77 Wr = Wcr(1:I2) +abs(Wcr(1,1));
78 Gr = (trapz(Ngr,Wr,2))/NfatSN^2;
79 Grr = [Grr;Gr];
80 Grmean = abs(mean([G_rr(I2-11);G_rr(I2-1)]));
81 Grmeanr = [Grmeanr;Grmean];
82
83 W_afstand = 30; %Voor de fitting line voor Wcr
84 xdata2 = N((50):I2-5,1);
85 myfun2 = @(w,xdata2) xdata2.*w(1)+w(2);
86 w0 = [0.1; 1];
87 [w] = lsqcurvefit(myfun2,w0,xdata2,Wcr((50):I2-5,1));
88 Gr2 = w(1);
89 Gr2r = [Gr2r;Gr2];

```

G.2. CY-ITT

For the CY-ITT it is the same case with the initial part of the code used. As the greater part of the code is comparable to the 4PB only the highlights are shown. Take care that as the CY-ITT sample is in a constant compression/tensile state, the measured displacement is captured in a peak-peak or amplitude form. From that realise that the captured displacement peak peak values are taking into consideration the linear incline resulting from the permanent deformation. The used script to find the these displacement and force amplitudes are given here first. The choice to use a fitting function over a

FFT formulations is personal and did not show a difference in the final result. The only reason to use a fitting function over FFT is the insight it provides over the computational advantage of the FFT.

```

1      %% ---- CURVE FITTING PART -----%%
2      for i=0:(c-1)
3          ydata= data((14+(i*step1):(489+i*step1)), [4]);          %10Hz op 513 30Hz op 489
4          xdata = data((14+(i*step1):(489+i*step1)), [5]);
5          force =data((14+(i*step1):(489+i*step1)), [1]);
6          time = xdata;
7          displacement = ydata;
8
9          yu = max(ydata);
10         yl = min(ydata);
11         yr = (yu-yl);
12         yz = ydata-yu+(yr/2);
13         zx = time(yz .* circshift(yz,[0 1]) ≤ 0);
14         per = 2*mean(diff(zx));
15         ym = mean(ydata)
16
17         myfun = @(x,time) x(1).*sin(2*pi*freq*time+x(2))+x(3)+x(4)*time;
18         x0 = [yr; 0.01; ym; 0.001];
19         [x] = lsqcurvefit(myfun,x0,time,displacement); %[x,resnorm] for R^2 error sum
20         xr = [xr;abs(x(1))];
21
22         fu = max(force);
23         fl = min(force);
24         f2r = (fu-fl);
25         fz = force-fu+(f2r/2);
26         zx = time(fz .* circshift(fz,[0 1]) ≤ 0);
27         per = 2*mean(diff(zx));
28         fm = mean(force);
29         f2 = f(2);
30
31         myfun2 = @(f,xdata) f(1)*sin(2*pi*freq*xdata+f(2))+f(3);
32         f0 = [f2r; 0.01; fm];
33         [f] = lsqcurvefit(myfun2,f0,xdata,force);
34         fr = [fr;abs(f(1))];
35
36         times = (linspace(time(1),time(end),2000)) ;
37         y1 = myfun(x,times(120:400,1));
38         [val, idtime] = max(y1);
39         y2 = myfun2(f,times(120:400));
40         [val2,idtime2] = max(myfun2(f,times(120:400)));
41
42         idtime11 = times(idtime+120);
43         idtime22 = times(idtime2+120);
44         Δ_t = idtime22-idtime11;
45         phi = 360*1*abs(Δ_t);
46
47         %%--figure--%%
48         % left to the reader

```

The total mixture results of each fitting script are stored together and used with the generic CY-ITT script presented here below.

```

1      %%--Calculations--%%
2      phirad = (data(1:L,4*i-2))*pi()/180;
3      phir = 180/pi*phirad;
4      sigma = 2*(data(1:L,4*i-1)/2)/(pi()*hoogte*omega)*10^3; %Mpa / N/mm2
5      epsilon = ((2*data(1:L,4*i)/2)/omega)*((1+3*poisson)/(4+pi()*poisson-pi())); % ...
6      displacement is stored as peak-peak
7      epsilon_r = [epsilon_r;(mean(epsilon(1:10,1))*2*10^6)]; %strain (um/m) % total ...
8      strain is peak-peak!
9      Smix = sigma./epsilon *(1+3*poisson); %MPa
10     %DE van MPa to Pa -> 10^6
11     DE = 2*pi()*.*epsilon.*sigma.*sin(phirad)*10^6 ; %4x because always in tension so ...
12     2x amplitude strain and 2x amplitude stress, 0.5 for single side J/m^3

```

```

11     for k=1:(L-1)
12         RDEC = (DE((k+1)) - DE(k)) / ((N(k+1)-N(k))*DE(k+1)); %positive
13         RDECr = [RDECr;RDEC];
14     end
15
16     %%--VECD--%%
17     DMR = E_finger/E_LVE;
18     e_pseudo = 2*epsilon*(E_LVE); %factor 2 for all tensile state of specimen
19     F_pseudo = (2*sigma+(2*0.034)) ./ (2*epsilon*E_LVE*DMR);
20     Wcr = 0.5*(1-F_pseudo) .* (e_pseudo.^2)*10^6; %J/m3
21     DMRr = [DMRr;DMR];
22
23     for k=1:(L-1)
24         G_r = (Wcr((k+1)) - Wcr(k)) / ((N(k+1)-N(k)));
25         G_rr = [G_rr;G_r];
26     end
27
28     %%--RDEC--%%
29     xdata = N(33:I2,1); %After 2000 load repetitions strain measured is assumed stable
30     myfun = @(x,xdata) xdata.*x(1)+x(2);
31     x0 = [0.1; 0.01 ];
32     [x,resnorm] = lsqcurvefit(myfun,x0,xdata,DE(33:I2,1));
33
34     PV = x(1)/DE(1)
35     PVde = abs(x(1)/(mean([DE(33,1);DE(I4,1)]))); % (mean([DE(17,1);DE(I2,1)])
36     Gradient = x(1);
37     Gradientr = [Gradientr;Gradient];
38     PVder = [PVder;PVde];
39     PVr = [PVr;PV];
40     PV50 = (1-(1+100/Nfat50)^x(1))/100;
41     PVmean = abs(mean([RDECr(I4-11);RDECr(I4-1)]))
42     PV50r = [PV50r;PV50];
43     PVmeanr = [PVmeanr;PVmean];
44     Smixr = [Smixr;Smix(1)];
45
46     %%--Trivial--%%

```